

CHARACTERISATION OF BOD1L, A NOVEL PLAYER IN THE DNA DAMAGE RESPONSE

by

RACHEL MARIA ANTONIA MOTTRAM

*A thesis submitted to the University of Birmingham for the degree of
DOCTOR OF PHILOSOPHY*

Institute of Cancer and Genomic Sciences

College of Medical and Dental Sciences

University of Birmingham

December 2019

UNIVERSITY OF
BIRMINGHAM

University of Birmingham Research Archive

e-theses repository

This unpublished thesis/dissertation is copyright of the author and/or third parties. The intellectual property rights of the author or third parties in respect of this work are as defined by The Copyright Designs and Patents Act 1988 or as modified by any successor legislation.

Any use made of information contained in this thesis/dissertation must be in accordance with that legislation and must be properly acknowledged. Further distribution or reproduction in any format is prohibited without the permission of the copyright holder.

Abstract

Many components of the DNA damage response are known to function across multiple pathways. Bi-orientation defect 1-like (BOD1L) was recently identified as a modulator of nucleolytic resection of stalled replication forks. However, its potential roles in the resolution of other types of DNA damage were unexplored.

My thesis demonstrates that BOD1L interacts with the 53BP1 effector RIF1. This interaction is critical for the recruitment of RIF1 to DNA double-strand breaks (DSBs) induced by ionising radiation (IR). Collectively, these proteins antagonise the inappropriate accumulation of BRCA1 at these breaks, thereby suppressing CtIP- and MRE11-dependent resection. In the absence of BOD1L, aberrant resection ultimately compromises genome stability and cell survival. Homologous recombination is unaffected by the depletion of BOD1L; however, this factor is required for the 53BP1-dependent process of non-homologous end joining. Furthermore, BOD1L and RIF1 also modulate resection of Camptothecin (CPT)-induced DSBs.

In summary, I have demonstrated a novel interaction between BOD1L and RIF1, which is fundamental to its control of DSB resection following exposure to IR or CPT. Therefore, alongside its function during replication stress, BOD1L preserves genome stability by influencing DSB repair pathway choice, ensuring appropriate resolution of DSBs inflicted by a variety of genotoxins.

Acknowledgements

This document would not be before you today without the support and encouragement that I received from people in every circle of my life. In particular, I wish to express my considerable gratitude to those I will name below.

I extend my sincerest thanks to Prof. Grant Stewart and Dr. Martin Higgs at the University of Birmingham for accepting me into their respective labs and supervising this research. Through an inimitable combination of enduring patience, intelligence, perception, a substantial musical back-catalogue (and the best speaker system I have ever encountered in any research environment), their guidance continually inspired me and kept me motivated day by day. My colleagues in the Stewart and Higgs labs, past and present, have always been on hand to offer much-appreciated direction and support. I am especially thankful to Dr. Rachel Bayley for her unwavering practical assistance, countless invaluable discussions, reliable words of encouragement and a ready smile. It was a true privilege to work alongside her.

I also wish to thank our collaborators, Prof. Simon Boulton and Valérie Borel at the Francis Crick Institute, London, for their contributions to the story you are about to read.

Adequately expressing my gratitude to my family for their support throughout this journey deserves an entire chapter in its own right, but I hope that these few words will suffice here.

This thesis simply could not have been completed without the sheer selflessness of my parents, Lynne and Steve, and my parents-in-law, Nick and Nicki. They devoted months of their lives to providing childcare for my son during the final year of my research, and looked after both of us during the writing of my thesis - even when this engendered travelling to a different county and, in the case of my parents, actually moving house. I am grateful to my sister-in-law, Naomi, for always finding the right words to uplift me, and for hauling me out of a writing rut at a critical point. Considerable thanks are also due to my husband, Martin, for remaining steadfast at my side throughout this journey. I can't imagine that I have always been easy to live with during course of this PhD. I expect that on many occasions, I failed to show my gratitude for all that my wonderful family sacrificed to support me. I hope they know that it meant the world to me, and always will.

Finally, I must acknowledge my son, Stephen, for being my sternest taskmaster during my write-up phase. He was ever ready to reprimand me with "Get back to your work, Mummy!" whenever I left my desk... but his most treasured gift was bringing more joy and love into the past two and a half years of my life than any one person could possibly deserve in an entire lifetime. And I am profoundly grateful for my second child, who is due to join our family soon. This little flutter of life within has been my constant companion throughout the crafting of my thesis, and thoughts of this child have kept me grounded and reminded me that there will indeed be life beyond the PhD.

Per Dominum de gratia et Gloria eius.

Table of contents

Chapter 1: Introduction	1
1.1: DNA damage	1
1.2: DNA replication and replication stress	2
1.2.1: An overview of mammalian DNA replication	2
1.2.2: Replication stress	4
1.2.3: Factors contributing to replication stress	5
1.3: The cellular response to replication stress.....	10
1.3.1: Functions of ATR/CHK1 pathway in resolving replication stress.....	10
1.3.2: ATR-Seckel syndrome.....	11
1.3.3: The FA pathway and its function in ICL repair and resolving replication stress..	12
1.3.4: Fanconi Anaemia.....	15
1.3.5: Mechanistic differences between replication-dependent and -independent ICL repair	19
1.3.6: Protecting replication forks from uncontrolled degradation	20
1.4: DNA double-strand breaks	23
1.4.1: Causes of double-strand breaks.....	23
1.5: DNA double-strand break signalling and repair	26
1.5.1: Detection of double-strand breaks and signal initiation	26
1.5.2: Homologous recombination	35
1.5.3: Non-homologous end joining	42
1.5.4: Error-prone DSB repair pathways	45
1.5.5: Structural variation in double-strand breaks	47
1.5.6: Coping with complex lesions.....	48

1.6:	Regulation of DSB repair pathway choice	50
1.6.1:	Cell cycle-dependent regulation	50
1.6.2:	Promotion of nucleolytic resection.....	54
1.6.3:	Suppression of resection.....	56
1.6.4:	Epigenetic control of repair pathway choice	59
1.7:	Human diseases arising from a defective DNA damage response	61
1.7.1:	Ataxia telangiectasia	62
1.7.2:	A-T-like disorder.....	63
1.7.3:	Nijmegen breakage syndrome	65
1.7.4:	DNA-PKcs severe combined immunodeficiency	67
1.7.5:	Cancer	68
1.8:	Therapeutic opportunities within the DNA damage response.....	69
1.9:	BOD1L.....	73
1.9.1:	Structural and preliminary functional detail	74
1.9.2:	Characterisation as a fork protection factor	76
1.9.3:	Characterisation as a member of the FA pathway.....	79
1.10:	Thesis aims	79
Chapter 2:	Materials and Methods.....	82
2.1:	General Reagents and Equipment.....	82
2.2:	Antibodies	82
2.3:	Mammalian cell culture.....	83
2.3.1:	General culture protocols	83
2.3.2:	Transfections.....	85
2.3.3:	Treatment with DNA damaging agents and chemical inhibitors.....	87
2.4:	Clonogenic survival assays.....	88

2.5:	Immunoblotting	89
2.5.1:	Preparation of whole cell extracts (WCE)	89
2.5.2:	Analysis of WCE by SDS-PAGE and Western blotting.....	89
2.6:	Native DNA fibre analysis	92
2.6.1:	Preparation and spreading.....	92
2.6.2:	Antibody staining of DNA fibres for immunofluorescence microscopy	93
2.7:	Immunofluorescence microscopy	94
2.7.1:	Preparation of samples for immunofluorescence microscopy	94
2.7.2:	Antibody staining and mounting.....	94
2.7.3:	Proximity ligation assays (PLA).....	96
2.7.4:	Visualisation of IdU foci.....	96
2.7.5:	Fluorescence microscopy and image analysis.....	97
2.8:	Identification of novel BOD1L interactors	98
2.8.1:	Generation of Bod1L-FLAG-GFP stable cell line	98
2.8.2:	Affinity purification pull-down and mass spectrometry.....	98
2.8.3:	Analysis of mass spectrometry data	98
2.8.4:	Immunoprecipitation	99
2.8.5:	Generation of GST-tagged BOD1L fragments	99
2.8.6:	GST pull-down assays.....	101
2.9:	Analysis of class switch recombination (CSR).....	101
2.9.1:	Generation of conditional Bod1L knockout mouse model	101
2.9.2:	Assessing CSR proficiency	102
2.10:	DNA repair assays	102
2.10.1:	I-SceI-based reporter assays	102
2.10.2:	TRF2 telomere fusion assays	104

Chapter 3: A role for BOD1L in repair of IR-induced DNA double-strand breaks	108
3.1: Introduction	108
3.2: BOD1L suppresses resection of IR-induced DSBs alongside its fork protection role	110
3.2.1: Depletion of BOD1L results in increased sensitivity to IR	112
3.2.2: BOD1L maintains genome stability in irradiated cells by contributing to the repair of IR-induced DSBs	114
3.2.3: BOD1L modulates DSB repair during G2 phase	117
3.2.4: BOD1L depletion results in increased accumulation of IR-induced ssDNA in G2 cells	121
3.2.5: Elevated DSB resection in the absence of BOD1L is suppressed by depletion of CtIP	127
3.3: Discussion.....	144
Chapter 4: The interaction of BOD1L with resection antagonist RIF1 and the implications for DSB repair	152
4.1: Introduction	152
4.2: Identification of a functional interaction between BOD1L and the resection antagonist RIF1	155
4.2.1: BOD1L interacts with the 53BP1 effector RIF1	156
4.2.2: Identification of the RIF1-binding domains of BOD1L.....	162
4.2.3: Recruitment of 53BP1, RIF1 and REV7 to DSBs is unaffected in the absence of BOD1L in G2 cells	163
4.2.4: Chromatin recruitment of RIF1 in G1 cells is dependent on BOD1L.....	168
4.2.5: Class-switch recombination is compromised in a Bod1L-deficient mouse model	171
4.2.6: BOD1L and RIF1 depletion alters recruitment of BRCA1 to DSBs in G1.....	172
4.2.7: Depletion of BOD1L or RIF1 leads to accumulation of IR-induced ssDNA	174

4.2.8:	Increased DSB resection during G1 is counteracted by depletion of CtIP and MRE11	178
4.2.9:	Increased genome instability in the absence of BOD1L or RIF1.....	180
4.3:	Discussion.....	185
Chapter 5:	The impact of BOD1L on DSB repair	194
5.1:	Introduction	194
5.2:	BOD1L regulates DSB repair as well as resection	195
5.2.1:	Depletion of BOD1L has no impact on HR proficiency.....	196
5.2.2:	Chromatin recruitment of RAD51 increases upon BOD1L depletion in G1 cells	197
5.2.3:	BOD1L is required for NHEJ.....	203
5.2.4:	The impact of BOD1L on SSA, a non-canonical resection-dependent repair pathway	205
5.3:	Discussion.....	209
Chapter 6:	Role of BOD1L in repair of Camptothecin-induced double-strand breaks.....	215
6.1:	Introduction	215
6.2:	BOD1L is involved in the repair of CPT-induced DSBs	217
6.2.1:	BOD1L and RIF1 contribute to cell survival and genome stability after exposure to CPT	218
6.2.2:	Resolution of CPT-induced DSBs is problematic in the absence of BOD1L or RIF1	221
6.2.3:	Resection of CPT-induced DSBs is increased in the absence of BOD1L or RIF1	225
6.2.4:	BOD1L is required for the recruitment of RIF1 to CPT-induced DSBs but does not affect BRCA1 localisation	234

6.2.5: Repair of CPT-induced DSBs by HR is unaffected in the absence of BOD1L or RIF1	238
6.3: Discussion.....	240
Chapter 7: Discussion	247
7.1: Summary and Model	247
7.2: BOD1L and the 53BP1/RIF1-mediated DSB end protection pathway	249
7.2.1: The interaction between BOD1L and RIF1	249
7.2.2: Suppression of nucleolytic resection	252
7.3: SETD1A: A novel fork protection factor that interactions with BOD1L	254
7.3.1: Interplay between fork protection mechanisms.....	256
7.3.2: Replication fork protection and the acquisition of PARPi resistance.....	258
7.4: BOD1L and human disease.....	258
7.4.1: Cancer therapeutics.....	259
7.4.2: Likely phenotypes for individuals harbouring BOD1L mutations	260
7.5: Extending the current study.....	262
7.5.1: Further insights into the role of BOD1L in 53BP1-dependent end protection..	263
7.5.2: Impact of BOD1L depletion on DSB repair pathways.....	265
7.5.3: Crosstalk between BOD1L and pro-/anti-recombinogenic pathways	267
7.5.4: Potential interactions with RIF1- and CtIP-dependent fork protection pathways	269
7.5.5: BOD1L and the repair of CPT-induced DSBs	269
7.6: Concluding remarks.....	271

List of figures

Figure 1.1: Factors contributing to replication stress.	7
Figure 1.2: Repair of inter-strand crosslinks by the Fanconi Anaemia pathway.	16
Figure 1.3: Sources of DNA double-strand breaks.	24
Figure 1.4: Assembly of DNA-PK.	29
Figure 1.5: MRN performs a scaffolding role during DSB detection and signal initiation.	31
Figure 1.6: Activation of ATM and downstream signalling.....	33
Figure 1.7: Overview of DSB repair by homologous recombination (HR).	37
Figure 1.8: Sub-pathways of the synaptic phase of HR and resolution of crossovers.....	41
Figure 1.9: Overview of DSB repair by non-homologous end joining (NHEJ).....	44
Figure 1.10: Cell cycle checkpoints.	52
Figure 1.11: Structural details of BOD1L.	75
Figure 1.12: Model for BOD1L-mediated protection of stalled replication forks.....	78
Figure 3.1: Depletion of BOD1L induces hyper-sensitivity to ionising radiation.	113
Figure 3.2: Prevalence of IR-induced micronuclei is elevated in the absence of BOD1L.	115
Figure 3.3: BOD1L is required for the resolution of IR-induced DSBs.	118
Figure 3.4: BOD1L-deficient cells initiate an IR-induced DNA damage response, but the completion of repair is compromised.	120
Figure 3.5: Defective repair of IR-induced DSBs in the absence of BOD1L is specific to G2 cells.	122
Figure 3.6: The level of IR-induced phosphorylation of RPA2 is higher in the absence of BOD1L.	124
Figure 3.7: Depletion of BOD1L increases the prevalence of nuclear ssDNA following IR.	126

Figure 3.8: BOD1L depletion has no detectable impact on the extent of resection of individual IR-induced DSBs.	128
Figure 3.9: More IR-induced DSBs are subjected to nucleolytic resection in BOD1L-depleted cells than in control cells.	129
Figure 3.10: Depletion of a panel of key nucleases in HeLa cells.	132
Figure 3.11: Depletion of key DSBR-associated nucleases reduces IR-induced resection in HeLa cells.	133
Figure 3.12: Depletion of a panel of key nucleases in U-2-OS cells.	135
Figure 3.13: IR-induced resection in U-2-OS cells is reduced by depletion of key DSBR-associated nucleases.	136
Figure 3.14: Depletion of CtIP rescues defective resection of IR-induced DSBs in the absence of BOD1L.	138
Figure 3.15: Depletion of CtIP rescues defective resection of IR-induced DSBs in the absence of BOD1L.	141
Figure 3.16: Co-depletion of CtIP rescues increased RPA2 fluorescence intensity observed in BOD1L-deficient cells.	142
Figure 3.17: RPA-P (S4/S8) phosphorylation in BOD1L-deficient cells is reduced by co-depletion with CtIP.	143
Figure 4.1: Schematic representation of Bod1L-Flag-GFP construct.	157
Figure 4.2: Confirmation of interaction between BOD1L and RIF1.	161
Figure 4.3: The interaction between BOD1L and RIF1 is mediated by both the N- and C-terminal regions of BOD1L.	164

Figure 4.4: Depletion of BOD1L in HeLa cells has no impact on IR-dependent recruitment of factors that antagonise resection.	166
Figure 4.5: Depletion of BOD1L in U-2-OS cells has no impact on IR-dependent recruitment of key resection antagonists.	167
Figure 4.6: Depletion of BOD1L in HeLa has no detectable impact on recruitment of REV7..	169
Figure 4.7: G1 recruitment of RIF1 is reduced by depletion of BOD1L.	170
Figure 4.8: Class switch recombination is compromised in the absence of BOD1L.	173
Figure 4.9: Depletion of BOD1L and RIF1 leads to increased prevalence of BRCA1-positive G1 nuclei after exposure to IR.	176
Figure 4.10: Accumulation of RPA2 at IR-induced DSBs is elevated in the absence of BOD1L and RIF1.	179
Figure 4.11: Increased G1 resection in the absence of BOD1L is counteracted by the depletion of CtIP or MRE11.	182
Figure 4.12: Depletion of RIF1 or BOD1L have a comparable impact on genome instability.	184
Figure 5.1: BOD1L and RIF1 depletion has no detectable impact on HR proficiency in asynchronous cells.	198
Figure 5.2: BOD1L depletion has no detectable impact on IR-induced RAD51 foci formation in an asynchronous pool of cells.	201
Figure 5.3: G1 recruitment of RAD51 increases in the absence of BOD1L or RIF1.	202
Figure 5.4: Depletion of BOD1L does not increase RAD51 recruitment to IR-induced DSBs in G2 cells.	204
Figure 5.5: Non-homologous end joining of de-protected telomeres is suppressed by depletion of BOD1L or RIF1.	206

Figure 5.6: Single-strand annealing assay optimisation attempts.....	208
Figure 6.1: Depletion of BOD1L or RIF1 results in higher sensitivity to CPT.	220
Figure 6.2: Cells depleted of BOD1L or RIF1 show more CPT-induced micronucleation.	222
Figure 6.3: Resolution of CPT-induced DSBs is compromised in the absence of BOD1L or RIF1.	224
Figure 6.4: Recruitment of 53BP1 to sites of CPT-induced damage is unaffected in the absence of BOD1L or RIF1.....	226
Figure 6.5: BOD1L- and RIF1-depleted cells exhibit increased accumulation of RPA2 at CPT- induced DSBs.	228
Figure 6.6: Depletion of BOD1L or RIF1 results in greater RPA32 phosphorylation in cells exposed to CPT.	231
Figure 6.7: RIF1 depletion, but not BOD1L depletion, has a mild impact on the extent of resection of individual CPT-induced DSBs.....	232
Figure 6.8: Depletion of BOD1L or RIF1 has no detectable impact on the number of CPT-induced DSBs resected.	233
Figure 6.9: Recruitment of RIF1 to CPT-induced DSBs is impaired in the absence of BOD1L.	236
Figure 6.10: Recruitment of BRCA1 to CPT-induced DSBs is unaffected by depletion of BOD1L or RIF1.....	237
Figure 6.11: HR-mediated repair of CPT-induced DSBs is unaffected in the absence of BOD1L or RIF1.	239
Figure 7.1: BOD1L-mediated regulation of DSB repair.	248
Figure 7.2: The interaction between BOD1L and RIF1.	250

List of tables

Table 2.1: Details of siRNA	86
Table 2.2: Antibody information and dilutions for immunoblotting	91
Table 2.3: Antibody information and dilutions for immunofluorescence	95
Table 2.4: Primer sequences for generation of GST-tagged BOD1L fragments.	100
Table 2.5: Details of plasmids.	107
Table 4.1: Proteins identified by mass spectrometry screen as being highly enriched in complexes containing mBod1L.	159

List of abbreviations

Alt-NHEJ	Alternative non-homologous end joining
Alt-EJ	As for Alt-NHEJ
APC/C	Anaphase-promoting complex/cyclosome
APLF	Aprataxin-PNK-like factor
AP-MS	Affinity purification mass spectrometry
ASH2L	Ash2-like histone methyltransferase complex subunit
Asp	Asparagine
A-T	Ataxia Telangiectasia
ATLD	AT-like disorder
ATM	Ataxia Telangiectasia mutated
ATR	Ataxia Telangiectasia mutated- and Rad3-related
ATRIP	ATR-interacting protein
AT-rich	Adenine/Thymine-rich DNA
BAC	Bacterial artificial chromosome
BARD1	BRCA1-associated ring domain protein 1
BIR	Break-induced replication
BLM	Bloom helicase
BOD1	Biorientation defect 1
BOD1L	Biorientation defect 1-Like
bp	Base pairs
BRCA1	Breast cancer susceptibility protein 1
BRCA2	Breast cancer susceptibility protein 2
BRCT	BRCA1 C-terminal domain
BrdU	Bromodeoxyuridine
BSA	Bovine serum albumin
cDNA	Complementary DNA
C-NHEJ	Canonical non-homologous end joining
C-terminus	Carboxyl terminus

CBX4	Chromobox 4
CCAR2	Cell cycle and apoptosis regulator 2
Cd19	B-lymphocyte surface antigen Cd19
Cdc45	Cell division cycle 45
Cdh1	Cadherin 1
CDT1	Chromatin licensing and DNA replication factor 1
CDT6	Chromatin licensing and DNA replication factor 6
CDK	Cyclin-dependent kinase
CENPF	Centromere protein F
CEP152	Centrosomal protein 152
CFS	Common fragile sites
CHD4	Chromodomain helicase DNA-binding protein 4
Chk1	Checkpoint protein 1
CldU	Chlorodeoxyuridine
CLL	Chronic lymphocytic leukaemia
CMG	Cdc45/MCM/GINS replicative helicase
CPT	Camptothecin
Cre	Cre recombinase
CRISPR	Clustered, regularly interspaced, short palindromic repeats
CSR	Class-switch recombination
CTCF	CCCTC-binding factor
CtIP	CtBP-interacting protein
CXXC1	CXXC-type zinc finger protein 1 (CpG-binding protein 1)
CYREN	Cell cycle regulator of NHEJ
DAPI	4',6-diamidino-2-phenylindole
dCTP	Deoxycytidine triphosphate
DDK	Dcf-dependent kinase
DDR	DNA damage response
DEB	Diepoxybutane
dHJ	Double Holliday junction

DNA	Deoxyribonucleic acid
DNA-PK	DNA-dependent protein kinase
DNA-PKcs	DNA-dependent protein kinase (catalytic sub-unit)
DNA2	DNA replication helicase/nuclease 2
dNTP	Deoxyribonucleotide triphosphate
DSB	Double-strand break
dsDNA	Double-stranded DNA
ECL	Enhanced chemiluminescence
EDTA	Ethylene-diamine-tetra-acetic acid
EdU	Ethynyldeoxyuridine
ERCC1	ERCC excision repair protein 1, endonuclease non-catalytic subunit
ERCC4	ERCC excision repair protein 4, endonuclease catalytic subunit (refer also to XPF)
ETAA1	Ewing's tumour associated antigen 1
EXO1	Exonuclease 1
EXD2	Exonuclease 3'-5' domain containing protein 2
FA	Fanconi anaemia
FAAP24	Fanconi anaemia-associated protein 24kDa
FANC[...]	Fanconi anaemia complementation group [...]
FISH	Fluorescence <i>in-situ</i> hybridisation
Fwd	Forward
G1	Cell cycle growth phase 1
G2	Cell cycle growth phase 2
GFP	Green fluorescent protein
GCR	Gross chromosomal rearrangement
GINS	<i>Go-Ichi-Ni-San</i> replication complex
Glu	Glutamic acid
GST	Glutathione S-transferase
Gy	Gray (ionising radiation unit)
H2A	Histone H2A

H2AK15	Histone H2A, lysine 15
γ H2AX	Phosphorylated (gamma)-histone H2AX
H ₂ O ₂	Hydrogen peroxide
H3K4	Histone H3 Lysine 4
H4K20 ^{Me2}	Histone H4 Lysine 20 di-methylation
HCl	Hydrochloric acid
HEAT	Huntingtin, elongation factor 3, protein phosphatase 2A, TOR1 domain
HELB	DNA helicase B
HERC2	HECT and RLD domain-containing E3 ubiquitin ligase 2
HR	Homologous recombination
HRP	Horseradish peroxidase
HU	Hydroxyurea
iBAQ	Intensity-based absolute quantification
ICL	Inter-strand crosslink
IdU	Iododeoxyuridine
IgA	Immunoglobulin A
IgG	Immunoglobulin G
IgM	Immunoglobulin M
IL-4	Interleukin 4
iPOND	Isolation of proteins on nascent DNA
IR	Ionising radiation
KCl	Potassium chloride
KMT	Lysine (K) methyltransferase
Ku70	ATP-dependent DNA helicase II, 70 kDa sub-unit
Ku80	ATP-dependent DNA helicase II, 80 kDa sub-unit
LIG3	DNA ligase 3
LIG4	DNA ligase 4
LPS	Lipopolysaccharide
Lys	Lysine
M	Mole (unit of concentration)

M (phase)	Cell cycle mitotic phase
MAD2L2	Mitotic arrest deficient 2-like 2
MCM	Minichromosome maintenance helicase
MDC1	Mediator of DNA damage checkpoint protein 1
MMC	Mitomycin C
MRE11	Meiotic recombination 11 homologue
MRI	Modulator of retroviral infection
MRN	MRE11-Rad50-Nbs1
MSH2	MutS homologue 2
N-terminus	Amino (NH ₂) terminus
NBS	Nijmegen breakage syndrome
NBS1	Nijmegen breakage syndrome protein 1
NEDD8	NEDD8 ubiquitin-like modifier (Neddylin)
NER	Nucleotide excision repair
NHEJ	Non-homologous end joining
nt	Nucleotide
OH·	Hydroxyl free radical
ORC	Origin recognition complex
PAXX	Paralogue of XRCC4 and XLF non-homologous end-joining factor
p53	Tumour protein 53
PAR	Poly(ADP-ribose)
PARP	Poly-(ADP-ribose) polymerase
PARPi	Poly-(ADP-ribose) polymerase inhibitor
PAXX	Paralogue of XCCR4 and XLF
PBZ	Poly(ADP-ribose)-binding zinc finger
PCNA	Proliferating cell nuclear antigen
PCR	Polymerase chain reaction
PFA	Paraformaldehyde
PIKK	PI-3 kinase-related kinase
PIPES	Piperazinediethanesulfonic acid

PLA	Proximity ligation assay
Plk3	Polo-like kinase 3
PP1	Protein phosphatase 1
Pre-RC	Pre-replicative complex
PTIP	Pax transactivation domain interacting protein
PTM	Post-translational modification
R-loop	RNA-DNA hybrid
RAD50	DNA repair protein RAD50
RAD51	DNA repair protein RAD51
RAD52	DNA repair protein RAD52
RBBP5	Retinoblastoma-binding protein 5
RECQL4	RecQ-like helicase 4
Rev	Reverse
REV7	Rev7 homologue
RFP	Red fluorescent protein
RFWD3	Ring finger and WD repeat domain 3
RIF1	Rap1-interacting factor 1
RNA	Ribonucleic acid
RNF8	Ring finger protein 8
RNF186	Ring finger protein 168
RNR	Ribonucleotide reductase
RPA	Replication protein A
RPA-P (S4/S8)	Phosphorylated replication protein A (Serines 4 and 8)
rpm	Revolutions per minute
S (phase)	Cell cycle synthesis phase
SAPK	Stress-activated protein kinase
SETD1A	SET domain-containing protein 1A
SET8	SET domain-containing protein 8
Ser	Serine
Shg1H	Shg1 homology domain

SHLD1	Shieldin sub-unit 1 (C20orf196)
SHLD2	Shieldin sub-unit 2 (FAM35A)
SHLD3	Shieldin sub-unit 3 (CTC-534A2.2)
siRNA	Small interfering RNA
SLX4	Structure-specific endonuclease sub-unit SLX4
SMARCAD1	SWI/SNF-related matrix-associated actin-dependent regulator of chromatin (sub-family A) containing DEAD/H box 1
SMARCAL1	SWI/SNF-related matrix-associated actin-dependent regulator of chromatin (sub-family A)-like 1
SDSA	Synthesis-dependent strand annealing
SS	Seckel syndrome
SSA	Single-strand annealing
SSB	Single-strand break
ssDNA	Single-stranded DNA
SUMO	Small ubiquitin-like modifier
TBS-T	Tris-buffered saline with Tween 20
TDP1	Tyrosyl-DNA phosphodiesterase 1
TIPIN	TIMELESS-interacting protein
TLS	Trans-lesion synthesis
TOPBP1	DNA topoisomerase-II binding protein 1
TopoI	Topoisomerase-I
TopoII	Topoisomerase-II
Thr	Threonine
TRESLIN	TOPBP1 interacting checkpoint and replication regulator
TRF2 ^{ΔBΔM}	Telomere repeat binding factor 2 (B- and M-domain-deficient mutant)
UAF1	USP1-associated factor 1
UBA1	Ubiquitin-like modifier activating enzyme 1
UBC13	Ubiquitin-conjugating enzyme 13
UBD	Ubiquitin-binding domain
UBE2T	Ubiquitin conjugating enzyme E2 T

UFB	Ultra-fine bridge
UHRF1	Ubiquitin-like with PHD and RING finger domains 1
USP1	Ubiquitin-specific peptidase 1
UV	Ultraviolet
v/v	Volume per volume (concentration)
V[D]J	Variable (Diversity) and Joining
w/v	Weight per volume (concentration)
WRN	Werner syndrome RecQ-like helicase
XLF	XRCC4-like factor
XPF	Xeroderma pigmentosum factor (refer also to ERCC4)
XRCC1	X-ray repair cross-complementing 1
XRCC2	X-ray repair cross-complementing 2
XRCC4	X-ray repair cross-complementing 4
XRCC5	X-ray repair cross-complementing 5
ZRANB3	Zinc finger Ran-binding domain-containing protein 3
$^1\text{O}_2$	Singlet oxygen molecule
53BP1	Tumour protein 53-binding protein 1

Chapter 1: Introduction

The objective of my doctoral studies will be to extend the characterisation of BOD1L (Biorientation Defect 1-Like), a recently-identified member of the DNA damage response (DDR); I will describe its published role in cells exposed to replication stress inducers in more detail in later sections (section 1.9). However, the potential role of BOD1L in the cellular response to other genotoxins is hitherto unexplored; this forms the basis of my studies. Therefore, I will begin by outlining the fundamental principles and exponents of the mammalian DNA damage response, with a particular focus on two types of DNA damage: replication stress and DNA double strand breaks.

1.1: DNA damage

DNA damage is defined as any deleterious modification of the DNA structure; this may constitute the disruption of a base, chemical alterations, or breakage of one or both phosphate backbones. Such damage can arise from a spectrum of endogenous and environmental sources, posing a considerable threat to the integrity of the genome. This has led to the evolution of a complex array of proteins and pathways, collectively termed the DNA damage response (DDR), which enables the cell to deal efficiently and appropriately with genetic damage in all its manifestations.

1.2: DNA replication and replication stress

The efficient and accurate replication of the genome and transfer of the genetic information to daughter cells is critical for survival. However, the integrity of this process is frequently challenged by insults from extra-cellular agents as well as endogenous sources. These insults may include physical obstacles to the unwinding of the DNA and progression of the replication fork, or inhibition of key enzymes associated with DNA synthesis. When replication is impaired, cells are said to be in a state of replication stress. To combat this potentially deleterious state, cells have evolved a suite of factors and pathways which respond to replication stress by pausing DNA replication until any obstacles have been removed. In the following sections, I will provide a brief overview of DNA replication, and will then describe replication stress in detail.

1.2.1: An overview of mammalian DNA replication

The process of faithfully replicating the genetic material in preparation for cell division is fundamental to all organisms. This process has been investigated and reviewed comprehensively elsewhere (for examples refer to Bleichert et al. (2017), Fragkos et al., 2015, Jain et al., 2018, Singh and Wu, 2019, Gambus, 2017), but will be summarised below for the purpose of context.

DNA replication is initiated at thousands of specific positions along the chromosomes – termed replication origins. The first step of initiation is the formation of the pre-replicative complex (pre-RC), which comprises the helicases MCM2-MCM7 and the origin recognition complex proteins ORC1-6, along with CDT1 and CDC6. Assembly of this complex occurs at all replication origins and can commence from late M phase. The preparation of replication origins in this

manner is termed 'licensing'. Origin firing, the second initiation step, occurs solely during S phase. Origins are fired in a controlled manner to balance replication accuracy and speed with the need to allocate resources appropriately. Early origins are fired first, with late origins following. Furthermore, a subset of origins is reserved to fire in case of any perturbation of replication; these origins may not be required if replication proceeds without obstacles (Zeman and Cimprich, 2014, Mazouzi et al., 2014).

During origin firing, a pair of bi-directional replication forks forms, each with an activated MCM2-7 helicase complex at its apex. The activities of cyclin-dependent kinases (CDKs) and Dbp-dependent kinases (DDKs) become critical at this point: firstly, to convert the pre-RC into a pre-initiation complex, and secondly, to incorporate Cdc45 and GINS into the MCM2-7 helicase to form a CMG complex at each fork. This latter conversion occurs at the transition from G1 to S phase and involves a number of other factors, including RECQL4, TRESLIN and TOPBP1 (DNA Topoisomerase-II binding protein 1). Collectively, the pre-RC and CMG complexes unwind the DNA at each origin and allow DNA synthesis to proceed in opposite directions. This process requires DNA helicases to unwind the DNA double helix, DNA polymerase enzymes α , δ and ϵ , tethering factors to join the helicase and polymerase enzymes, a polymerase co-factor known as proliferating cell nuclear antigen (PCNA), and replication protein A (RPA) to stabilise the single-stranded DNA. The replication machinery is collectively known as the replisome (Munoz and Mendez, 2017, Mazouzi et al., 2014, Zeman and Cimprich, 2014). At the point where two opposing replication forks meet, the replisome dissociates from the DNA in a process known as

termination. This disassembly is reliant on specific polyubiquitination of MCM7 by the Cul2^{LRR1} and TRAIIP ubiquitin ligases (Moreno and Gambus, 2015, Priego Moreno et al., 2019).

1.2.2: Replication stress

Replication stress is not a specific form of DNA damage, but a complex cellular state. In fact, there are currently no definitive markers or characteristics to identify it. Whilst it is acknowledged that replication stress can pose major problems for genomic integrity, a number of features that result from replication stress – and which can therefore serve as indicators of the state – may also contribute to its exacerbation. For example, chromosomal nicks and gaps result from unresolved replication stress, but also lead to its amplification. In view of this ambiguity, a combination of approaches represents the most robust strategy for the examination of replication stress, including single-molecule analysis of fork progression through DNA fibre assays, genome stability assays and quantification of 53BP1 bodies (Zeman and Cimprich, 2014).

Replication stress frequently gives rise to tracts of single-stranded DNA (ssDNA) due to continued activity of the replicative helicase after the stalling of the DNA polymerase. RPA, a heterotrimeric complex with a high affinity for ssDNA due to its multiple oligonucleotide/oligosaccharide-binding folds (Marechal and Zou, 2015) rapidly coats this ssDNA and acts as a signal to recruit the ATR (Ataxia-Telangiectasia Mutated- and Rad3-Related) kinase. Accordingly, the presence of ssDNA and increased phosphorylation of ATR substrates, such as RPA (Ser 33) or CHK1 (Ser 345) can be used as indicators of replication stress. Whilst

phosphorylation of H2AX, a histone variant, may also increase during replication stress, this modification is associated with multiple kinases and various manifestations of DNA damage, and is therefore not a specific indicator (Zeman and Cimprich, 2014).

1.2.3: Factors contributing to replication stress

A multitude of factors, both endogenous and extra-cellular, can pose a threat to DNA replication, and ultimately to viability at the cellular and whole organism level.

It is now known that endogenous sources play a substantial role in inducing replication stress. Research into the properties of common fragile sites (CFS), which are liable to break upon exposure to chemical inhibitors of replication, has given key insights into DNA structural features that are likely to be problematic for the replisome (Munoz and Medez, 2017). For instance, secondary structures arising at repetitive DNA sequences (Mazouzi et al., 2014) and AT-rich regions can act as barriers to fork progression. Short tandem repeats, known as microsatellites, do not impede replication but reduce the fidelity of the process due to the increased risk of polymerase slippage in such regions (Munoz and Mendez, 2017). Physiological processes, or mistakes in these processes, may also render the DNA template unrecognisable to the replication machinery; examples include erroneous ribonucleotide incorporation and base damage or inter-strand crosslinks (ICLs) arising from endogenous sources. Furthermore, collisions between replication and transcription machinery may also be a source of replication stress (Helmrich et al., 2013). Such collisions are more likely in larger genes. There is some speculation that cells may have evolved strategies to reduce the frequency of these events

(such as origin depletion in highly-transcribed regions and the temporal separation of transcription and replication) (Bermejo et al., 2012), but this remains a point of contention. Collisions can nonetheless be problematic when they do occur, resulting in topological stress and the formation of DNA-RNA hybrids known as R-loops. There is a further risk that R-loops may collide with the replication or transcription machinery (Zeman and Cimprich, 2014, Munoz and Mendez, 2017). Sources of replication stress are summarised in figure 1.1.

The capacity of chemical agents to induce replication stress is the subject of ongoing investigation. Such agents are frequently employed in research settings as well as therapeutic contexts (refer to section 1.8). Replication stress may be induced by chemicals such as hydroxyurea (HU), which depletes the pool of dNTPs available for incorporation into nascent DNA through inhibition of ribonucleotide reductase (RNR) (Munoz and Mendez, 2017, Mehta and Haber, 2014, Timson, 1975). There can be considerable deleterious consequences of chronic, unresolved replication stress arising from HU exposure, such as the collapse of stalled forks into DSBs (Petermann et al., 2010). Chemical treatments such as Cisplatin prevent DNA unwinding and replication forks progression by the induction of DNA crosslinks (which are predominantly intra-strand). Other agents interfere with the activities of fundamental replication-associated enzymes. These compounds selectively target cells in which active DNA replication is taking place; as such, they are effective specifically in S phase, during which DNA is most vulnerable to damage (Vesela et al., 2017). Aphidicolin, for example, triggers a conformational change in DNA polymerase α , thereby specifically inhibiting the incorporation

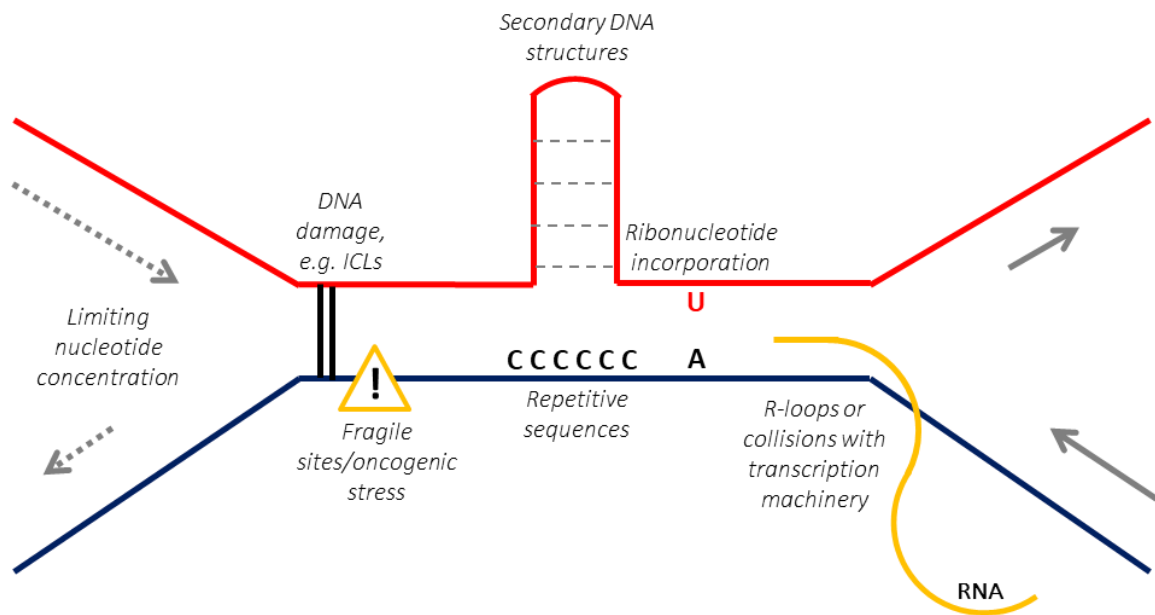


Figure 1.1: Factors contributing to replication stress.

The progression of DNA replication may be impaired by multiple factors, such as a limiting nucleotide concentration, damaged DNA, fragile sites and oncogenic stress, repetitive DNA sequences, secondary DNA structures, erroneous incorporation of ribonucleotides, RNA-DNA hybrids and collisions with the transcription machinery. Adapted from Zeman & Cimprich, 2014.

of dCTP into nascent DNA. Due to the uncoupling of helicase and polymerase activities, cells are unable to progress through S phase. Camptothecin inhibits Topoisomerase I, part of the enzyme family which is essential for the control of supercoiling during DNA replication. TopoI fulfils its function through generation of a TopoI-DNA cleavage complex. This is normally a transient interaction. CPT prevents the dissociation of this complex, depleting the pool of TopoI and leading to chronic torsional stress. Single-ended DSBs can also arise when the trapped cleavage complex encounters a replication fork (Hsiang et al., 1989). Etoposide acts via a corresponding mechanism but targets TopoII (Vesela et al., 2017). Finally, ionising radiation (IR) and ultraviolet radiation (UV) are well-established sources of DNA double-strand breaks (DSBs) and DNA adducts, respectively; if unresolved, this damage may also halt the progression of the replisome (Munoz and Mendez, 2017).

As mentioned above, ICLs are a potent source of replication stress, as these structures act as a physical block to DNA replication or transcription due to the impairment of strand separation. ICLs are generated through the covalent linkage of pairs of base or phosphate backbone modifications that have occurred on complementary strands of DNA. This form of DNA damage is therefore potentially lethal; it has been suggested that a cell can sustain fewer than 20 unrepaired ICLs (Noll et al., 2006). Since BOD1L plays a crucial role in combating replication stress and has also been shown to associate with the Fanconi Anaemia (FA) pathway (section 1.9) – which is fundamental to the resolution of these lesions – an understanding of ICL formation and repair provides valuable context for my studies.

The mechanism of ICL formation has been extensively studied since the seminal work of Louis Goodman and colleagues that paved the way for the introduction of ICL-inducing agents as a leukaemia treatment after the Second World War (Goodman et al., 1946). Rapid, uncontrolled cycling and proliferation are hallmarks of cancerous cells. These agents are therefore eminently suited to the treatment of neoplastic tissues due to the impact of ICLs on DNA replication (Rycenga and Long, 2018).

Over 70 years after their introduction, ICL-inducing drugs remain a mainstay for the chemotherapeutic treatment of cancer. It is now understood that the four classes of these drugs in routine use (nitrogen mustards and other alkylating agents, Mitomycins, psoralens and platinum compounds such as Cisplatin) have relatively similar mechanisms of action. The formation of a crosslink is dependent on the drug's two chemically active groups, each of which can react with bases on complementary DNA strands (Eastman, 1983).

In the case of platinum compounds or alkylating drugs, side chains are activated within the cell by the displacement of chloride ions by water molecules, thus facilitating their reactivity with DNA bases – typically guanosine or adenosine. Around 90% of the resultant lesions are intra-strand crosslinks, with 1-2% being ICLs (Eastman, 1983, Rycenga and Long, 2018). The planar rings found in Mitomycins and psoralens become able to interact with bases on opposite strands of DNA following photon-dependent activation. Approximately 15% of Mitomycin-induced DNA lesions are ICLs, and over 50% involve DNA adducts (Rycenga and Long, 2018). In psoralen-based chemotherapy, this photon dependence has been harnessed to facilitate

targeted treatments by using UVA irradiation to activate the drug in a directed manner. Activated psoralens are efficient ICL inducers; up to 90% of total lesions are ICLs (Rycenga and Long, 2018, Deans and West, 2011).

The detection and resolution of ICLs is primarily mediated through ATR/FA pathway (discussed in detail in section 1.3).

1.3: The cellular response to replication stress

A robust response to replication stress is a fundamental pre-requisite to the preservation of genome integrity. This response, which is centrally regulated by the ATR kinase, involves the recruitment of a specialised network of proteins to maintain the stability of stalled replication forks; alongside this, progression through the cell cycle is paused. Collectively, these steps prevent the replication of damaged DNA and conserve resources to ensure that DNA replication can be completed after the resolution of damage (Zeman and Cimprich, 2014). The key components of the replication stress response, and the consequences of an impaired response, are detailed below.

1.3.1: Functions of ATR/CHK1 pathway in resolving replication stress

During replication stress, ATR and its functional partner ATRIP (ATR-interacting protein) are recruited to stalled replication forks. This recruitment is driven by the detection of tracts of RPA-associated ssDNA, which arise following the dissociation of the replication machinery from

the fork (Byun et al., 2005). The separation of the replisome components from one another is prevented by TIMELESS in association with TIPIN (TIMELESS-interacting protein); furthermore, this heterodimer also functions to stabilise the replication fork (Leman and Noguchi, 2012, Her et al., 2018).

ATR is activated upon interaction with ETAA1 (Ewing's tumour-associated antigen 1) or TOPBP1. This activation has multiple downstream consequences: the suppression of new origin firing, the activation of the S-phase DNA damage checkpoint, the recruitment of additional replication stress response factors, the regression of stalled forks and the loading of RAD51 to prevent nucleolytic degradation of these structures (refer to section 1.3.5). In addition, ATR phosphorylates a number of substrates that help to maintain the fidelity of DNA replication under replication stress. These substrates include constituents of the replisome, the key checkpoint protein CHK1 (Buisson et al., 2015, Zeman and Cimprich, 2014) and the histone variant H2AX (termed γ H2AX following phosphorylation at Ser139) (Chanoux et al., 2009, Her et al., 2018). CHK1 functions as a key mediator of ATR-dependent activities during replication stress (Buisson et al., 2015). Activated CHK1 (phosphorylated at Ser317 and Ser345) triggers cell cycle arrest at the G2/M checkpoint, inhibits spurious origin firing and allows stalled replication forks to be repaired (Zuazua-Villar et al., 2015).

1.3.2: ATR-Seckel syndrome

Seckel syndrome (SS) is an autosomal recessive form of microcephalic primordial dwarfism, primarily attributable to mutations in *ATR*. It is clinically heterogeneous, but typical features

include intra- and extra-uterine growth delay, malformation of the digits, characteristic “bird-like” facial features and cellular hypersensitivity to agents that induce replication stress (Seckel, 1960). In contrast to a multitude of syndromes associated with defects in the DDR (refer to section 1.7 for further examples), predisposition to cancer is not a typical feature of Seckel syndrome, with malignancies reported in only a small number of affected individuals (Qvist et al., 2011).

Another unique feature of SS is its genetic heterogeneity. Causal mutations in a number of genes have been identified. Several studies have highlighted compound heterozygous and splice site mutations in *ATR* which dramatically reduce the protein expression of this fundamental kinase ((O'Driscoll et al., 2003, Mokrani-Benhelli et al., 2012); accordingly, in several patients, the disease was mapped to chromosome 3q22.1-q22.4 – a region that includes *ATR* (Goodship et al., 2000). Some years later, mutations in its binding partner ATRIP were also implicated in SS (Ogi et al., 2012). This latter observation illustrated the importance of the ATR-ATRIP interaction in maintaining a robust response to DNA damage to ensure timely and faithful DNA replication and genome stability ((Khetarpal et al., 2016). In addition, other cases have been attributed to mutations in *CENPJ* (Centromere protein J) (Khetarpal et al., 2016, Al-Dosari et al., 2010), *CEP152* (Centrosomal protein 152) (Kalay et al., 2011) and *CTIP* (Qvist et al., 2011).

1.3.3: The FA pathway and its function in ICL repair and resolving replication stress

The Fanconi Anaemia (FA) pathway – so-named for the syndrome that arises when it is defective – plays a critical regulatory role in alleviating replication stress through the resolution

of DNA inter-strand crosslinks (ICLs). Over 20 years of research has revealed a specialised network of 22 proteins responsible for the resolution of ICL-related replication stress. These proteins have been designated FANCA to FANCW (Nepal et al., 2017). As will be discussed further in section 1.9.3, BOD1L has been classified as a FA-like protein; it stabilises RAD51 (another FA-like protein, termed FANCR) at stalled forks to promote HR-mediated repair and prevent deleterious over-resection (Higgs et al., 2015). As such, this pathway is of particular relevance to my thesis.

Opposing replication forks may converge at either side of an inter-strand crosslink (ICL); this is detected by the FANCM sub-unit in complex with FAAP24 (Fanconi anaemia-associated protein, 24 kDa). This heterodimer, which is reminiscent of a structure-specific nuclease pair, binds to the lesion and recruits the core FA complex, an octomeric complex comprising the FANCA sub-units A, B, C, E, F, G and L as well as FAAP100. This core complex functions as an E3 ubiquitin ligase and is the key effector of the FA pathway (Kim and D'Andrea, 2012). Recent cryo-EM and mass spectrometry studies shed light on the assembly of the complex and its functionality. The centre of the core complex contains a FANCB-FAAP100 heterodimer. FANCL, located in the base of the complex, associates with the central heterodimer via interactions with its coiled-coil domains. The base of the complex also contains the substrate recognition module, which comprises FANCC, FANCE and FANCF. FANCB-FAAP100 also forms crosslinks with FANCG, which is thought to be required for the interaction of FANCA with the core complex (Shakeel et al., 2019).

The recruitment of the FA core complex is dependent upon the presence of UHRF1 (ubiquitin-like with PHD and RING finger domains 1) (Liang et al., 2015) as well as phosphorylation of FANCM by ATR: a key effector of the response to replication stress (Ceccaldi et al., 2016b). The mono-ubiquitination of FANCD2 (Lys 561) and FANCI (Lys 523) by the E2 ubiquitin ligase UBE2T (FANCT) in co-operation with the FANCL component of the core complex also represents a major regulatory event (Kim and D'Andrea, 2012, Michl et al., 2016). There is incomplete understanding of the specific dynamics of FANCD2/I ubiquitination and de-ubiquitination, but both processes are essential for FA pathway function (Ceccaldi et al., 2016b).

Following its activation, FANCD2/I is then recruited to converged replication forks (Kottemann and Smogorzewska, 2013). FANCD2/I acts as a co-ordinating platform for the incoming nucleases ERCC4, MUS81 and SLX1 (guided by a Ubiquitin Binding Domain, UBD). Where replication stress has been triggered by the presence of an ICL, these nucleases create incisions at each side of the crosslink, facilitating its detachment from one parental DNA strand; this process is termed 'unhooking'. The ERCC4-ERCC1 complex has been shown to play a key role at this stage (Kottemann and Smogorzewska, 2013, Ceccaldi et al., 2016b).

This nucleolytic processing effectively converts the converged forks into a DSB-like structure (Kottemann and Smogorzewska, 2013). Finally, the DNA break is repaired by homologous recombination (Ceccaldi et al., 2016b), which will be covered in depth in section 1.5.2. The extensively-studied cancer predisposition proteins, BRCA1 (FANCD1) and BRCA2 (FANCS), are crucial for HR-mediated repair of these structures; this is a key example of the complex

interplay between the FA pathway and a multitude of other DDR-associated factors and processes (Michl et al., 2016, Kim & D'Andrea, 2012). Upon completion of the repair, FANCD2/I is de-ubiquitinated by USP1 in complex with UAF1 (Kim and D'Andrea, 2012). Nucleotide excision repair (NER) facilitates removal of any remaining adducts (Rycenga and Long, 2018).

Certain classes of DNA crosslinks, such as those induced by psoralens, do not present significant obstacles to the progress of DNA replication. Such ICLs may be bypassed or 'traversed' via the DNA translocase activity of FANCM, allowing repair of the ICL to be delayed. Alternatively, NER-associated DNA glycosylase enzymes may directly cleave the crosslink without the need to dismantle the replisome (Rycenga & Long, 2018).

1.3.4: Fanconi Anaemia

Affecting 1 to 5 individuals per 1,000,000 births (Kim and D'Andrea, 2012), Fanconi Anaemia (FA) arises due to a defective cellular response to ICLs and associated replication stress. The proteins of the FA pathway, along with a spectrum of known interactors, are critical for this response. Bi-allelic germline mutations in any one of the 22 identified FA genes result in a syndrome characterised by progressive failure of the bone marrow leading to pancytopenia (a deficiency in blood cells of all lineages), a cellular sensitivity to ICL-inducing agents, constitutive genome instability and a predisposition to haematological cancers (Heyer et al., 2010, Kim and D'Andrea, 2012). It is thought that the bone marrow failure observed in affected individuals can be explained by the over-expression of p53 – one of the key safeguards of

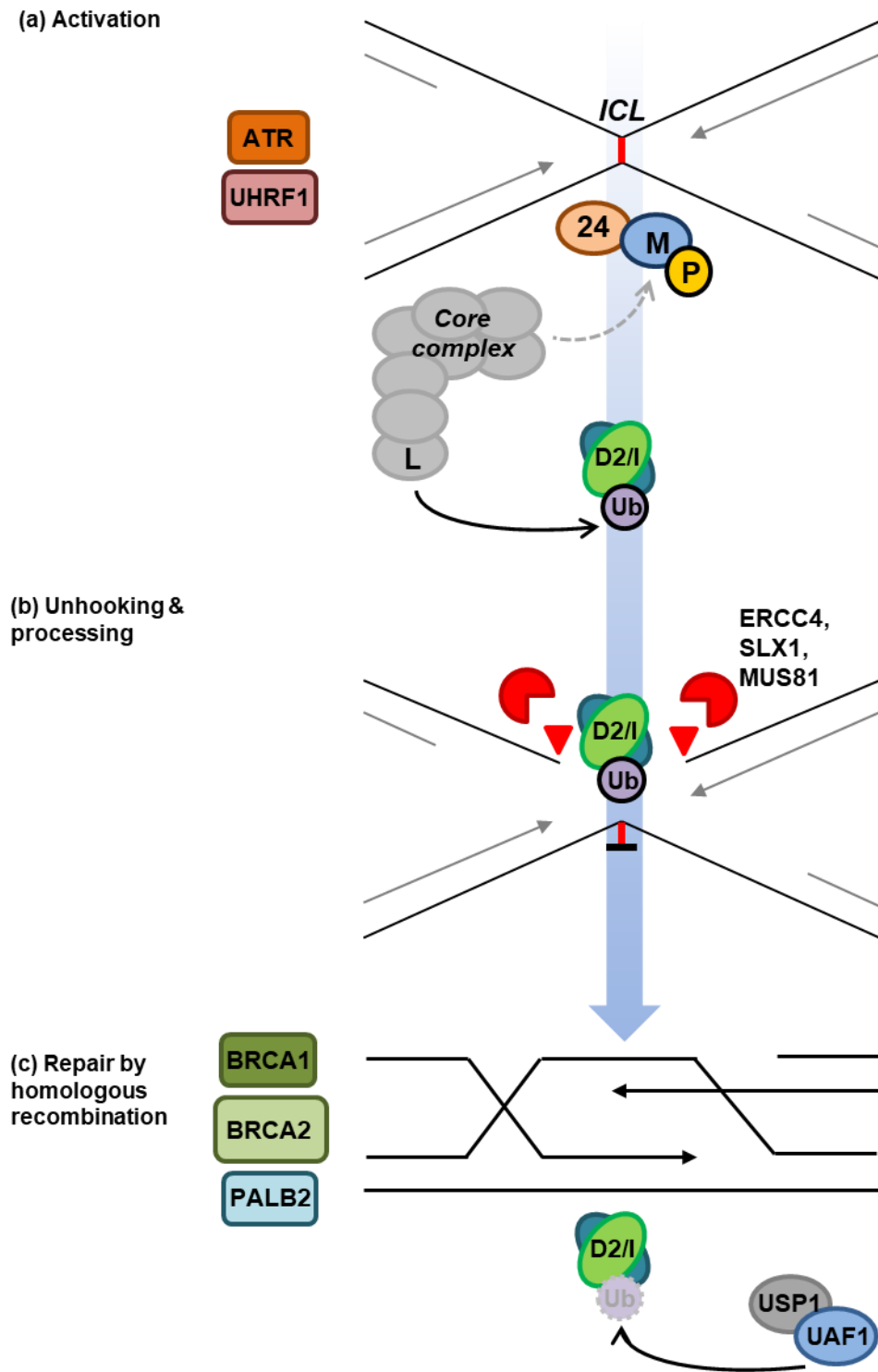


Figure 1.2: Repair of inter-strand crosslinks by the Fanconi Anaemia pathway.

(a) During activation of the FA pathway, the convergence of opposing replication forks either side of an ICL is detected by FANCM-FAAP24. The core complex is then recruited. UHRF1 and ATR-mediated phosphorylation of FANCM are required at this stage. The FANCL sub-unit mono-ubiquitinates FANCD2/I. (b) This mono-ubiquitinated heterodimer functions as a platform to recruit nucleases, including ERCC4, SLX1 and MUS81; nucleolytic processing detaches the crosslink (unhooking). (c) The resultant DSB-like structure is repaired by homologous recombination. Once repair is completed, FANCD2/I is deubiquitinated by USP1 and UAF1.

Adapted from Kotteman & Smogorzewska, 2013.

genomic integrity – in the haematopoietic stem cells of developing fetuses with FA; additionally, the bone marrow of FA patients is under-proliferative from birth (Kottemann and Smogorzewska, 2013, Ceccaldi et al., 2016b). Affected individuals may also exhibit other congenital features such as thumb abnormalities or café-au-lait spots (Shimamura & Alter, 2010).

In recent years, it has been suggested that the associated genes may be classified as ‘*bona fide* FA’ or ‘FA-like’ genes (Ceccaldi et al., 2016b). *Bona fide* FA gene mutations are associated with the most typical FA patient phenotypes. On the other hand, mutations in FA-like genes may give rise to atypical FA clinical presentations, potentially lacking features usually associated with the disease; alternatively, the classification of these genes as part of the FA network may be based solely on an individual patient. For example, the 8 members of the FA core complex are considered *bona fide* FA proteins, as is the prominent homologous recombination (HR)-associated factor, breast cancer susceptibility protein 2 (BRCA2, also designated as FANCS), which stabilises stalled replication forks in preparation for repair by HR (Ceccaldi *et al.*, 2016).

The recent elucidation of the FA core complex structure provides insights into the severity of the FA phenotype associated with mutations in *FANCL* or *FANCB*. The encoded sub-units fulfil key structural and catalytic functions within the FA core complex, and mutations in these sub-units are thought to disrupt the entire complex, abrogating any ubiquitin ligase activity. Conversely, the complex can sustain alterations in its peripheral components and maintain residual catalytic activity (Shakeel *et al.*, 2019).

Multiple novel FA genes have been identified and characterised in recent years. For example, REV7, which plays a fundamental role in the regulation of DNA repair pathway choice (refer to section 1.6.3) and DNA repair by trans-lesion synthesis (TLS), was shown to be a *bona fide* FA protein and designated FANCV. Bluteau and colleagues identified a patient who displayed a range of typical FA features but lacked mutations in any known FA pathway genes. Whole-exome sequencing revealed a homozygous mutation in REV7, c.354T>A; furthermore, the authors demonstrated that the bone marrow failure in this patient could be attributed to a deficiency in REV7-mediated DNA damage repair (Bluteau et al., 2016). Furthermore, bi-allelic mutations in *RFWD3* (Ring finger and WD repeat domain 3), which encodes an E3 ubiquitin ligase, were recently found to be responsible for a classical case of FA. Whole-exome sequencing revealed a 2-bp insertion which led to the generation of a premature stop codon as well as a missense mutation which disrupted the critical RPA2-binding WD40 domain. The pathogenic nature of these mutations was confirmed by cellular complementation studies (Knies et al., 2017).

A frequently-used diagnostic tool in suspected FA is the exposure of patient-derived cells to ICL inducers, such as Mitomycin C (MMC) or diepoxybutane (DEB); as would be expected, acute hypersensitivity to these agents results in major chromosomal aberrations due to breakages at common fragile sites (Kim and D'Andrea, 2012, Kottemann and Smogorzewska, 2013, Ceccaldi et al., 2016).

1.3.5: Mechanistic differences between replication-dependent and -independent ICL repair

Although the key stages of ICL repair are broadly similar across all cell cycle stages, there are some differences between the precise mechanisms involved. ICL repair involves a combination of nucleotide excision repair (NER) and trans-lesion synthesis (TLS) pathways (Williams et al., 2013). Following the detection of an ICL, an incision complex is loaded; this complex cleaves one strand of DNA upstream and downstream of the crosslink. TLS polymerases (including DNA polymerase κ and ζ) synthesise new DNA between these incisions, bypassing the crosslink (Sarkar et al., 2006, Klug et al., 2012). A second incision complex then excises the crosslink from the other strand of DNA, and the resultant gap is filled by DNA polymerase δ (Hashimoto et al., 2016).

The manner in which ICLs are detected is cell cycle dependent. During replication-coupled (S-phase) repair, stalled DNA polymerases serve as a signal for the presence of an ICL. In contrast, dedicated pathways have evolved to detect these lesions outside S-phase (Williams et al., 2013).

A key facet of replication-dependent resolution of ICLs is the generation of a DSB following the removal of the crosslink. This is repaired by homologous recombination (discussed in depth in section 1.5.2) to restore the integrity of the chromosome (Williams et al., 2013).

1.3.6: Protecting replication forks from uncontrolled degradation

Replication forks are inherently vulnerable structures. For DNA replication to take place, the double helix must be unwound, exposing unstable ssDNA. Carefully controlled processing of nascent DNA strands by nuclease enzymes is thought to be an essential aspect of the response to replication stress; however, over-processing is likely to be deleterious, leaving stalled forks incompetent for repair and re-start and resulting in genome instability (Mijic et al., 2017). Cells have therefore evolved robust mechanisms to shield replication forks from spurious nuclease activity. The mechanisms underlying these critical processes have remained elusive in mammalian cells until relatively recently. As will be discussed further in section 1.9.2, BOD1L was recently identified as a novel fork protection factor (Higgs et al., 2015); these pathways are therefore of key relevance to this thesis.

One highly conserved mechanism for the prevention of nucleolytic attack of stalled replication forks is fork reversal. This involves the re-modelling of forks into 4-way structures when they are intercepted by DNA lesions, allowing for the continuation of DNA replication. This conversion is performed by DNA translocase enzymes, such as SMARCAL1 (SWI/SNF-related matrix-associated actin-dependent regulator of chromatin [sub-family A]-like 1) (Kolinjivadi et al., 2017) and ZRANB3 (Zinc finger Ran-binding domain-containing protein 3) (Vujanovic et al., 2017). The formation of this intermediate structure is a key step in the process of re-starting stalled replication forks. Re-start may occur via multiple mechanisms. Firstly, fork reversal may preserve the stability of the stalled fork until the arrival of a converging fork from a neighbouring origin. Alternatively, it may allow for the resolution of the intervening lesion by

DNA excision pathways or homologous recombination, the latter of which is preceded by regulated nucleolytic processing (refer to section 1.5.2). Nascent DNA strands may also be annealed to provide an undamaged template, facilitating by-pass of the lesion; this is known as template switching (Bhat and Cortez, 2018).

However, there is also the possibility of a more deleterious scenario: uncontrolled nucleolytic attack of the nascent DNA strand. One arm of a reversed fork is similar in structure to a single-ended DSB and is therefore vulnerable to cleavage by nucleases which are adapted for processing these structures (refer to section 1.5.2) (Quinet et al., 2017, Mijic et al., 2017). Adequate protection of reversed forks is therefore essential. To this end, BRCA2 plays a critical mediating role. Whilst BRCA2 is well known for its role in homologous recombination-mediated repair of DNA damage (section 1.5.2), it also functions independently of this role to load the RAD51 recombinase onto stalled forks and stabilise the resulting nucleofilaments. The C-terminus of BRCA2 harbours a RAD51-binding domain. BRCA2 binds to ssDNA at the fork, thereby displacing bound RPA, before transferring RAD51 monomers onto the ssDNA. BRCA2 stabilises the RAD51-ssDNA filaments through its C-terminus and BRC repeat domains, preventing nuclease access (Mijic et al., 2017, Schlacher et al., 2011, Bhat and Cortez, 2018).

Multiple nucleases have been implicated in fork degradation in the absence of functional protection pathways. The nuclease involved in this deleterious processing appears to be context-dependent. For instance, In BRCA2-deficient cells, stalled forks are targeted for degradation by MRE11: the nuclease component of the MRN complex, which is a key player in

DSB signalling and repair (refer to sections 1.5.1-1.5.2) (Schlacher et al., 2011). On the other hand, it was demonstrated that BOD1L, which is the focus of my thesis, protects stalled forks from uncontrolled nucleolytic processing by DNA2 (DNA replication helicase/nuclease 2) (Higgs et al., 2015, refer also to section 1.9). Furthermore, RIF1 (Rap1-interacting factor 1), a key downstream effector of the resection antagonist 53BP1 (tumour protein 53-binding protein 1) was recently highlighted as a novel fork protection factor. Garzón and colleagues demonstrated that, in a role analogous to that of BOD1L, RIF1 and protein phosphatase 1 (PP1) shield nascent DNA at stalled replication forks from the nuclease and helicase activities of DNA2 and WRN (Werner syndrome helicase) (Garzon et al., 2019). Somewhat paradoxically, the nuclease CtIP (CtBP-interacting protein) also functions to prevent DNA2-mediated fork degradation; however, this was shown to be unique to cells deficient in BRCA1, but not BRCA2 (Przetocka et al., 2018). These observations illustrate the considerable crosstalk between replication fork protection and other DNA repair pathways, the full extent of which is gradually being revealed.

Replication fork protection involves a careful balancing act. A recent study demonstrated that whilst SMARCAL1-dependent formation of reversed forks allows for protection of nascent DNA strands in wild-type settings, these structures are prone to extensive degradation in the absence of BRCA2/RAD51-mediated protection (Kolinjivadi et al., 2017). It is therefore unsurprising that pathways which antagonise spurious fork reversal are now being revealed. Malacaria and colleagues recently demonstrated that the mediator protein RAD52 inhibits

excessive recruitment of SMARCAL1 to stalled forks to regulate levels of fork reversal (Malacaria et al., 2019).

1.4: DNA double-strand breaks

A DSB involves the simultaneous breakage of both phosphate backbones within a single turn of the double helix (Mehta and Haber, 2014). They are widely regarded as being among the most deleterious lesions, posing a major threat to genomic integrity. Even relatively “simple” breaks are extremely difficult to repair and have the potential to be highly damaging to cellular viability. DSBs can arise from a multitude of sources, both endogenous and extra-cellular; as such, cells have evolved robust pathways to resolve this damage and maintain the stability of the genome.

1.4.1: Causes of double-strand breaks

DNA double-strand breaks can be induced by a plethora of exogenous agents, with IR and many chemotherapeutic compounds being among the most well-characterised sources. Additionally, DSBs can arise in the course of a number of normal cellular processes and are known to fulfil key physiological roles (refer to figure 1.2).

IR is a potent source of DSBs, and the lesions generated by this agent have been studied extensively. IR results in many DNA single-strand breaks (SSBs); during exposure to high-dose IR, there is increased likelihood that two such lesions will occur in opposite DNA strands within

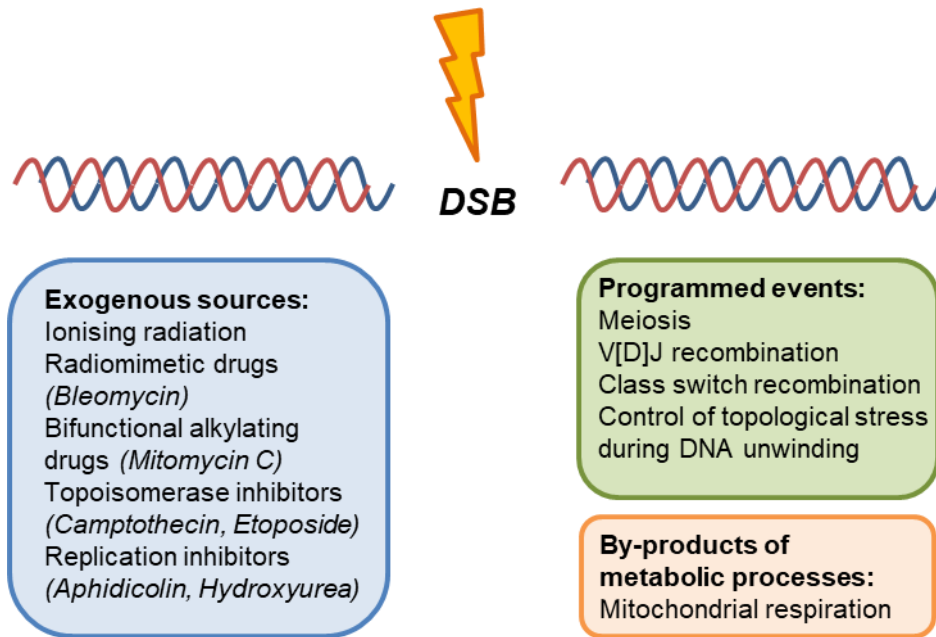


Figure 1.3: Sources of DNA double-strand breaks.

DSBs arise from a multitude of exogenous sources, as by-products of physiological processes and as programmed events. V[D]J: Variable, Diversity and Joining fragments.

the same turn of the double helix, resulting in a DSB (Mehta and Haber, 2014). The radiolytic radical species associated with IR lead to oxidative damage to the sugar-phosphate backbone and terminal nucleotides, as well as phosphoglycolate adducts that require complex processing in advance of repair (Cejka, 2015, Jackson and Bartek, 2009). Other classes of DNA-damaging drugs, namely bifunctional alkylating agents, topoisomerase inhibitors and replication inhibitors, can also induce DSBs, amongst a spectrum of additional effects (Jackson and Bartek, 2009).

In specific scenarios, DSBs may also be generated through physiological events. The contribution of endogenous DNA-damaging events to disease should not be underestimated; epidemiological data has demonstrated that exposure to environmental mutagens alone is insufficient to explain the considerable sporadic cancer incidence observed in the human population, and endogenous processes must therefore play a role. The most prevalent endogenous source of DSBs is the generation of reactive oxygen species (ROS), such as hydrogen peroxide (H_2O_2), hydroxyl free radicals ($OH\cdot$) and singlet oxygen molecules (1O_2), which are by-products of processes such as mitochondrial respiration, and can inflict damage to bases as well as SSBs and DSBs (De Bont and van Larebeke, 2004).

Moreover, some DSBs are essential for normal cellular function, playing vital roles in programmed genetic rearrangements and transient topological modifications of the DNA. The generation of substantial immune receptor diversity in lymphoid cells through the process of Variable, Diversity and Joining (V[D]J) recombination requires carefully programmed DSB

formation and resolution. Similarly, class switch recombination (CSR) in mature B cells further modulates the immune response by creating new immunoglobulin isotypes with altered effector properties. This process requires the induction of DSBs in pre-determined 'switch' regions in the immunoglobulin heavy chain region (Soulas-Sprauel et al., 2007, Khan and Ali, 2017). DSB formation during meiotic recombination also facilitates the controlled exchange of genetic material between non-homologous chromatids to promote gametic diversity. Lastly, Topoisomerase enzymes play a fundamental role in suppressing topological stress by inducing transient SSBs and DSBs during cellular processes which require the unwinding of the DNA double-helix, such as transcription and DNA replication (Khan and Ali, 2017).

1.5: DNA double-strand break signalling and repair

As my doctoral studies will involve the investigation of a potential role for BOD1L in DNA double-strand break repair, I will describe these pathways in more detail below. The principal pathways – template-dependent homologous recombination (HR) and template-independent NHEJ (non-homologous end joining) can be divided into detection, signal initiation and repair stages, and each involve several sub-pathways (Forget and Kowalczykowski, 2010).

1.5.1: Detection of double-strand breaks and signal initiation

Considerable advances have been made towards the elucidation of the DSB signalling cascade, and the proteins and complexes involved in the detection of DSBs and the initiation of signalling

have been extensively studied (Ciccia and Elledge, 2010). Key factors and pathways are described below.

Roles of PARylation: PARylation by PARP enzymes is a post-translational modification implicated in a wealth of physiological processes. Multiple ADP ribose monomers are conjugated onto Glu, Asp, Lys or Ser residues of substrate proteins, forming linear or branched chains (Pears et al., 2012). Although the principal roles of PARPs are in SSB repair, PARPs are also known to bind to DSBs and are activated during the early stages of DSB detection. Indeed, the inhibition of this PTM sensitises cells to DSB inducers and impairs the resolution of these lesions. There are multiple proposed functions of PARylation in DSB repair signalling: to promote recruitment of other DSB repair factors, many of which have PAR-binding motifs, to modify these factors to influence their interactions with DNA and with other repair pathway components (Beck et al., 2014), and to facilitate chromatin remodelling (Chen et al., 2018).

To date, PARP1, PARP2 and PARP3 have been identified as DNA damage responders. Whilst PARP1 and PARP2 activation has been linked to multiple types of DNA lesion, including DSBs, recent evidence is suggestive of a specific role in DSB resolution for PARP3. The two zinc finger domains of PARP1 recognise the key hallmarks of damaged DNA: unpaired nucleotides and an exposed phosphate backbone. Upon binding to DSBs, PARP1 assembles into dimers, resulting in conformational changes to the enzyme's catalytic domain that up-regulate the synthesis of poly(ADP-ribose), thereby creating a feedback loop to enhance DSB-dependent signalling (Beck et al., 2014). Whilst PARP1 has no apparent role in canonical NHEJ (which remains viable in

PARP1-deficient murine cells), it is a pre-requisite for non-canonical alternative NHEJ (alt-NHEJ) (refer to section 1.5.4) and facilitates the re-start of stalled replication forks by promoting HR-mediated repair (Pears et al., 2012, Couto et al., 2011).

Initial PARylation by PARP1 triggers recruitment of PARP2, which further propagates the PARylation signal through the conjugation of additional ADP ribose units onto existing PAR chains. It was recently demonstrated that the resultant branched structures act as a signal for the histone chaperone Aprataxin-PNK-like factor (APLF), which promotes removal of histone H3 during the repair of DNA damage to allow for chromatin remodelling. Furthermore, the accumulation of PAR, which has a net negative charge, at the site of damaged DNA leads to electrostatic repulsion of the nearby chromatin (Chen et al., 2018)

Finally, emerging evidence supports the importance of PARP3 in canonical NHEJ. The recruitment of the Ku70/Ku80 heterodimer to DSBs is aided by the poly(ADP-ribose)-binding zinc finger (PBZ) domain of Ku70. PARP3 co-operates with this heterodimer to suppress short-range nucleolytic resection at these sites by CtIP and MRE11, thereby promoting NHEJ-mediated repair (section 1.5.3). Furthermore, it has been suggested that PARP3 acts with APLF to support the re-ligation step of NHEJ (Couto et al., 2011, Beck et al., 2014).

DSB detection and assembly of DNA-PK: Within seconds of the induction of a DSB, the Ku70/Ku80 heterodimer is recruited to the site of damage. Owing to its ring-like structure, this

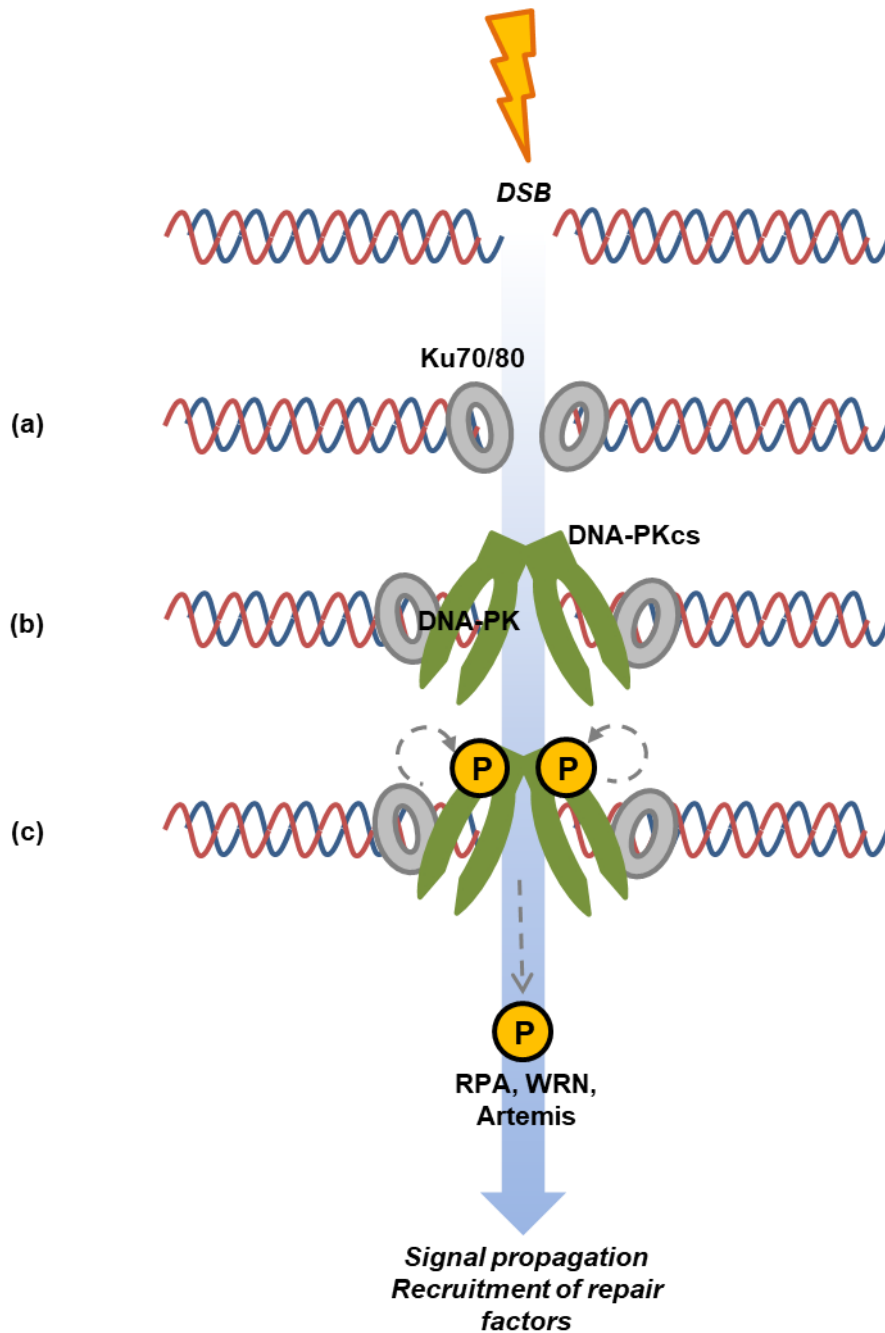


Figure 1.4: Assembly of DNA-PK.

The Ku70/80 dimer is rapidly recruited to DSBs, stabilising the damaged DNA (a). This triggers the recruitment of DNA-PKcs. Together with Ku70/80 and associated DSB ends, this forms the DNA-PK holoenzyme (b). DNA-PK is activated by autophosphorylation and proceeds to phosphorylate a number of downstream, substrates, including RPA, WRN and Artemis, thereby propagating the DNA damage signal and promoting the recruitment of the required repair factors (c). Adapted from Davis et al., 2014.

dimer has a high affinity for DSB ends. An individual heterodimer is loaded onto each exposed end, where it functions as a platform for the recruitment of downstream repair factors and acts to stabilise the damaged DNA. Furthermore, Ku70/Ku80 rapidly recruits the catalytic subunit of DNA-PK, termed DNA-PKcs (Davis et al., 2014). In complex with Ku70/Ku80 and bound DSB ends, DNA-PKcs forms the holoenzyme DNA-PK (DNA-dependent protein kinase). The binding of DNA-PKcs engenders a slight shift in the position of bound Ku70/Ku80 (Wyman and Kanaar, 2006). This shift is followed by autophosphorylation-based activation of DNA-PK and the phosphorylation of multiple downstream targets, including replication protein A (RPA) (Shrivastav et al., 2008). Collectively, these processes function to propagate DDR signalling, triggering the recruitment of additional repair factors and facilitating their access to the damaged DNA. In addition to its signalling function, DNA-PK also supports the activity of MRE11 and RAD50 in bridging the gap between the broken DNA ends, but opposes the nuclease activity of the MRN complex in order to prevent spurious processing of the DSB (Wyman and Kanaar, 2006, Davis et al., 2014).

Roles of MRN during DSB detection and early signalling: The MRN complex, recruited promptly upon detection of a DSB, is a highly conserved complex comprising Meiotic recombination 11 homologue A (MRE11), RAD50 and Nijmegen breakage syndrome protein 1 (NBS1). MRN is equipped for DNA binding through the properties of its subunits. MRE11, which serves as the functional core of the complex, has 2 DNA-binding motifs, as well as an N-terminal phosphoesterase domain. RAD50's Walker A and B sequences also facilitate DNA binding. NBS1 includes a C-terminal MRE11-interacting motif (van den Bosch et al., 2003). Whilst the

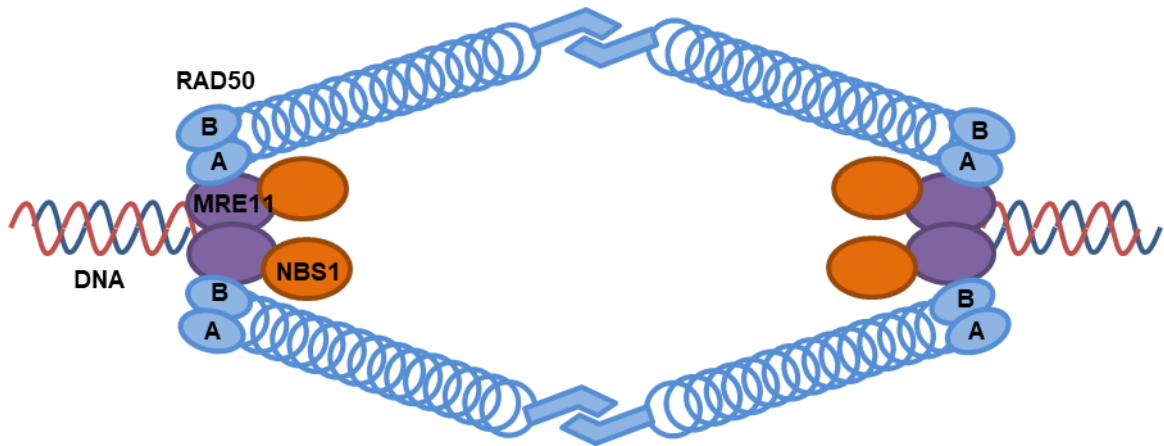


Figure 1.5: MRN performs a scaffolding role during DSB detection and signal initiation.

The MRN complex binds to DSB ends via the DNA-binding motifs of MRE11 and RAD50's Walker A and B domains (denoted as A and B, respectively). NBS1 interacts with the complex with a C-terminal MRE11-binding sequence. RAD50 and MRE11 bridge the gaps between the broken ends of the DSB through oligomerisation of RAD50's protruding coiled coil domains. Adapted from van der Bosch et al., 2003.

endo- and exonuclease activities of MRE11 play key roles in the processing of DNA at a DSB site to initiate repair (Shibata et al., 2014), it is widely acknowledged that the scaffolding role of this complex is its most critical function at the point of DSB detection. Structural studies implicate RAD50, in complex with MRE11, in the formation of bridges between DNA ends. The protruding coiled coil domains of RAD50 allow for the formation of oligomers at broken DNA ends, thereby maintaining their proximity to one another to facilitate faithful repair (Wyman and Kanaar, 2006).

ATM: The initiation and amplification of IR-induced DDR signalling is primarily attributable to the master regulatory kinase, ATM (Ataxia-telangiectasia mutated), which is activated via multiple routes. Activation of ATM by autophosphorylation of S1981 occurs within minutes following treatment with IR. Furthermore, the detection of DNA damage triggers the conversion of ATM from an inactive homodimer to a catalytically active monomer. Optimal activation of ATM is dependent upon the activity of the MRN complex; in MRE11-deficient cells, there is a notable reduction in the phosphorylation of ATM target proteins (Adams et al., 2006, Paull, 2015).

ATM activation initiates a cascade of downstream signalling, during which the histone analogue H2AX is phosphorylated (creating the phosphorylated variant γ H2AX), along with a plethora of other proteins which harbour SQ or TQ target motifs (Matsuoka et al., 2007). The key mediator protein MDC1 (mediator of DNA damage checkpoint protein 1) interacts with γ H2AX in a phosphorylation-dependent manner to propagate the DDR signal and recruit critical factors,

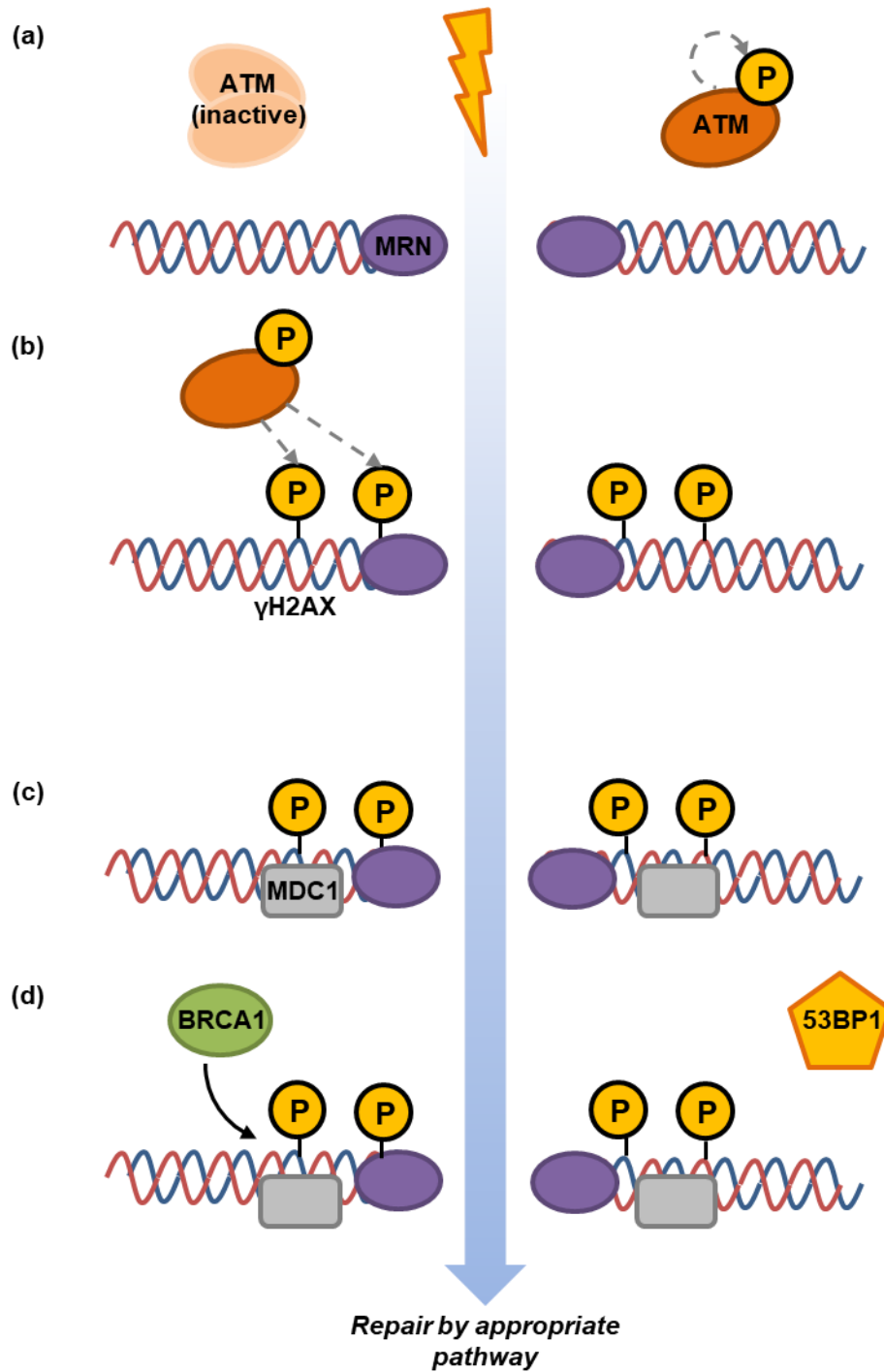


Figure 1.6: Activation of ATM and downstream signalling.

Upon detection of a DSB, ATM is converted from an inactive dimer to a monomer and is activated by autophosphorylation at S1981. Optimal activation is achieved by the activity of the MRN complex (a). ATM phosphorylates downstream targets, including the histone analogue H2AX, forming γ H2AX (b). The mediator protein MDC1 interacts with γ H2AX, propagating the DNA damage signal to promote recruitment of BRCA1 and 53BP1.

including the additional mediator protein BRCA1 (breast cancer susceptibility protein 1) to damaged chromatin (Stewart et al., 2003). The BRCT2 domain of a third mediator, 53BP1 (tumour protein 53-binding protein 1) also interacts directly with γ H2AX, promoting its recruitment to damaged chromatin following ATM activation (Baldock et al., 2015). These proteins are key determinants of appropriate repair pathway selection (to be discussed in detail in section 1.6).

Roles of Ubiquitination: Ubiquitin and ubiquitin-like modifiers are eminently suited to the modulation of DSB repair and other dynamic processes due to the capacity for easy reversal by de-ubiquitinating enzymes (DUBs). Moreover, as ubiquitin itself may also be modified, diverse signalling is possible through the creation of complex chains (Schwertman et al., 2016). Ubiquitination is a three-step post-translational modification involving the activation of ubiquitin by E1 enzymes followed by co-operation between E2 conjugating enzymes and E3 ubiquitin ligases to attach ubiquitin moieties to lysine residues of substrate proteins (Komander and Rape, 2012).

Along with phosphorylation, ubiquitination plays a fundamental role at the early stages of DDR signalling in order to direct 53BP1 to sites of DNA damage. In response to ATM and ATR signalling, MDC1 binds to H2AX in the locality of the damaged chromatin. This binding triggers the recruitment of a ubiquitin E3 ligase complex, comprising RNF8, HERC2 and UBC13 along with UBA1 (Stewart et al., 2009). This is followed by the localisation of RNF168, which ubiquitinates Lysine 15 of histone H2A in the vicinity of the damaged DNA. Ubiquitinated

H2AK15 acts as a signal to direct the recruitment of 53BP1. This modification is performed exclusively by RNF168 as a downstream consequence of ATM/ATR signalling; this underlies the specificity of 53BP1 recruitment to damaged regions of chromatin (Zimmermann and de Lange, 2014). Histone ubiquitination allows for chromatin remodelling to facilitate access of the DSB repair machinery to these regions (Kee and Huang, 2015).

The recruitment of BRCA1 to DSBs is also supported by ubiquitin-based signalling. Through its BRCT (BRCA1 C-terminus) domains, BRCA1 interacts with RAP80 (receptor-associated protein 80), which harbours two ubiquitin-interacting motifs (UIM) and a SUMO-interacting motif (SIM) (Lombardi et al., 2017, Sobhian et al., 2007). These motifs allow RAP80 to recruit BRCA1, in complex with its interacting partner BARD1 (BRCA1-associated ring domain protein 1) to poly-ubiquitinated MDC1 at DSB sites with a preference for polymers linked to Lys63 or Lys6 (Sobhian et al., 2007).

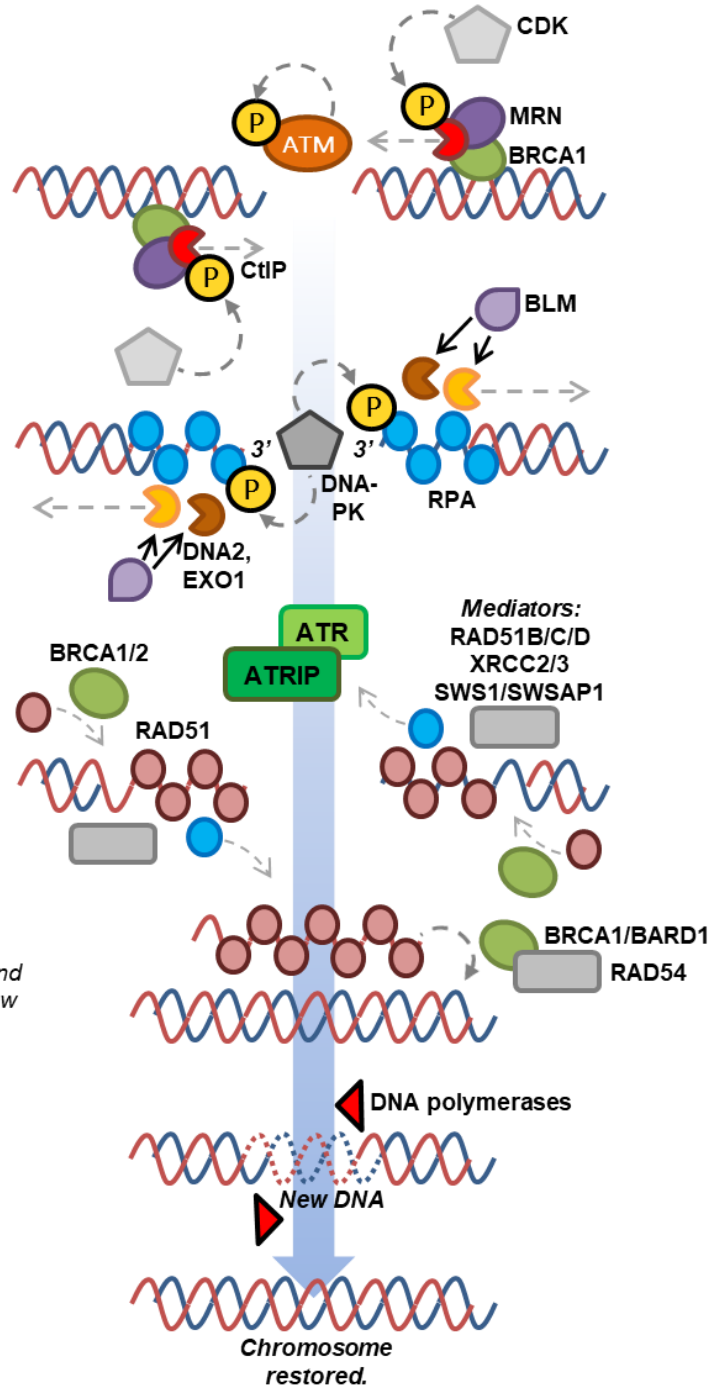
1.5.2: Homologous recombination

Following the initiation of DDR signalling, the resolution of a DSB can proceed by HR, in which undamaged DNA from the homologous sister chromatid is used as a template for repair, or NHEJ, which involves direct re-ligation of the broken DNA ends (Heyer et al., 2010). HR and its related sub-pathways will be described below.

HR can be divided into three stages: pre-synaptic, synaptic and post-synaptic. During the first phase (figure 1.3a), the DNA ends at either side of the DSB are subjected to processing by nuclease enzymes. Initial short-range resection is first carried out to expose short 3' ssDNA tails, approximately 20 nt in length (Gong *et al.*, 2016). This resection is primarily attributable to the 3'-5' exonuclease functions of tetrameric assemblies of CtIP (Davies *et al.*, 2015) in association with the MRN complex and BRCA1 (Chen *et al.*, 2008). Additionally, mass spectrometry analysis of the CtIP interactome revealed EXD2 (exonuclease 3'-5' domain-containing 2) as a co-factor of MRN, which supports its nucleolytic activity, aids recruitment of RPA, promotes HR and maintains genome stability (Broderick *et al.*, 2016).

HR requires the generation of extensive tracts of ssDNA, which are generated from the 3' overhangs by the action of further nucleases, DNA replication helicase/nuclease 2 (DNA2) and Exonuclease 1 (EXO1). These catalyse long-range resection in the 5'-3' direction by two overlapping pathways, both requiring the Bloom helicase (BLM). Biochemical analyses demonstrated that BLM is recruited to DSBs ends by MRN. DNA2 subsequently interacts with BLM to resect DNA in a manner dependent on the nuclease activity of DNA2 and the helicase

(a) Pre-synapsis:
*Resection & formation of
 RAD51-ssDNA
 nucleofilament*



(b) Synapsis:
*Homology searching, strand
 invasion & synthesis of new
 DNA using homologous
 template.*

(c) Post-synapsis:
*Ligation of nascent &
 existing DNA to restore
 chromosome.*

Figure 1.7: Overview of DSB repair by homologous recombination (HR).

Repair of DSBs by canonical HR involves the use of the homologous sister chromatid as a template to produce an accurate repair fragment. During pre-synapsis (a), DSB ends are subjected to two stages of nucleolytic processing. Short-range resection is carried out by CtIP in complex with MRN and BRCA1; the formation of this complex is dependent on CDK-mediated phosphorylation of CtIP. This is followed by long-range resection by DNA2 and EXO1, both of which are stimulated by BLM. RPA is recruited to the exposed ssDNA, which serves as a platform for the recruitment of ATR and ATRIP. RPA is displaced by RAD51 to form a nucleofilament; this is facilitated by mediators including RAD51 homologues. In the synaptic phase (b), the RAD51-ssDNA nucleofilament performs a homology search to locate suitable template DNA and invades the complementary strand. RAD51 dissociates from the strand in a RAD54-dependent process to allow DNA polymerases to synthesise new DNA. During post-synapsis (c), the chromosome is restored by annealing of the existing and nascent DNA strands; in a small fraction of cases, this involves the formation of crossovers, which must be resolved.

function of BLM to promote DNA unwinding (Nimonkar et al., 2011). A more recent study suggested that the helicase domain of DNA2 also has the capacity to unwind kilobases of dsDNA; however, this activity is only observable in a nuclease-deficient variant of DNA2 and is therefore unlikely to make a substantive contribution to the preparation of DNA for resection (Pinto et al., 2016). Additionally, EXO1-dependent resection is supported by BLM, which strengthens the binding of this nuclease to DNA (Nimonkar et al., 2011).

Both of the above long-range pathways are also reliant on existing RPA-bound ssDNA, demonstrating the fundamental requirement for an initiating short-range resection step prior to the extension of the ssDNA tails (Nimonkar et al., 2011). RPA rapidly binds to the extended 3' overhangs, which may comprise thousands of nucleotides (Gong *et al.*, 2016). This heterotrimeric complex is rapidly recruited, stabilising it and suppressing the formation of secondary structures. Whereas RPA may bind to all ssDNA within the nucleus, it has been shown that RPA recruited to ssDNA following resection is phosphorylated by DNA-PKcs at Serine residues 4 and 8 of the RPA32 subunit (Ashley et al., 2014). RPA-bound ssDNA provides a platform for the recruitment of ATR, along with its obligate regulatory partner ATRIP (Cortez et al., 2001). The formation of ATR foci can be observed 1-2 h after IR; this occurs in an MRN-dependent manner, and considerably later than recruitment of ATM (Adams et al., 2006, Ciccia and Elledge, 2010).

The final stage of pre-synapsis involves the loading of the highly-conserved RAD51 recombinase onto ssDNA, thereby forming a RAD51-ssDNA nucleofilament. The presence of RPA poses a

barrier to this process; RPA must therefore be displaced to facilitate RAD51 nucleation on the ssDNA strand. This exchange and nucleofilament formation are catalysed by an array of mediator proteins. RAD51 paralogues, comprising RAD51B, -C and -D, XRCC2 and -3, SWS1 and SWSAP1, represent one class of mediators. These proteins bear structural resemblance to the ATPase domain of RAD51 (Godin et al., 2016). Moreover, BRCA1 and BRCA2 also mediate loading of RAD51 onto ssDNA. The precise mechanisms of action of mediator proteins in mammalian cells remain to be elucidated, but it is understood that they are required to regulate RAD51 function and overcome the inhibitory effects of loaded RPA (Shrivastav et al., 2008, Heyer et al., 2010, Shibata et al., 2011). In *Saccharomyces cerevisiae* (a model in which the steps of HR are well characterised), Rad52 performs a role analogous to human BRCA2 during pre-synapsis; conversely, human RAD52 is not a pre-requisite for this stage of canonical HR unless cells are deficient of BRCA2 (Godin et al., 2016, Wright et al., 2018).

Synapsis is the second stage of HR (figure 1.3b). A sequence homology search is undertaken by the RAD51-ssDNA nucleofilaments to locate a suitable homologous tract of undamaged DNA for use as a repair template – typically the undamaged sister chromatid. It is thought that the nucleofilament probes dsDNA for complementary sequence regions through transient destabilisation of the double helix. This process, referred to as base-flipping, remains unclear, but it is known that additional factors are involved (Wright et al., 2018). For instance, a recent study demonstrated that BRCA1 and its functional partner BARD1 both interact with RAD51 and enhance the interaction of the RAD51 nucleofilament with homologous DNA (Zhao et al., 2017). Short homologous regions of only 8 nt are sufficient to prolong the nucleofilament-

ssDNA interaction during homology searches. It is clearly of considerable importance that filaments dissociate efficiently from non-homologous sequences; this process is not fully understood in mammalian cells (Wright et al., 2018).

Upon location of a suitable region of homology, the nucleofilament forms a transient association with the partially unwound duplex DNA in a synaptic complex; this process is stimulated by the ATP-dependent translocase RAD54 (Rossi and Mazin, 2008, Shibata et al., 2011). The nucleofilament then binds to the complementary region of DNA, forming a displacement loop (D-loop) – so-named because the existing base pairing in the duplex DNA is disrupted to allow the invasion and binding of the nucleofilament (Wright et al., 2018). Following this strand exchange, RAD51 then dissociates from the nucleofilament in a process catalysed by RAD54. This allows DNA polymerases to access the resultant primer-template junction and synthesise new DNA until a sufficient length is produced to anneal to the second end of the resected DSB (Wright et al., 2018, Godin et al., 2016).

During the post-synaptic stage of HR (figure 1.3c, figure 1.4), the restoration of intact duplex DNA is completed by the appropriate sub-pathway: synthesis-dependent strand annealing (SDSA), break-induced replication (BIR) or double Holliday junction (dHJ) formation. The main pathway in somatic cells appears to be SDSA, during which the nascent DNA strand anneals to the opposite end of the DSB, bridging the gap between the existing and newly-synthesised strands. This circumvents the potential formation of crossovers (Wyman and Kanaar, 2006, Heyer et al., 2010). Alternatively, if the DSB arose through the collapse of a stalled replication

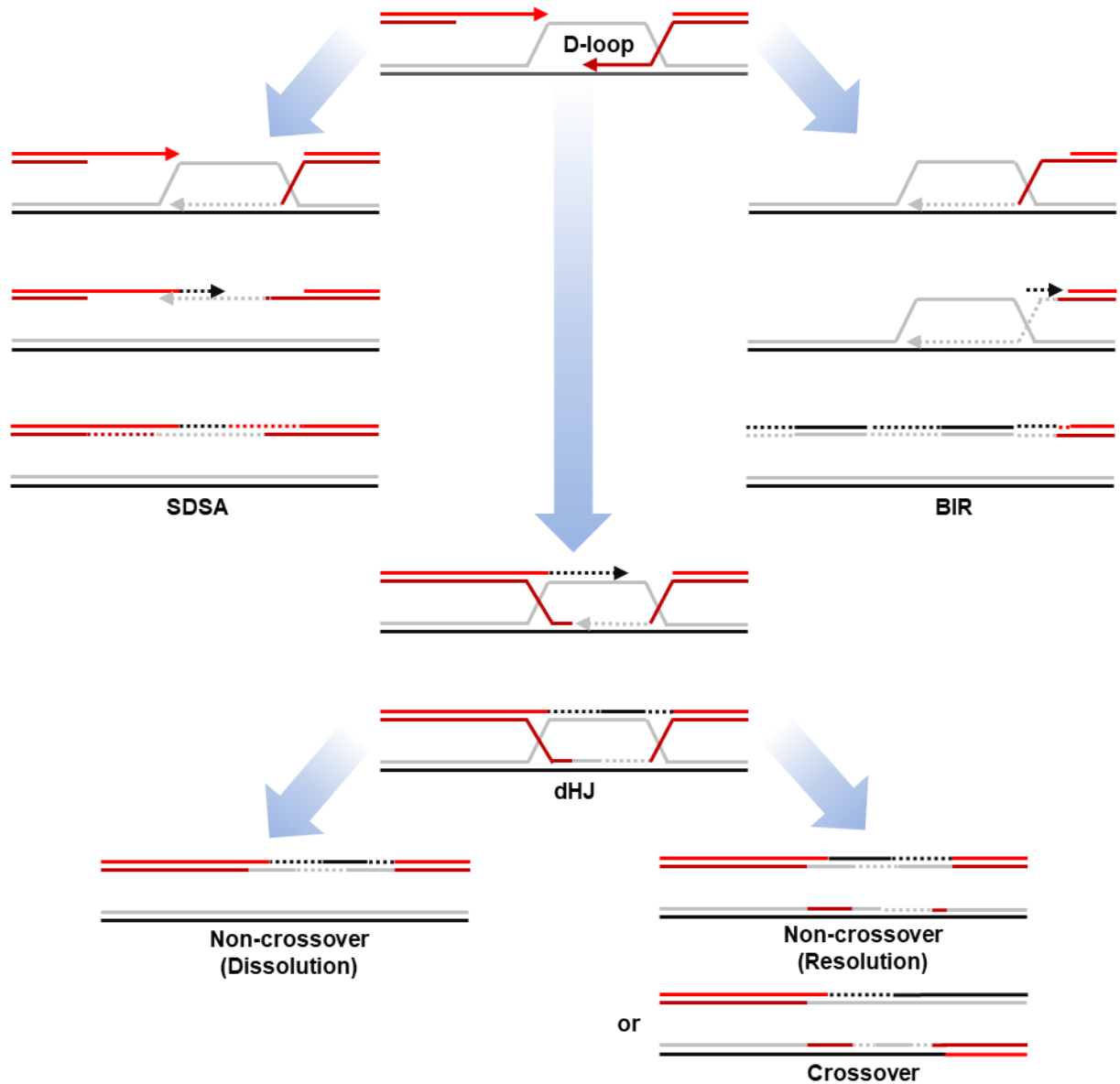


Figure 1.8: Sub-pathways of the synaptic phase of HR and resolution of crossovers.

Restoration of the repaired chromosome occurs via one of 3 sub-pathways. In synthesis-dependent strand annealing (SDSA), newly-synthesised DNA anneals to the opposite end of the DSB. No crossovers are formed. A small proportion of repairs result in double Holliday junctions (dHJs). These may dissolve or be resolved by dHJ resolvase enzymes or BLM/Topo3, leaving the original DNA sequences intact. Some crossovers may remain, leading to chromosomal rearrangements. In break-induced replication (BIR), the D-loop may be converted to a new replication fork to continue DNA replication. This occurs where DSBs have occurred through the collapse of replication forks. Adapted from Mehta & Haber, 2014.

fork (Petermann et al., 2010) and no second end is available for annealing, the D-loop can form a new replication fork (BIR). In a small percentage of cases, crossed DNA structures (dHJs) can result during the restoration of the chromosome. Whilst dHJ formation is an essential aspect of meiotic recombination for the generation of genetic diversity in gametes, it can lead to deleterious genomic rearrangements during HR-mediated repair. Crossovers may be resolved by dHJ resolvase enzymes or through the combined activities of BLM helicase and Topoisomerase 3 (Wyman and Kanaar, 2006, Heyer et al., 2010). RAD52 may play a role in the annealing of existing and nascent DNA strands due to its capability to join tracts of ssDNA bound by RPA. However, the mild phenotype of RAD52-deficient mammalian cells does not support a critical role in HR for this factor; it is therefore unlikely to be the primary mediator of this step (Wright et al., 2018).

1.5.3: Non-homologous end joining

In contrast to HR, NHEJ involves the direct re-ligation of the DNA ends at either side of the break with no repair template and minimal nucleolytic processing of the damaged DNA. Of these two pathways, NHEJ is regarded as the more error-prone due to the potential for re-ligation of non-contiguous ends, which can result in deleterious chromosomal rearrangements or loss of genetic information at the repair site. However, the kinetics of NHEJ-mediated repair are advantageous to cells; NHEJ offers a faster and more straightforward pathway for the restoration of chromosomal integrity (Huertas, 2010, Shibata et al., 2011). It is therefore the most frequently-used pathway for DSB repair, responsible for the resolution of around 80% of

radiation-induced DSBs (Kakarougkas and Jeggo, 2014). The canonical and alternative modes of NHEJ are described below.

Following the detection of a DSB by the ring-like Ku70/Ku80 heterodimer, DNA-PKcs is rapidly recruited to the site of damage DNA and activated, forming the DNA-PK holoenzyme (figure 1.5a). This activation marks the initiation of repair by NHEJ (Davis et al., 2016, Ciccia and Elledge, 2010). At this stage, DNA-PKcs is phosphorylated. The most well-characterised of these phosphorylations takes place at Threonine 2609. This site was previously thought to be autophosphorylated, but it is now known that these sites are ATM targets which are modified in response to the detection of DSBs. Conversely, a second phosphorylation site at Serine 2056 is recognised as a site of autophosphorylation. It has been speculated that the phosphorylation of these regions produce antagonistic effects in terms of nucleolytic processing of DSB ends (discussed in section 1.5.6). Multiple other phosphorylation sites have been identified, but their functions in modulating NHEJ remain unclear (Davis et al., 2016).

Finally, formation of the pre-ligation complex and re-ligation of the DSB ends is performed by the XRCC4/LIG4 complex with support from the stimulatory action of an XRCC4 homologue, XRCC4-like factor (XLF) (figure 1.5d) (Ciccia and Elledge, 2010). Recent single-molecule studies with immunofluorescence microscopy have shed further light on these processes. Using a system based on *Xenopus laevis* cell-free egg extract, Graham and colleagues demonstrated that single XLF dimers function as bridges between DSB ends prior to the assembly of the synaptic complex – a precursor to ligation. Furthermore, synapsis occurs as a two-step process.

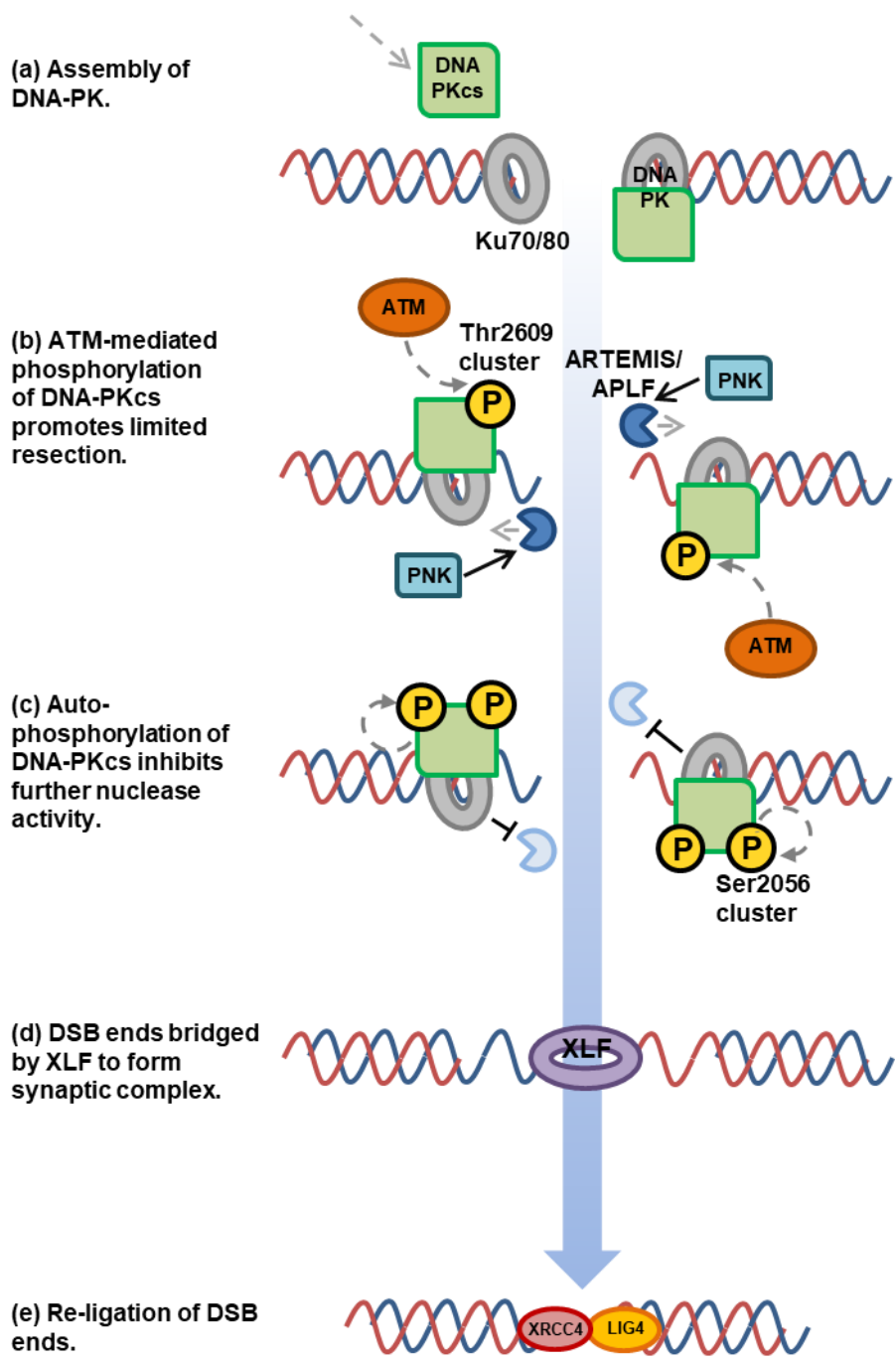


Figure 1.9: Overview of DSB repair by non-homologous end joining (NHEJ).
 During DSB repair by canonical NHEJ, the Ku70/Ku80 heterodimer rapidly recruits DNA-PKcs; the Ku/DNA-PKcs/DNA complex forms the DNA-PK holoenzyme (a). DNA-PKcs is then phosphorylated at the Thr2609 cluster, which promotes minimal resection by ARTEMIS and APLF to remove DNA adducts. This processing is stimulated by PNK (b). DNA-PKcs is then autophosphorylated at the Ser2056 cluster to inhibit further nuclease activity. The synaptic complex is formed when XLF dimers form bridges between DSB ends (c). The ends are then brought closer to one another to facilitate ligation by XRCC4 and LIG4.

The ends of the DSB are initially held at some distance from one another before being brought into proximity to facilitate ligation (figure 1.5e) (Graham et al., 2018, Graham et al., 2016).

The properties of the NHEJ machinery and a number of supporting factors contribute to the fidelity of this crucial ligation step. A structural motif of LIG4, known as insert1, allows for the flexible assembly of the LIG4 complex that permits tolerance of complex ends and sampling of alternative ends in the event of mismatches (Conlin et al., 2017). In addition, tyrosyl-DNA phosphodiesterase 1 (TDP1) was recently shown to be essential for efficient and accurate NHEJ. Overall end-joining proficiency is reduced in the absence of TDP1. Moreover, end-joining fidelity is compromised, with cells deficient of this protein exhibiting an increased frequency of erroneous insertion-associated repair events. The NHEJ-related functions of TDP1 are dependent on its catalytic activity (Li et al., 2017). Modulator of retroviral infection (MRI, also termed cell cycle regulator of NHEJ, CYREN) also functions as a versatile adaptor protein during canonical NHEJ, interacting with a suite of NHEJ-associated proteins, such as Ku70, Ku80 and XRCC4, via its N- and C-terminal domains (Hung et al., 2018).

1.5.4: Error-prone DSB repair pathways

Alongside the DSB repair pathways described above, several non-canonical pathways have been described. These are typically regarded as error-prone; despite being reliant on some nucleolytic processing, repairs involve little or no utilisation of homologous template DNA and typically result in deletions at the DSB site. Two non-canonical pathways, single-strand annealing (SSA) and alternative NHEJ (alt-EJ), will be described below.

Single-strand annealing becomes a viable pathway for repair when DSBs are flanked by homologous repeat regions (a relatively frequent occurrence in large eukaryotic genomes). As for canonical HR, SSA is dependent on resection; in contrast to HR, however, it occurs independently of RAD51 (Heyer et al., 2010). The DSB is primed for repair by CtIP-mediated processing to expose 3'-ended homologous sequences at either side of the break. These sequences function as a bridge across the DSB and are annealed by RAD52 (Symington, 2002, Bhargava et al., 2016). Interestingly, FANCA, a member of the Fanconi Anaemia core complex (refer to section 1.3.3), was recently shown to catalyse strand annealing in a RAD52-independent manner (Benitez et al., 2018). Next, the non-homologous regions are cleaved by the endonuclease ERCC excision repair 1 (ERCC1) in complex with the exonuclease Xeroderma pigmentosum group F-complementing protein (XPF). Finally, DNA polymerases synthesise new DNA to fill any remaining gaps, allowing the resultant strands to be joined by DNA ligases (Symington, 2002, Bhargava et al., 2016). Due to the loss of genetic material involved, SSA is inherently mutagenic and is therefore typically down-regulated relative to other pathways. However, multiple studies have demonstrated increased utilisation of SSA when alternative pathways, such as canonical NHEJ, are unavailable (Mansour et al., 2008, Escribano-Diaz et al., 2013).

For a number of years, alternative NHEJ (alt-EJ) was considered to be a back-up in case of failure of the canonical pathway. Later studies have indicated that the switch to alt-EJ is triggered specifically by the absence of Ku, but not through the impairment of NHEJ caused by loss of

other core repair factors, such as DNA-PKcs or XRCC4 (Mansour et al., 2013). DSB end structure is also a key determinant of NHEJ sub-pathway selection (Chang et al., 2017). In preparation for repair by alt-EJ, limited processing of the DSB ends may be performed by MRN and CtIP, exposing regions including 2-20 nt of microhomology which can be used to facilitate re-ligation. The ligation step is then performed by X-ray repair cross-complementing 1 (XRCC1) and Ligase 3 (LIG3) (Ciccio and Elledge, 2010, Chang et al., 2017).

Several factors have been implicated specifically in non-canonical end joining. Firstly, PARP1 is an essential regulator of this repair pathway, hence its alternative designation of PARP-EJ (Mansour et al., 2013). Pol θ , an atypical DNA polymerase, also promotes alt-EJ and suppresses recombination. Alongside its functions in DNA replication, it contributes to the formation of the pre-ligation complex and the annealing of processed DNA strands (Kent et al., 2015, Mateos-Gomez et al., 2015).

1.5.5: Structural variation in double-strand breaks

There is considerable variability in the structural complexity of the damaged ends of a DSB, which is determined by how the break arises. At one end of the spectrum, chemically 'simple' DSBs, such as those induced by restriction endonucleases, may have blunt ends or short 5'/3' overhangs. Multiple systems have been generated which allow the induction and visualisation of DSBs at defined genomic loci by specific enzymes, such as the rare-cutting I-SceI (Gunn and Stark, 2012) or FokI (Bitinaite et al., 1998). These DSBs are valuable in research settings, allowing repair kinetics to be monitored at individual, known sites of damage. Enzymatically-

induced DSBs are typically reparable by direct re-ligation of the DSB ends with no preliminary processing (Wyman and Kanaar, 2006).

Conversely, DSBs inflicted by exogenous agents may include chemical alterations, secondary DNA structures or protein adducts. IR, for instance, results in oxidative damage to the sugar-phosphate backbone of the DNA, which creates SSBs. DSBs are generated when two such lesions occur on opposite DNA strands in proximity to one another. These DSBs typically include a 5' hydroxyl group and 3' phosphoglycolate adduct, rendering direct re-ligation of the broken ends impossible (Schipler and Iliakis, 2013, Mehta and Haber, 2014).

An additional layer of complexity has also been described in cells exposed to ionising radiation or radiomimetic drugs. These forms of assault can lead to clustered DNA damage, in which multiple DNA lesions – DSBs, SSBs, abasic sites or oxidised bases – occur within a region of approximately 20 bp. The complexity of the individual lesions, as well as their proximity to one another, poses considerable challenges to the DNA damage repair machinery (Sutherland et al., 2002).

1.5.6: Coping with complex lesions

Previous studies have consistently suggested that misprocessing of complex DSBs is the main factor underlying the deleterious outcomes associated with this form of DNA damage;

furthermore, errors in processing are considerably more likely for DSBs than for lesions involving only one strand of the DNA (Schipler and Iliakis, 2013).

The repair pathways described above are applicable to scenarios involving chemically 'simple' DSBs, such as those induced by restriction endonucleases. However, exogenous agents, including IR, are a major source of DSBs. The complex ends associated with these DSBs require additional processing prior to the initiation of repair. To some extent, the cellular HR machinery is able to cope with such complexity due to the extensive processing inherently associated with this pathway. Any damaged bases are likely to be removed by nucleolytic resection, although this may negatively impact on the kinetics of repair (Schipler and Iliakis, 2013). For instance, CtIP, BRCA1 and the MRN complex have been shown to process DSBs arising from Topoisomerase II (TopoII) trapping (Aparicio et al., 2016). Furthermore, when faced with bulky protein adducts at DSB ends, MRN is effectively 'converted' in an NBS1- and ATP-dependent manner into a complex which is specialised to handle these adducts using both its endo- and exonuclease activities (Deshpande et al., 2016).

Conversely, specialised mechanisms and additional factors are inevitably required prior to re-ligation of DSB ends via NHEJ. The most well-characterised of these is the ARTEMIS nuclease, which works in co-operation with a second nuclease, Aprataxin and PNKP-like factor (APLF), and requires the kinase/phosphatase activity of polynucleotide kinase (PNK). In association with DNA-PK, ARTEMIS utilises its endonuclease activity to target DSB ends associated with complex structures, such as gaps, flaps, DNA hairpin structures and 5' or 3' overhangs

(Malyarchuk et al., 2013, Wyman and Kanaar, 2006). The removal of these structures facilitates the continuation of repair by the standard NHEJ machinery. Resection of complex breaks is carefully controlled by post-translational modifications. Initial phosphorylation of DNA-PKcs at Thr2609 permits minimal nucleolytic end processing by ARTEMIS. In contrast, subsequent autophosphorylation at Ser2056 protects ends from excessive resection and acts as an inhibitor of HR-mediated repair (Davis et al., 2016, Ciccia and Elledge, 2010).

1.6: Regulation of DSB repair pathway choice

The selection of the appropriate repair pathway for each DSB is carefully controlled by a multitude of factors. The complex interplay between these determinants maintains a finely-tuned balance between repair pathways.

1.6.1: Cell cycle-dependent regulation

It is understood that NHEJ, although error-prone, is the favoured pathway for the repair of 75-80 % of DSBs, irrespective of the cell cycle stage (Shibata et al., 2011). Time-lapse fluorescence microscopy studies of live cells have confirmed that NHEJ predominates during G1 and G2 phases, with a gradual shift towards increased HR during late S and G2 phases, and peak HR utilisation during mid-S phase. Interestingly, repair pathway choice for a DSB is not determined at the point of damage. Instead, it can be adjusted according to replication dynamics within the cell (Karanam et al., 2012). There is scant evidence that HR can occur outside S and G2

phases (Saleh-Gohari and Helleday, 2004); this is understandable due to the requirement of the homologous sister chromatid as a template for HR-mediated repair.

Erroneous repair of DSBs is a major cause of genome instability (Schipler and Iliakis, 2013). Selecting the appropriate pathway for the repair of DSBs is therefore fundamental for survival at the cell and whole organism level. A major consideration which governs repair pathway choice is the presence or absence of an intact sister chromatid to use as a template for repair. HR-mediated repair is template-dependent; as such, this pathway must be suppressed outside late S and G2 phases or in non-replicated chromosomal regions. This precise regulation is partly achieved by cell cycle-dependent control of nucleolytic resection, which is an essential precursor to HR (Shrivastav et al., 2008).

The activity of cyclin-dependent kinases (CDKs) oscillates throughout the cell cycle and reaches peak levels during S and G2 phases of the cell cycle. thereby providing a suitable tool for implementing cell cycle-dependent control of resection (Harashima et al., 2013). Four CDKs have been identified in humans (CDK1, CDK2, CDK4 and CDK6); these target substrates harbouring a serine or threonine residue with a neighbouring downstream proline (S/T-P). CDK activity is controlled via an interaction with a specific cyclin which serves a regulatory function. These kinases and associated cyclins play a key role in governing passage through cell cycle checkpoints (figure 1.6). Accordingly, their activity is down-regulated in response to DNA damage in order to provide sufficient time to effect repair, thus preventing the potentially deleterious consequences of passage through the cell cycle with unresolved DNA damage. In

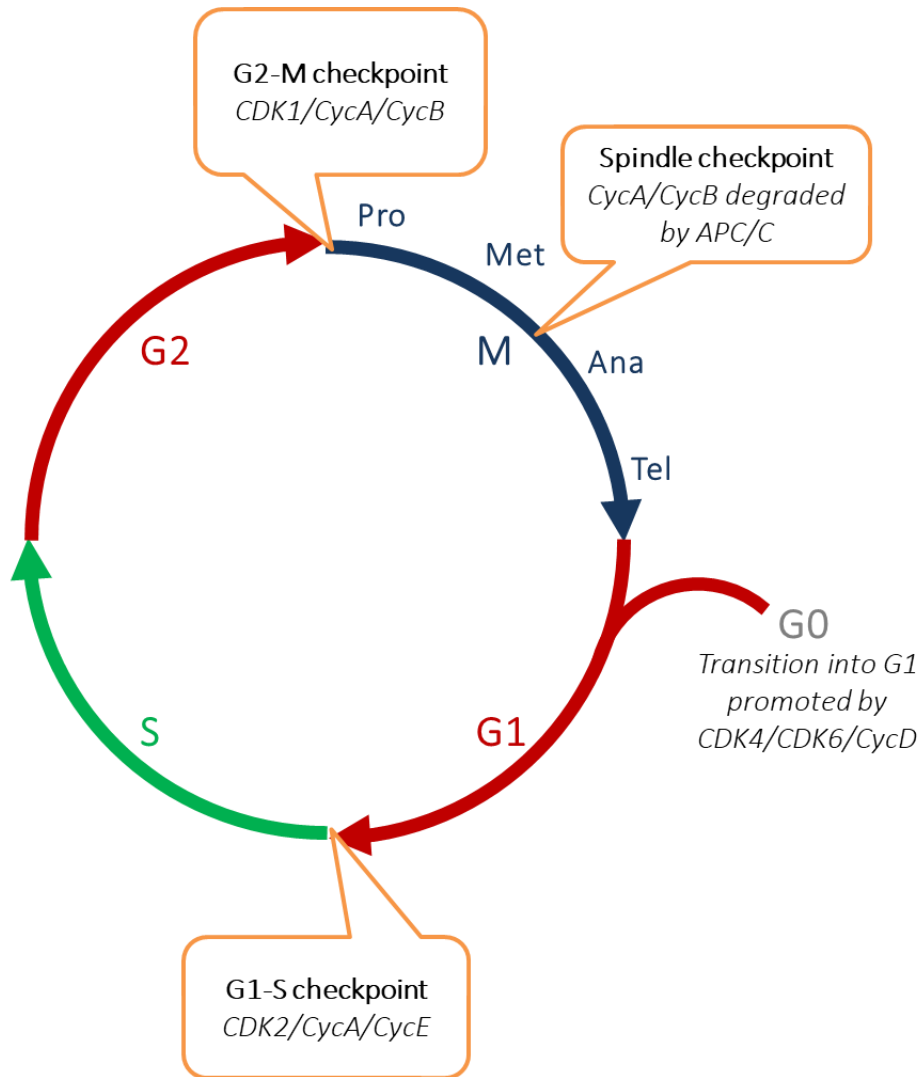


Figure 1.10: Cell cycle checkpoints.

Uni-directional progression through the cell cycle is ensured by three checkpoints, which are governed by cyclins and cyclin-dependent kinases (CDKs). Quiescent (G0) cells require CDK4 and CDK6 activity in combination with Cyclin D for transition into G1. CDK2 along with Cyclins A and E allow entry into S-phase. The onset and progression of mitosis is controlled by CDK1 in association with Cyclins A and B. Finally, upon correct alignment of chromosomes on the metaphase plate, the completion of M phase is permitted by APC/C-mediated degradation of Cyclins A and B.

a contrasting but equally important role, CDKs also phosphorylate a plethora of factors associated with DSB repair. This phosphorylation is essential for nucleolytic resection of DSBs and results in the up-regulation of HR (Ferretti et al., 2013).

CDK-mediated phosphorylation of CtIP remains the most widely accepted mechanism for the modulation of resection dynamics (Ferretti *et al.*, 2013). CDK2-mediated phosphorylation of this nuclease and its suppressors exerts multiple direct and indirect effects on resection levels. Firstly, phosphorylation of Thr847 promotes resection through the stimulation of CtIP activity, although the exact mechanism for this remains unknown (Ferretti et al., 2013). Moreover, the presence of CDK-phosphorylated CtIP impedes the interaction between 53BP1 – a key antagonist of resection – and its major downstream effector, RIF1, which also serves to up-regulate CtIP-mediated resection indirectly (Zimmerman and de Lange, 2014). Thirdly, phosphorylation of CtIP at Ser327 permits its interaction with BRCA1; the formation of this complex is generally viewed as a further pre-requisite for short-range resection (Chen et al., 2008), although one study suggests that this interaction is dispensable for efficient resection (Polato et al., 2014). Phosphorylation of Ser327 is facilitated by interaction between MRE11, CDK2 and CtIP, which brings the kinase into proximity with its substrate. However, there is no convincing evidence to suggest that MRE11 or other components of the MRN complex are controlled by CDK-mediated phosphorylation. Studies to date have yielded conflicting results; whilst NBS1 has been demonstrated to be a CDK substrate, there is no consensus regarding the impact of this apparent phosphorylation on resection (Chen et al., 2008, Ferretti et al., 2013). Additionally, the 5'-3' exonuclease EXO1 is phosphorylated by CDK1 and CDK2 at four sites

(Ser639, Thr732, Ser815, and Thr824); these modifications promote resection and efficient HR, thereby contributing to the maintenance of genome stability (Tomimatsu et al., 2014).

Until recently, it was not understood why canonical NHEJ does not consistently out-compete HR to resolve DSBs, particularly in late S and G2 phases when both pathways are viable. The identification of CYREN as a cell cycle-dependent regulator of NHEJ provided key insights into this unanswered question. The depletion of CYREN in cells expressing TRF2^{ΔBΔM}, which leads to exposure of the telomeres to the cellular end-joining machinery, led to a marked increase in chromatid-type telomere fusions. These fusions are characteristic of post-replicative cells. This implicated CYREN in the suppression of NHEJ in S and G2. Furthermore, an increase in NHEJ was observed in CYREN knockout cell lines relative to wild-type cells. Finally, this study revealed that CYREN preferentially suppresses NHEJ at DSBs with 3' overhangs, protecting these overhangs to provide favourable environments for HR-mediated repair (Arnoult et al., 2017).

1.6.2: Promotion of nucleolytic resection

Since the two main categories of DSB repair have differential requirements for ssDNA at the break site, resection serves as a robust tool for commitment of each lesion to the appropriate pathway. Resolution of DSBs by HR relies upon the initiating step of short-range resection followed by long-range resection; indeed, it has been demonstrated that short-range resection in isolation is sufficient to block NHEJ, but it cannot initiate HR (Bakr et al., 2016). Conversely, NHEJ is suppressed at resected DNA ends due to the low affinity of the Ku70/Ku80 heterodimer for ssDNA (Ciccia and Elledge, 2010, Huertas, 2010). In the absence of Ku70/Ku80, repair

dynamics shift towards HR or alt-EJ, an error-prone, non-canonical end-joining pathway which is dependent on PARP1 (Bakr et al, 2016).

Multiple studies have revealed that pathway choice is underpinned by the nuclease activities of CtIP and the MRN complex. Following induction of DNA damage by laser micro-irradiation, Sartori and colleagues demonstrated that CtIP is recruited exclusively to lesions in S- or G2-phase nuclei. CtIP was also shown to interact with MRN, modulating its function to promote resection and consequent repair by HR (Sartori et al., 2007). A subsequent study further elucidated the details of the CtIP-MRN interaction and highlighted the importance of the critical HR factor BRCA1 in this context. It was demonstrated that CtIP forms a complex with BRCA1 by interacting with the BRCT domains of this protein, and with the MRN complex via a direct association with Nbs1. As discussed above, the formation of this complex is cell cycle-dependent, and short-range resection is thereby restricted to late S and G2 phases of the cell cycle (Chen et al. 2008). A further aspect of CtIP regulation was also described. In a 2014 study, CtIP was revealed as a substrate of the E3 ubiquitin ligase complex, APC/C^{Cdh1} (anaphase promoting complex/cyclosome), which targets this nuclease for ubiquitin proteasome system (UPS)-mediated degradation outside G2 phase, thus ensuring that DSBs resection is prevented and breaks are repaired by NHEJ. The interaction between CtIP and the adaptor protein Cdh1 was found to be essential for clearance of CtIP from sites of DNA damage; abrogating this interaction led to aberrant DSB resection and dysregulated HR (Lafranchi et al., 2014).

The multi-functional transcription factor CCCTC-binding factor (CTCF) has also been implicated in the promotion of CtIP-dependent resection. It was demonstrated previously that CTCF promotes HR; however, the underlying mechanism was not fully understood until recently. In a 2019 study, Hwang and colleagues highlighted three routes by which CTCF promotes CtIP activity. Firstly, it directly interacts with MRE11 in a DNA damage-dependent manner and localises to DSBs via this interaction. Secondly, it interacts with CtIP, promoting the recruitment of this nuclease to DSBs. Finally, CTCF also strengthens the interaction between CtIP and MRE11, thereby indirectly stimulating CtIP recruitment to sites of DNA damage (Hwang et al., 2019).

1.6.3: Suppression of resection

Alongside the factors which promote resection and HR, a suite of DNA end protection factors exists to antagonise nuclease activity and promote NHEJ. The apical factor of this cascade is 53BP1 (TP53BP1, Tumour protein 53-binding protein 1), the function of which has been studied extensively. In response to phosphorylation by ATM at 28 N-terminal S/TQ motifs, 53BP1 is recruited to DSBs; the presence of this factor at DSBs as a scaffold is critical for the fulfilment of its role as an antagonist of resection and driver of end joining (Bakr et al., 2016, Symington and Gautier, 2011, Bothmer et al., 2011, Bunting et al., 2010).

ATM-dependent phosphorylation of 53BP1 is also essential for the successful recruitment of several downstream effectors, of which RIF1 (Rap1-interacting factor 1) was the first to be identified. As with 53BP1, RIF1 is required for NHEJ, and end-joining is defective in the absence

of RIF1 – both in the context of DNA damage repair and the re-ligation of programmed DSBs during CSR. Indeed, the end-to-end fusion of artificially de-protected telomeres which lack a functional Shelterin complex is markedly reduced in the absence of RIF1, illustrating that this protein is required for NHEJ (Chapman et al., 2013). As such, *Rif1*^{-/-} mouse models exhibit immunodeficiency due to their inability to develop sufficient immune diversity (Chapman et al., 2013, di Virgilio et al., 2013). RIF1 also regulates nucleolytic resection directly through crosstalk with the BRCA1-CtIP-MRN complex. During G1, when HR is inviable due to the absence of suitable template DNA, recruitment of this complex to damaged chromatin is antagonised by RIF1, preventing short-range resection by CtIP and MRE11 (Chapman et al., 2013, Escribano-Diaz et al., 2013, di Virgilio et al., 2013). Conversely, in late S and G2 phases, BRCA1 and its functional partner BARD1 overcome this block to resection by ubiquitination of histones at the DSB site, promoting the dissociation of 53BP1-RIF1 from the DNA and allowing nuclease access (Densham and Morris, 2017). Furthermore, CDK2-phosphorylated CtIP also impedes the interaction between 53BP1 and RIF1 (Zimmerman and de Lange, 2014).

As well as RIF1, several additional effectors of 53BP1 have been identified, including Pax transactivation domain interacting protein (PTIP) and REV7 (also known as MAD2L2). The precise role of PTIP in 53BP1-dependent DSB end protection remains to be fully elucidated; however, it is accepted that there is some redundancy between this factor and RIF1. Depletion of PTIP is sufficient to recapitulate a number of the defects associated with RIF1 deficiency, including an elevation in DSB end resection during G1 and NHEJ-mediated fusion of de-protected telomere ends (Zimmerman and de Lange, 2014). It is thought that PTIP acts via

ARTEMIS, an endonuclease with known functions in promoting NHEJ (Wang et al., 2014). REV7 has also been shown to promote NHEJ and inhibit HR in a 53BP1-dependent manner (Xu et al., 2015a, Boersma et al., 2015). It is now understood that the key function of REV7 is the recruitment of a distal 53BP1 effector complex known as Shieldin. This heterotrimeric complex, which comprises C20orf196 (SHLD1), FAM35A (SHLD2) and CTC-534A2.2 (SHLD3), was characterised independently in four recent CRISPR/Cas9 screens which aimed to identify novel 53BP1 interactors associated with PARPi resistance in BRCA1-deficient cells. REV7 facilitates the localisation of this complex to DSBs via its interaction with SHLD2, where it functions to shield DNA ends from unscheduled resection and promote repair of the lesion by NHEJ (Gupta et al., 2018a, Dev et al., 2018, Findlay et al., 2018, Noordermeer et al., 2018).

Pathways that negatively regulate resection independently of 53BP1 have also been identified. For instance, the helicase HELB suppresses long-range DNA resection during G1 via a feedback inhibition mechanism. HELB is recruited to tracts of resected ssDNA through its interaction with RPA; at high nuclear concentrations, it limits resection by BLM, DNA2 and EXO1 via its 5'-3' translocase activity. During late S and G2 phases, CDK-mediated phosphorylation of HELB triggers its export from the nucleus, removing the obstacle to long-range resection. Indeed, forced maintenance of nuclear HELB during these phases abrogates DNA end resection. In contrast to 53BP1 and RIF1, HELB is not required for NHEJ in the context of CSR or the repair of IR-induced DSBs (Tkac et al., 2016). Nevertheless, due to its role in effecting cell cycle-dependent control of long-range resection, one may speculate that it contributes to the suppression of inappropriate HR.

Although nucleolytic resection of DSB ends has widely been viewed as a key point of distinction between HR and NHEJ, recent studies have indicated that this distinction may not be clear-cut. Canonical NHEJ may also proceed in a resection-dependent manner during G1, but this resection differs from that which takes place as a precursor to HR. Resection-dependent NHEJ is initiated by a PLK3-mediated CtIP-BRCA1 interaction and continues through EXO1, EXD2 and MRE11 exonuclease activity; the endonuclease activity of MRE11 is dispensable. Resection is then completed by ARTEMIS (Biehs et al., 2017).

1.6.4: Epigenetic control of repair pathway choice

Post-translational protein modifications are known to influence a host of cellular processes, including DNA repair pathway choice. Alongside phosphorylation, a spectrum of other post-translational modifications, such as methylation, acetylation, ubiquitination and SUMOylation, are also known to influence resection dynamics and repair pathway choice (Ceccaldi et al., 2016a).

As discussed in section 1.5.1, histone ubiquitination plays a key role in directing 53BP1 to sites of damaged chromatin during the early stages of DSB detection and signalling. Ubiquitination of H2AK15 by RNF168 occurs solely as a consequence of ATM/ATR signalling in response to DNA damage, allowing for the specific recruitment of 53BP1 to regions requiring repair (Zimmerman and de Lange, 2014).

Histone methylation also impacts on the recruitment of 53BP1. It has been known for some time that 53BP1 is preferentially recruited to di-methylated Histone H4K20 in pre-replicative chromatin to promote NHEJ during G1; it dissociates as cells enter S phase to allow HR in post-replicative chromatin, at which time there is homologous template material available to facilitate repair (Zimmerman and de Lange, 2014). Appropriate targeting of 53BP1 to damaged chromatin is crucial for the selection of optimal repair pathways, especially in S-phase cells which can contain tracts of both pre- and post-replicative chromatin (Simonetta et al., 2018). However, the precise mechanism underlying the regulated binding and dissociation of 53BP1 remained unknown until recently. Pellegrino and colleagues highlighted the importance of the H4K20^{Me2} mark, levels of which are close to saturation prior to DNA replication, as a signal for the recruitment of 53BP1 specifically to non-replicated chromatin. In this study, it was demonstrated that resection as a precursor to HR-mediated repair is at its most efficient in damaged chromatin where H4K20 di-methylation, and therefore 53BP1 localisation, is minimal. Artificial enhancement of H4K20^{Me2} by over-expression of the histone methyltransferase SET8 during S-phase restored 53BP1 recruitment and suppressed resection (Pellegrino et al., 2017). These results were corroborated by a second study, which further demonstrated that the two-fold dilution of H4K20^{Me2} after DNA replication triggers the dissociation of 53BP1 and its downstream effectors from damage sites in post-replicative chromatin, thereby allowing access by BRCA1 to promote resection (Simonetta et al., 2017).

Whilst the CDK-mediated phosphorylation of CtIP is well characterised as a means of influencing DSB repair dynamics in a cell cycle-dependent fashion (as discussed in section 1.6.1), further studies have also implicated other modifications of CtIP in the fine-tuning of DSB end resection. NEDDylation involves the conjugation of NEDD8 to lysine residues in substrate proteins and has known functions in the DDR. The process is analogous to ubiquitination, requiring a chain of E1, E2 and E3 enzymes to transfer the modifying peptide to its target protein. NEDDylation has been proposed as a determinant of repair pathway choice through the control of CtIP-dependent resection. This resection is up-regulated in the presence of small molecule inhibitors of NEDDylation; furthermore, the interaction between CtIP and BRCA1 appeared to be compromised in these conditions (Jimeno et al., 2015). In contrast, constitutive SUMOylation (the conjugation of the small peptide SUMO onto target proteins) of CtIP at lysine 896 by the E3 SUMO ligase CBX4 has been shown to be essential for CtIP-dependent resection (Soria-Bretones et al., 2017).

1.7: Human diseases arising from a defective DNA damage response

A functional DDR is fundamental to the successful passage through the cell cycle and the maintenance of genome stability. As would therefore be expected, a multitude of human diseases can be attributed to mutations in key components of the DDR. A selection of relevant examples will be outlined below.

1.7.1: Ataxia telangiectasia

Ataxia Telangiectasia (A-T) was described in the mid-20th century as an autosomal recessive syndrome involving progressive decline of neurological function. Affected individuals display unusual gait and posture due to loss of muscular co-ordination (ataxia) along with prominent dilation of capillaries in the sclera of the eyes and elsewhere on the face (telangiectasia). Additional typical features include growth retardation, predisposition to lymphoid cancers and a high frequency of respiratory tract infection due to immunodeficiency; furthermore, there is increased radiosensitivity at the cellular level (Boder and Sedgwick, 1958, Taylor et al., 1975, Taylor and Byrd, 2005).

A-T is clinically heterogeneous; this likely reflects the fact that over 400 causal mutations in *ATM* have been identified. Eighty-five percent of these are bi-allelic mutations. In the majority of cases, these mutations result in a reduction of functional ATM protein to negligible levels (Ball and Xiao, 2005, Savitsky et al., 1995). However, some patients (such as those with a heterozygous mutation in *ATM*) have residual levels of functional protein, which is typically associated with reduced disease severity (Taylor and Byrd, 2005).

ATM is a master regulator of the DDR, and of DSB repair in particular; this explains the marked increase in kinase activity in wild-type cells exposed to IR relative to untreated cells, and the profound sensitivity to this agent in A-T patient-derived cells. The dysregulation of the DDR in the absence of functional ATM underlies all phenotypic manifestations of A-T (Taylor et al., 1975, Ball and Xiao, 2005). The reduced growth rate frequently observed in A-T patients results

from unresolved DNA damage combined with the failure of the G1-S, S-phase and G2-M checkpoints (refer to figure 1.6). Patients also exhibit increased cancer predisposition due to constitutive genome instability arising from impairment of the DDR. Immunodeficiency in affected individuals can be attributed to an inability to repair physiologically programmed DSBs during the process of V[D]J recombination, which is a pre-requisite for the generation of immune diversity (Taylor and Byrd, 2005, Ikuta *et al.*, 1986). Furthermore, it was recently suggested that the predominantly cytoplasmic localisation of ATM in post-mitotic cells, such as neurons, may account for the progressive neurological symptoms observed in A-T patients. This localisation allows for the association of ATM with organelles which produce reactive oxygen species (ROS), which may play a role in neurodegeneration. Indeed, increased levels of oxidative stress were observed in brains of Atm-deficient mice (Choy and Watters, 2018).

Confirmation of a clinical diagnosis of A-T involves the exposure of patient-derived cells to IR and assessing levels of ATM protein by immunoblotting. Increased sensitivity to radiation along with negligible ATM protein levels are reliable indicators of the disease. Sequencing of the *ATM* gene to identify the associated mutations is usually performed as a secondary step, and an ATM kinase activity assay can provide additional verification in the rare instances when ATM protein levels are close to normal (Taylor and Byrd, 2005).

1.7.2: A-T-like disorder

A-T-like disorder is an incredibly rare DDR-linked disorder, with only a handful of cases reported internationally. Patients exhibit many features typically associated with A-T, including

cerebellar ataxia (albeit with a later onset than for classical A-T), cellular radiosensitivity and an impairment of DDR signalling. Notably, telangiectasia are absent, and patients are immunocompetent with respect to levels of total IgG, IgA and IgM (although some specific functional antibodies may be deficient) (Taylor et al., 2004).

In some of the first reported instances, patients identified from two families were diagnosed with an A-T-like disorder (ATLD) based on clinical presentation. None of the patients had mutations in ATM; furthermore, all had normal ATM protein levels. Sequencing of the components of MRN complex (MRE11, RAD50 and NBS1), which also play a role in early-stage sensing of DSBs along with ATM (van den Bosch et al., 2003), revealed truncating and missense mutations in MRE11 and reduced levels of all proteins; this distinguished this disorder from classical A-T at the molecular level. The identified mutations were shown to compromise the interaction of MRE11 with other members of the MRN complex, but did not abrogate these interactions entirely (Stewart et al., 1999).

Examinations of the phenotypic manifestations of ATLD at the cellular level have revealed multiple similarities to A-T, as well as a number of key contrasts. As for A-T patient-derived cells, ATLD cells exhibit an increased sensitivity to IR, but this is not due to a major DDR defect. ATLD patient cells are also unable to suppress DNA synthesis after IR exposure as the S-phase DNA damage checkpoint is inactive; notably, however, the impact of MRE11 mutations on the functionality of this checkpoint is less pronounced than for ATM mutations. Additionally, there is reduced IR-induced activity of stress-activated protein kinases (SAPKs) in ATLD patient-

derived cells. Conversely, the induction of p53 following exposure to γ irradiation is normal in ATLD, whereas radiation-induced p53 induction is impaired in cells carrying a mutation in ATM. Furthermore, immunofluorescence microscopy analyses have demonstrated that ATLD cells show negligible recruitment of the MRN complex to IR-induced lesions in ATLD patient cells; MRN focus formation in cells exposed to IR is unaffected in ATM patient-derived cells (Stewart et al., 1999, Taylor et al., 2004).

1.7.3: Nijmegen breakage syndrome

Nijmegen breakage syndrome (NBS) is a rare disease inherited in an autosomal recessive manner, and is caused by bi-allelic mutations in NBS1. This gene was formerly termed p95 and had already been shown to encode a DDR-associated protein that interacts with MRE11 and RAD50 (Chrzanowska et al., 2012, Carney et al., 1998). *NBS1* maps to chromosome 8q and encodes a 754 aa protein. Screening of *NBS1* in multiple patients of Slavic and German ethnic origin revealed a 5 bp deletion. This mutation generates an erroneous stop codon at position 218, leading to severe polypeptide truncation (Chrzanowska et al., 2012, Matsuura et al., 1998); this underlies the absence of full-length NBS1 protein in patient cells.

NBS is characterised by microcephaly identified at birth, along with other features that become apparent with age: a mild extra-uterine growth delay, recurrent infections due to immunodeficiency, a predisposition to early-onset malignancies, especially haematological cancers, and a potential decline in cognitive function. At the cellular level, patient-derived cells exhibit heightened sensitivity to IR, chromosomal inversions and translocations and

chromosomal breakage in unperturbed cells; this is accompanied by the failed suppression of DNA synthesis after IR and the absence of full-length NBS1 protein (Taalman et al., 1983, Chrzanowska et al., 2012).

The first affected individuals identified were 2 members of same Dutch family who presented with microcephaly at birth, subsequent growth delay, cognitive impairment, immunodeficiency and café-au-lait spots on the skin. Cytogenetic analyses of patient lymphocytes revealed reciprocal chromosomal translocations centred around the common fragile sites of chromosomes 7 and 14, as well as spontaneous chromosome breakages. Immunodeficiency was observed in both individuals (Weemaes et al., 1981).

Whilst the clinical presentations were acknowledged to be strikingly similar to those of other known syndromes involving chromosomal breakage, these diagnoses were ruled out on the basis of clinical and cytogenetic observations. Firstly, the lack of skeletal abnormalities or pancytopenia distinguished this disease from FA. A-T was also ruled out clinically due to the absence of ataxia or telangiectasia. Finally, a diagnosis of Bloom syndrome was ruled out. Quadriradial chromosomes are characteristic of Bloom syndrome, but were absent in the Dutch patients. It was concluded that a novel syndrome had been identified; this was designated Nijmegen breakage syndrome (NBS) (Weemaes et al., 1981).

1.7.4: DNA-PKcs severe combined immunodeficiency

Severe combined immunodeficiency (SCID) arises due to the failed differentiation of B and T lymphocyte lineages (Bosma et al., 1983). It has been demonstrated in multiple animal models as well as in humans that this disorder can be attributed to C-terminal deletions in the catalytic sub-unit of DNA-PK (DNA-PKcs). These mutations compromise the functionality of the holoenzyme, impairing NHEJ in the context of V[D]J recombination: a requirement for the generation of immune diversity. Defective V[D]J recombination has consistently been implicated in the development of SCID (Meek et al., 2001, Bosma et al., 1983, Wiler et al., 1995). Conversely, there is no consensus regarding the potential importance of DNA-PKcs in CSR within this context. A recent study proposed that DNA-PKcs mutations also underlie CSR defects in SCID patients (Bjorkman et al., 2015); however, this conflicted with multiple earlier studies which suggested that DNA-PKcs does not function in this process (Bosma et al., 2002, Kiefer et al., 2007).

As would be expected, the failure to generate sufficient immune cell diversity across multiple lineages results in profound immunodeficiency, with affected individuals frequently succumbing to opportunistic infections during childhood. Patients also exhibit a predisposition to the development of cancers, neurological defects and hypersensitivity to radiation at the cellular level (Morio, 2017).

1.7.5: Cancer

Perhaps the most frequently cited example of a human disease associated with defective DNA repair is cancer, with genomic instability being one of the defining hallmarks of this complex disease (Lengauer et al., 1998, Jackson and Bartek, 2009). Therefore, a functional DDR can be regarded as an anti-tumour barrier to reduce the frequency of malignant cellular transformations. Tumour cells typically exhibit gross chromosomal rearrangements (GCRs), missense/nonsense mutations, and gene deletions/amplifications (Lengauer et al., 1998), all of which can arise following progression through the cell cycle with unrepaired DNA damage. DDR defects are characteristic of many, if not most, tumour cells. Furthermore, these cells proliferate more rapidly than normal cells. Upon exposure to chemotherapeutic agents, a high proportion of tumour cells are in S phase, during which cells are most vulnerable to DNA damage. Catastrophic levels of DNA damage are induced, and tumour cells are unable to repair this damage effectively (Jackson and Bartek, 2009).

Interestingly, a link has been proposed between BOD1L and cancer. As will be discussed further in section 7.4.2, a number of mutations in BOD1L – mainly in the N-terminus – are associated with chronic lymphocytic leukaemia (CLL) as well as myelodysplasia, which is a precursor to the development of this cancer (Dr. Martin Higgs and Prof. Tatjana Stankovic, unpublished). This further highlights the critical role of the DDR in suppressing cancer development.

1.8: Therapeutic opportunities within the DNA damage response

The DDR provides a wealth of therapeutic opportunities, particularly for the treatment of cancer. Typical approaches involve targeting DDR pathways with inhibitors and/or harnessing the inherent hypersensitivity of cancerous tissues to DNA-damaging agents, many of which have defective DNA repair pathways (Jackson and Bartek, 2009). Despite numerous advances, this remains an area of extensive research; the development of drug resistance due to restoration of repair pathways and toxicity in healthy tissues are challenges that must be overcome. Current successful strategies for DDR-related treatment approaches, future perspectives and remaining challenges are summarised below.

Genomic instability in cancer arises through a combination of accumulated DNA damage, impaired DNA repair capacity and the inappropriate transition of cells through cell cycle prior to the completion of repair (Lord and Ashworth, 2012, Lengauer et al., 1998). DNA-damaging agents as therapy may therefore have a more profound impact on tumour cells than on the surrounding unaffected tissue. Non-surgical avenues for treatment of cancer typically involve the use of DNA-damaging agents, which can be divided into several classes. Radiotherapy (such as ionising radiation) and radiomimetic drugs generate single- and double-stranded breaks in the DNA; furthermore, the reactive oxygen species (ROS) released upon exposure to radiation can damage DNA bases. Alkylating drugs, such as Mitomycin C, engender replication stress due to the generation of bulky adducts on the DNA (Jackson and Bartek, 2009). DNA replication inhibitors also impede replication and lead to chronic replication stress by various means. Aphidicolin, for example, inhibits DNA polymerase α (Krokan et al., 1981), whereas hydroxyurea

functions by depleting the pool of available nucleotides (Mehta and Haber, 2014). Replication inhibitors can also induce chromosomal damage during S-phase. Topoisomerase inhibitors, such as the TopoI inhibitor Camptothecin, trap topoisomerase in enzyme-DNA complexes, impeding replication and generating single-ended DNA breaks. Finally, a class of agents known as antimetabolites inhibit appropriate base pairing, resulting in base damage and S-phase lesions, which may prove irreparable in DDR-deficient cancer cells (Helleday et al., 2008).

Exploiting the known DNA repair defects present in many cancers through the use of DDR inhibitors can allow for the targeted impairment of malignant cells due to synthetic lethality. Conversely, the impact on healthy tissue is minimal due to compensation by alternative repair pathways; as such, these treatments are associated with reduced side effects compared to DNA damage inducers (Helleday et al., 2008). A key clinical example is the use of poly(ADP ribose) polymerase inhibitors (PARPi). Whilst there is no consensus as to the mechanisms of PARPi activity in tumour cells, two possible scenarios are that sensitivity to PARPi arises due to the persistence of unrepaired spontaneous lesions or through the maintenance of PARP at sites of DNA damage (Pears et al., 2012, Lord and Ashworth, 2012, Helleday et al., 2008, D'Andrea, 2018). The clinical applicability of PARPi has been demonstrated in HR-deficient cancers, such as BRCA1- or BRCA2-mutated breast and ovarian cancers or those with defects in proteins associated with recombination (Helleday et al., 2008). Furthermore, inhibitors of other fundamental DDR components, including ATM, ATR, CHK1 and DNA-PKcs, are undergoing development for clinical application (O'Connor, 2015). A recent study also demonstrated that CtIP-deficient cells are hyper-sensitive to PARPi; as the expression of this key nuclease is often

down-regulated in breast cancer, this may provide novel therapeutic opportunities in the future (Wang et al., 2015b).

The key challenges associated with harnessing DDR pathways or deficiencies for therapeutic ends are the possibility of off-target effects and the development of resistance to treatments. Bone marrow suppression is commonly associated with chemotherapeutic regimens (particularly those incorporating DNA-damaging agents) due to the rapid rate of cellular proliferation in the bone marrow (Helleday et al., 2008). This has obvious implications for immune competence. Moreover, IR, to which approximately 40% of positive patient outcomes can be attributed, generates considerable numbers of SSBs and DSBs in healthy tissues as well as cancerous cells. This side effect underlies the dose-limiting toxicity of this agent (O'Connor, 2015). As discussed above, however, progress has been made in this area following the clinical introduction of DDR inhibitors as monotherapies.

In addition, the development of treatment-resistant malignancies remains an ongoing problem. For instance, acquired resistance to PARPi has been widely studied. Broadly, the mechanisms of resistance in BRCA1- and BRCA2-deficient tumours are based upon the restoration of HR or the development of reliance on alternative pathways for replication fork protection; these mechanisms are intrinsically linked to the key functions of BRCA1 and BRCA2 in the DDR. Firstly, HR restoration can arise due to secondary mutations in BRCA1 or BRCA2, an altered methylation status of the BRCA1 promoter which triggers a shift from low to high protein expression, or the loss of 53BP1-dependent DNA end protection, which leads to the up-

regulation of resection. It has been known for some time that secondary loss of 53BP1 in BRCA1-deficient cells restores HR, resulting in resistance to PARPi (D'Andrea, 2018). Recent studies have demonstrated the importance of the Shieldin complex, a distal 53BP1 effector, in DNA end protection; loss of any component of this trimeric complex leads to PARPi resistance (Dev et al., 2018, Gupta et al., 2018a, Noordermeer et al., 2018, Findlay et al., 2018, D'Andrea, 2018). Secondly, the up-regulation of ATR/CHK1-dependent replication fork protection pathways also confers resistance to PARPi by compensating for loss of BRCA1- and BRCA2-dependent fork protection (Edwards et al., 2008, Sakai et al., 2008).

There is growing interest in combining DDR inhibitors with conventional chemotherapy or DNA-damaging agents in order to increase the efficacy of these treatments. Clinical trials are already underway for a number of regimens. PARP inhibitors, for example, have been trialled in combination with systemic platinum-based chemotherapy or alkylating agents, and ATR inhibitors are being tested alongside chemotherapy or Olaparib. These novel approaches may be applicable to multiple types of tumour (O'Connor, 2015), Helleday et al., 2008). Furthermore, a recent study yielded promising results with the use of KU60648, an inhibitor of DNA-PKcs, as a radiosensitiser in osteosarcoma cells (Mamo et al., 2017). However, there are several key questions to address when designing combined treatment plans. The optimal dosages and timings of exposure to DNA-damaging agents and potential sensitisers will need to be determined. Additionally, any variability in the efficacy of the sensitising agent in different genetic backgrounds must be identified. Finally, the impact of combined therapies on normal tissue will be a key consideration (O'Connor, 2015, Helleday et al., 2008). Such informed

management approaches may facilitate patient stratification and the selection of appropriate treatments based on predicted responses to maximise the likelihood of positive outcomes.

1.9: BOD1L

The DDR remains the subject of intensive investigation; scores of novel players are identified each year, and the complex network of pathways is gradually being elucidated. However, there are undoubtedly many factors which remain to be investigated. In this context, my laboratory recently demonstrated that BOD1L plays a key role in the resolution of replication stress. Below, I will describe the findings of this study and outline our current understanding of BOD1L.

A diverse array of proteins involved in combating replication stress is recruited to replication forks during DNA replication. Examination of the proteomic content of nascent chromatin therefore provides a useful means of identifying novel factors associated with the DDR. One technique for achieving this is iPOND (isolation of proteins on nascent DNA) (Sirbu et al., 2012). To identify novel replication stress responders, an iPOND screen was undertaken by our laboratory, modified to overcome the sensitivity of many proteins to the standard conditions. iPOND involves the labelling of newly-replicated DNA with the thymidine analogue EdU (ethynyldeoxyuridine), using a Click reaction to link biotin-azide to EdU-labelled DNA, and the purification of nascent DNA and associated proteins using Streptavidin-agarose beads. These proteins can then be resolved by SDS-PAGE and characterised by mass spectrometry (Higgs et al., 2015, Sirbu et al., 2012). As well as components of the replication machinery, this screen

also revealed a previously uncharacterised factor, Biorientation defect 1-like (BOD1L), which was subsequently shown to play a role in the maintenance of genome stability during replication stress. Furthermore, BOD1L was designated as a novel FA-like gene in the ATR/FA pathway (Higgs et al., 2015).

1.9.1: Structural and preliminary functional detail

BOD1L is a 3051 aa protein, named for the sequence similarity of its N-terminal domain to the mitotic spindle regulator BOD1 (figure 1.7). Within its amino acid sequence are 5 confirmed target sites for ATM/ATR phosphorylation, as well as numerous other putative ATM/ATR phosphorylation motifs. It was therefore hypothesised that BOD1L may be involved in the DDR.

BOD1 is a highly-conserved protein that localises to kinetochores and spindle poles at mitosis and plays vital roles in chromosome biorientation at the metaphase plate (Porter et al., 2007). Using siRNA-mediated depletion, Higgs and colleagues demonstrated that despite the similarity between the sequences of BOD1 and BOD1L (figure 1.7), there was no overlap in the functions of the two proteins. Hyper-phosphorylation of H2AX and RPA2 was observed upon knockdown of BOD1L, indicating an elevation in DNA damage signalling and nucleolytic resection of DNA lesions, respectively; in contrast, loss of BOD1 resulted in severe spindle alignment defects (Higgs et al., 2015).

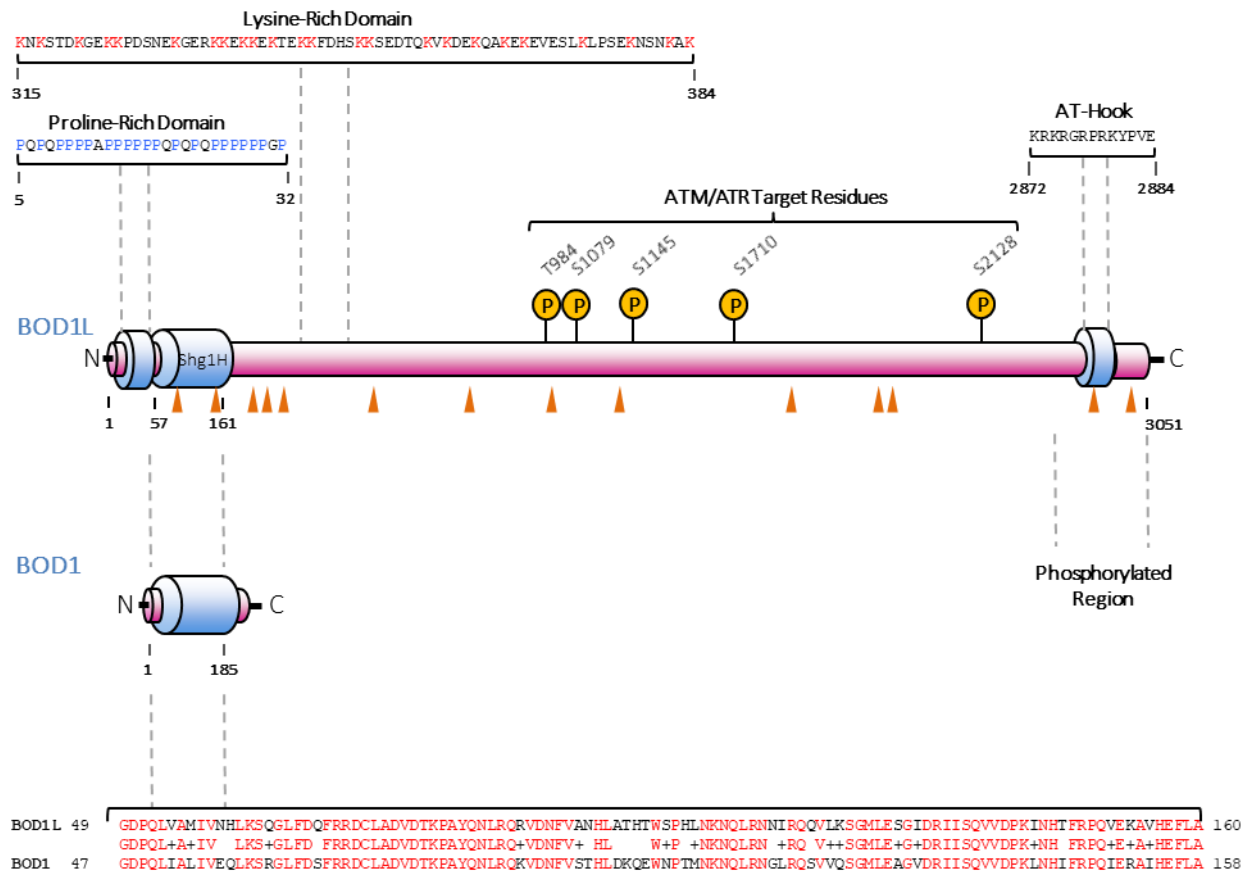


Figure 1.11: Structural details of BOD1L.

Schematic diagram of the human mitotic spindle regulator BOD1 and BOD1L structures, illustrating regions of sequence homology. Confirmed ATM/ATR phosphorylation target sites are shown above the structure; additional putative targets are denoted with arrowheads below the structure. Other potential domains are also shown.

1.9.2: Characterisation as a fork protection factor

In agreement with the iPOND data, which suggested a role for BOD1L at replication forks, subsequent experiments using a variety of techniques confirmed that BOD1L was required to resolve replication stress. DNA fibre analysis was used to examine the progression of ongoing forks after exposure of cells to HU. Opposing forks from the same origin typically progress at similar rates; as such, disparities between these rates can indicate problematic re-start or increased fork stalling (Conti et al., 2007, Rodríguez-López et al., 2002). BOD1L-deficient cells were shown to exhibit a marked increase in the asymmetry of sister replication forks upon treatment with HU, suggesting that BOD1L is required for the re-starting and/or progression of replication forks. Moreover, BOD1L-depleted cells subjected to replication stress exhibited an increase in nucleolytic resection of stalled forks, as evidenced by an increase in both RPA2 and RPA-P (S4/S8) foci (Higgs et al., 2015).

Furthermore, cells treated with BOD1L siRNA showed severe impairment of MMC-induced RAD51 focus formation. In addition to its role in HR-mediated repair pathways, RAD51 is known to stabilise damaged replication forks to ensure they can be repaired and re-started (Costanzo, 2011). Interestingly, MMC-induced RAD51 foci formation could be re-established in BOD1L-depleted cells by co-depletion of either BLM or FBH1: two helicases which inhibit RAD51-dependent pathways of DNA repair. This co-depletion also reduced levels of RPA-P (S4/S8) foci, showing that over-resection of stalled replication forks had been alleviated. This led to the conclusion that BOD1L stabilises RAD51 at stalled forks through the inhibition of BLM and FBH1 (Higgs *et al.*, 2015).

Assessments of fork resection by DNA fibre analyses supported the role of BOD1L as a fork protection factor. Sequential pulsing of replicating cells with the thymidine analogues CldU and IdU, treatment with HU and measurements of the relative length of each labelled tract of ssDNA allowed for quantification of fork degradation during replication stress. A decrease in the ratio of the two labels to less than 1 would be indicative of increased fork resection. In the absence of BOD1L, the mean IdU:CldU ratios were reduced to levels comparable with those observed in BRCA2-depleted cells. Since BRCA2 is essential for the loading and stabilisation of RAD51 onto ICLs during replication stress (Godthelp et al., 2006), this was taken as a further indication of fork degradation in the absence of BOD1L. Notably, ratios were restored to control levels by the depletion of DNA2, but not by the inhibition of MRE11 with Mirin. This led Higgs and colleagues to conclude that BOD1L-mediated stabilisation of RAD51 at stalled forks prevents excessive DNA2-mediated resection of stalled replication forks; however, MRE11 does not play a role in aberrant fork resection in the absence of BOD1L. As a consequence, forks remain competent for repair and genome stability is maintained (Higgs et al., 2015). This model is summarised in figure 1.8.

It is interesting to note that no equivalent defect was observed for IR-induced DNA damage, suggesting that there was no overall defect in the recruitment of RAD51, but a problem with the stabilisation of the protein specifically at replication forks.

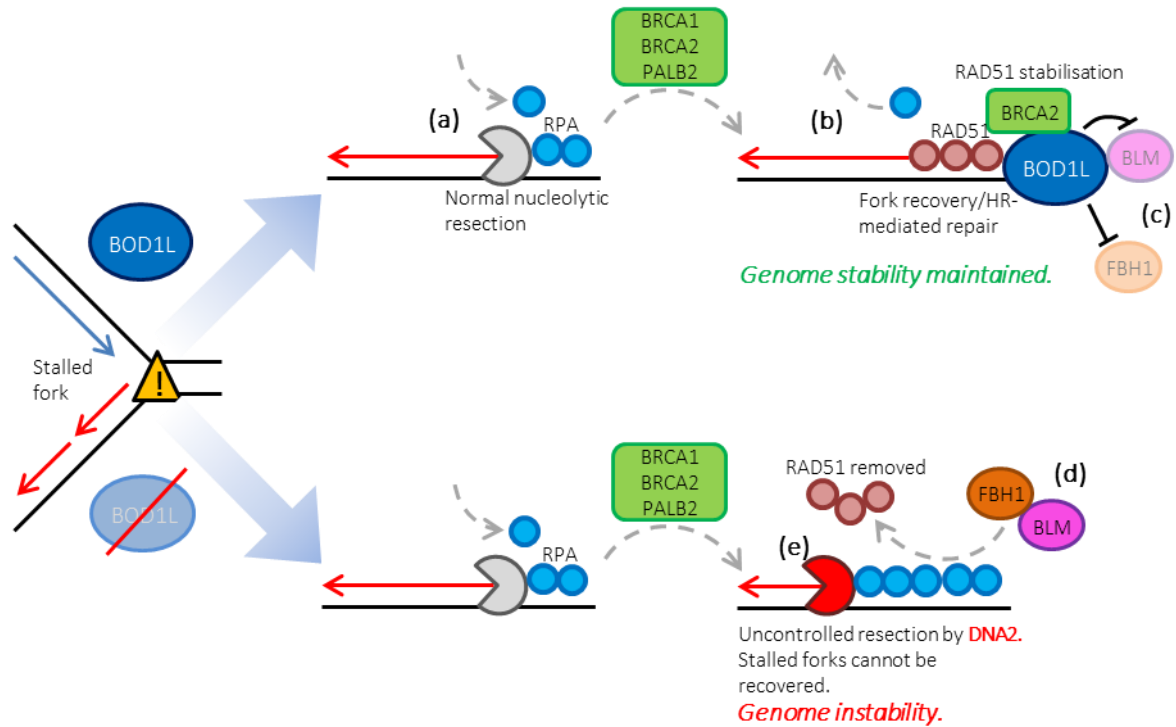


Figure 1.12: Model for BOD1L-mediated protection of stalled replication forks.

In the event of an obstacle to the progression of replication, stalled forks undergo regulated nucleolytic resection as a precursor to repair by homologous recombination (a). RPA is loaded onto the exposed ssDNA. The activities of BRCA1, BCRA2 and PALB2 facilitate the displacement of RPA (b), allowing RAD51 to be loaded. The stability of the resultant RAD51 nucleofilaments is maintained by BOD1L through the inhibition of BLM and FBH1 (c). Forks are repaired by HR and genome stability is maintained. When BOD1L is lost, FBH1 and BLM remove RAD51 from stalled forks (d), permitting unrestricted nucleolytic processing by DNA2 (e). These forks are thus rendered irreparable. Unrepaired forks, in combination with elevated levels of new origin firing, result in genome instability. Adapted from Higgs *et al.*, 2015.

Furthermore, cells depleted of BOD1L exhibited an increase in micronuclei formation, ultra-fine bridges (UFBs) early in mitosis (which are indicative of improperly replicated DNA), chromosomal breakage and 53BP1 body formation, all of which are characteristic manifestations of unresolved replication stress. Importantly, restoration of the observed chromosomal damage to control levels was achieved when murine Bod1l was stably expressed to complement loss of the endogenous protein (Higgs et al., 2015).

1.9.3: Characterisation as a member of the FA pathway

During the course of their studies on BOD1L, Higgs and colleagues also demonstrated that the depletion of BOD1L phenocopied loss of FANCA, a core component of the Fanconi Anaemia pathway. Moreover, as is characteristic of cells deficient in FA pathway members, exposure of BOD1L-depleted cells to the ICL inducer MMC led to severe chromosomal breakage. These observations suggested that BOD1L acts in the FA pathway and is required for an effective cellular response to replication stress (Higgs et al., 2015). Indeed, BOD1L has been proposed as an FA-like factor in recent reviews (D'Andrea, 2018), despite the fact that no mutations in BOD1L have been discovered to date in patients with an FA-like disorder.

1.10: Thesis aims

Robust DNA damage repair mechanisms are critical to the maintenance of genome stability. Earlier published work by Higgs and colleagues identified BOD1L as a previously

uncharacterised factor with a key role in maintaining genome stability through the protection of stalled replication forks during replication stress. BOD1L was shown to participate in the repair of S-phase DNA damage by preventing spurious resection of stalled forks (Higgs et al., 2015). However, prior to the commencement of my doctoral studies, the potential role of BOD1L in the response to other forms of DNA damage had not been explored. This provided the basis for my investigations.

The first aim of my thesis was to determine whether BOD1L also functioned in other aspects of the DDR. Numerous proteins involved in the prevention of replication stress-induced DNA damage also contribute to the repair of DSBs; I therefore hypothesised that BOD1L may also function in the resolution of these lesions. I initially focused on DSBs inflicted by IR, a potent inducer of this type of DNA damage. Given its demonstrated role in the suppression of stalled fork resection, I next investigated the hypothesis that BOD1L performed an analogous function at IR-induced DSBs.

Nucleolytic resection of DSBs is tightly regulated to ensure appropriate DSB repair pathway selection. Key pathways have evolved to antagonise resection in situations where homologous recombination-mediated repair would be inviable. I therefore considered the possibility that BOD1L may suppress inappropriate DSB resection via interactions with 53BP1 or its downstream effectors, as these factors are among the most well-characterised resection antagonists. Insights from an ongoing collaboration with Prof. Simon Boulton led me to focus on a potential interaction between BOD1L and RIF1.

Finally, I sought to extend the characterisation of BOD1L's role further by examining its importance in the repair of DSBs induced by Camptothecin. This TopoI inhibitor generates single-ended DSBs in S-phase, which bear structural similarities to stalled replication forks as well as IR-induced double-ended DSBs.

Chapter 2: Materials and Methods

2.1: General Reagents and Equipment

Laboratory chemicals were purchased from Sigma or Thermo Fisher Scientific, except where otherwise stated. Kits for isolation of plasmid DNA from bacterial cultures were obtained from Invitrogen (Thermo Fisher Scientific). Purified 18 Ω water was used for all experimental procedures.

Centrifugation (with the exception of cell culture samples) was performed in Grant benchtop micro-centrifuges or an Allegra X-30R fitted with either SX4400 or F0630 rotors (Beckman Coulter).

Menzel Gläser Superfrost® microscope slides and 12 mm coverslips were purchased from Thermo Fisher Scientific.

2.2: Antibodies

Commercial primary antibodies were sourced from Abcam or Bethyl Laboratories Inc., unless stated otherwise. The antibody against BOD1L was generated as a custom order and the anti-CtIP antibody was produced in the laboratory from a hybridoma cell line. Secondary antibodies (Alexa Fluor 594-conjugated anti-mouse IgG and Alexa Fluor 488-conjugated anti-rabbit IgG)

were obtained from Life Technologies. Table 2.2 provides full details of all antibodies with relevant dilutions.

2.3: Mammalian cell culture

2.3.1: General culture protocols

HeLa and U-2-OS cell lines were obtained from ATCC and maintained at 37 °C with 5 % CO₂ in a humidified incubator. HeLa cells were cultured in Dulbecco's Modified Eagle Medium (DMEM) with L-glutamate supplemented with 10 % (v/v) foetal bovine serum (FBS) and 1 % (v/v) Penicillin/Streptomycin solution (from stock containing 10,000 units/ml Penicillin and 10,000 µg/ml Streptomycin). U-2-OS cells were maintained in McCoy's 5A medium with 10 % (v/v) FCS.

All tissue culture plastic-ware was supplied by Corning and cell culture media and solutions by Gibco (Life Technologies). Cryo-vials were obtained from Greiner Bio-One. For cell culture, centrifugation steps were carried out in an Allegra X-12 centrifuge with SX4750 rotor (Beckman Coulter). Unless otherwise stated, centrifugation steps were performed at room temperature.

Cultures were passaged sufficiently to maintain sub-confluent conditions. After aspiration of media, cells were washed in phosphate-buffered saline (PBS) before incubation at 37 °C with TrypLE™ Express cell dissociation reagent for 3-5 min. Flasks were tapped to release adherent

cells before the addition of appropriate fresh media. A proportion of the suspension (typically 1/15 for HeLa and 1/10 for U-2-OS) was then transferred to a new flask containing fresh media.

After a maximum of 20 passages, cultures were replaced with new cells retrieved from short-term storage at -80 °C. Vials of cells were thawed rapidly before being transferred to fresh T75 flasks containing appropriate medium, pre-warmed to 37 °C. After 4-6 hours, the thawed cells were examined; once adhering to the flask, the medium was aspirated and replaced with fresh pre-warmed medium after a wash with PBS.

For storage, cells in confluent T75 flasks were washed in PBS and treated with cell dissociation reagent as described above. The suspension was diluted with appropriate fresh media and centrifuged at 1,600 rpm for 4 min to collect the cells as a pellet. The pellet was re-suspended in PBS and the centrifugation step repeated. The pellet was then re-suspended in freezing medium comprising appropriate cell medium (DMEM or McCoy's 5A) with 10% FCS and 10% dimethyl sulphoxide (DMSO). Cells were frozen without antibiotics. The contents of each confluent T75 were frozen in 2 Cryo-vials, each containing 1 ml cell suspension. Tubes were transferred to Nalgene™ Cryo freezing containers for controlled cooling to -80 °C. For short-term storage (up to 6 months), tubes were retained at -80 °C; long-term stocks were also maintained in liquid nitrogen.

2.3.2: Transfections

Custom and SMARTpool™ siRNA was obtained from Dharmacon (Horizon Discovery Ltd.)

Further details, including custom siRNA sequences, are provided in table 2.1.

To perform RNAi-mediated knockdowns, 5×10^5 cells were plated into 60 mm dishes to achieve 40-60% confluence at the point of transfection. HeLa cells were plated and maintained at 37 °C for 4 h prior to transfection. siRNA transfections were carried out with Oligofectamine reagent in Opti-MEM reduced serum medium according to the manufacturer's standard protocol. siRNA was used at a final concentration of 100 nM for single transfections or 50 nM per target for multiple transfections (for which the optimal concentrations were determined by titration and Western blotting). Details of specific siRNA are provided in table 2.1.

Eighteen hours post-transfection, the cells were rescued after by adding DMEM with 20% FCS to the dishes. For U-2-OS, cells were transfected 24 h after plating and rescued 4-6 h post-transfection by complete replacement of the transfection medium with fresh culture medium (as described in section 2.3.1). Unless otherwise stated, all experiments were performed 72 h post-transfection.

For plasmid transfections, Lipofectamine 2000 was used in accordance with the manufacturer's standard protocol. In brief, the required quantity of plasmid DNA was diluted in Opti-MEM

Table 2.1: Details of siRNA

siRNA Target	Supplier	Catalogue No./Sequence
Control	Dharmacon	D-001810-10
BOD1L	Dharmacon	L-017033-02
BLM	Dharmacon	L-007287-00
BRCA1	Dharmacon	L-003461-00
CtIP	Dharmacon (Custom)	GCUAAAACAGGAACGAAUC[dT]
DNA2	Dharmacon	L-026431-01
EXO1	Dharmacon	L-013120-00
MRE11	Dharmacon	L-009271-00
RAD52	Dharmacon	L-011760-00
RIF1	Dharmacon	L-027983-01

References: BOD1L – Higgs *et al.*, 2015. RIF1 – Chapman *et al.*, 2013. The Control siRNA is a pool of 4 non-targeting siRNAs, engineered with a minimum of 3 mismatches to any human protein-coding gene and modifications to both strands to reduce potential off-target effects.

reduced serum medium. Lipofectamine 2000 was diluted separately in Opti-MEM and the diluted reagents were incubated at room temperature for 5 min before being combined and incubated for a further 25 min. Transfection complexes were applied to cells at approximately 60% confluence. Transfections were carried out in antibiotic-free medium appropriate to the cell line (prepared as described in section 2.2.1 but omitting Penicillin/Streptomycin). Following incubation (3-6 h for U-2-OS cells or overnight for HeLa), the transfected cells were rescued by replacement of the transfection medium with standard culture medium. Cells were washed twice in standard medium after aspiration of the transfection media to remove traces of Lipofectamine 2000.

Twenty-four hours prior to experimental treatments, cells to be analysed by SDS-PAGE and immunoblotting were re-plated into 100 mm culture dishes to achieve 90-100% confluence at the point of harvesting.

2.3.3: Treatment with DNA damaging agents and chemical inhibitors

To permit cell cycle-specific immunofluorescence microscopy analyses, coverslips were treated with 3 μ M Aphidicolin for 40 minutes immediately prior to the induction of DNA damage.

To induce DSBs, cells were irradiated with a dose of 3 Gy (unless otherwise stated). Irradiated and non-irradiated control cells were returned to the incubator and maintained at 37 °C until they were harvested at the required time points for analyses.

Alternatively, cells were treated with 1 μ M Camptothecin for 1 h at 37 °C and then harvested immediately for analysis by Western blotting and immunofluorescence microscopy (sections 2.5.1 and 2.7.1). For quantification of CPT-induced micronuclei, cells were treated as described above; after 1 h, the CPT was washed out and cells were cultured in standard growth medium for 24 h prior to harvesting.

To inhibit the exonuclease activity of MRE11, cells were treated with Mirin (in full: Z-5-(4-hydroxybenzylidene)-2-imino-1,3-thiazolidin-4-one) at a final concentration of 50 μ M (Dupré et al., 2008). This treatment was applied for 40 min prior to the induction of DNA damage.

2.4: Clonogenic survival assays

Twenty-four hours after siRNA transfections, cells were re-suspended and counted using a haemocytometer slide. Serial dilutions were prepared and used to seed four 60 mm dishes per conditions.

Twenty-four hours after plating at low density, the cells were treated with IR or CPT and allowed to proliferate for 10-14 days in standard conditions. At the end of this period, the culture medium was removed by aspiration and surviving colonies stained with Crystal Violet solution for 5 min. After staining, dishes were washed once in PBS and 3 times in water before being

allowed to air-dry. The number of colonies per dish was then quantified manually, and the proportion of viable colonies was calculated.

2.5: Immunoblotting

2.5.1: Preparation of whole cell extracts (WCE)

Cells were harvested to prepare WCE by washing in PBS and treatment with cell dissociation reagent as described above. After dilution with fresh media, the suspension was centrifuged for 4 min at 1,600 rpm. The collected pellet was re-suspended in PBS and centrifugation was repeated. PBS was then removed by aspiration and pellets were snap-frozen in liquid nitrogen before storage at -80 °C. WCE were obtained by sonication of the thawed pellets in UTB buffer (8 M urea, 50 mM Tris, 150 mM β -mercaptoethanol) and clarified by centrifugation at 4 °C. Lysates were quantified using the Bradford protein assay according to standard protocols; 96-well plates were analysed on an iMark Microplate Absorbance Reader (Bio-Rad) with a bovine serum albumin (BSA) standard curve for reference. Quantified lysates were stored at -80 °C.

2.5.2: Analysis of WCE by SDS-PAGE and Western blotting

To prepare samples for immunoblotting, 50 μ g of WCE was denatured at 95 °C in Laemmli buffer for 10 min. Samples were loaded in duplicate (50 μ g protein per gel lane) onto denaturing polyacrylamide gels (6% v/v acrylamide with a 12% lower layer) along with a full range molecular weight marker (Amersham ECL Rainbow Marker, GE Healthcare). Proteins were resolved by electrophoresis at 25 mA per gel for 5 h.

Following electrophoresis, proteins were transferred to BioTrace™ NT nitrocellulose membrane (Pall Corporation) in standard transfer buffer (25 mM Tris, 192 mM Glycine, 20% methanol v/v). Membranes were probed with primary antibodies overnight at 4 °C; details of antibodies and concentrations are provided in table 2.2. After primary labelling, membranes were washed with TBS-T and incubated with horseradish peroxidase (HRP)-conjugated secondary antibodies for 1 h at room temperature. Following final washes with TBS-T, proteins were visualised using chemiluminescence with either Amersham™ ECL Western Blotting Detection Reagents (GE Healthcare) or Immobilon™ Western (Millipore) sensitive ECL systems and Amersham™ Hyperfilm chemiluminescent film (GE Healthcare) according to standard manufacturer protocols. Exposed films were developed in a Konica Minolta SRX-101A automatic developer.

Table 2.2: Antibody information and dilutions for immunoblotting

Antigen	Host species	Dilution	Supplier	Cat. No.	Usage notes
<i>Primary</i>					
53BP1	Rabbit	1/1000	Novus	NB100-904	
BLM	Rabbit	1/1000	Bethyl Laboratories Inc.	A300-110A	Antibody freshly diluted from stock for each procedure.
BOD1L	Rabbit	1/1000	Custom	N/A	Antibody freshly diluted from stock for each procedure.
CHK1	Mouse	1/1000	Santa Cruz Biotechnology	DCS-310	
P-CHK1 (S345)	Rabbit	1/1000 in 5% BSA	Abcam	ab58567	
CtIP	Mouse	1/200	Gift from Dr. Roger Grand	N/A	Antibody freshly diluted from stock for each procedure. Sensitive ECL reagents used for detection.
DNA2	Rabbit	1/500	Abcam	ab96488	Sensitive ECL reagents used for detection.
EXO1	Rabbit	1/1000	Bethyl Laboratories Inc.	A302-640A	
H2A	Rabbit	1/2000	Millipore	07-146	
Mitosis (CENPF)	Mouse	1/1000	BD Transduction	610768	
MRE11	Rabbit	1/1000			
RIF1	Rabbit	1/1000	Bethyl Laboratories Inc.	A300-568A	
RPA2	Mouse	1/1000	Abcam	ab2175	
RPA2	Mouse	1/1000	Calbiochem	NA18	
P-RPA (S4/S8)	Rabbit	1/1000	Bethyl Laboratories Inc.	A300-245A	Used only for Western blotting.
<i>Secondary</i>					
Ig/HRP	Goat (α -Mouse)	1/10000	Agilent Dako	P0447	Secondary antibody for WB
Ig/HRP	Goat (α -Rabbit)	1/3000	Agilent Dako	P0448	Secondary antibody for WB

References: BOD1L – Higgs *et al.*, 2015. RIF1: Chapman *et al.*, 2013. Sources: The CtIP antibody stock was a gift from Dr. Roger Grand, University of Birmingham. The stock was expanded in the lab using a hybridoma cell line provided by Dr. Richard Baer, Columbia University. The antibody diluent was 5% milk in TBS-T. Diluted primary antibodies were stored at 4 °C with the addition of 0.1% sodium azide as a bacteriostatic agent.

2.6: Native DNA fibre analysis

2.6.1: Preparation and spreading

The thymidine analogue Iododeoxyuridine (IdU) (Sigma-Aldrich) was thawed, diluted in appropriate cell culture medium and pre-equilibrated in the CO₂ incubator prior to use to avoid oxidative damage to cells. Twenty-four hours after siRNA transfections (section 2.3.2), diluted IdU was applied to cells at a final concentration of 10 µM. Treated cells were incubated in standard conditions for a further 24 h before exposure to IR or CPT according to the doses stated. At the given time points, the culture medium was removed and cells were washed twice in ice-cold PBS. Cells were re-suspended according to standard protocols (section 2.2.1) and the cell concentration for each sample was adjusted to 5 x 10⁵/ml in ice-cold PBS. Samples were stored on ice for up to 2 h.

Spreading was performed in triplicate for each condition. In preparation, 2 µl cell suspension was applied to labelled microscope slides and allowed to settle. Seven microlitres of spreading buffer (200 mM Tris at pH 7.4, 50 mM EDTA, 0.5% SDS) was then added. The sample was mixed to promote cell lysis and left for 2 min. Lysed cells were then spread down the slide by gravity. Once dry, slides were fixed in a 3:1 solution of methanol : acetic acid for a minimum of 10 min prior to air-drying, and were stored at 4 °C until staining.

2.6.2: Antibody staining of DNA fibres for immunofluorescence microscopy

Slides were washed twice in water and twice in blocking solution (1% BSA in PBS with 0.1% Tween-20) before being incubated in blocking solution for 1 h. Diluted mouse primary antibody against Bromodeoxyuridine (BrdU) was applied to cover each slide (approximately 100 μ l). Slides were covered with rectangular coverslips and incubated in the dark for 1 h.

Following primary antibody labelling, antibodies and coverslips were removed and slides were washed 3 times in PBS. Slides were fixed in 4% PFA for 10 min before being washed 3 times in PBS and 3 times in blocking solution. Anti-mouse secondary antibody (Alexa Fluor 594), diluted 1/500 in blocking solution, was applied and slides were incubated for 90 min as described above.

After final washing steps, (2 x PBS, 3 x blocking solution, 2 x PBS), Fluoroshield™ mounting medium (Sigma-Aldrich) was applied to each slide, followed by a fresh rectangular coverslip. Once dried, coverslip edges were sealed with transparent nail varnish, and slides were stored at -20 °C prior to analysis.

2.7: Immunofluorescence microscopy

2.7.1: Preparation of samples for immunofluorescence microscopy

Twenty-four hours in advance of experimental treatments, cells were re-suspended, transferred from 60 mm dishes and grown on 12 mm round glass coverslips in 100 mm dishes.

To prepare coverslips for analysis, cells were treated for 5 min with ice-cold pre-extraction buffer (0.25 % Triton X-100, 10 mM NaCl, 1.5 mM MgCl₂, 150 mM sucrose, 5 mM PIPES). Cells were then fixed for 10 min in 3.6% PFA and washed twice in ice-cold PBS. Coverslips were blocked in 10% FBS with 0.1% sodium azide in advance of antibody staining.

2.7.2: Antibody staining and mounting

Details pertaining to specific antibodies are provided in table 2.3. Fixed and permeabilised coverslips were transferred to lidded chambers and incubated in primary antibodies for 2 h at room temperature. Following three washes with PBS, coverslips were moved to fresh chambers and probed with secondary antibodies for 1 h at room temperature in the dark. Coverslips were washed as above, blotted dry and mounted onto Menzel Gläser Superfrost® microscope slides using Vectashield Antifade Mounting Medium with DAPI (Vector Laboratories). Coverslip edges were sealed with transparent nail polish, and slides were stored at 4 °C.

Table 2.3: Antibody information and dilutions for immunofluorescence

Antigen	Host species	Dilution	Supplier	Cat. No.	Usage notes
<i>Primary</i>					
53BP1	Rabbit	1/300	Novus	NB100-904	
BOD1L	Rabbit	1/500	Custom	N/A	
BRCA1	Mouse	1/1000	Santa Cruz Biotechnology	sc-6954	
BrdU (IdU)	Mouse	1/500	BD Biosciences	347580	Used for native fibre/foci staining.
CENPF	Rabbit	1/1000	Abcam	ab5	
γ H2AX (S139)	Mouse	1/1000	Abcam	ab26350	
Mitosisin (CENPF)	Mouse	1/1000	BD Transduction	610768	
RAD51	Rabbit	1/500	Calbiochem	PC130-100	
REV7	Mouse	1/500	BD Transduction	612266	Not successfully optimised for IF.
RIF1	Rabbit	1/1000	Bethyl Laboratories Inc.	A300-568A	
RPA2	Mouse	1/200	Abcam	ab2175	
RPA2	Mouse	1/200	Calbiochem	NA18	
P-RPA (S4/S8)	Rabbit	1/1000 in TBS	Bethyl Laboratories Inc.	IHC-00422	Optimised for immunofluorescence; not used for Western blotting.
<i>Secondary</i>					
Alexa Fluor 594-IgG	Goat (α - Mouse)	1/1000	Life Technologies	A-11032	Secondary antibody for IF
Alexa Fluor 488-IgG	Goat (α - Rabbit)	1/1000	Life Technologies	A-11034	Secondary antibody for IF

ECL: Enhanced chemiluminescence. TBS: Tris-buffered saline. Except where otherwise stated, the antibody diluent was 3% FCS in PBS. Antibody sources/references: BOD1L – Higgs *et al.*, 2015.

2.7.3: Proximity ligation assays (PLA)

PLA was performed using the Duolink™ In Situ Fluorescence kit (Sigma) in accordance with the manufacturer's standard protocol. Briefly, cells grown on coverslips were pre-extracted, fixed in 3.6% PFA and blocked as described in section 2.7.1. A humidified chamber was used for all incubations. Primary antibody incubation was carried out for 1 h at room temperature before two washes with the provided Wash Buffer A. Coverslips were then incubated with the prepared PLUS and MINUS PLA probes for 1 h at 37 °C before two washes with Wash Buffer A. The ligation reaction then was carried out for 30 min. After a further two washes with Wash Buffer A, amplification was performed at 37 °C for 100 min; during this stage, coverslips were shielded from light. After two final washes with Wash Buffer B (provided), coverslips were mounted with Duolink™ In Situ Mounting Medium with DAPI and stored at -20 °C.

2.7.4: Visualisation of IdU foci

To permit the examination of native IdU focus formation, transfected cells on coverslips were supplemented with 10 µM IdU for 24 h prior to the induction of DNA damage. At the appropriate time points following DNA damage, cells were harvested as for standard immunofluorescence, but with two consecutive 5-min pre-extraction steps prior to fixation (Sartori et al., 2007).

After harvesting, cells were prepared for immunofluorescence microscopy as in section 2.7.1. Cells were stained with primary antibodies against IdU and CENPF followed by incubation with secondary antibodies (table 2.3) before being mounted as described above.

2.7.5: Fluorescence microscopy and image analysis

Fixed and stained coverslips were examined on a Nikon Eclipse Ci setup with CoolLED pe-300 illumination. Quantification was performed at the microscope under the Plan Fluor 60x oil objective. Light intensity was optimised for each experiment depending on antibody staining efficiency, and intensity conditions were then kept constant for each experiment.

Images were acquired using an Andor Zyla SCMOS camera in conjunction with the Plan Fluor 60x or Plan Fluor 100x oil objectives. After adjustment for staining efficiency, acquisition settings were kept constant for each experimental replicate.

For fluorescence intensity calculations, acquired images were analysed using ImageJ software v.1.51 (NIH). Green (CENPF) and red (RPA2) channel images were converted to 8-bit format. A mask was generated from the 8-bit green image which included only CENPF-positive cells; this was overlaid onto the corresponding 8-bit red image, allowing calculation of the mean RPA2 intensity per unit area in the unmasked (CENPF-positive) regions.

2.8: Identification of novel BOD1L interactors

2.8.1: Generation of Bod1L-FLAG-GFP stable cell line

A bacterial artificial chromosome (BAC) encoding murine Bod1L tagged with FLAG-GFP (hereafter Bod1L-FLAG-GFP) was generated by fusing genomic mBod1L to an existing FLAG-GFP construct using a BAC sub-cloning kit. This was then stably transfected into HeLa cells. Alongside this, an empty FLAG-GFP vector was stably transfected to generate a control HeLa (Prof. Simon Boulton and Valérie Borel, Francis Crick Institute, London).

2.8.2: Affinity purification pull-down and mass spectrometry

Bod1L-FLAG-GFP and FLAG-GFP control cells were cultured as monolayers, harvested and lysed. Immune complexes were isolated using an anti-GFP antibody and extensively washed; bound proteins were then resolved by SDS-PAGE. Gel slices were excised, digested with trypsin and processed for analysis by mass spectrometry (Prof. Simon Boulton and Valérie Borel, Francis Crick Institute, London).

2.8.3: Analysis of mass spectrometry data

Samples were analysed with an Orbitrap Fusion mass spectrometer (Thermo Scientific). In order to provide an accurate determination of the relative abundance of all proteins identified in each sample, intensity-based absolute quantification (iBAQ) was used. For each protein, this involved calculating the sum of the intensities for all tryptic peptides and dividing this value by

the number of theoretically observable peptides using MaxQuant software v.1.5.3.8 (Cox & Mann, 2008, www.maxquant.org).

2.8.4: Immunoprecipitation

HeLa nuclear cell extracts (Cilbiotech) were clarified by centrifugation at 44,000 x g and incubated with 5 µg relevant antibodies or an IgG control. Following incubation for 3 h at 4 °C, immune complexes were isolated with protein-A Sepharose (GE Healthcare). Purified complexes and a 5% input control were loaded onto polyacrylamide gels and analysed by SDS-PAGE. Polypeptides were transferred to nitrocellulose membranes and visualised by immunoblotting and chemiluminescence (section 2.5).

2.8.5: Generation of GST-tagged BOD1L fragments

Six overlapping fragments of BOD1L with N-terminal GST tags were generated by PCR amplification of BOD1L cDNA. The resultant fragments were cloned into the pGEX4T1 vector at the Sall and NotI restriction sites. Primer sequences are listed in table 2.4. Fragment sizes ranged from 500-652 aa and collectively spanned the full length of BOD1L. Proteins were expressed in *E. coli* and purified with GST affinity reagents.

Table 2.4: Primer sequences for generation of GST-tagged BOD1L fragments.

Primer name	Supplier	Sequence
BOD1L F1 Fwd	Sigma-Aldrich	TATCCTGTCGACATGGCCACCAACCCACAGCCGCAG
BOD1L F1 Rev	Sigma-Aldrich	CGAGTTAGCGGCCGGGGTTTCTTTGGAATCTTCTTCATA
BOD1L F2 Fwd	Sigma-Aldrich	CACGACGTCGACGAAAAAGAAGAGAGGCTTTTAAGA
BOD1L F2 Rev	Sigma-Aldrich	CGTTTGAGGGGCCGCTTCTCCTTTGCTAATGGTAACTT
BOD1L F3 Fwd	Sigma-Aldrich	AGAACGGTCGACACAAAGAGCTTGTTAGAAGAGAAA
BOD1L F3 Rev	Sigma-Aldrich	ACGGATAGCGGCCGCAGTTGCCACATCCTCAGTTTGTCC
BOD1L F4 Fwd	Sigma-Aldrich	ATCACCAAGGAGGGCGGCCTGGTGGACATGGCCAAG
BOD1L F4 Rev	Sigma-Aldrich	GGAGATGGTGGTGTCTCCACCTTCTCCAGCTG
BOD1L F5 Fwd	Sigma-Aldrich	GAGTCCGCCGAGGGCGACTCCCAGATCGGCACCGTG
BOD1L F5 Rev	Sigma-Aldrich	GTTGGCGTTGCCCTCAGGCCCGGCCGGCGGAGTA
BOD1L F6 Fwd	Sigma-Aldrich	GAGTGAGTCGACTTGGCAGTGAGCACCCAGGAGGGG
BOD1L F6 Rev	Sigma-Aldrich	TTGTAGAGGGGCCGCTTATCGCTTCGCTTTTTTCACAGG

Forward and reverse primer sequences for amplification of sections from BOD1L cDNA in preparation for cloning GST-tagged fragments.

2.8.6: GST pull-down assays

HeLa nuclear cell extracts were clarified as in section 2.8.4. Following affinity purification, GST-tagged BOD1L fragments or GST alone (1 µg per assay) were incubated with clarified nuclear cell extracts for 3 h at 4 °C. Tagged proteins were then isolated with glutathione Sepharose. Isolated protein complexes were separated by SDS-PAGE along with a 5% sample of nuclear cell extract as an input control before analysis by immunoblotting and chemiluminescence (described in section 2.5).

2.9: Analysis of class switch recombination (CSR)

2.9.1: Generation of conditional Bod1L knockout mouse model

The creation of a B-cell-specific conditional Bod1L knockout mouse model and control animals was carried out by our collaborators (Prof. Simon Boulton and Valérie Borel, Francis Crick Institute, London). Parental mouse strains were sourced from EUCOMM. A conditional knockout line (Bod1L^{F/F}) had previously been established using embryonic stem cells engineered with CRISPR/Cas9 genome editing. In this line, functional Bod1L expression is abrogated by a Cre recombinase-induced deletion of exon 3. These animals, along with Bod1L-proficient controls (Bod1L^{+/+}), were crossed with Cd19^{+/^{Cre}} mice to induce a B-cell-specific knockout of Bod1L in the resultant progeny (Bod1L^{F/F} Cd19^{+/^{Cre}}) and Bod1L-proficient control mice (Bod1L^{+/+} Cd19^{+/^{Cre}}), respectively.

2.9.2: Assessing CSR proficiency

To assess the proficiency of CSR, B-cells were extracted from Bod1L-deficient animals and Bod1L-proficient controls. Differentiation was stimulated by culturing cells with lipopolysaccharide (LPS) for 96 h with or without interleukin 4 (IL-4) supplementation. Flow cytometry was then used to examine cell surface immunoglobulin expression (Prof. Simon Boulton and Valérie Borel, Francis Crick Institute, London, Dr. Rachel Bayley).

2.10: DNA repair assays

2.10.1: I-SceI-based reporter assays

I-SceI reporter cell lines and plasmids were a kind gift from Dr. Jeremy Stark. Plasmid details are provided in table 2.5. These reporter lines and the associated assay protocols have been described comprehensively (Gunn and Stark, 2012); an overview is provided here. Cells were cultured in standard media for HeLa cells described in section 2.2.2 and passaged 1-2 times per week

The DR-GFP cell line was used to assess repair by homologous recombination (HR). The reporter cassette within this cell line includes truncated N- and C-terminal GFP fragments either side of a restriction site for the rare-cutting endonuclease, I-SceI (termed SceGFP). Downstream of this region is a fragment which encompasses the central portion of the GFP coding sequence but lacks the N- or C-terminal regions (iGFP). When I-SceI is transiently expressed, this induces a DSB in SceGFP; HR-proficient cells repair this break using iGFP as a

homologous template. This generates a functional GFP coding sequence; expression of GFP can then be analysed as an indicator of HR proficiency.

Single-strand annealing (SSA) was assessed in the SA-GFP cell line. In this line, the repair cassette comprises a 5' section of the GFP coding sequence (5'GFP) situated upstream of the 3' section that harbours the I-SceI recognition site (Sce3'GFP). There is a short (~260nt) region of sequence homology shared by these sections. Expression of I-SceI results in a DSB in the Sce3'GFP section. The short homologous region is sufficient to act as a bridge to facilitate repair by SSA, thereby generating a functional GFP sequence.

For DNA repair assays, cells were seeded into 60 mm dishes (5×10^5 per dish) 24 prior to transfection to achieve 40-60 % confluence at the point of transfection. Cells were then transfected with the relevant siRNA as above (section 2.3.2) and rescued after 4 hours.

Once cells had reached 60-80% confluency, they were transfected with 4 μ g I-SceI expression vector and 1 μ g pRFP using Lipofectamine 2000 as described in section 2.3.2. The cells were rescued with fresh media 3 hours after transfection.

Forty-eight hours after DNA transfections, cells were then harvested for analysis by flow cytometry. The cells were re-suspended as described in section 2.2.1, transferred to 15 ml

screw-cap centrifuge tubes and centrifuged at 1,200 rpm for 4 min. The culture medium was aspirated and the pellets were re-suspended in PBS and re-centrifuged. After re-suspension in fresh PBS, an equal volume of 3.6% PFA solution was added to a final concentration of 1.8% PFA. Cells were then fixed on ice for 15 min.

Following fixation, the cells were pelleted by centrifugation as described above. The fixative solution was removed by aspiration and the pellet was washed by re-suspension in fresh PBS to remove traces of PFA. Cells were again pelleted and re-suspended in 1 ml PBS before being stored on ice for a maximum of 4 hours before analysis.

Immediately prior to flow cytometry, the cell suspensions were vortexed and filtered with a 30 μm nylon mesh filter (CellTrics™).

Screening for GFP-positive cells (those which had successfully reconstructed a functional GFP sequence by the repair pathway of interest) was carried out on a Beckman Coulter Cyan flow cytometer. Data were analysed using FlowJo™ v.10.6.1 (Becton Dickinson).

2.10.2: TRF2 telomere fusion assays

HeLa cells were seeded into 60 mm dishes and transfected with the relevant siRNA as described above. Twenty-four hours after siRNA transfections, cells were transfected with a plasmid

encoding a dominant-negative TRF2 allele (TRF2^{ΔBAM}) as described in section 2.2.2 (refer to table 2.5 for plasmid details). The following day, cells were transferred to 100 mm dishes and cultured for a further 24 h before being harvested.

Prior to harvesting, cells were incubated with 0.1 µg/ml Colcemid for 3 h. Cells were diluted with PBS and transferred to a 15 ml polypropylene centrifuge tube. Pellets were collected by centrifugation at 1000 rpm for 5 min, after which the supernatant was discarded and the pellets re-suspended in 5 ml 75 mM KCl (pre-warmed to 37 °C).

The cell suspension was incubated at 37 °C for 10 min with gentle agitation every 2 min before centrifugation at 1200 rpm for 5 min. The supernatant was then poured off and the pellets re-suspended in the residual volume of KCl.

Cells were then fixed in pre-chilled fixative solution (3:1 methanol : acetic acid, freshly prepared). The first 1 ml of fixative was added dropwise whilst agitating tubes on a vortex mixer; a further 9 ml was added without agitation. After fixation, cells were stored at 4 °C for at least 30 min before spreading.

To prepare for spreading, cells were centrifuged for 5 min at 1000 rpm; afterwards, 9 ml of fixative solution was removed and the cell pellets were re-suspended in the remaining 1 ml.

Microscope slides were soaked in fixative solution, and spreading was commenced before the slides had dried. For each condition, 15 μ l cell suspension was dropped onto slides from a height of 20-30 cm. Remaining cells were transferred to -20 °C for storage. Slides were heated to 80 °C for 1 min and allowed to air-dry overnight in a fume hood before being stored at 4 °C.

Spread metaphases were stained using Duolink™ In Situ Mounting Medium with DAPI, covered with rectangular coverslips (22 x 50 mm) and sealed with transparent nail polish. Slides were analysed at 100x magnification using the microscope setup described above.

Table 2.5: Details of plasmids.

Section reference	Protocol/application	Plasmid	Source/Reference
2.8.5	GST-BOD1L fragment cloning	pGEX4T1	
2.10.1	I-SceI reporter assays	pCAGGS-I-SceI	Dr. Jeremy Stark (Gunn & Stark, 2012)
	I-SceI reporter assays	pRFP	Dr. Jeremy Stark (Gunn & Stark, 2012)
2.10.2	Telomere fusion assay	pLPC-Myc-TRF2 ^{ABΔM}	Smogorzewska <i>et al.</i> , 2002

Expression vectors used during the course of this study.

Chapter 3: A role for BOD1L in repair of IR-induced DNA double-strand breaks

3.1: Introduction

The recently-identified DDR protein BOD1L plays a critical role in maintaining genome stability during replication stress. BOD1L functions to protect stalled replication forks through the inhibition of the anti-recombinase activities of BLM and FBH1, thereby stabilising RAD51 at these sites. The shielding of stalled forks from excessive nucleolytic resection ensures that they can be repaired in a timely manner by HR, which allows for the continuation of DNA replication and preserves genome integrity. In the absence of BOD1L, RAD51 is displaced by BLM and FBH1, which exposes stalled forks to uncontrolled resection by DNA2, ultimately compromising genome stability (Higgs et al., 2015).

To date, there have been no investigations into the potential role of BOD1L in other aspects of the DNA damage response, despite the fact that it is well established that certain factors function in several DDR pathways. For example, alongside its well-characterised role in homology search and strand invasion during HR, RAD51 participates in the repair of ICLs independently of HR. RAD51 carrying a T131P mutation in its Walker A domain is deficient in ICL repair whilst its function in HR is unaffected (Wang et al., 2015a). Additionally, BLM is required for nucleolytic resection of DNA lesions as a precursor to HR, but also co-operates with components of the Fanconi Anaemia (FA) pathway to suppress replication stress-induced micronucleation (Naim and Rosselli, 2009). Likewise, some pathways are involved in the resolution of multiple types of lesion. For instance, HR is important for the repair of collapsed

DNA replication forks but is also fundamental to the resolution of double-strand breaks (DSBs) (Heyer et al., 2010).

DSBs arise from a variety of sources, including some physiological processes as well as extra-cellular agents. These lesions involve the simultaneous breakage of both phosphate backbones within a single turn of the DNA double helix (Mehta & Haber, 2014). If unrepaired, DSBs can severely compromise a multitude of cellular processes, including DNA replication and transcription; furthermore, small- or large-scale chromosomal aberrations may result. As such, they pose a considerable threat to cell viability and genome stability (Shrivastav et al., 2008). IR is acknowledged to be one of the most potent DSB inducers (Soulas-Sprauel et al., 2007, Zeman and Cimprich, 2014, Mehta and Haber, 2014). DSBs in late S and G2-phase cells may be resolved by either of the two major repair pathways: HR or NHEJ. HR is not a viable DSB repair pathway outside these phases.

Repair pathway choice is influenced by the cell cycle due to the necessity of a homologous sister chromatid as a template for HR-mediated repair. Conversely, NHEJ is template-independent and is not restricted post-replicative phases (Heyer et al., 2010). Outside late S/G2, additional control measures exist to down-regulate nuclease activity – a pre-requisite for HR. The stimulatory activity of BRCA1 is required for CtIP-mediated resection. Recruitment of BRCA1 is antagonised by components of the 53BP1 end protection pathway when DNA replication has not been completed and there is no template for HR (Chen et al., 2008). During these phases, DSB repair is completed by NHEJ.

Nucleolytic resection is a key determinant of repair pathway choice. Short-range 3'-5' resection is firstly carried out by CtIP and MRE11. As CtIP activation requires phosphorylation by CDKs, which are active during late S/G2 phases, this resection is therefore limited to these phases (Huertas, 2010). The short 3' overhangs are subsequently extended by DNA2 and EXO1, both of which are supported by the activity of BLM (Nimonkar et al., 2011). In view of its function in the modulation of resection, I hypothesised that BOD1L may participate in the repair of IR-induced DSBs. This chapter therefore aims to investigate this potential role. It was of particular importance to determine whether BOD1L influences the resection of IR-induced DSBs, and to identify other known DDR factors involved. The impact of BOD1L deficiency on genome stability in cells exposed to IR was also examined.

3.2: BOD1L suppresses resection of IR-induced DSBs alongside its fork protection role

To investigate any uncharacterised roles of BOD1L in DSB repair, I first examined the impact of BOD1L depletion on cellular survival after IR. Indeed, cells lacking BOD1L were more sensitive to IR than control cells. Immunofluorescence microscopy also revealed that BOD1L-deficient cells displayed more IR-induced genomic instability. These analyses further highlighted a G2-specific increase in γ H2AX and RPA2 recruitment to IR-induced DSBs in BOD1L-depleted cells, indicating compromised DSB resolution and a higher level of IR-induced DSB resection. These observations were confirmed by immunoblotting. The nature of this aberrant resection in the absence of BOD1L was probed using native DNA fibre and IdU focus analysis; these experiments suggested that BOD1L controls the number of DSBs resected, but not the extent of resection

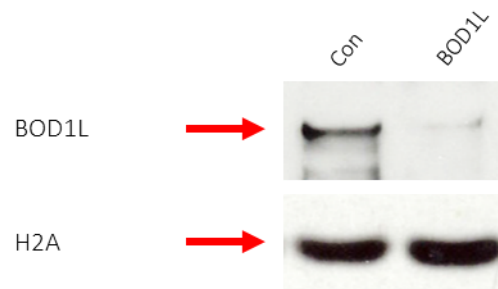
at individual breaks. Finally, to identify the nucleases involved in BOD1L-mediated suppression of DSB resection, cells were depleted of BOD1L along with a subset of relevant factors, and resection was monitored.

3.2.1: Depletion of BOD1L results in increased sensitivity to IR

Higgs and colleagues demonstrated that BOD1L plays a key role in the resolution of replication stress. In wild-type cells, BOD1L ensures that stalled replication forks are subjected to controlled nucleolytic resection to facilitate HR, a pathway which is also essential for the repair of DSBs. I therefore proposed that BOD1L may also be involved in the resolution of IR-induced DSBs, and that cell viability would be compromised in the absence of this factor. To investigate the impact of BOD1L depletion on cell survival following exposure to IR, clonogenic survival assays were performed. Twenty-four hours after siRNA-mediated depletion of BOD1L, HeLa cells were plated at low density, with cell numbers adjusted for siRNA condition and irradiation dose. In parallel, siRNA-transfected cells were cultured at normal density and harvested for Western blot analysis after 3 days to confirm depletion of BOD1L. Cells at low density were subjected to ionising radiation in doses ranging from 2 Gy to 8 Gy. After incubation in standard conditions for a further 10 days, surviving colonies were stained with Crystal Violet solution and quantified by eye.

Successful depletion of BOD1L was first confirmed by Western blotting (Figure 3.1a). BOD1L-deficient cells were more sensitive to IR than control cells. The depletion of this factor resulted in a two- to five-fold reduction in cell viability (Figure 3.1b). Although this is a relatively modest reduction in cell viability, similarly modest defects have been observed upon inhibition or loss of key DNA damage repair factors, such as the apical signalling kinase ATM (Xu and Baltimore, 1996), the end resection regulator 53BP1 and its downstream effectors, such as RIF1

(a)



(b)

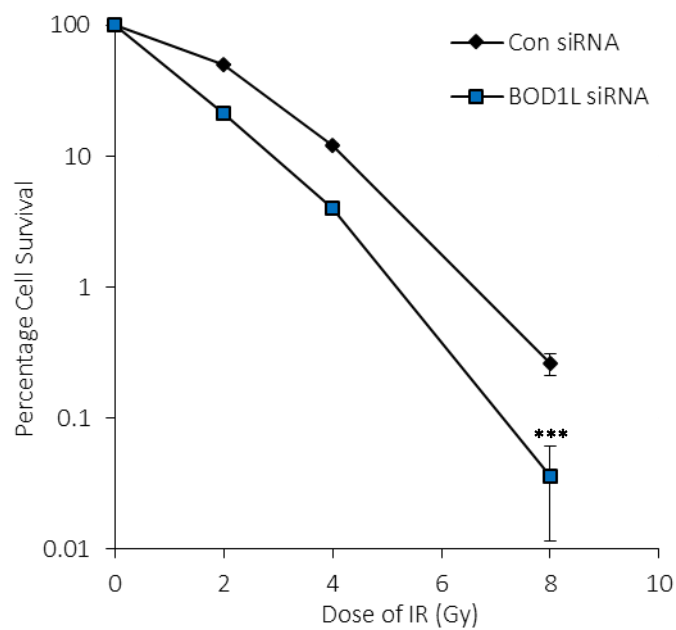


Figure 3.1: Depletion of BOD1L induces hyper-sensitivity to ionising radiation.

HeLa cells were treated with siRNA against BOD1L and a non-targeting control. Knockdown was confirmed by Western blotting (a). These cells were plated at low density and subjected to the indicated doses of ionising radiation (IR). Irradiated cells were returned to standard culture conditions for a further 10 days to allow colony formation, after which the surviving colonies were stained with Crystal Violet solution and quantified. The proportion of viable colonies was calculated for each condition (b). Data shown in (b): Three technical repeats of the assay were performed, with 3 dishes per condition included in each assay. Statistics: Student's T-test for Control vs. BOD1L. 8 Gy: $p = 0.00002$. Error bars indicate SEM.

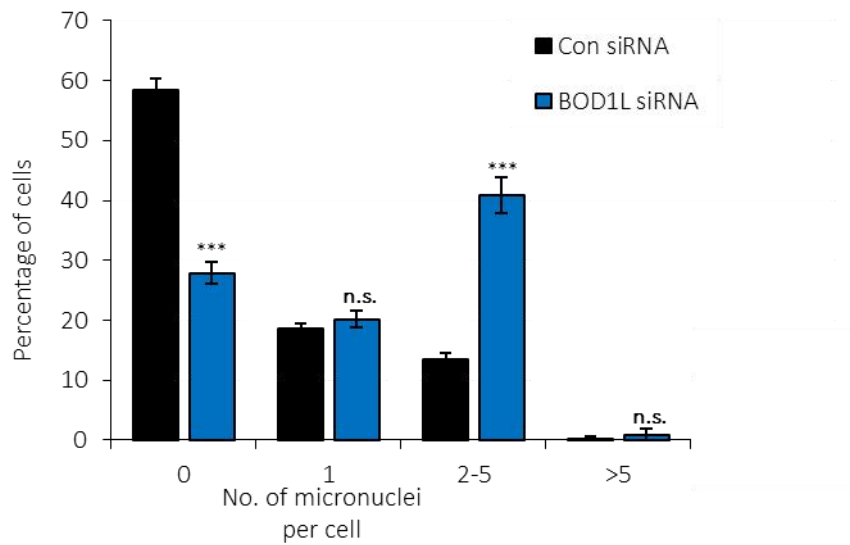
(Chapman et al., 2013, Silverman et al., 2004). It can therefore be concluded that BOD1L promotes cell survival following exposure to IR.

3.2.2: BOD1L maintains genome stability in irradiated cells by contributing to the repair of IR-induced DSBs

The results of the survival assays described above demonstrate that BOD1L is required for cell viability following IR exposure. Given these results, I hypothesised that BOD1L may ensure genome stability and cell survival by contributing to the repair of IR-induced lesions. To investigate this, I first examined the impact of BOD1L loss on genome integrity, which is genome instability (Tucker and Preston, 1996, Naim and Rosselli, 2009). To this end, HeLa cells transfected with siRNA against BOD1L or a non-targeting control were irradiated with 3 Gy IR and harvested after 24 h for analysis. Cells were pre-extracted, fixed and mounted, and micronuclei enumerated by immunofluorescence microscopy.

The proportion of cells with IR-induced micronuclei was elevated in BOD1L-depleted cells relative to controls. In particular, the proportion of nuclei with between two and five associated micronuclei was 13.5% in control cells and more than three-fold higher in those lacking BOD1L (figure 3.2). These results indicate that BOD1L is required for the maintenance of genome stability following exposure to IR.

(a)



(b)

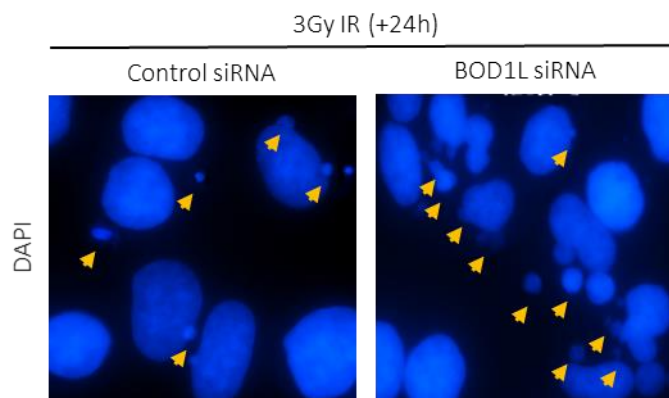


Figure 3.2: Prevalence of IR-induced micronuclei is elevated in the absence of BOD1L.

The proportion of cells with of micronuclei was quantified in asynchronous HeLa cells transfected with siRNA against BOD1L or a non-targeting control sequence. Quantifications were performed 24 hr after irradiation with 3 Gy IR (a). Representative images are shown in (b), with micronuclei indicated by arrowheads.

Data shown in (a): 3 technical repeats with ≥ 100 nuclei analysed per condition in each experiment. Statistics: Students T-test for Control vs. BOD1L. 0: $p = 0.00002$. 1: $p = 0.26$. 2-5: $p = 0.0003$. >5: $p = 0.11$. Error bars indicate SEM.

To extend my investigations, I monitored focus formation of γ H2AX. The histone variant H2AX is phosphorylated by ATM during the initial stages of DSB detection and signalling and γ H2AX can therefore serve as a proxy for the induction of the DDR (Matsuoka et al., 2007). HeLa cells were transfected with control or BOD1L siRNA, irradiated and harvested for immunofluorescence microscopy as described above. After coverslips had been stained with antibodies against γ H2AX and mounted with DAPI, the number of nuclei with at least 10 γ H2AX foci was scored for all conditions.

In non-irradiated cells, the proportion of focus-positive nuclei was 7.9% in control cells. This proportion more than doubled in the absence of BOD1L. This difference was also observed at late time points post-irradiation. Twenty-four hours after exposure to IR, the majority of control cells had resolved γ H2AX foci; conversely, almost one third of BOD1L-depleted cells retained at least 10 γ H2AX foci at this time (figure 3.3). These results provide further evidence that BOD1L is required for the successful completion of DSB repair in cells exposed to IR.

I next hypothesised that BOD1L may preserve genome stability by contributing directly to the repair of IR-induced DSBs. In order to examine this, HeLa cells were stained with antibodies against 53BP1: a widely-used indicator of the presence of DSBs (Symington and Gautier, 2011, Bothmer et al., 2010, Bunting et al., 2010). Cells were depleted of BOD1L using siRNA and exposed to 3 Gy IR. Coverslips were harvested at multiple time-points up to 24 h post-irradiation. Non-irradiated coverslips were also harvested and treated as described above.

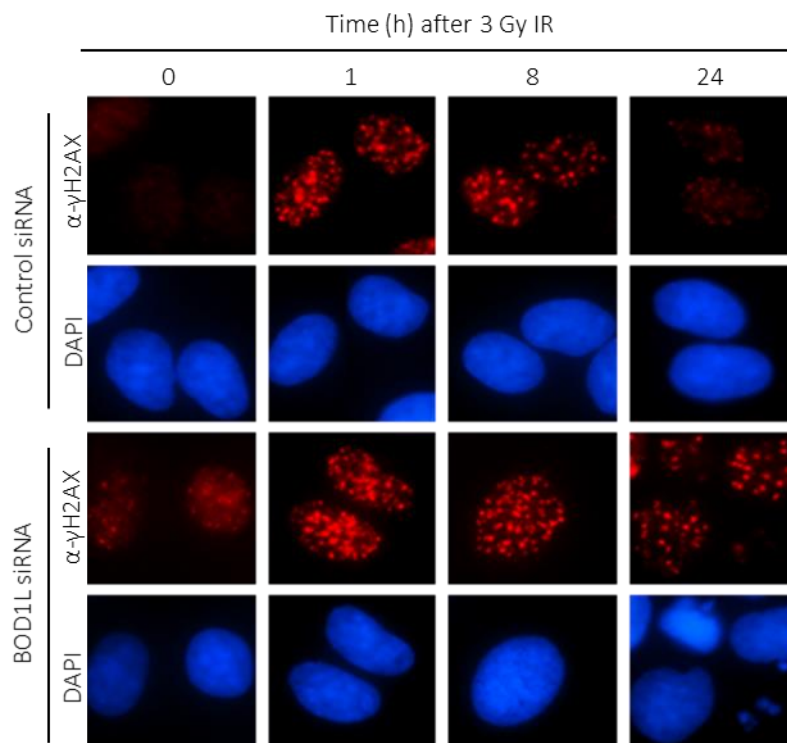
After staining, coverslips were mounted in DAPI and immunofluorescence microscopy was used to assess the proportion 53BP1-positive cells.

The proportions of nuclei with 53BP1 foci were similar for control and BOD1L-depleted cells at early time points, but a discontinuity was observed 24 h post-irradiation. While the majority of 53BP1 foci in control cells had been cleared by this time point, approximately 41.0% of BOD1L-depleted cells retained foci after 24 h (figure 3.4). These data illustrate that the initiation of the DNA damage response is unaffected in the absence of BOD1L; however, the failure to resolve these foci by 24 h after damage is suggestive of problematic repair of DSBs in BOD1L-depleted cells.

3.2.3: BOD1L modulates DSB repair during G2 phase

BOD1L functions during S-phase to protect stalled replication forks from uncontrolled resection (Higgs et al., 2015). I considered the possibility that BOD1L's function in DNA repair may not be confined to S-phase cells, speculating that it may also modulate G2 resection as a precursor to HR. I hypothesised that if this were the case, DSB repair would be impaired in G2 cells deficient of BOD1L. This would lead to a G2-specific increase in γ H2AX-positive nuclei in BOD1L-depleted cells.

(a)



(b)

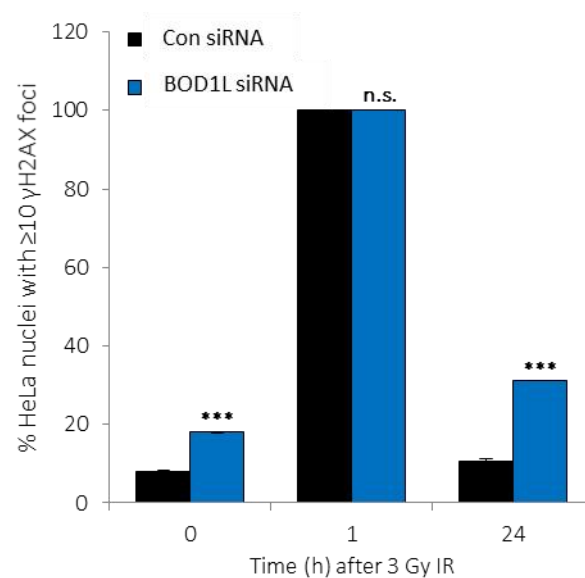


Figure 3.3: BOD1L is required for the resolution of IR-induced DSBs.

HeLa cells were treated with the named siRNAs and exposed to 3 Gy IR. Coverslips were pre-extracted, fixed and stained with antibodies against γ H2AX. The proportion of nuclei with at least 10 γ H2AX foci was assessed by immunofluorescence microscopy at the indicated time points after exposure to IR. Representative images of γ H2AX foci in control- and BOD1L-depleted cells are shown (a) with quantifications in (b).

Data shown in (b): 3 independent experiments with ≥ 100 nuclei analysed per experiment. Statistics: Students T-test for Control vs. BOD1L. Untreated: $p = 0.00001$. 1 hr: $p = 1$. 24 hr: $p < 0.00001$. Error bars indicate SEM.

To examine cell cycle-specific recruitment of γ H2AX to IR-induced DSBs, I transfected HeLa cells with control or BOD1L siRNA. Prior to irradiation, cells were treated with the DNA polymerase α inhibitor Aphidicolin (Krokan et al., 1981). This prevented the transition of any damaged cells from S-phase to G2 between irradiation and analysis, and also ensured that no cells damaged in G1 entered S-phase. Cells were exposed to 2 Gy IR and harvested for immunofluorescence microscopy at multiple time points until 24 h post-irradiation.

Coverslips were pre-extracted, fixed in PFA and stained with antibodies against γ H2AX. To distinguish between G1 and G2 cells, coverslips were co-stained with antibodies against CENPF. Expression of this centromeric protein peaks during late S/G2 phase (Zhu et al., 1995); as such, CENPF-positive cells were regarded as G2 cells and CENPF-negative as G1 cells. The mean number of γ H2AX foci per nucleus was quantified in G1 and G2 cells.

γ H2AX focus formation in G1 cells was unaffected by depletion of BOD1L; numbers of foci for control and BOD1L-deficient cells were indistinguishable at all time points analysed (figure 3.5a). In contrast, G2 cells depleted of BOD1L contained significantly more foci per nucleus than controls at 8 h post-IR (figure 3.5b). These data implied an increase in unrepaired DNA damage during G2.

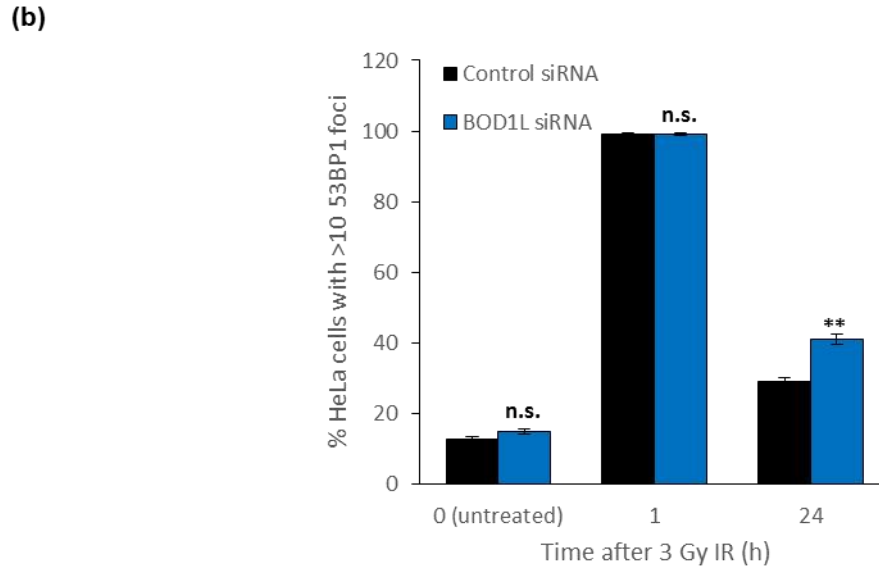
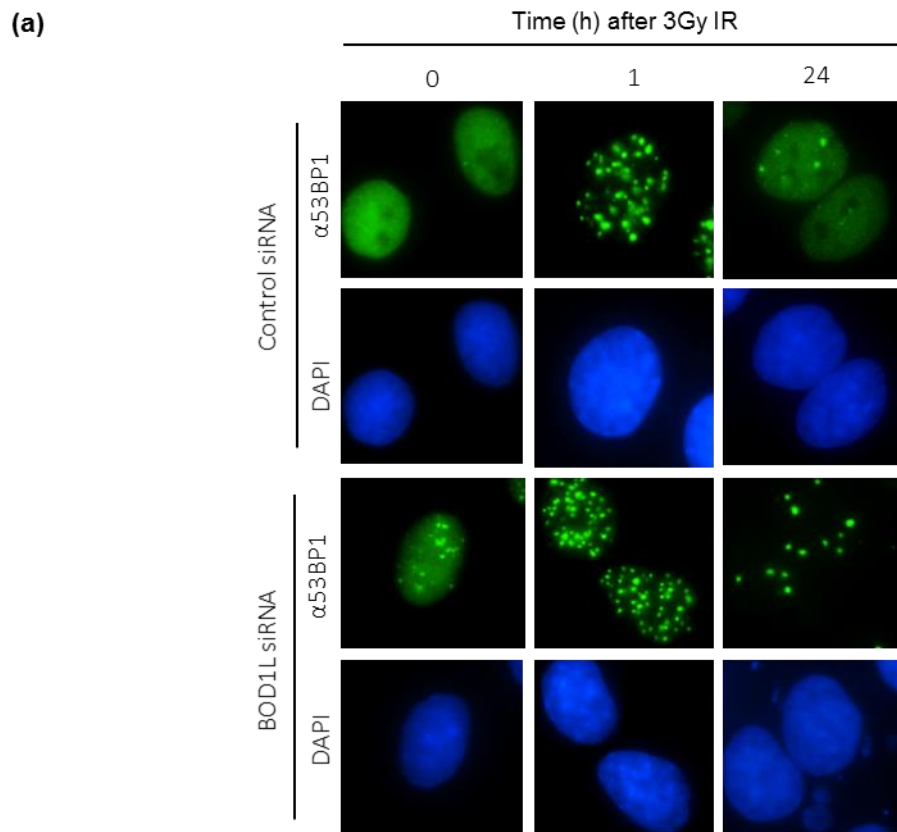


Figure 3.4: BOD1L-deficient cells initiate an IR-induced DNA damage response, but the completion of repair is compromised.

HeLa cells transfected with siRNA against BOD1L or a non-targeting control sequence were exposed to 3 Gy IR and harvested for immunofluorescence microscopy at the indicated time points. Coverslips were pre-extracted, fixed and stained with antibodies against 53BP1. Representative images are shown in (a). The proportion of nuclei with at least 10 53BP1 foci was calculated; quantifications are shown in (b).

Data shown in (b): 3 independent experiments with ≥ 100 nuclei analysed per condition in each experiment. Statistics: Student's T-test for Control vs. BOD1L. Untreated: $p = 0.10$. 1 h: $p = 0.82$. 24 h: $p = 0.003$.

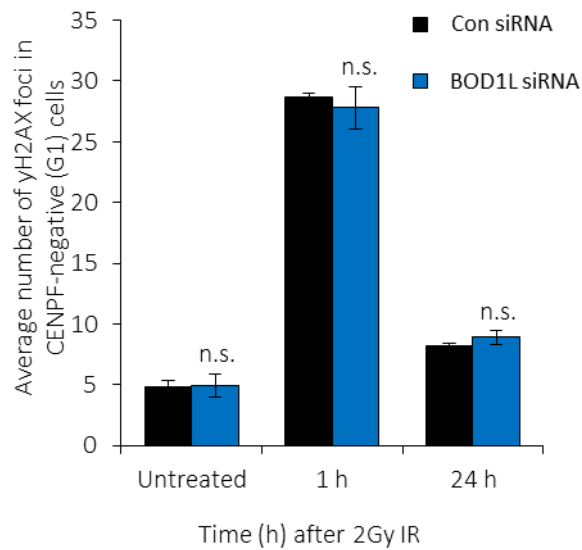
3.2.4: BOD1L depletion results in increased accumulation of IR-induced ssDNA in G2 cells

As outlined above, the G2-specific impairment of DSB repair in the absence of BOD1L provided further support for the notion that this protein functioned as a modulator of DSB resection following exposure to IR. To determine whether BOD1L influenced the resection of IR-induced DSBs, HeLa cells were depleted of BOD1L with siRNA, treated with 3 Gy IR and harvested for analysis by Western blotting over a 24-hour time course. Membranes were probed with primary antibodies against BOD1L, the ssDNA-binding protein RPA2 and phosphorylated RPA2 (RPA-P S4/S8), followed by incubation with HRP-conjugated secondary antibodies and visualisation by chemiluminescence. Levels of phosphorylated RPA2 protein can be monitored to provide an indication of the amount of resection that has taken place within a sample of cells (Ashley et al., 2014).

Successful depletion of BOD1L was verified by Western blotting. Importantly, the level of RPA2 was consistent across all samples. There was negligible RPA2 phosphorylation in control cells, with detectable levels observed only at 24 hours post-irradiation. In contrast, BOD1L-depleted cells exhibited a marked increase in RPA2 phosphorylation, even in unperturbed cells. Levels of phosphorylated protein increased following irradiation and reached peak levels 8 hours after treatment (figure 3.6). This result suggested that more IR-induced nucleolytic resection occurred in the absence of BOD1L.

Whilst the above approach provided a means to examine changes in DSB resection, it did not allow for the identification of the cell cycle phase(s) in which aberrant resection took place. It

(a)



(b)

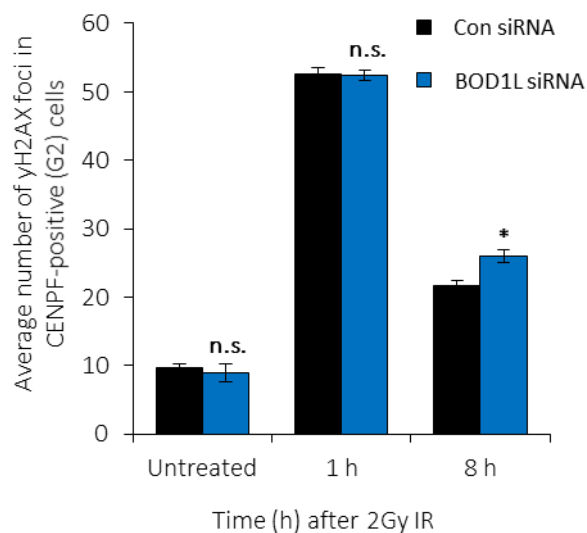


Figure 3.5: Defective repair of IR-induced DSBs in the absence of BOD1L is specific to G2 cells.

HeLa cells were transfected with the named siRNAs, pre-treated with Aphidicolin prior to irradiation and harvested for analysis at the indicated time points following exposure to 3 Gy IR. Coverslips were pre-extracted and fixed prior to staining with antibodies against γ H2AX and CENPF. γ H2AX foci were quantified by immunofluorescence microscopy in CENPF-negative (G1) nuclei (a) and CENPF-positive (G2) nuclei (b).

Data shown in (a) and (b): 3 independent experiments with ≥ 100 nuclei analysed per condition in each experiment. Statistics for CENPF-negative analyses: Student's T-test for Control vs. BOD1L. Untreated: $p > 0.05$. 1 hr: $p > 0.05$. 24 hr: $p > 0.05$.

Statistics for CENPF-positive analyses: Student's T-test for Control vs. BOD1L. Untreated: $p > 0.05$. 1 hr: $p > 0.05$. 8 hr: $p < 0.05$. Error bars indicate SEM.

was therefore important to determine whether elevated resection could be detected specifically in G2 cells in the absence of BOD1L. To this end, HeLa cells treated with siRNA against BOD1L or a non-targeting control were irradiated with 3 Gy IR. Prior to irradiation, cells were treated with Aphidicolin as described in section 3.3.2. Cells were harvested, pre-extracted, fixed in PFA and mounted with DAPI at time points ranging from 1-24 hours after irradiation.

The gold standard for monitoring changes in nucleolytic resection by immunofluorescence microscopy is to probe cells with antibodies against RPA32-P (S4/S8). However, other experiments presented in this chapter showed that RPA2 phosphorylation occurs at relatively low levels in response to IR (refer to figures 3.10, 3.12a and 3.14) when compared with other inducers of DNA damage, such as Camptothecin (figure 3.12b). It was therefore difficult to make comparisons between protein levels in different conditions. Moreover, preliminary investigations in our lab revealed that this antibody was associated with a high fluorescent background signal in irradiated cells. Cells were therefore stained with antibodies against RPA2 and CENPF; as outlined above, Aphidicolin pre-treatment and CENPF expression were used to facilitate the identification of G2 phase cells. The proportion of RPA2-positive G2 nuclei (those with at least 10 RPA2 foci) was assessed by immunofluorescence microscopy.

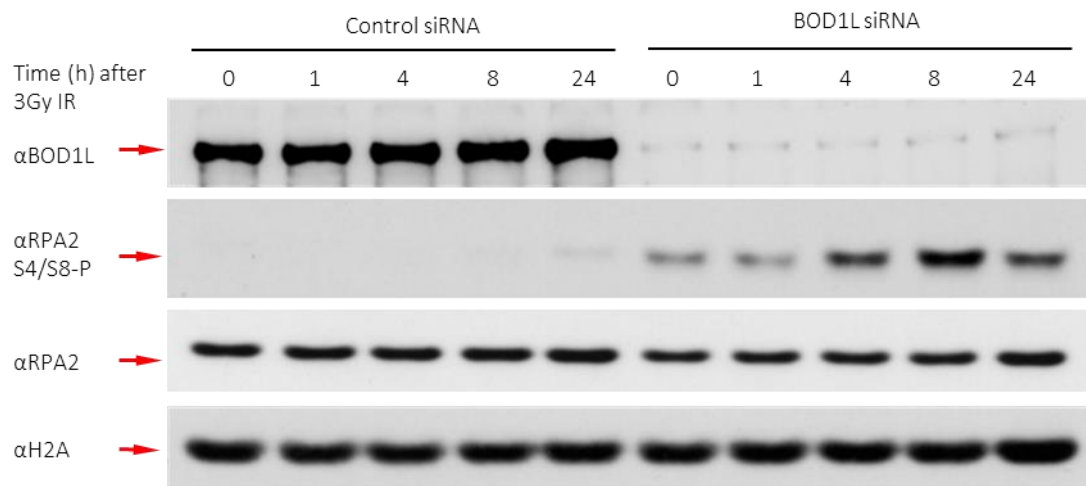


Figure 3.6: The level of IR-induced phosphorylation of RPA2 is higher in the absence of BOD1L.

HeLa cells treated with the named siRNA were subjected to 3 Gy IR and harvested for analysis at the time points given. Whole-cells extracts were resolved by SDS-PAGE and transferred to nitrocellulose membranes, which were then probed with the named antibodies.

In control cells, the proportion of RPA2-positive nuclei reached its peak (37.9%) 4 hours post-irradiation and had begun to decline after 8 hours. By 24 h after irradiation, the majority of cells were negative for RPA2 foci. The proportion of RPA2-positive nuclei in BOD1L-depleted cells was significantly higher than for control cells at all time points following irradiation, with the highest proportion (83.3%) being recorded 8 hours after treatment. Twenty-four hours after irradiation, 35.8% of BOD1L-depleted nuclei retained RPA2 foci (figure 3.7). These data suggest that resection of IR-induced DSBs during G2 is more prevalent in the absence of BOD1L.

There were two possible scenarios that could explain the observed increase in RPA2 focus formation in the absence of BOD1L: either an increase in the number of DSBs resected per nucleus, or a greater extent of resection per DSB. It was not possible to distinguish between these scenarios in the analyses described thus far. Therefore, to gain further insight, I cultured control- and BOD1L-depleted cells in media supplemented with 10 μ M IdU and irradiated them with 10 Gy IR. Cells were harvested and lysed after 24 h and spread onto slides for native DNA fibre analysis to assess the extent of resection at individual DSBs. As outlined in figure 3.8a, HCl denaturation is omitted from this protocol, meaning that only resected tracts of ssDNA are exposed; these regions were delineated by staining DNA fibres with anti-IdU antibodies and measured using ImageJ software. The depletion of BOD1L did not have any detectable effect on ssDNA tract length (figure 3.8b).

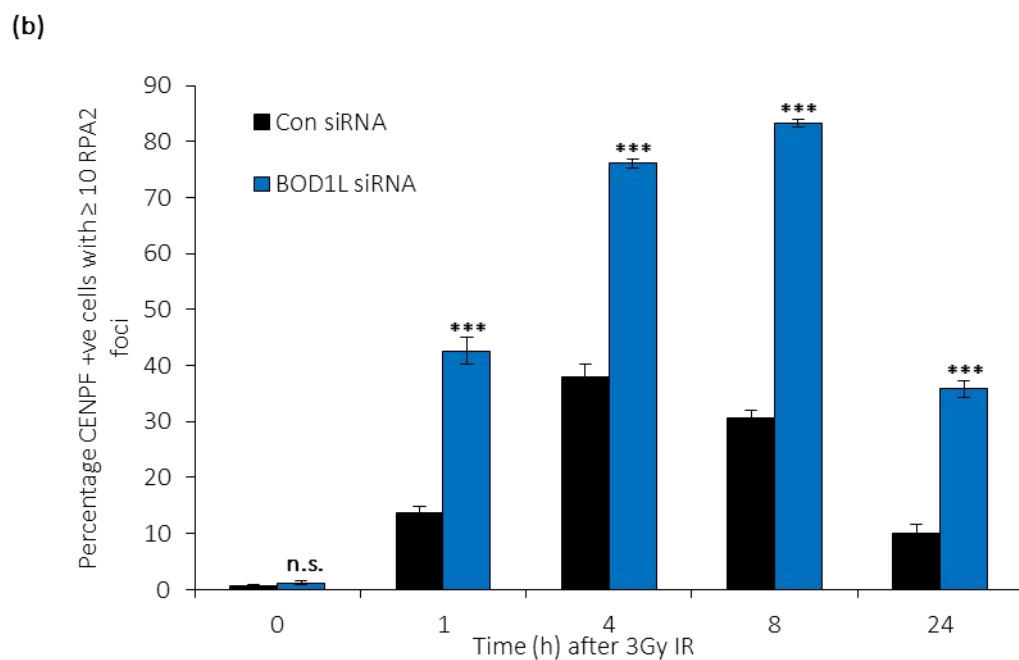
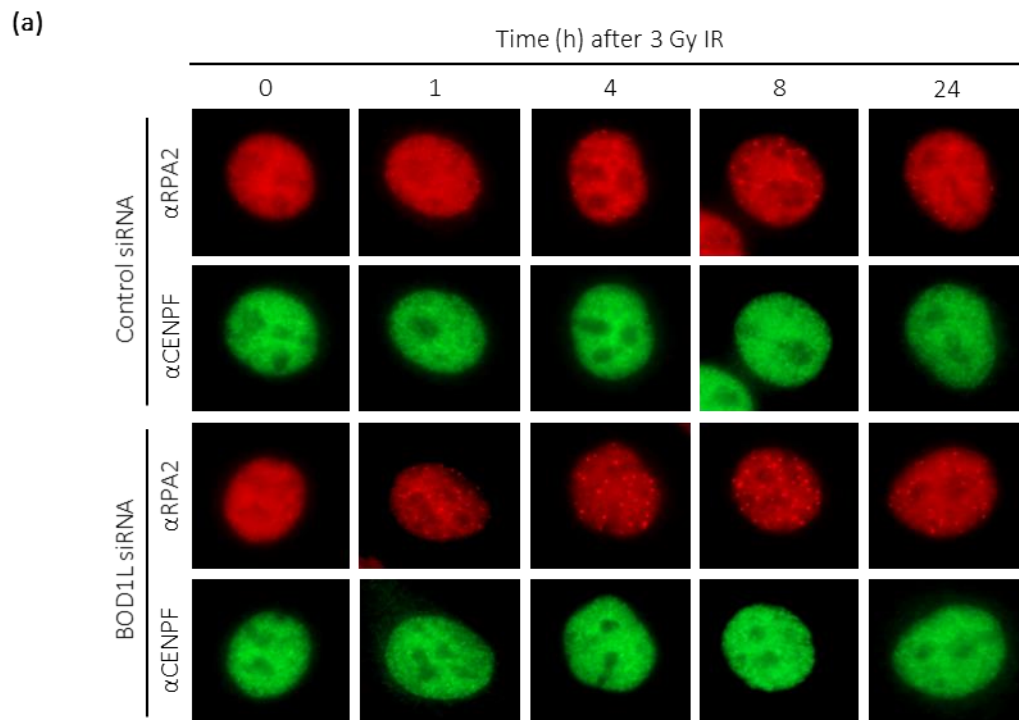


Figure 3.7: Depletion of BOD1L increases the prevalence of nuclear ssDNA following IR.

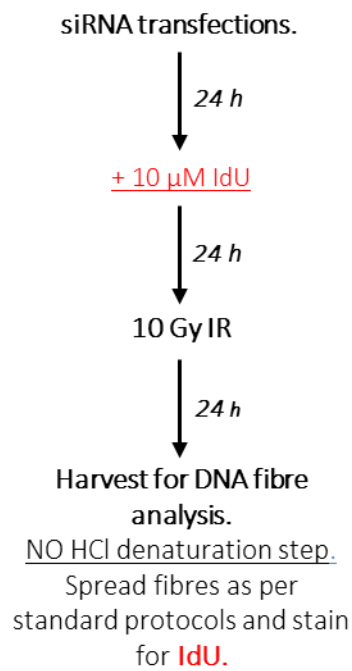
HeLa cells were treated with siRNA targeting BOD1L and a control sequence, pre-treated with Aphidicolin and exposed to 3 Gy IR. Cells were harvested for analysis at the indicated time points following IR. Coverslips were pre-extracted and fixed prior to staining with the named antibodies. Representative images of RPA foci in late S/G2 (CENPF-positive) HeLa cells are shown in (a). The proportion of late S/G2 cells (CENPF-positive) with at least 10 RPA2 foci was quantified at the time points given (b). Data shown in (b): 3 independent experiments with ≥ 100 nuclei analysed per experiment. Statistics: Student's T-test for Control vs. BOD1L. 0 hr (untreated): $p > 0.05$. 1 hr: $p < 0.0005$. 4 hr: $p < 0.0005$. 8 hr: $p < 0.0005$. 24 hr: $p < 0.0005$. Error bars indicate SEM.

In parallel, cells cultured and irradiated as above were harvested for immunofluorescence microscopy after 24 h and stained with antibodies against IdU and CENPF, thereby allowing for the identification of late S/G2-phase cells (figure 3.9a). The number of IdU foci per cell was analysed by immunofluorescence microscopy as an indicator of the number of DSBs resected per cell. In contrast to the results of the native fibre analyses, BOD1L depletion was found to have a significant impact on the number of IdU foci, with more foci per cell in the absence of BOD1L (figure 3.9b). Based on these observations, it was apparent that BOD1L did not suppress the extent of resection at DSBs, but restricted the number of DSBs resected. I therefore concluded that, rather than acting as physical block to the progress of resection at individual DSBs, it was more likely that BOD1L influenced the activity of key nucleases to effect a global suppression of resection in cells exposed to IR.

3.2.5: Elevated DSB resection in the absence of BOD1L is suppressed by depletion of CtIP

BOD1L suppresses aberrant resection of stalled replication forks by inhibiting the nuclease DNA2 (Higgs et al., 2015). The previous sections of this chapter provided evidence of a parallel role for BOD1L in the modulation of IR-induced DSB resection; however, the nucleases responsible for unscheduled resection in the absence of BOD1L had not been investigated in this novel context. For this reason, I set out to identify the relevant nucleases from a panel of well-characterised factors associated with resection of DSBs: CtIP and MRE11, which perform short-range resection in the 3'-5' direction, and DNA2 and EXO1, which are responsible for long-range resection with support from BLM (Heyer et al., 2010, Nimonkar et al., 2011).

(a)



(b)

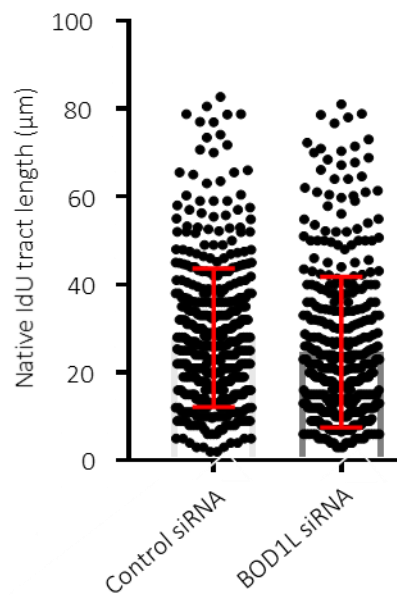
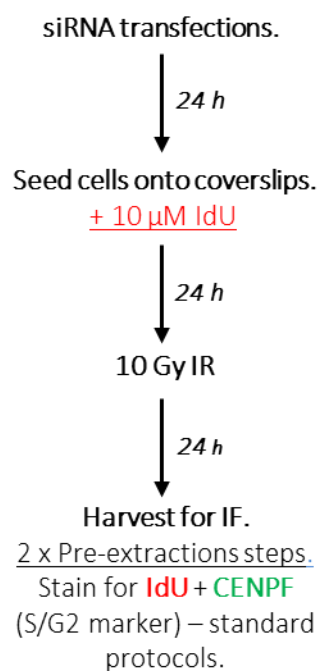


Figure 3.8: BOD1L depletion has no detectable impact on the extent of resection of individual IR-induced DSBs.

HeLa cells were transfected with siRNA against BOD1L or a non-targeting control sequence. The following day, the culture medium was supplemented with IdU. After 24 h, cells were treated with 10 Gy IR. Cells were harvested, stained with antibodies against IdU and spread for DNA fibre analysis, omitting the HCl denaturation step. Fluorescence microscopy images were acquired and native IdU tract length was measured using ImageJ software. The workflow is summarised in (a); native IdU tract lengths are shown in (b).

Data shown in (b): 3 independent experiments with ≥ 100 tracts measured per condition in each experiment. Statistics: T-test for Control vs. BOD1L: $p > 0.05$. Bars indicate the standard deviation from the population mean.

(a)



(b)

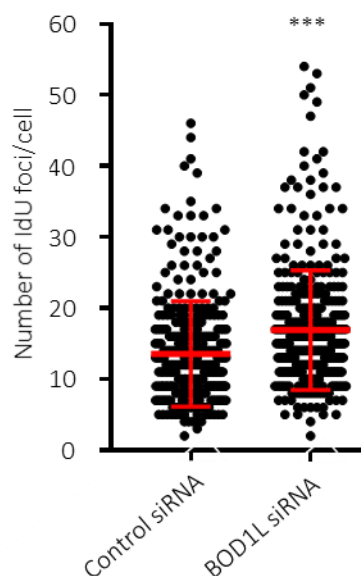


Figure 3.9: More IR-induced DSBs are subjected to nucleolytic resection in BOD1L-depleted cells than in control cells.

HeLa cells were transfected with Control or BOD1L siRNA and cultured with 10 μ M IdU. After 24 h, cells were treated with 10 Gy IR. Coverslips were harvested and stained with antibodies against IdU and the S/G2 marker CENPF. The number of IdU foci per CENPF-positive cell was quantified by immunofluorescence microscopy. The workflow is summarised in (a); the numbers of foci per cell are shown in (b).

Data shown in (b): 3 independent experiments with ≥ 100 nuclei analysed per condition in each experiment. Statistics: T-test for Control vs. BOD1L: $p < 0.0005$. Bars indicate the standard deviation from the population mean.

As proof of principle, the above-mentioned nucleases were depleted with siRNA in HeLa and U-2-OS cells, with the exception of MRE11, which was inhibited with Mirin. In addition to single knockdowns of the named nucleases, BLM was also co-depleted with DNA2 and with EXO1 to account for the functional relationships between these factors (Heyer et al., 2010, Nimonkar et al., 2011). Due to the established role of the named nucleases in DSB resection and repair, I predicted that ssDNA accumulation would be reduced in the absence of these nucleases. siRNA-transfected cells were exposed to 3 Gy IR and harvested for immunofluorescence microscopy and Western blotting after 8 h. Cells grown on coverslips for microscopy were treated with Aphidicolin prior to irradiation to prevent transition of cells through S-phase, thereby facilitating specific identification of damaged G2 nuclei. Western blotting was used to confirm knockdown of the relevant proteins, and also to compare levels of RPA2 phosphorylation between conditions. Coverslips were treated with antibodies against RPA2 and co-stained with CENPF to permit the identification of G2 nuclei. The localisation of RPA2 to IR-induced DSBs was quantified by immunofluorescence microscopy as an indication of IR-induced accumulation of ssDNA.

Depletion of the target nucleases was first verified by Western blotting in HeLa cells; this also confirmed that levels of total RPA2 were unaltered by nuclease depletion. Somewhat surprisingly, CtIP depletion and MRE11 inhibition both led to a notable increase in RPA-P (S4/S8) levels, with a lesser increase seen upon co-depletion of BLM and EXO1; this result counter-intuitively implied an increase in resection in the absence of these nucleases (figure 3.10). Nevertheless, the depletion of the candidate nucleases in the same cells resulted in a two- to

threefold reduction of IR-induced RPA2 focus formation in G2 nuclei relative to the control condition, with the most pronounced impact observed upon depletion of CtIP. The exception to this was the depletion of EXO1, which did not have any discernible impact on RPA2 recruitment (figure 3.11). This latter observation may have reflected the fact that EXO1 participates in long-range resection, which takes place after the initial short-range resection by CtIP and MRE11; the knockdown of this nuclease would therefore not be expected to abrogate all resection (Huertas, 2010).

For further verification of these results, the depletion of the same panel of nucleases was repeated in a second cell line, U-2-OS, using the same experimental setup as described for HeLa. In parallel, to verify the functionality of Mirin at the relevant concentration, U-2-OS cells were treated for 1 hr with 1 μ M Camptothecin (CPT), with or without the addition of 50 μ M Mirin. These cells were harvested and stained with antibodies against RPA2 and RPA-P (S4/S8). CPT-treated cells typically show high levels of RPA2 phosphorylation. It was anticipated that correctly-functioning Mirin would considerably impair this phosphorylation through its inhibition of MRE11, which is responsible for initiating short-range resection along with CtIP (Dupré et al., 2008).

Depletion of the relevant factors was first confirmed by Western blotting; in fact, the efficiency of the knockdowns—particularly the dual depletions of BLM/DNA2 and BLM/EXO1—was generally higher in this cell line than in HeLa. Furthermore, although levels of RPA2 remained constant across all conditions, a reduction in levels of IR-induced RPA-P (S4/S8) was observed

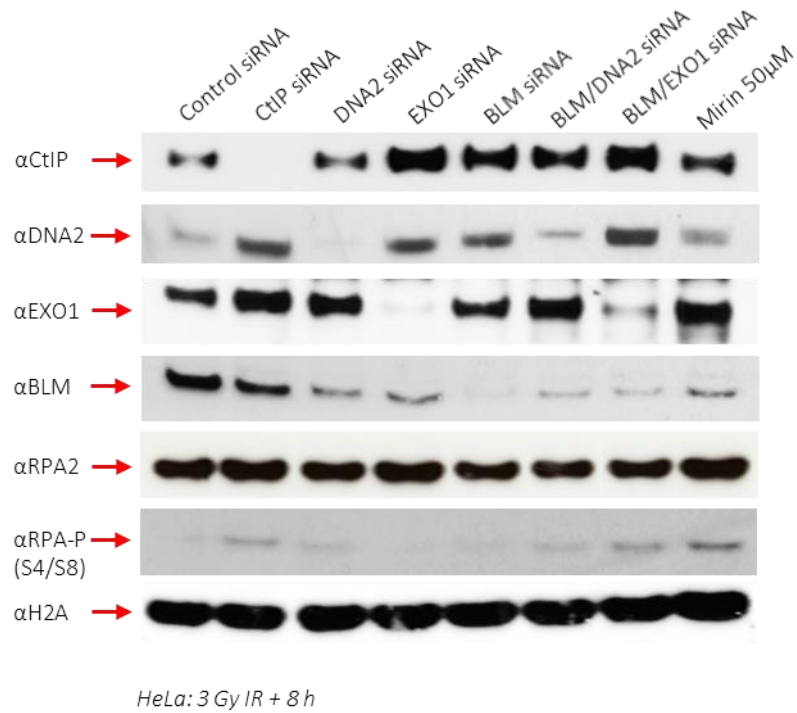
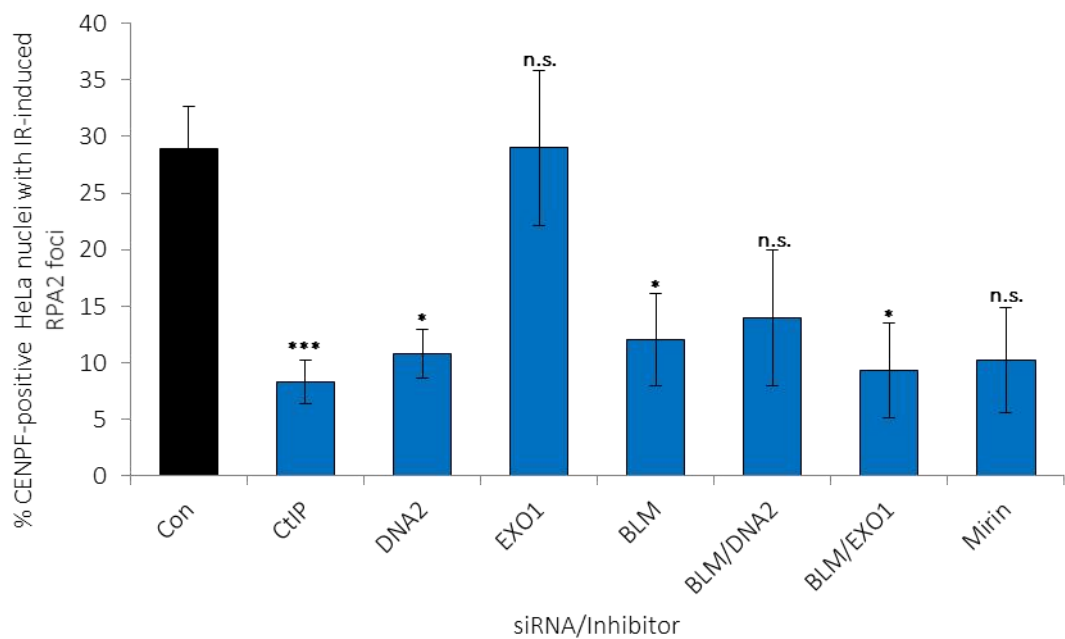


Figure 3.10: Depletion of a panel of key nucleases in HeLa cells.

HeLa cells were treated with the indicated siRNA/inhibitor, exposed to 3 Gy IR and harvested after 8 h for analysis by SDS-PAGE and Western blotting. Membranes were probed with the named primary antibodies and labelled with HRP-conjugated secondary antibodies before visualisation by chemiluminescence.

(a)



(b)

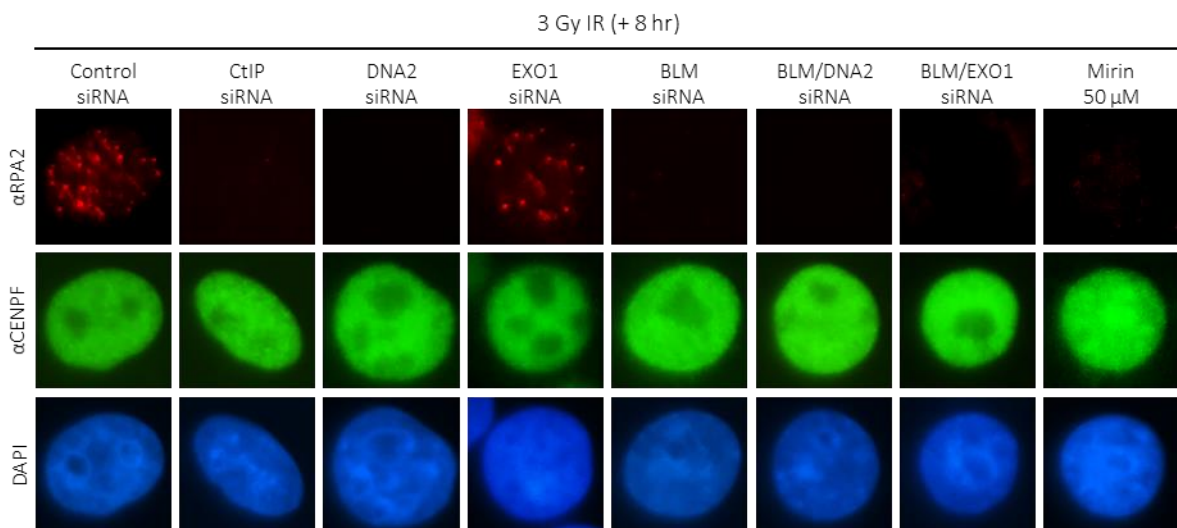


Figure 3.11: Depletion of key DSBR-associated nucleases reduces IR-induced resection in HeLa cells.

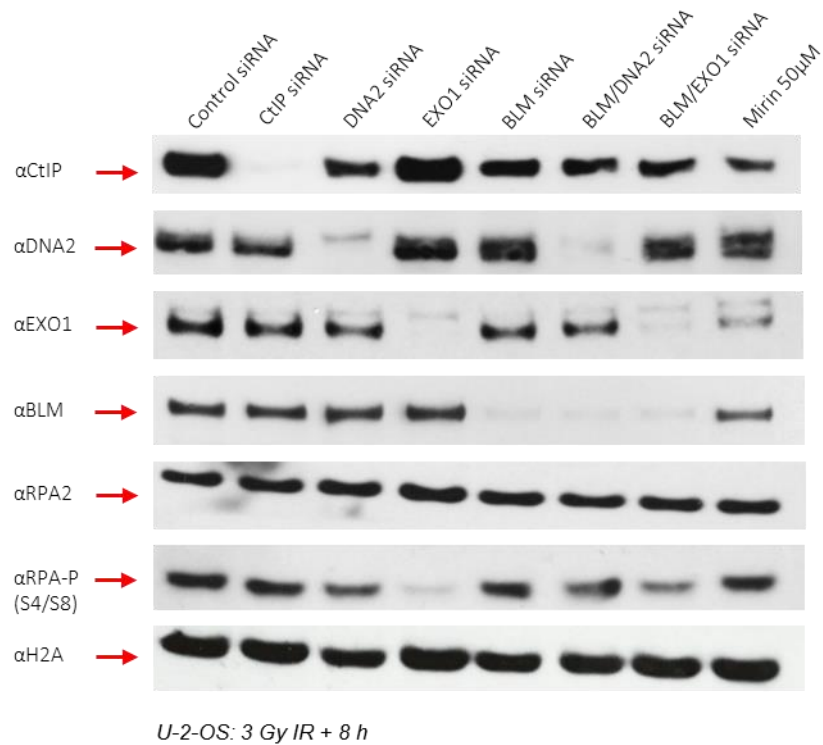
HeLa cells were treated with the indicated siRNAs/inhibitor, pre-treated with 3 μ M Aphidicolin and harvested 8 h following exposure to 3 Gy IR. Cells on coverslips were pre-extracted, fixed and stained with antibodies against RPA2 and CENPF. The proportion of CENPF-positive cells with at least 10 RPA2 foci was assessed by immunofluorescence microscopy (a). Representative images are shown in (b).

Data shown in (a) are from 3 independent experiments with ≥ 100 cells analysed per condition in each experiment. Statistics: Student's T-test for Control vs. KD/inhibitor. CtIP: $p = 0.007$. DNA2: $p = 0.01$. EXO1: $p = 0.99$. BLM: $p = 0.03$. BLM/DNA2: $p = 0.10$. BLM/EXO1: $p = 0.02$. Mirin: $p = 0.05$. Error bars indicate SEM.

upon depletion or inhibition of the full nuclease panel (figure 3.12a). Additionally, as predicted, Mirin had no impact on the prevalence of RPA2 foci, but CPT-induced RPA-P (S4/S8) foci were not detected in cells treated with this inhibitor (figure 3.12b). This confirmed that Mirin functioned as expected to inhibit MRE11 activity. Immunofluorescence analysis revealed that the depletion of CtIP, DNA2, BLM/DNA2, BLM/EXO1 and the inhibition of MRE11 resulted in a significant reduction in the proportion of cells with RPA2 foci from 38.9 % to between 6.7 % and 11.0 %. Upon depletion of EXO1 or BLM, this proportion was also reduced, albeit to a lesser degree (figure 3.13). These results demonstrated that the depletion of key pro-resection factors reduced resection of IR-induced DSBs in this experimental setup.

Having validated my planned protocol, I moved on to identify the nucleases which specifically play a role in the aberrant resection of DSBs in BOD1L-deficient cells. There was considerable variation observed in the positive control experiments performed in HeLa cells. The depletion of key nucleases in HeLa did not consistently lead to the reduction in both IR-induced RPA2 foci formation and S4/S8 phosphorylation as expected. As such, U-2-OS cells were selected for subsequent studies of DSB resection in the absence of BOD1L. BOD1L was co-depleted with the described panel of nucleases in U-2-OS cells; as above, cells were exposed to 3 Gy IR (with Aphidicolin pre-treatment in advance of irradiation for microscopy coverslips) and harvested after 8 h for immunofluorescence microscopy and Western blotting. Coverslips were stained with antibodies against RPA2 and CENPF.

(a)



(b)

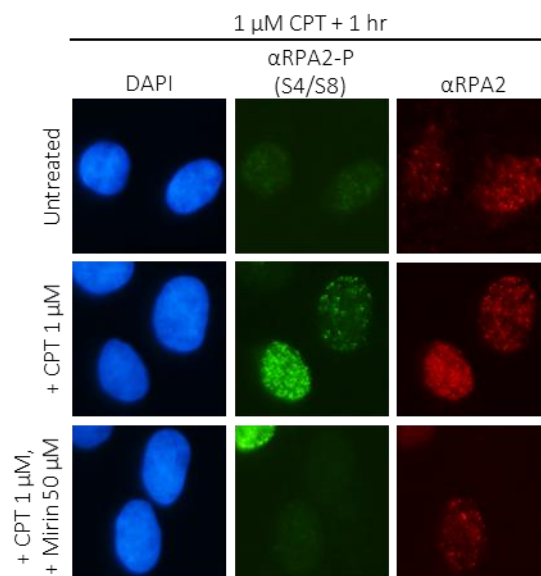


Figure 3.12: Depletion of a panel of key nucleases in U-2-OS cells.

U-2-OS cells treated with the named siRNA/inhibitor were irradiated with a dose of 3 Gy and harvested 8 h post-irradiation. Whole-cell extracts were prepared and analysed by SDS-PAGE and Western blotting. Membranes were probed with the indicated primary antibodies, incubated with HRP-conjugated secondary antibodies and visualised by chemiluminescence (a). U-2-OS cells were seeded onto coverslips and treated with CPT or Mirin as described. After 1 h, coverslips were harvested for immunofluorescence microscopy, pre-extracted and fixed before being stained with the named antibodies (b).

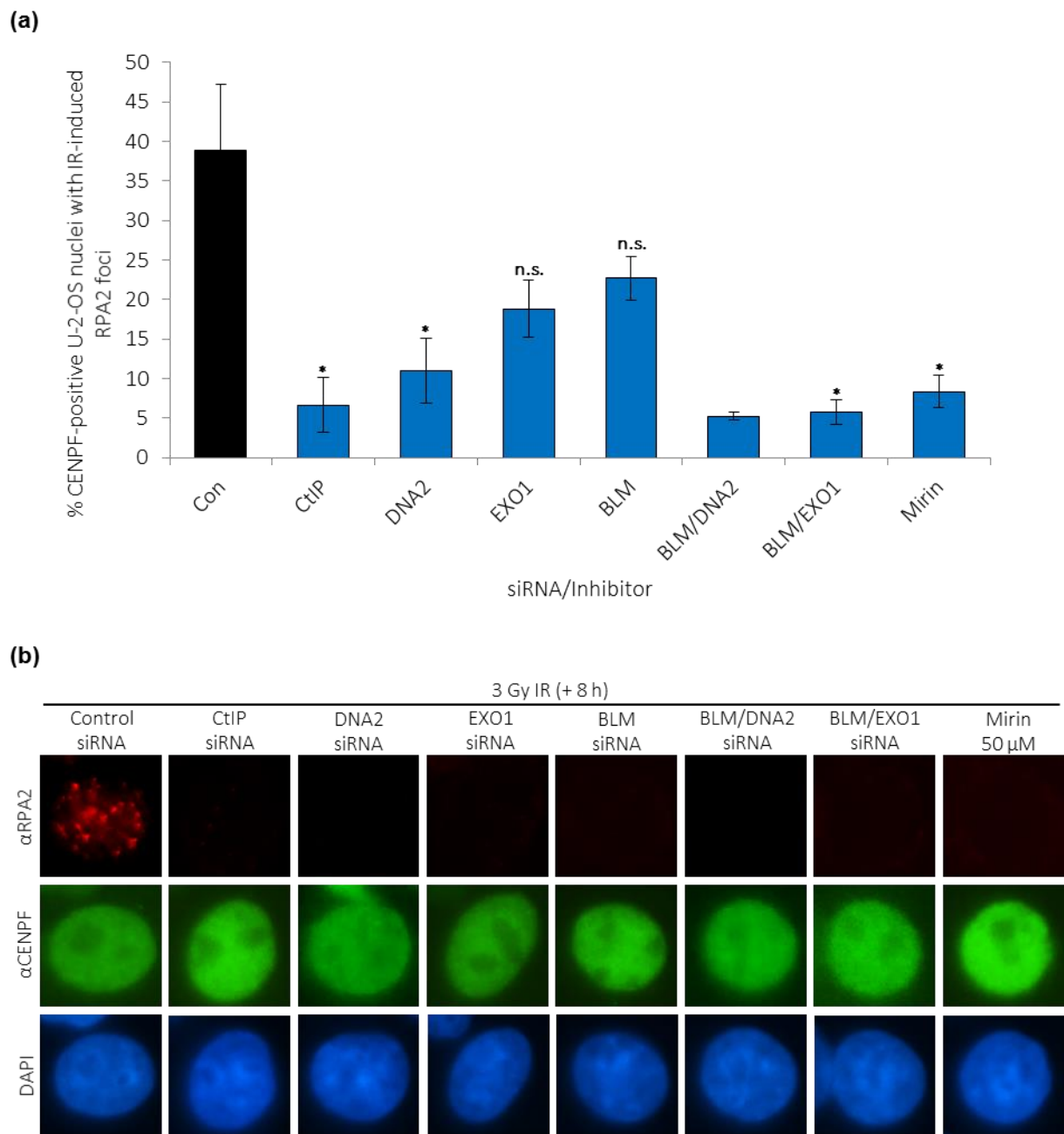


Figure 3.13: IR-induced resection in U-2-OS cells is reduced by depletion of key DSB-associated nucleases.

U-2-OS cells were treated with the indicated siRNAs/inhibitor, pre-treated with 3 μ M Aphidicolin, exposed to 3 Gy IR and harvested after 8 h. Coverslips were pre-extracted, fixed and stained with antibodies against RPA2 and CENPF. The proportion of CENPF-positive nuclei with at least 10 RPA2 foci was assessed by immunofluorescence microscopy (a). Representative images are shown in (b).

Data shown in (a): 3 independent experiments with ≥ 100 cells analysed per condition in each experiment. Statistics: Student's T-test for Control vs. KD/inhibitor. CtIP: $p = 0.02$. DNA2: $p = 0.04$. EXO1: $p = 0.09$. BLM: $p = 0.13$. BLM/DNA2: $p = 0.05$. BLM/EXO1: $p = 0.02$. Mirin: $p = 0.02$. Error bars indicate SEM.

The depletion of BOD1L and all nucleases of interest was demonstrated by Western blotting (figure 3.14). The recruitment of RPA2 to ssDNA was examined with immunofluorescence microscopy; the proportion of G2 (CENPF-positive) cells with at least 10 RPA2 foci was calculated. In support of my earlier findings, the depletion of BOD1L alone led to a significant increase in the proportion of RPA2-positive nuclei from one third to nearly half of G2 cells. Depleting CtIP and BLM/DNA2 along with BOD1L gave the most pronounced reductions in RPA2 focal accumulation, whilst depleting BOD1L with DNA2, EXO1 or BLM was less consequential. The combined knockdown of EXO1 and BLM in BOD1L-deficient cells had a greater impact than the single knockdowns. Inhibition of MRE11 in cells lacking BOD1L suppressed RPA focus formation, but only to a level slightly lower than control cells (figure 3.15). A number of important conclusions were drawn based on these observations. Firstly, as the increase in IR-induced DSB resection in BOD1L-deficient cells was rescued by co-depletion with CtIP, this suggested a prominent role for CtIP in the aberrant resection observed in the absence of BOD1L. As a similar result was observed for the depletion of BLM and DNA2 in combination with BOD1L, this also implied a role for these nucleases. Interestingly, the depletion of DNA2 in combination with BOD1L was insufficient to rescue uncontrolled resection. This contrasted with the findings of the previous study on BOD1L's role in the DDR, in which it was demonstrated that BOD1L suppresses DNA2 to restrict resection of stalled replication forks (Higgs et al., 2015); this implied that BOD1L may function via a novel mechanism in cells exposed to IR.

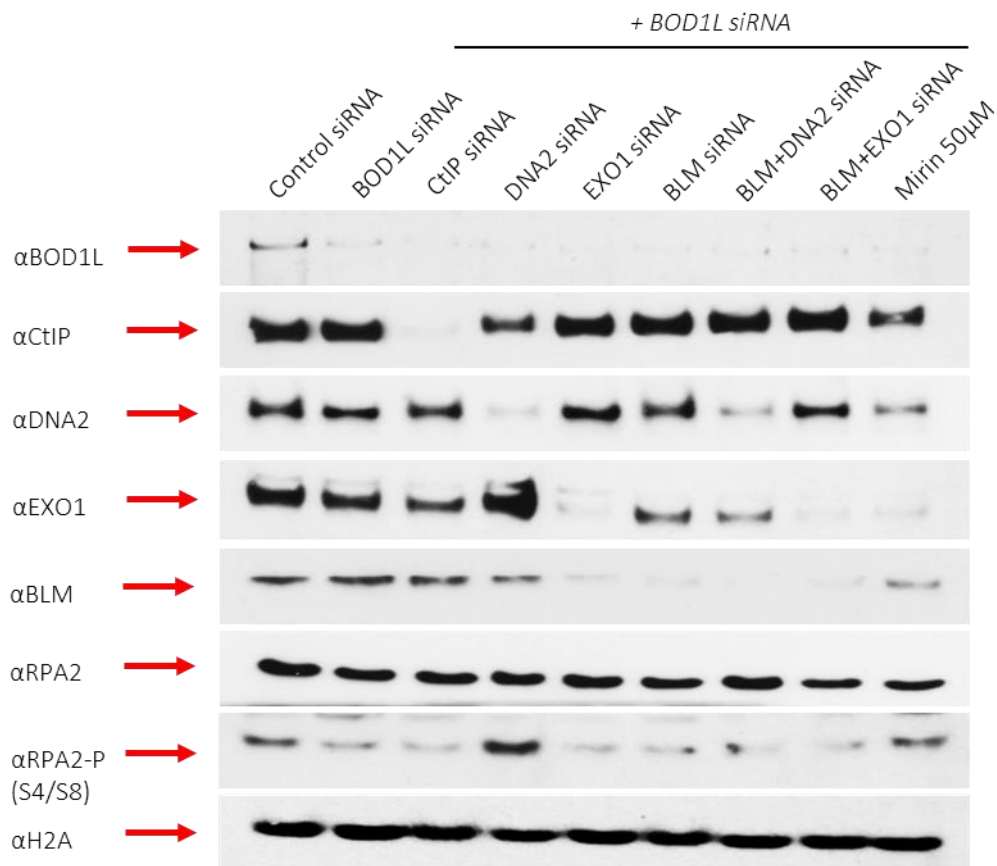


Figure 3.14: Depletion of CtIP rescues defective resection of IR-induced DSBs in the absence of BOD1L.

U-2-OS cells were treated with the indicated siRNA or inhibitor, exposed to 3 Gy IR and harvested after 8 h for analysis. Whole-cell extracts were prepared and analysed by SDS-PAGE and Western blotting. Membranes were probed with the named primary antibodies, incubated with HRP-conjugated secondary antibodies and visualised by chemiluminescence.

One shortfall with the scoring of RPA2 focus-positive cells was the potential for subjectivity during analyses. Furthermore, quantifying only focus-positive cells would mean that differences in focus intensity would be overlooked; such differences could be indicative of altered levels of resection. To overcome these caveats, a set of fluorescence microscopy images from the above experiments was analysed using a software-based intensity calculation protocol, as summarised in figure 3.16a. ImageJ was used to calculate the mean RPA2 intensity per unit area in CENPF-positive control cells and those depleted of BOD1L and BOD1L/CtIP. The mean RPA2 intensity was higher in BOD1L-depleted cells than controls, and co-depletion of BOD1L with CtIP reduced this intensity (figure 3.16b). These data provided further support for the importance of CtIP in aberrant resection in BOD1L-deficient cells.

Next, I investigated changes in RPA-P (S4/S8) protein levels in response to the depletion of BOD1L and CtIP as a proxy for nucleolytic resection. To this end, I transfected U-2-OS cells with siRNA against BOD1L, CtIP or both proteins, alongside a non-targeting control sequence. Transfected cells were irradiated with 15 Gy IR and harvested 8 h post-damage for analysis by Western blotting. As expected, RPA2 phosphorylation was negligible in all non-irradiated cells. In agreement with earlier results from this chapter, depletion of BOD1L resulted in a high level of IR-induced RPA2 phosphorylation. CtIP-deficient cells exhibited minimal levels of phosphorylated RPA2. Importantly, co-depletion of BOD1L and CtIP reduced RPA-P (S4/S8) to levels lower than those observed in cells depleted of BOD1L alone (figure 3.17). These results collectively illustrated that CtIP-mediated resection of IR-induced DSBs increased in BOD1L-

depleted cells, suggesting that CtIP played a key role in the uncontrolled resection of IR-induced DSBs in the absence of BOD1L.

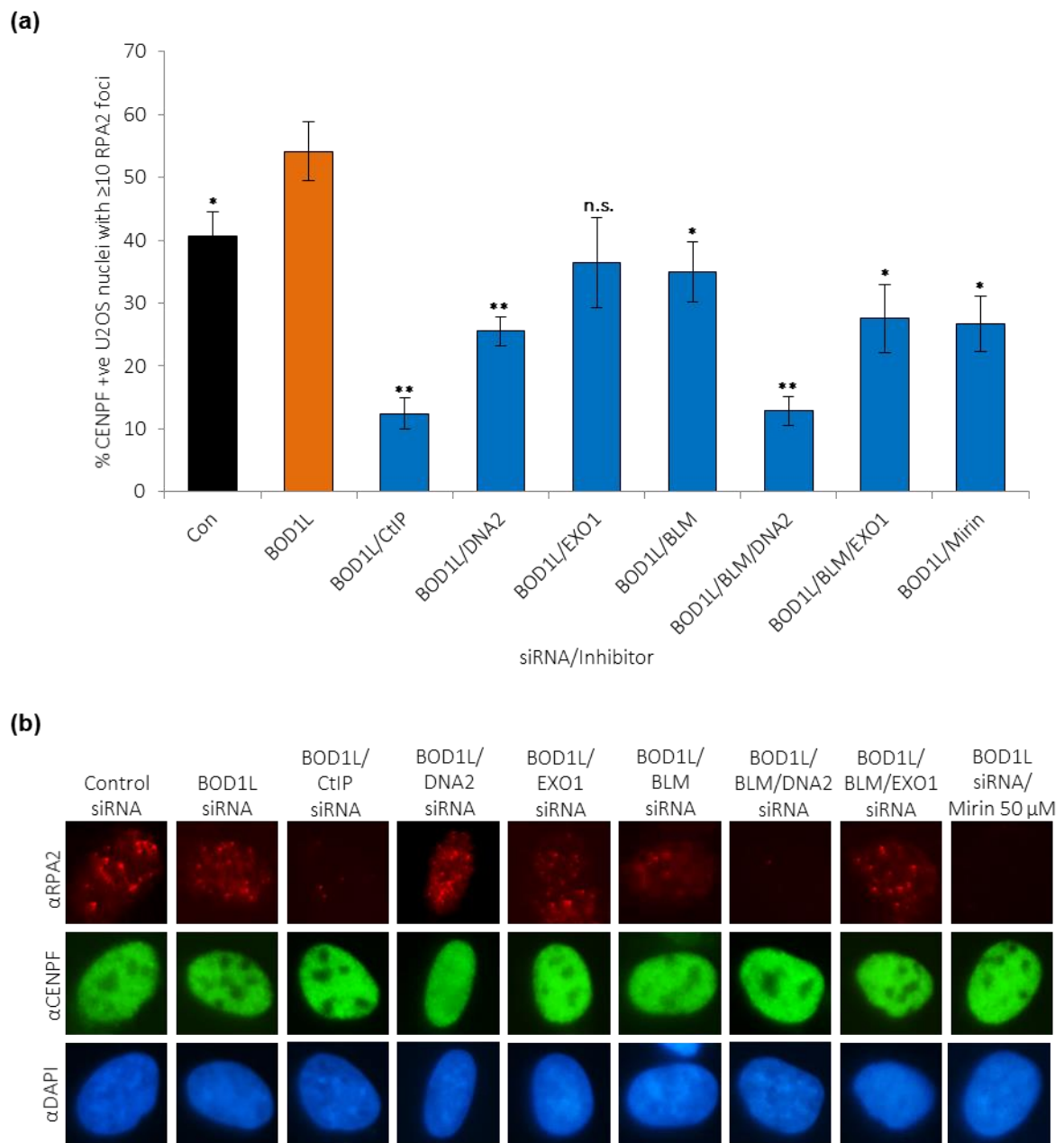


Figure 3.15: Depletion of CtIP rescues defective resection of IR-induced DSBs in the absence of BOD1L.

U-2-OS cells were treated with the indicated siRNA/inhibitor, pre-treated with Aphidicolin and irradiated with 3 Gy IR. After 8 h, cells were harvested for immunofluorescence microscopy. Coverslips were pre-extracted, fixed and stained with antibodies against RPA2 and CENPF. The proportion of CENPF-positive nuclei with at least 10 RPA2 foci was quantified. Proportions are shown in (a) with representative images in (b).

Data shown in (a): 3 independent experiments with ≥ 100 cells quantified per condition in each experiment. Statistics: Student's T-test for Control/KD vs. BOD1L. Control: $p = 0.04$. BOD1L/CtIP: $p = 0.001$. BOD1L/DNA2: $p = 0.005$. BOD1L/EXO1: $p = 0.11$. BOD1L/BLM: $p = 0.04$. BOD1L/BLM/DNA2: $p = 0.007$. BOD1L/BLM/EXO1: $p = 0.02$. BOD1L/Mirin: $p = 0.01$. Error bars indicate SEM.

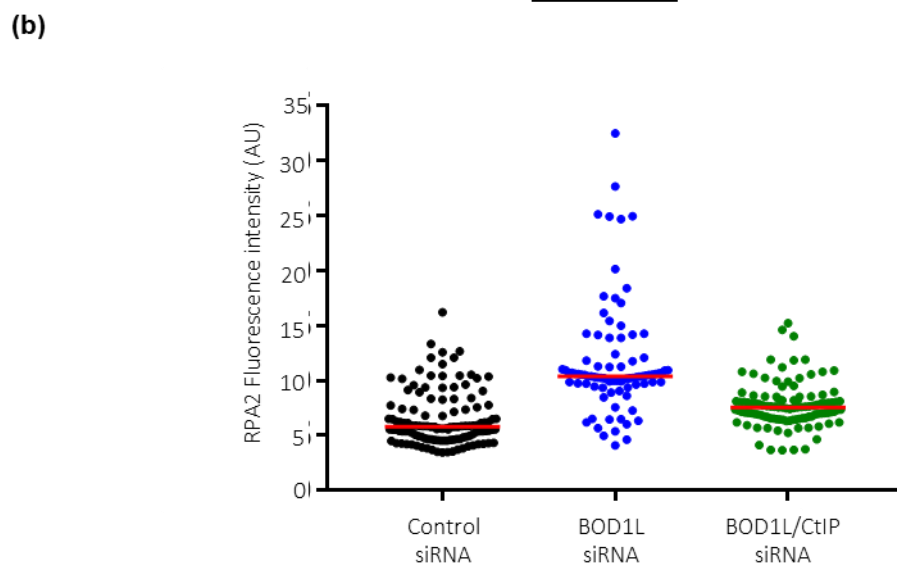
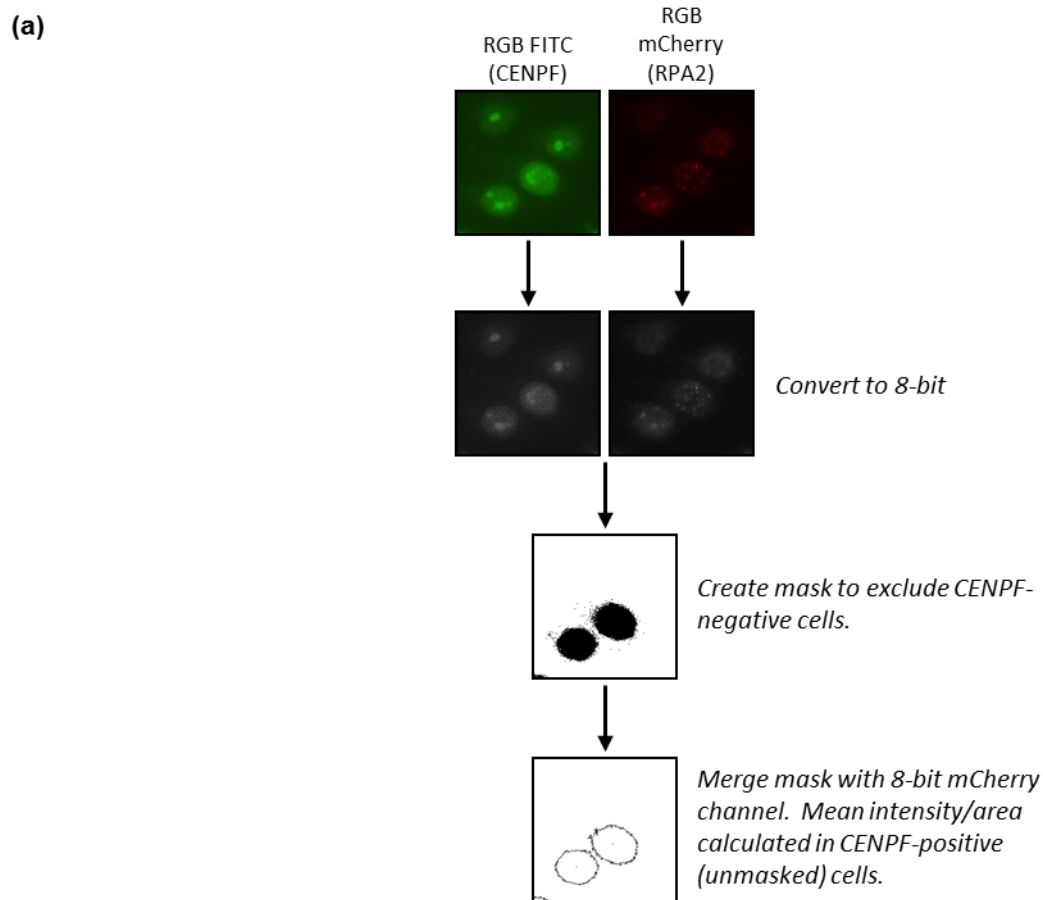


Figure 3.16: Co-depletion of CtIP rescues increased RPA2 fluorescence intensity observed in BOD1L-deficient cells.

Following treatment of U-2-OS cells as described in figure 3.15, immunofluorescence microscopy images were acquired in the FITC and mCherry channels and analysed using ImageJ software. Images were converted to 8-bit format and a mask was created to delineate CENPF-positive cells. This mask was merged with the mCherry channel image, and the mean mCherry fluorescence intensity per area was calculated in CENPF-positive cells (a). Intensity quantifications for 3 independent experiments are shown in (b).

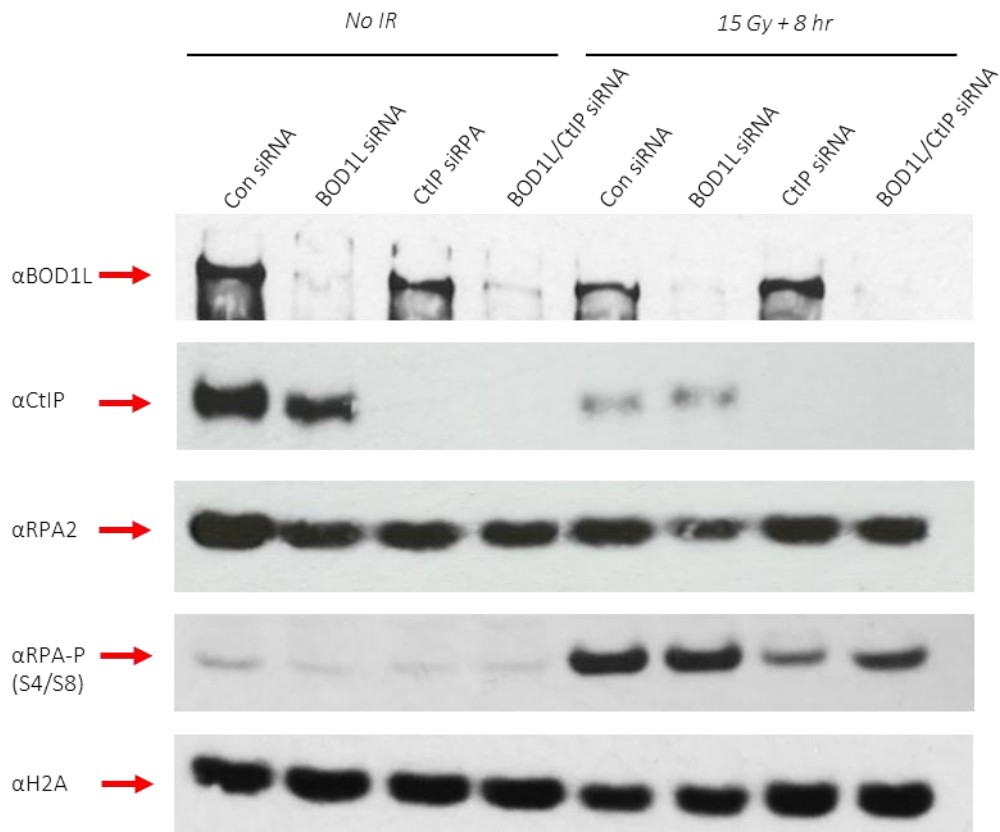


Figure 3.17: RPA-P (S4/S8) phosphorylation in BOD1L-deficient cells is reduced by co-depletion with CtIP.

U-2-OS cells were transfected with the indicated siRNA and irradiated with a dose of 15 Gy IR. After 8 h, cells were harvested and whole-cell extracts prepared for SDS-PAGE and Western blotting. Membranes were probed with the named primary antibodies, incubated with HRP-conjugated secondary antibodies and then visualised with chemiluminescence.

3.3: Discussion

The founding work into the role of BOD1L in the DDR by Higgs and colleagues revealed that this factor suppresses resection of stalled replication forks, allowing them to be repaired by HR and thereby contributing to the maintenance of genome stability (Higgs et al., 2015). I therefore proposed that BOD1L may also modulate the resection of DSBs in cells exposed to IR, which is a potent inducer of these lesions (Mehta and Haber, 2014). I first investigated cell viability and DSB signalling and repair in BOD1L-depleted cells treated with IR, hypothesising that these would be impaired if BOD1L were required for the resolution of IR-induced DSBs. In support of my predictions, cell survival was significantly compromised in the absence of BOD1L, as demonstrated by a clonogenic survival assay. I subsequently demonstrated by immunofluorescence microscopy that BOD1L-deficient cells failed to resolve 53BP1 and γ H2AX foci by 24 h post-irradiation. These observations collectively suggested that whilst BOD1L was dispensable for the initiation of IR-induced DDR signalling, it was required to complete repair of DSBs. It was also worthy of note that the persistence of IR-induced γ H2AX foci was apparent in BOD1L-depleted G2 cells, but not in G1 cells, suggesting a specific role in the repair of G2 DNA damage.

One key consideration when inducing DSBs with IR and examining G2 nuclei is that IR-induced DNA damage is not restricted to G2 cells. S-phase nuclei may also sustain DNA damage following exposure to IR, allowing for the possibility of damaged S-phase cells entering G2 phase between irradiation and analysis. I acknowledged that this could artificially elevate the proportion of cells exhibiting DNA damage foci and attempted to prevent this scenario by

treating cells with the DNA polymerase α inhibitor Aphidicolin prior to irradiation. This prevented the transition of S-phase cells to G2, thereby ensuring that any CENPF-positive nuclei identified were G2 cells that had been irradiated whilst in this phase.

A fully functional DDR is essential for the maintenance of genome stability. Failure to resolve DNA damage in a timely and appropriate manner can ultimately lead to cell death. Surviving cells may exhibit micronuclei: a hallmark of genome instability (Naim and Rosselli, 2009, Tucker and Preston, 1996). I therefore examined the prevalence of micronuclei in BOD1L-depleted cells following irradiation. Cells depleted of BOD1L exhibited more micronucleation than control cells, suggesting that BOD1L was crucial for the resolution of IR-induced DSBs and maintenance of genome stability after IR exposure. These results demonstrated that the role of BOD1L as a genome stability factor was not restricted to cells experiencing replication stress.

BOD1L's role in the DDR during replication stress involves the indirect suppression of nucleolytic resection of stalled replication forks. I hypothesised that it could also influence the resection of DSBs in cells exposed to IR to facilitate repair. A role in resection modulation was supported by the aforementioned G2-specific failure of BOD1L-depleted cells to clear IR-induced γ H2AX foci; resection of DSBs as a precursor to HR is primarily restricted to G2 cells (Heyer et al., 2010). To investigate this, I examined IR-induced recruitment of RPA2 in BOD1L-deficient cells by immunofluorescence microscopy. RPA2 rapidly binds to ssDNA, such as tracts exposed by nucleolytic resection of a DNA lesion, to stabilise it and prevent the formation of secondary structures (Nakajima et al., 2015). However, ssDNA can be exposed by any

physiological process that requires the DNA double-helix to be unwound, such as transcription or DNA replication. Whilst RPA2 is frequently used to provide an indication of fluctuating levels of resection, it must be noted that this protein is recruited to all nuclear ssDNA, and not solely to resected sites. With this caveat in mind, I also monitored the phosphorylation of RPA2 at S4 and S8 by immunoblotting. RPA2-P (S4/S8) is specifically associated with nucleolytic resection (Ashley et al., 2014).

My immunofluorescence microscopy studies revealed an increase in IR-induced accumulation of RPA2 at DSBs in BOD1L-deficient cells. In agreement with the above hypothesis, this was suggestive of a role for BOD1L in suppressing nucleolytic resection of DSBs. The corresponding elevation in RPA2 phosphorylation shown by Western blotting further supported this notion. It is particularly of note that both RPA2 recruitment and phosphorylated RPA2 levels reached their peaks at 8 hours after exposure to IR. As these two markers follow the same pattern of accumulation and resolution in BOD1L-depleted cells subjected to irradiation, it can be concluded that the changing RPA2 focal accumulation is likely, at least in part, to be the result of altered levels of resection.

The nature of this defective resection in the absence of BOD1L was probed further using native DNA fibre analysis and the enumeration of IdU foci by immunofluorescence microscopy. This provided a sensitive means of distinguishing between an increased number of DSBs resected per cell versus a greater extent of resection at individual breaks in BOD1L-deficient cells. Having demonstrated a significant increase in IdU foci but no detectable change in the mean length of

ssDNA tracts at resected DSBs, I concluded that BOD1L functioned to restrict the number of DSBs resected in cells exposed to IR. In this manner, BOD1L may preserve genome stability in cells exposed to IR by effecting a shift in repair dynamics to favour the more rapid, template-independent NHEJ pathway.

It is known that in the context of replication stress, DNA2 is responsible for unscheduled resection of stalled replication forks in the absence of BOD1L. However, it was not known whether the increased resection of IR-induced DSBs in BOD1L-deficient cells was attributable to DNA2, or to other nucleases. The latter scenario would suggest that BOD1L operates via distinct mechanisms to repair different types of DNA lesion. I therefore set out to identify the nucleases which promote aberrant resection of IR-induced DSBs in the absence of BOD1L by co-depleting BOD1L with a panel of candidate factors, exposing cells to IR and analysing the proportion of RPA2-positive cells in each condition by immunofluorescence microscopy. As resection in advance of HR-mediated repair typically occurs only during G2 phase, analyses were confined to G2 (CENPF-positive) nuclei.

There was a significant reduction in the proportion of RPA2 focus-positive cells upon depletion of BOD1L with CtIP, which suggested that this nuclease was required for the increased IR-induced ssDNA accumulation observed in BOD1L-deficient cells. As further verification of the relevance of this nuclease, IR-induced RPA2 (S4/S8) phosphorylation was assessed in cells depleted of BOD1L and CtIP by Western blotting. As mentioned earlier, this post-translational modification is specifically associated with resected regions of ssDNA (Ashley et al., 2014). In

agreement with the abrogation of RPA2 focus formation, there was a reduction in IR-induced RPA2 phosphorylation upon co-depletion of these proteins. Moreover, I carried out software-based analysis of RPA2 intensity in cells depleted of BOD1L or BOD1L with CtIP. This enabled me to assess changes in RPA2 recruitment in an unbiased manner, accounting for any fluctuations in antibody staining efficiency or background fluorescence that could have been problematic whilst making observations solely by eye. In line with my earlier observations, RPA2 fluorescence intensity was higher in BOD1L-depleted cells than in control cells; this intensity was reduced upon co-depletion of BOD1L and CtIP. Collectively, these data suggested that CtIP played a prominent role in over-resection of DSBs in the absence of BOD1L. This points towards a scenario in which BOD1L regulates the activity of this nuclease directly or indirectly to suppress uncontrolled resection of IR-induced DSBs during G2.

It is well established that short-range DSB resection by CtIP underpins all subsequent resection associated with DSB repair. It could therefore be argued that lower levels of resection would be expected for depletion of CtIP irrespective of a cell's BOD1L status; indeed, this has been demonstrated by previous studies (Sartori et al., 2007). However, the results discussed above lent credibility to the proposal that CtIP specifically played a role in over-resection of DSBs in the absence of BOD1L, implying that BOD1L may influence the resection of IR-induced DSBs by modulating the activity of CtIP in a manner that remained to be determined.

Notably, the knockdown of DNA2 alone in BOD1L-depleted cells had less impact on the resection of IR-induced DSBs than on stalled replication forks. In addition, the depletion of BLM

alone had only a modest impact on the level of resection in BOD1L-deficient cells. In the context of replication stress, siRNA-mediated knockdown of either BLM or DNA2 in BOD1L-deficient cells was sufficient to rescue the aberrant resection of stalled replication forks observed in cells depleted of BOD1L alone (Higgs et al., 2015). This contrast suggested that BOD1L modulated resection of IR-induced DSBs via a novel mechanism, and not in the same manner by which it protects stalled replication forks from inappropriate nuclease activity. It implied that uncontrolled resection of IR-induced DSBs in the absence of BOD1L was attributable to alternative nucleases. My demonstration of the importance of CtIP in aberrant resection, as discussed in this chapter, was in line with this assertion.

It was therefore somewhat surprising that the depletion of BLM and DNA2 in combination had such a pronounced impact on DSB resection in BOD1L-deficient cells; the result was comparable to that of CtIP depletion in the absence of BOD1L. I considered the possibility that these nucleases in combination played a key role in aberrant DSB resection in BOD1L-deficient cells; however, this may well be an overly simplistic interpretation. Unanswered questions remain concerning the role of BLM in BOD1L-mediated DNA damage repair. As was discussed by Higgs and colleagues regarding BOD1L's role in replication stress, it was not known whether BOD1L inhibits DNA2-mediated resection by directly suppressing BLM activity, or by limiting access to stalled forks by the stabilisation of RAD51 (Higgs et al., 2015). As such, the impact on resection of BLM/DNA2 depletion in the absence of BOD1L could not be regarded as definitive evidence for the importance of these factors in aberrant resection of IR-induced DSBs. Further investigations will therefore be required in order to elucidate the complex

interplay between BOD1L, BLM and DNA2 in this aspect of the DDR. As well as supporting the current experiments with native fibre and IdU focus analyses in BLM/DNA2- and BOD1L/BLM/DNA2-depleted cells to confirm the suspected resection defect, the impact of these depletions on IR-induced RAD51 focus formation could also be examined.

In summary, these data demonstrated that alongside its role during replication stress, BOD1L facilitated the repair of IR-induced DSBs and maintained genome stability and cell viability following exposure to IR. It fulfilled this role by preventing uncontrolled CtIP-mediated resection of IR-induced DSBs.

Nucleolytic resection of DSBs is a carefully controlled process. Whilst resection is fundamental to HR, unregulated resection can render lesions irreparable and ultimately lead to genome instability (Higgs et al., 2015). To maintain appropriate resection and facilitate repair, a well-characterised DSB end protection network exists to antagonise nuclease activity. The apical factor of this network is 53BP1, which is recruited to DSBs following phosphorylation by ATM (Symington and Gautier, 2011, Bothmer et al., 2010, Bunting et al., 2010). When resection and HR would be inappropriate for the repair of a particular lesion, 53BP1 and its downstream effectors antagonise the recruitment of BRCA1 to the site of damage, thereby preventing short-range resection by CtIP and allowing for repair by NHEJ (Chen et al, 2008). I hypothesised that there could be interplay between BOD1L and this anti-resection pathway as a means of regulating nuclease activity. The experiments of the following chapter therefore aimed to investigate the mechanisms through which BOD1L regulates resection of IR-induced DSBs.

Chapter 4: The interaction of BOD1L with resection antagonist RIF1 and the implications for DSB repair

4.1: Introduction

The results presented in Chapter 3 demonstrate that BOD1L plays a role in suppressing nucleolytic resection of IR-induced DSBs. One scenario which could explain these findings is that BOD1L may modulate DSB resection by regulating one or more of the factors which antagonise this process. This cascade of DNA end protection factors ensures that resection is suppressed during phases of the cell cycle in which no homologous sister chromatid is available as a template for repair (Heyer et al., 2010).

Several anti-resection and pro-NHEJ factors have been identified. The first, whose role in end protection is well characterised, is 53BP1, which is recruited to DSBs following ATM phosphorylation at multiple sites within its N-terminus (Symington & Gautier, 2011, Bothmer et al., 2010, Bunting et al., 2010). These phosphorylation events are a pre-requisite for the interaction of 53BP1 with several key downstream effectors, including RIF1 and PTIP (Zimmerman & de Lange, 2014). RIF1 is essential for 53BP1-mediated cellular processes. Along with 53BP1, it antagonises short-range nucleolytic resection outside late S/G2, promotes non-homologous end joining and functions in class-switch recombination (CSR), which requires NHEJ-mediated repair of programmed DSBs (Feng et al., 2013, Chapman et al., 2013, Escribano-Diaz et al., 2013, di Virgilio et al., 2013). Whilst the precise role of PTIP is not fully understood,

it is acknowledged that there may be some functional overlap between PTIP and RIF1. For instance, the increase in DSB end resection and abrogation of dysfunctional telomere fusion observed in the absence of RIF1 can be recapitulated by depleting PTIP (Zimmerman and de Lange, 2014). Collectively, 53BP1 and RIF1 recruit REV7 to damaged chromatin (Xu et al., 2015a, Boersma et al., 2015). It was recently demonstrated that RIF1/REV7-mediated inhibition of resection involves the Shieldin complex, which physically protects DSB ends from nucleolytic processing. A series of studies identified this complex as a distal effector of 53BP1. Comprising newly-characterised C20orf196 (SHLD1), FAM35A (SHLD2) and CTC-534A2.2 (SHLD3), the Shieldin complex is targeted to DSBs via the interaction between SHLD2 and REV7, where it restricts DNA end resection and promotes NHEJ (Dev et al., 2018, Gupta et al., 2018, Noordermeer et al., 2018, Findlay et al., 2018).

Post-translational histone modifications play a key role in fine-tuning DSB repair pathway choice. Ubiquitination of histones at sites of DNA damage is carried out in an ATM-dependent manner by the E3 ligases RNF8 and RNF168 (Wang and Elledge, 2007, Stewart et al., 2009). In particular, it has been shown that RNF168-mediated mono-ubiquitination of H2A/H2AX at K13-15 is critical for the initiation of downstream DDR signalling (Mattioli et al., 2012). This promotes the recruitment of 53BP1 and BRCA1 to damaged chromatin (Uckleemann and Sixma, 2017), and crosstalk between post-translational modifications ensures the selection of the appropriate repair pathway. Whilst ubiquitination of H2A at K13-15 by RNF168 favours 53BP1-mediated end protection and repair by NHEJ, this block to resection can be overcome by the

ubiquitination of H2A at K127-129 by BRCA1 and its functional interactor BARD1 (Chapman et al., 2012, Densham et al., 2016).

Furthermore, a recent study revealed that histone methylation can dictate repair pathway choice for DSBs in pre- and post-replicative chromatin while DNA replication is ongoing. During this phase, incompletely-replicated DNA exists alongside replicated regions; the mechanism by which 53BP1-mediated end protection was directed specifically to lesions in non-replicated DNA to promote NHEJ was not previously understood. Simonetta and colleagues demonstrated that pre-replicative chromatin contains the highest possible concentration of histone H4 di-methylation of lysine 20 (H4K20^{Me2}), which provides a binding site for 53BP1. In these regions, 53BP1, in complex with RIF1 and REV7, are reliably recruited to DSBs, thereby suppressing the accumulation of BRCA1 and subsequent nucleolytic resection. Following DNA replication, the 50 % reduction in the concentration of H4K20^{Me2} triggers the dissociation of 53BP1-RIF1-REV7 from damaged chromatin, allowing for recruitment of BRCA1 and repair by HR (Simonetta et al., 2018).

In this context, the work described in this chapter aimed to elucidate the potential interactions between BOD1L and key resection antagonists, and to investigate their impact on DSB resection and repair.

4.2: Identification of a functional interaction between BOD1L and the resection antagonist RIF1

Although it has been shown that BOD1L suppresses excessive resection of IR-induced DSBs during G2, how this occurs is unclear. To investigate the hypothesis that BOD1L regulates resection antagonists to influence resection, initial experiments focused on the identification of novel BOD1L interactors using pull-downs of GFP-tagged murine Bod1L and characterisation of the resultant interacting proteins by mass spectrometry. These approaches revealed an interaction between Bod1L and the resection antagonist RIF1, which was confirmed and further characterised by immunoprecipitation and pull-down approaches. Cellular studies were subsequently performed to assess the recruitment of 53BP1 pathway components to IR-induced DSBs in BOD1L-depleted cells during G1 and G2. The proficiency of class switch recombination (CSR), a fundamental 53BP1-dependent process, was assessed in control and Bod1L-deficient mouse models. Finally, the collective role of BOD1L and RIF1 in the maintenance of genome stability was analysed using immunofluorescence techniques.

4.2.1: BOD1L interacts with the 53BP1 effector RIF1

The identification of potential novel BOD1L interactors may shed light on its role as a suppressor of DSB resection. In order to identify uncharacterised BOD1L-protein interactions in a sensitive, quantitative and unbiased manner, an approach involving affinity purification and mass spectrometry (AP-MS) was adopted. This technique has been utilised to identify novel protein-protein interactions within the DDR, allowing the identification of multi-protein complexes as well as binary interactions in near-physiological cellular states (Li et al., 2015).

The required constructs and cell lines were generated at the Francis Crick Institute, London, UK, as part of an ongoing collaboration with Prof. Simon Boulton and Valérie Borel. Firstly, a HeLa cell line stably expressing murine Bod1L tagged with FLAG-GFP (Bod1L-FLAG-GFP) was generated (figure 4.1); this construct was created by fusing genomic mBod1L to an existing FLAG-GFP construct using a BAC sub-cloning kit. Alongside this, a control cell line expressing an empty FLAG-GFP vector was created. This approach enabled the rapid and robust affinity purification of tagged Bod1L using validated reagents. Protein isolation with antibodies targeting epitope tags is widely used in mass spectrometry-based protein interaction studies as a means of overcoming the potential cross-reactivity associated with antibodies against endogenous proteins. Additionally, validated enrichment reagents and protocols are readily available (Smits and Vermeulen, 2016).

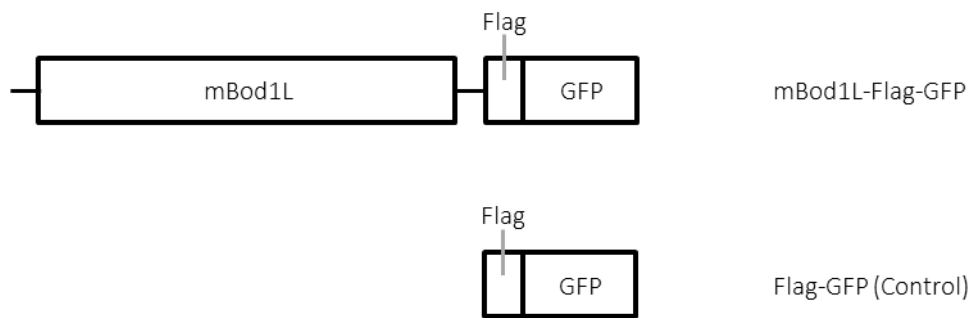


Figure 4.1: Schematic representation of Bod1L-Flag-GFP construct.

Murine Bod1L genomic DNA (along with linker sequences at both termini of the mBod1L sequence) was fused to Flag-GFP using a BAC sub-cloning kit to generate Bod1L-Flag-GFP. HeLa cells stably transfected with this construct were used to prepare mass spectrometry samples to identify novel Bod1L interactors. Control samples were prepared from cells stably expressing Flag-GFP alone.

Constructs generated by Prof. Simon Boulton and Valérie Borel, Francis Crick Institute, London.

Monolayers of cells harbouring Bod1L-FLAG-GFP or the control vector were cultured, harvested and lysed to generate whole-cell extracts. Immune complexes were isolated by incubation with an anti-GFP antibody and extensively washed; bound proteins were then separated by SDS-PAGE. Gel slices were excised and processed for mass spectrometry, with relative protein abundances determined by intensity-based absolute quantification (iBAQ). In iBAQ, the sum of the intensities of all tryptic peptides is calculated for each protein and divided by the number of theoretically observable peptides. The resultant intensities provide an accurate determination of the relative abundance of all proteins identified in a sample.

The top 30 proteins that were enriched in the Bod1L-containing complexes compared to controls by iBAQ are shown in Table 4.1. In addition to the successful identification of Bod1L in FLAG-bound immune complexes, the screen also showed enrichment of several key proteins, confirming its validity. For example, members of the COMPASS complex and several associated proteins, including ASH2L, RBBP5, and CXXC1 (the latter of which is involved in the localisation of the complex) (Couture and Skiniotis, 2013, Lee and Skalnik, 2005) were amongst the most highly enriched proteins. This was anticipated due to the interaction of BOD1L with the histone methyltransferase SETD1A (Higgs et al., 2018). Moreover, the complete MCM replicative helicase (MCM2-7) was identified in the screen, along with other proteins associated with DNA replication (Zhai et al., 2017). This is in line with BOD1L's known role in stabilising stalled replication forks (Higgs et al., 2015). Furthermore, DNA repair proteins such as MSH2, XRCC5 and RAD50 were also identified (Heyer et al., 2010, Noll et al., 2006). The identification of these

Table 4.1: Proteins identified by mass spectrometry screen as being highly enriched in complexes containing mBod1L.

Protein name	Gene name
Bi-orientation defect 1-like	<i>Bod1l</i>
Set1/Ash2 histone methyltransferase complex subunit ASH2	<i>ASH2L</i>
Retinoblastoma-binding protein 5	<i>RBBP5</i>
CpG-binding protein Cfp1	<i>CXXC1</i>
Structural maintenance of chromosomes flexible hinge domain-containing protein 1	<i>SMCHD1</i>
Cullin-associated NEDD8-dissociated protein 1	<i>CAND1</i>
Structural maintenance of chromosomes protein 2	<i>SMC2</i>
DNA replication licensing factor MCM5	<i>MCM5</i>
DNA mismatch repair protein Mlh1	<i>MLH1</i>
DNA replication licensing factor MCM3	<i>MCM3; HCC5</i>
DNA replication licensing factor MCM7	<i>MCM7</i>
X-ray repair cross-complementing protein 6	<i>XRCC6</i>
DNA replication licensing factor MCM4	<i>MCM4</i>
Fanconi anemia group I protein	<i>FANCI</i>
Structural maintenance of chromosomes protein	<i>SMC4</i>
DNA replication licensing factor MCM2	<i>MCM2</i>
Chromodomain-helicase-DNA-binding protein 4	<i>CHD4</i>
Mitotic checkpoint protein BUB3	<i>BUB3</i>
DNA mismatch repair protein Msh6	<i>MSH6; GTBP</i>
DNA mismatch repair protein Msh2	<i>MSH2</i>
SWI/SNF complex subunit SMARCC2	<i>SMARCC2</i>
X-ray repair cross-complementing protein 5	<i>XRCC5</i>
DNA replication licensing factor MCM6	<i>MCM6</i>
Structural maintenance of chromosomes protein 1A	<i>SMC1A</i>
DNA damage-binding protein 1	<i>DDB1</i>
Telomere-associated protein RIF1	<i>RIF1</i>
E3 ubiquitin-protein ligase RNF213	<i>RNF213</i>
DNA repair protein RAD50	<i>RAD50</i>
Scaffold attachment factor B2; Scaffold attachment factor B1	<i>SAFB2; SAFB</i>

HeLa cells stably expressing mBod1L-Flag-GFP or Flag-GFP alone were cultured and lysed. Tagged Bod1L and bound proteins were isolated with an anti-Flag antibody and affinity purification. Following extensive washing, samples were separated by SDS-PAGE and gel slices were processed for mass spectrometry. The top 30 proteins enriched in Bod1L-containing complexes relative to control samples are shown above. Proteins belonging to key functional categories have been highlighted. Orange: SETD1A (COMPASS) complex members & associated proteins. Green: proteins involved in DNA replication. Blue: DNA damage repair proteins.

Mass spectrometry and data analysis carried out by Prof. Simon Boulton and Valérie Borel, Francis Crick Institute, London.

proteins is consistent with the role of BOD1L as a DNA repair factor and further demonstrated the ability of the screen to highlight potential interactions between BOD1L and other proteins within the DDR network. Interestingly, the 53BP1 effector RIF1 (Feng et al., 2013, Chapman *et al.*, 2013, Escribano-Diaz et al., 2013, di Virgilio et al., 2013) was found to be enriched in Bod1L-containing complexes, suggesting a previously unknown interaction between BOD1L and RIF1.

One consideration was that the addition of tags to Bod1L could have interfered with the protein's normal sub-cellular localisation or its interactions with other proteins. Immunoprecipitation was therefore used to confirm the suggested interaction between BOD1L and RIF1. To this end, nuclear cell extracts from HeLa cells were clarified by high speed centrifugation, and proteins immunoprecipitated using antibodies against BOD1L, RIF1, or an IgG control. Immune complexes were isolated with protein-A Sepharose and analysed by SDS-PAGE and Western blotting alongside an input control. Membranes were probed with antibodies against BOD1L and RIF1, followed by HRP-coupled secondary antibodies.

Both BOD1L and RIF1 were immunoprecipitated by their respective antibodies, but were absent from the IgG control; these observations confirmed the validity of the experiment. Moreover, RIF1 was detected in immune complexes containing BOD1L, suggesting an interaction between the two factors. In agreement with this, BOD1L was also present in RIF1-containing immune complexes in the reciprocal assay (figure 4.2). These results further supported an interaction between BOD1L and RIF1.

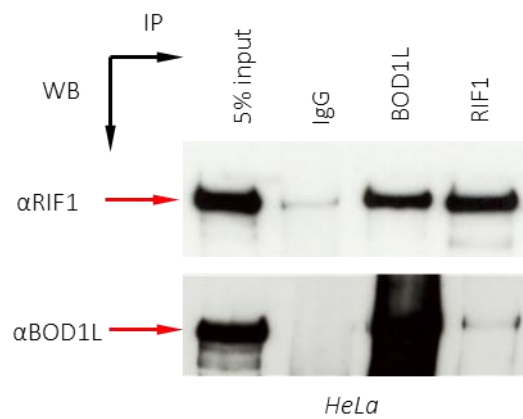


Figure 4.2: Confirmation of interaction between BOD1L and RIF1.

Nuclear extracts from HeLa cells were clarified by centrifugation, and then incubated with antibodies against BOD1L, RIF1, or an IgG control. Immune complexes were then isolated using protein-A Sepharose; complexes were analysed, along with a 5% input control, by SDS-PAGE and Western blotting. Membranes were probed with the indicated antibodies, and polypeptides detected using chemiluminescence.

Since RIF1 is known to antagonise nucleolytic resection during G1 (Feng et al., 2013, Chapman *et al.*, 2013, Escribano-Diaz et al., 2013, di Virgilio et al., 2013), this suggests a potential mechanism by which BOD1L may influence resection dynamics.

4.2.2: Identification of the RIF1-binding domains of BOD1L

Having revealed a previously unknown interaction between BOD1L and RIF1, the next objective was to identify the regions of BOD1L which are required for this interaction. As BOD1L contains no recognisable protein-protein interaction domains (Higgs et al., 2015), there were no specific candidate regions on which to focus these analyses; a search of the whole protein sequence was therefore necessary.

To this end, I generated 6 overlapping BOD1L fragments with N-terminal GST tags in the pGEX4T1 expression vector. These fragments ranged from 500-652 aa in length and collectively spanned the full length of the protein (figure 4.3a). The tagged proteins were then expressed and purified from *E. coli* using GST affinity reagents.

Purified GST-tagged BOD1L fragments or GST alone were incubated with clarified HeLa nuclear cell extracts. The tagged proteins and their interactors were subsequently isolated with glutathione Sepharose and analysed by SDS-PAGE and Western blotting. As can be observed in figure 4.3b, RIF1 was pulled down with fragments 1 and 2 and 6, but not by any other

fragments (figure 4.3b). It is therefore apparent that sequences within both the N- and C-terminal regions of BOD1L are required for its interaction with RIF1.

4.2.3: Recruitment of 53BP1, RIF1 and REV7 to DSBs is unaffected in the absence of BOD1L in G2 cells

The preceding data indicate that BOD1L interacts with the 53BP1 effector RIF1. In light of the anti-resection functions of RIF1 (Feng et al., 2013, Chapman *et al.*, 2013, Escribano-Diaz et al., 2013, di Virgilio et al., 2013), I therefore hypothesised that this interaction may act as a mechanism to suppress G2 resection, and that perturbation of this interaction may underlie the increased G2 resection observed in BOD1L-deficient cells (Chapter 3). To investigate this hypothesis, the impact of BOD1L depletion on the chromatin recruitment of three key resection antagonists was examined in G2 cells: 53BP1, the apical anti-resection factor, its principal effector RIF1, which suppresses BRCA1-mediated resection, and REV7, which contributes to DNA end protection by recruitment of the Shieldin complex.

Forty-eight hours after siRNA-mediated depletion of BOD1L, cells on coverslips were pre-treated with Aphidicolin, exposed to 3 Gy IR and harvested for immunofluorescence analyses after 8 h, as described in Chapter 3. Cells were then stained with antibodies against 53BP1, RIF1 and REV7, along with the S/G2 marker CENPF.

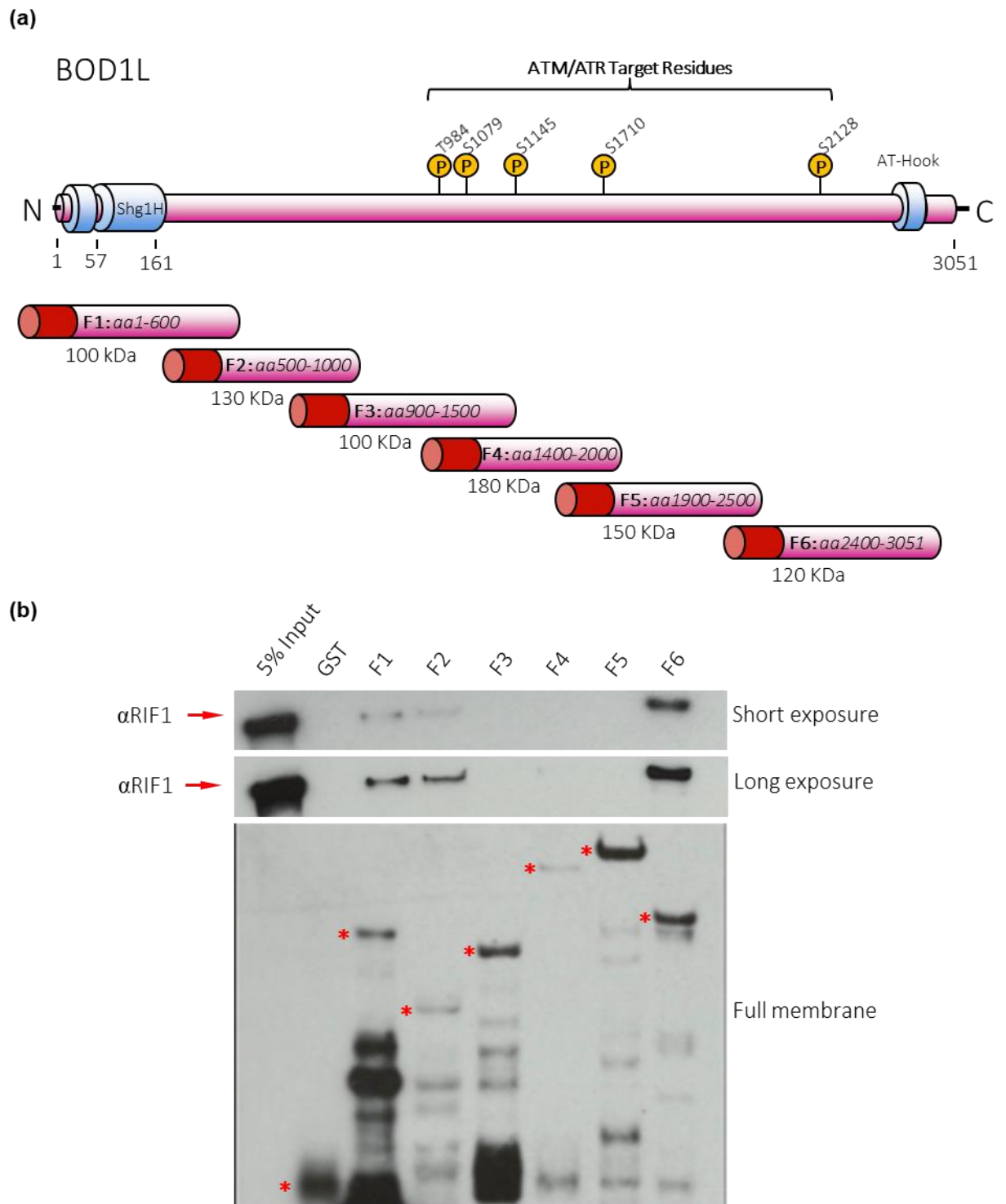


Figure 4.3: The interaction between BOD1L and RIF1 is mediated by both the N- and C-terminal regions of BOD1L. Six overlapping fragments of BOD1L, spanning the full amino acid sequence, were cloned and fused to N-terminal GST tags (a). For GST pull-down assays, purified tagged proteins (or purified GST alone) were incubated with HeLa whole-cells extracts, after which the GST-tagged proteins and bound complexes were isolated with protein-A Sepharose. Isolated protein complexes, along with a 5% sample of nuclear cell extract as input control, were analysed by SDS-PAGE and Western blotting, and membranes were then probed with antibodies against RIF1 (b). The bottom panel shows a Ponceau-stained membrane prior to immunodetection, with GST and tagged fragments F1-F6 denoted by an asterisk (*).

Successful depletion was first confirmed by immunoblotting (figure 4.4a). Next, the proportion of focus-positive G2 nuclei (CENPF-positive nuclei with at least 10 foci) was assessed by immunofluorescence microscopy. There was no significant difference in the proportion of 53BP1-positive G2 nuclei (figure 4.4b-c) between control and BOD1L-depleted cells; a comparable result was obtained when these experiments were repeated in U-2-OS cells (figure 4.5b-c). Similarly, there were no observable changes in the proportion of RIF1-positive nuclei (Figure 4.4d-e). These observations were recapitulated in U-2-OS cells (figure 4.5d-e). These results are not suggestive of a role for BOD1L in the recruitment of 53BP1 or RIF1 to IR-induced DSBs during G2.

In light of these observations, I postulated that the localisation of end protection components downstream of RIF1 may be compromised in the absence of BOD1L, potentially explaining the aberrant resection of IR-induced DSBs observed in G2 cells. The proportion of G2 nuclei with at least 10 REV7 foci was therefore also quantified in HeLa cells treated as described above. Initial observations revealed that the anti-REV7 antibody produced a high fluorescent background. Therefore, the ability of the antibody to detect REV7 foci at DSBs specifically was verified by depleting REV7 in HeLa cells and immunostaining with this antibody. Although the observed foci were small, their formation was abrogated in the absence of REV7 (figure 4.6a), demonstrating the capacity of the antibody to delineate REV7 foci at IR-induced DSBs, albeit with considerable spurious signal.

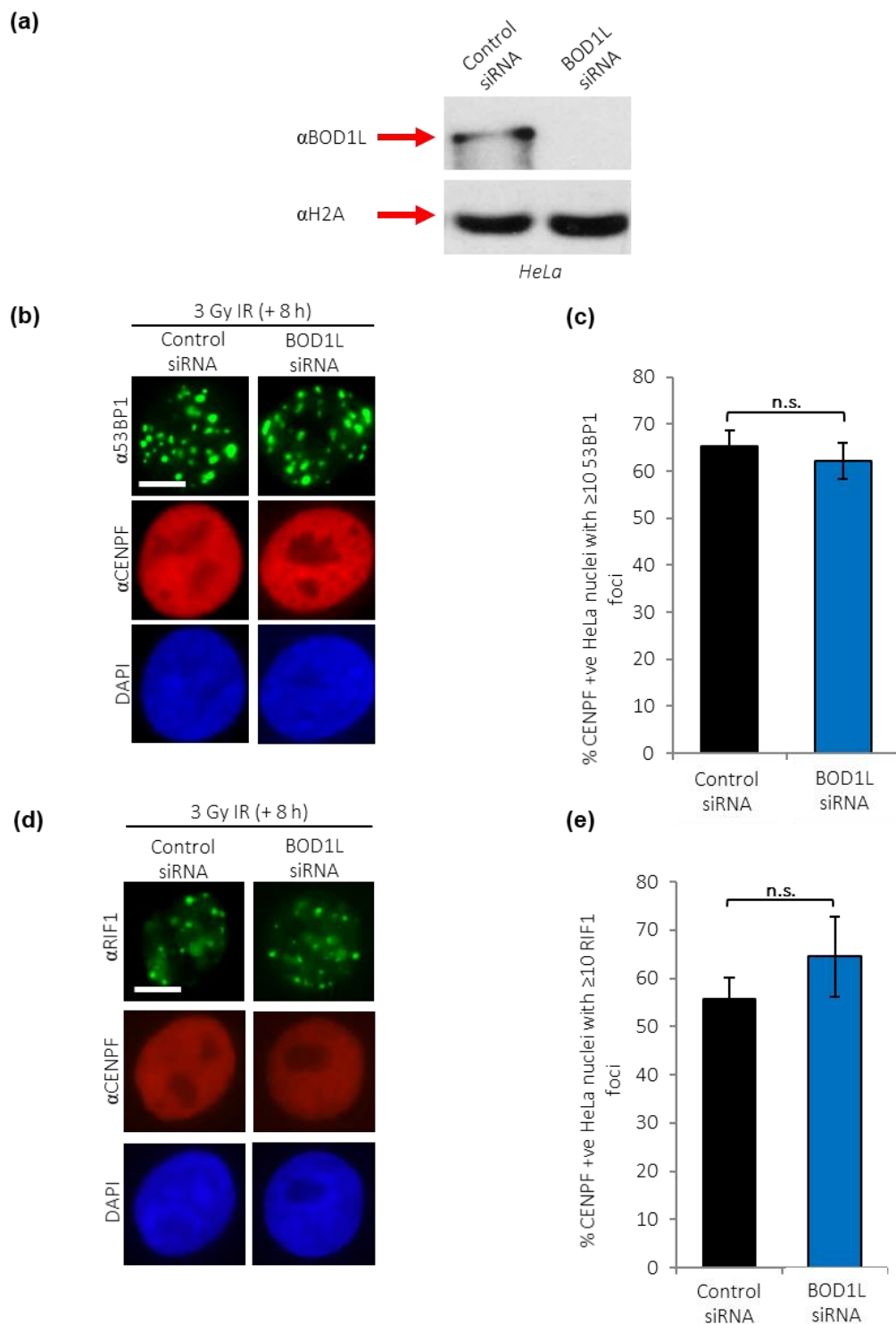


Figure 4.4: Depletion of BOD1L in HeLa cells has no impact on IR-dependent recruitment of factors that antagonise resection. HeLa cells were treated with the named siRNA, subjected to 3 Gy IR and harvested after 8 h for analysis. Whole-cells extracts were analysed by SDS-PAGE and Western blotting; membranes were probed with the indicated antibodies (a). Cells grown on coverslips and treated as above were pre-extracted and fixed for immunofluorescence microscopy before being labelled with antibodies against 53BP1/RIF1 and CENPF. The proportion of CENPF-positive (G2) cells with ≥ 10 53BP1 foci (b/c) in control and BOD1L-depleted cells was enumerated (statistics: Student's T-test for Control vs. BOD1L: $p = 0.49$). The proportion of CENPF-positive cells with RIF1 foci (d/e) was also assessed in cells treated as described above (statistics: Student's T-test for Control vs. BOD1L siRNA, $p = 0.40$). Scale bar = 10 μ M. Data shown in (c) and (e) represent mean data from 3 independent experiments, ≥ 100 cells per condition in each experiment. Error bars indicate SEM.

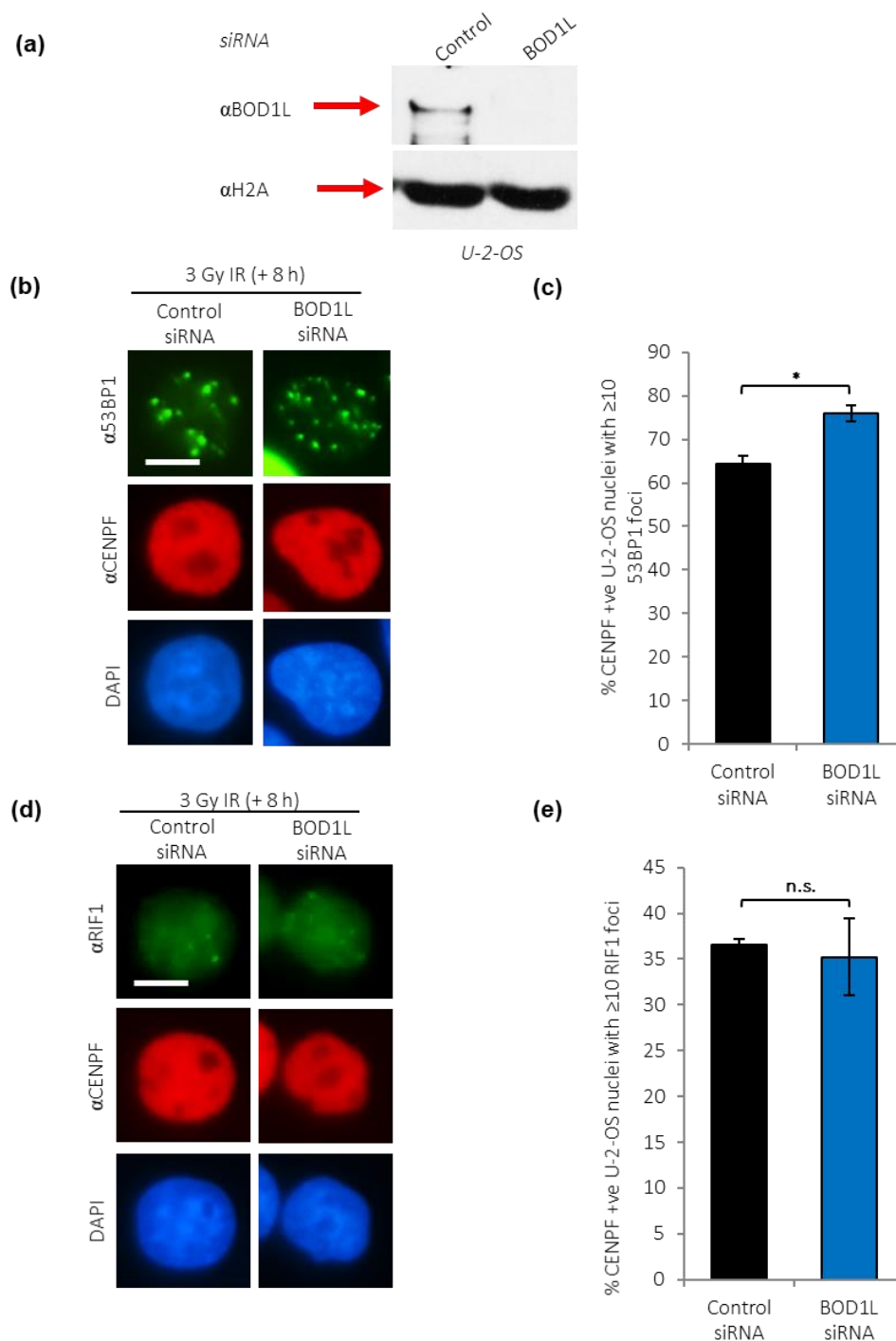


Figure 4.5: Depletion of BOD1L in U-2-OS cells has no impact on IR-dependent recruitment of key resection antagonists.

U-2-OS cells were treated with the indicated siRNA, subjected to 3 Gy IR and harvested after 8 h for analysis. Whole-cells extracts were analysed by SDS-PAGE and Western blotting to confirm protein depletion (a). Cells grown on coverslips and treated as above were pre-extracted and fixed for immunofluorescence microscopy before being labelled with antibodies against 53BP1/RIF1 and CENPF. The proportion of CENPF-positive (G2) cells with ≥ 10 53BP1 foci (b/c) in control and BOD1L-depleted cells was enumerated (statistics: Student's T-test for Control vs. BOD1L: $p = 0.01$). The proportion of G2 cells with RIF1 foci (d/e) was also assessed in cells treated as described above (statistics: Student's T-test for Control vs. BOD1L siRNA, $p = 0.81$). Scale bar = 10 μ M.

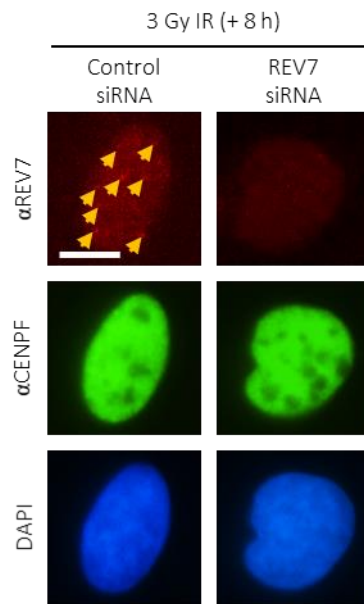
Data shown in (c) and (e): 3 independent experiments with ≥ 100 cells per condition in each experiment. Error bars indicate SEM.

Having demonstrated the functionality of the REV7 antibody, I then assessed the recruitment of REV7 to IR-induced DSBs in G2 cells. Negligible differences were observed in REV7 focus formation (Figure 4.6b-c) between control and BOD1L-depleted cells. However, any change in recruitment of REV7 in the absence of BOD1L may have gone undetected due to the high fluorescent background signal produced by the antibody. The modulation of REV7 recruitment by BOD1L during G2 cannot therefore be ruled out based on these experiments.

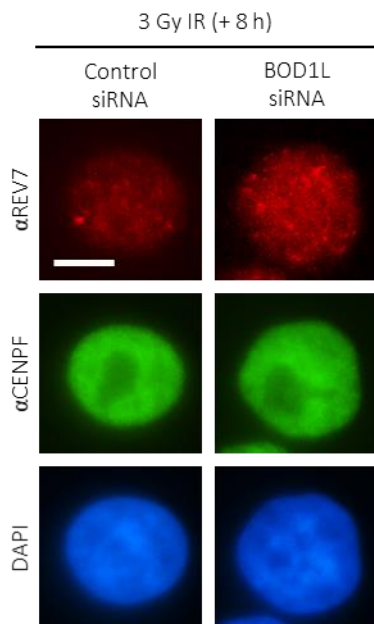
4.2.4: Chromatin recruitment of RIF1 in G1 cells is dependent on BOD1L

Multiple previous studies have demonstrated that the primary role of RIF1 as a suppressor of resection occurs in G1, during which it functions as an effector of 53BP1-mediated DNA end protection and promotes NHEJ (Feng et al., 2013, Chapman et al., 2013, Escribano-Diaz et al., 2013, di Virgilio et al., 2013). However, I had not yet investigated the impact of BOD1L on resection, or on the localisation of RIF1 to IR-induced DSBs, during G1. Chromatin recruitment of RIF1 in the absence of BOD1L was therefore examined in this phase of the cell cycle. HeLa cells were irradiated, harvested and stained as in section 4.3.3, but the quantification of nuclei with RIF1 foci by immunofluorescence microscopy was restricted to CENPF-negative cells. In contrast to the observations in G2 cells, depletion of BOD1L had a significant impact on the recruitment of RIF1 during G1, reducing the proportion of RIF1-positive nuclei from 83.7% to 47.3% (figure 4.7). This suggests that BOD1L is required to recruit RIF1 to sites of IR-induced DNA damage during G1.

(a)



(b)



(c)

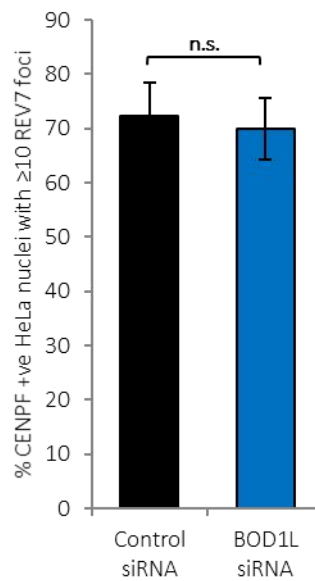
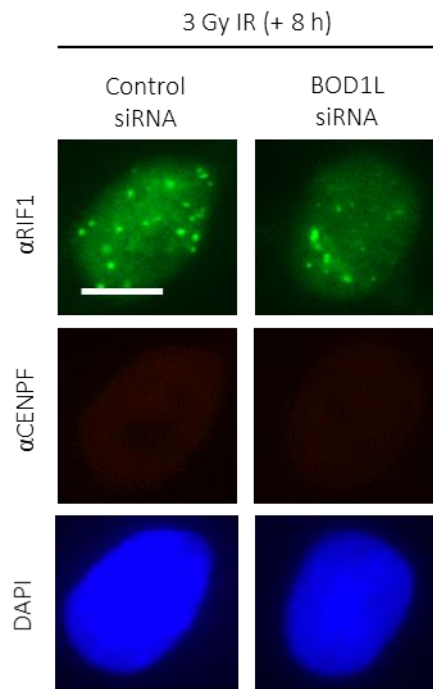


Figure 4.6: Depletion of BOD1L in HeLa has no detectable impact on recruitment of REV7.

HeLa cells were transfected with the indicated siRNAs, grown on coverslips and harvested for analysis 8 hours after a dose of 3 Gy IR. Coverslips were stained with the denoted antibodies (a). Representative images of REV7 foci in CENPF-positive (G2) cells are shown (b), and the proportion of REV7-positive G2 nuclei in the presence/absence of BOD1L was calculated. Scale bar = 10 μ M. Statistics: Student's T-test for Control vs. BOD1L siRNA, $p = 0.79$) (c).

Data shown in (c) represent mean data from 3 independent experiments, $n \geq 100$ cells/condition in each experiment. Error bars indicate SEM.

(a)



(b)

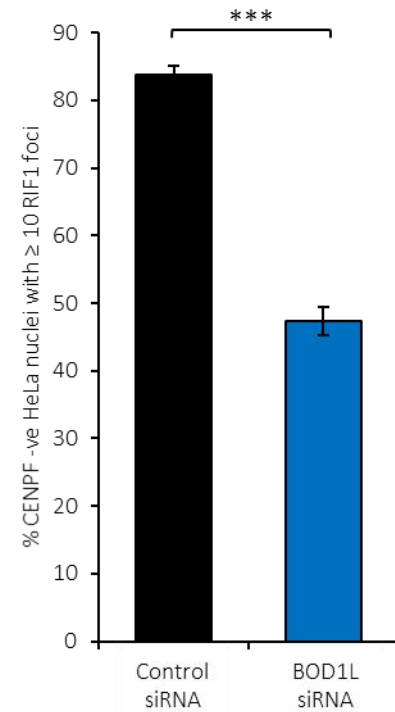


Figure 4.7: G1 recruitment of RIF1 is reduced by depletion of BOD1L.

HeLa cells were treated with siRNA against BOD1L or a non-targeting control sequence. Cells were grown on coverslips, subjected to 3 Gy IR and harvested for immunofluorescence analysis. Representative images of cells stained for the denoted antibodies are shown (a), and the proportion of G1 (CENPF-negative) nuclei with RIF1 foci was calculated (statistics: Student's T-test for Control vs. BOD1L siRNA, $p = 0.0001$) (b).

Data shown in (b): 3 independent experiments, $n \geq 100$ cells/experiment.

4.2.5: Class-switch recombination is compromised in a Bod1L-deficient mouse model

It has been shown by multiple previous studies that RIF1 is a fundamental effector of 53BP1-dependent class switch recombination (CSR), which involves NHEJ-mediated repair of programmed DSBs to generate immunoglobulin diversity (Chapman et al., 2013, di Virgilio et al., 2013). Having demonstrated in the previous section that BOD1L is required for the correct localisation of RIF1 in the context of G1 DSB repair, I hypothesised that CSR may be impaired in the absence of BOD1L.

However, one roadblock to examining the impact of BOD1L on CSR was the absence of an appropriate animal model. To overcome this obstacle, our collaborators (Prof. Simon Boulton and Valérie Borel, Francis Crick Institute, London) generated a conditional Bod1L knockout mouse models (Bod1L^{F/F}) using CRISPR/Cas9-engineered embryonic stem cells. In these animals, the deletion of exon 3 of Bod1L can be induced by the provision of Cre recombinase. To examine CSR specifically, these animals, along with Bod1L-proficient controls (Bod1L^{+/+}), were crossed with Cd19^{+/-}/Cre mice to induce a B-cell-specific knockout of Bod1L in the resultant progeny. B-cells were then extracted from Bod1L-deficient and control animals, and differentiation was stimulated by culturing cells with lipopolysaccharide (LPS) in the presence or absence of interleukin 4 (IL-4) for 96 h. Cell surface immunoglobulin expression was then examined by flow cytometry (Prof. Simon Boulton and Valérie Borel).

In every case, there was a striking reduction in surface immunoglobulin expression in Bod1L-deficient B-cells when compared to control cells (Figure 4.8). These data were consistent with

the hypothesis that BOD1L was essential for functional class switch recombination, in agreement with its role in recruiting RIF1 to DSBs. However, a mild but reproducible defect in B-cell maturation in the absence of Bod1L was also observed, suggesting that further experiments in alternative systems would be worthwhile.

4.2.6: BOD1L and RIF1 depletion alters recruitment of BRCA1 to DSBs in G1

Previous studies demonstrated significant crosstalk between the pro-resection BRCA1 pathway and the 53BP1 pathway that antagonises resection (Chapman et al., 2012). In late S/G2 cells, an undamaged sister chromatid is available as a template for DSB repair. During these phases, BRCA1 antagonises RIF1 recruitment to damaged chromatin, thereby facilitating CtIP-mediated resection of DSBs as a precursor to HR. Conversely, although there is no change in the expression of BRCA1 between G1 and G2, recruitment of this protein to DSBs is inhibited by 53BP1 and its downstream effectors in G1. 53BP1 pathway components physically block DNA end resection, preventing HR and driving repair by NHEJ (Escribano-Diaz et al., 2013, Chen et al., 2008).

In this context, it was postulated that BOD1L, via its interaction with RIF1, may influence the recruitment of BRCA1 to IR-induced DSBs in order to regulate resection. To investigate this, IR-induced BRCA1 focus formation at DSBs was analysed in HeLa cells depleted of BOD1L, RIF1, or both factors in combination. Cells were irradiated and harvested as described in previous sections, and then probed with antibodies against BRCA1 and CENPF. As previously,

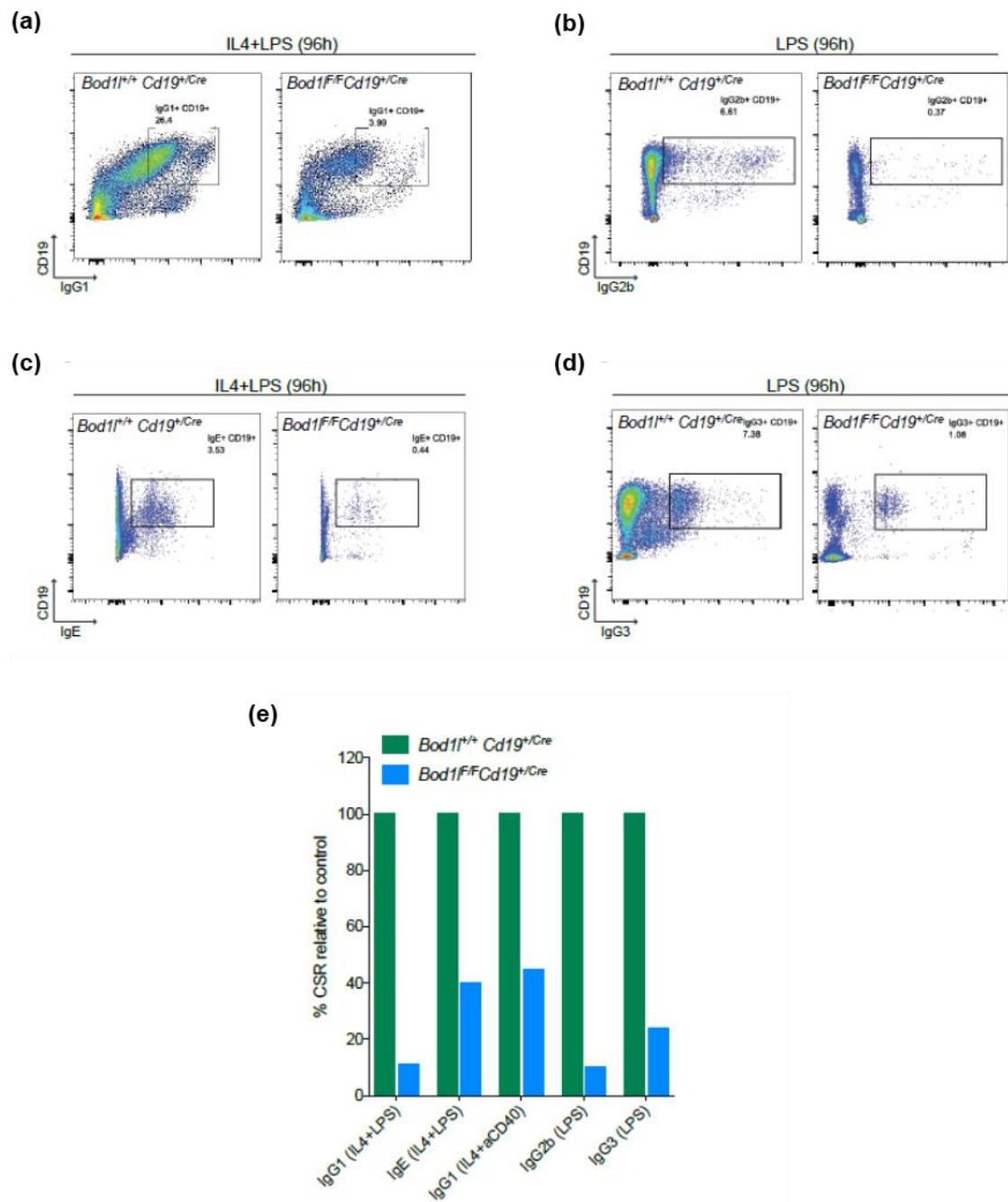


Figure 4.8: Class switch recombination is compromised in the absence of BOD1L.

B-cells extracted from control (*Bod1L^{+/+} Cd19^{+/-}Cre*) and *Bod1L*-deficient (*Bod1L^{F/F} Cd19^{+/-}Cre*) mice were cultured with lipopolysaccharide (LPS) +/- interleukin 4 (IL-4) to stimulate differentiation. After 96 h, cell surface expression of IgG1, IgG2b, IgE and IgG3 was assessed by flow cytometry (a-d). Data represent a single experiment. Surface expressions of IgGs are summarised in (e). IgG concentrations in *Bod1L*-deficient mice were normalised to those from the corresponding controls, with control mice being assigned concentrations of 100%. Data represent 2 mice per condition.

With thanks to Dr. Rachel Bayley, Prof. Simon Boulton and Valérie Borel.

nuclei without CENPF expression were regarded as G1 cells. Immunofluorescence microscopy was used to determine the number of nuclei with BRCA1 foci for each condition.

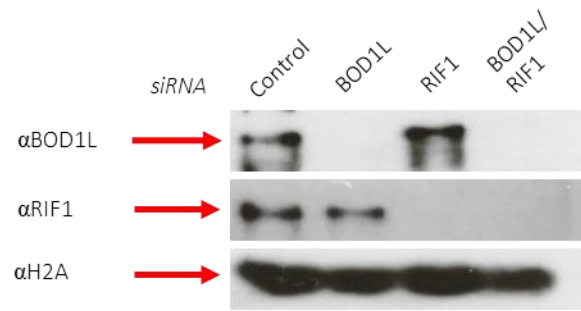
As expected, the proportion of irradiated cells with at least 10 BRCA1 foci was minimal in G1, but this increased significantly upon depletion of BOD1L or RIF1. The depletion of both proteins had no additive effect (figure 4.9b-c). These data suggest that BOD1L and RIF1 function within the same pathway to antagonise BRCA1 recruitment to IR-induced DSBs during G1.

In contrast, the absence of these proteins had no detectable impact on the proportion of BRCA1-positive nuclei during G2. As shown in figure 4.9d-e, 71.0% of control-depleted cells were BRCA1 focus-positive, and no significant alteration was observed upon depletion of BOD1L or RIF1 or in the absence of both proteins. As the chromatin recruitment of BRCA1 was unaffected by the depletion of these proteins during G2, these data point towards a mechanism for BOD1L's control of DSB resection which is not underpinned by the modulation of G2 BRCA1 localisation.

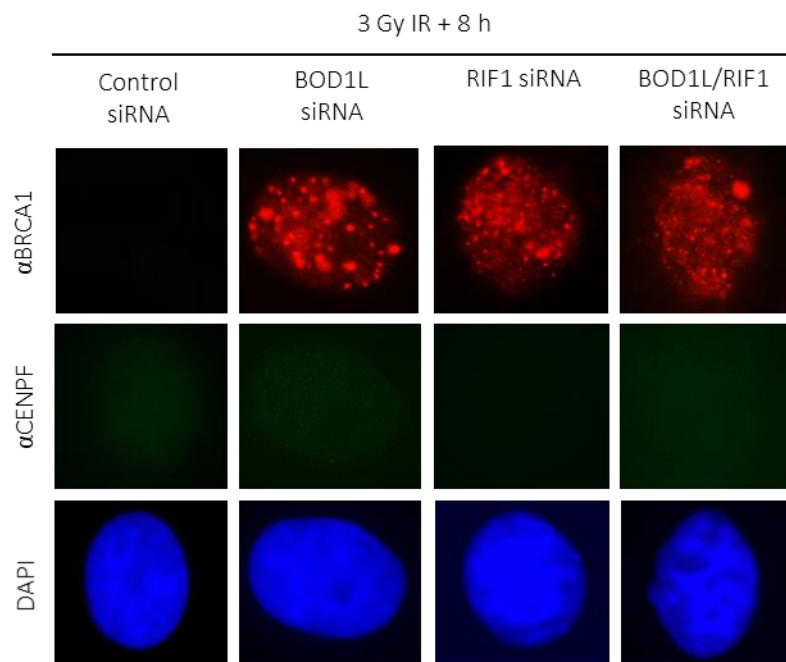
4.2.7: Depletion of BOD1L or RIF1 leads to accumulation of IR-induced ssDNA

The data presented in the preceding sections of this chapter demonstrate that BOD1L depletion results in reduced localisation of RIF1 to IR-induced DSBs and a subsequent increase in BRCA1 accumulation at these sites in G1. As BRCA1 recruitment is a pre-requisite for short-

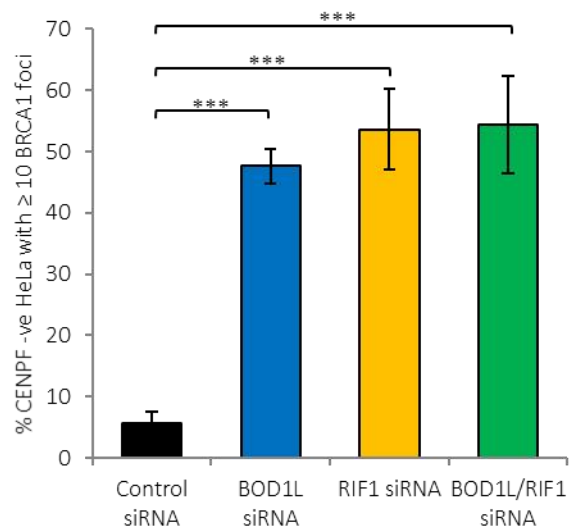
(a)



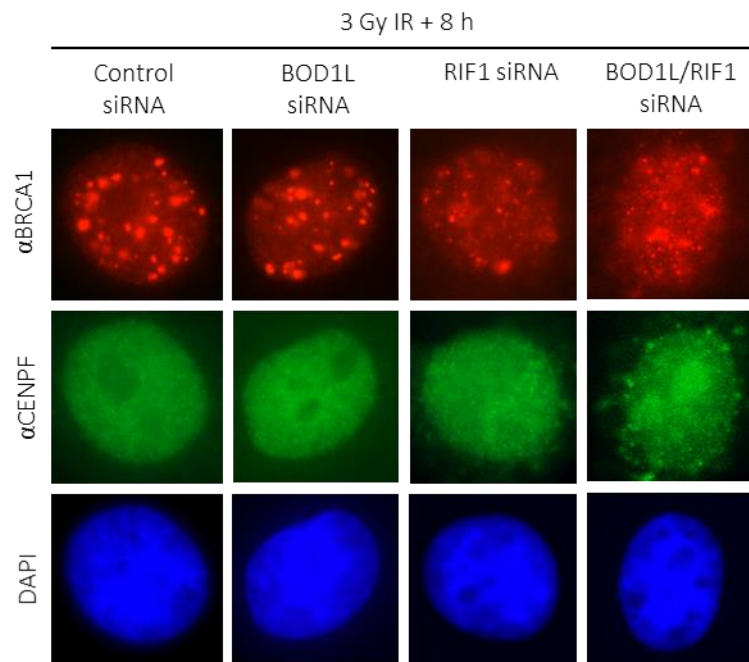
(b)



(c)



(d)



(e)

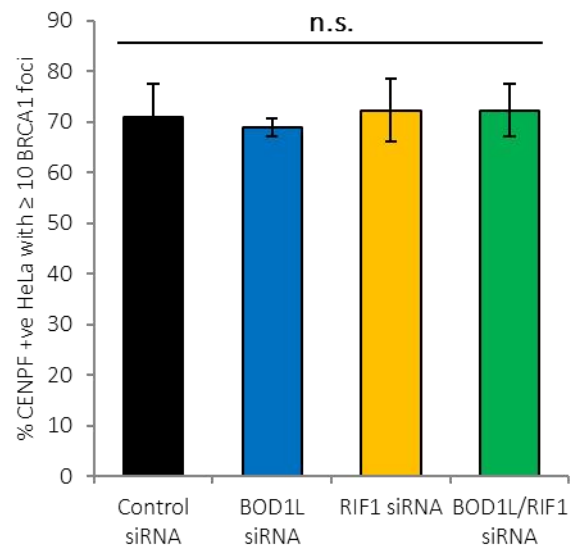


Figure 4.9: Depletion of BOD1L and RIF1 leads to increased prevalence of BRCA1-positive G1 nuclei after exposure to IR.

HeLa cells were treated with BOD1L and RIF1 siRNA, individually and in combination. Transfected cells were grown on coverslips, exposed to 3 Gy IR and harvested after 8 hr for Western blotting and immunofluorescence analyses. Successful protein depletions were demonstrated by Western blotting (a). Coverslips were then stained with the indicated antibodies; CENPF was included as a marker of cell cycle phase. The proportion of BRCA1-positive G1 nuclei (CENPF-negative with at least 10 BRCA1 foci) was quantified. Representative images are shown in (a) with quantifications in (b). Statistics: Student's T-test for Control vs. KD. BOD1L: $p = 0.0002$, RIF1: $p = 0.002$, BOD1L/RIF1: $p = 0.003$. Quantification of BRCA1 focus-positive cells was also carried out in G2 nuclei; representative images are shown in (c) with quantifications in (d). Statistics: Student's T-test for Control vs. KD. BOD1L: $p = 0.78$, RIF1: $p = 0.89$, BOD1L/RIF1: $p = 0.88$. Data shown in (b) and (d): 3 independent experiments, $n \geq 100$ cells/experiment.

range nucleolytic resection of DSBs (Chen et al., 2008), it was therefore of interest to discover whether this altered localisation was associated with an increase in resection of IR-induced DSBs during G1. Therefore, control cells and those depleted of BOD1L or RIF1, singly and in combination, were irradiated, harvested after 8 hr and stained for RPA2 and CENPF. The proportion of RPA2-positive cells (those with a least 10 foci) was quantified by immunofluorescence microscopy in both G1 and G2 phases of the cell cycle, using CENPF staining to distinguish between phases.

In G1, the proportion of cells with RPA2 foci was 17.7%; this rose significantly in cells depleted of BOD1L, RIF1, or both proteins. The increase in levels of RPA2 accumulation was strikingly similar across all conditions (figure 4.10a-b). These results are consistent with the hypothesis that BOD1L, along with RIF1, suppresses inappropriate resection of DSBs during G1; furthermore, they support the notion that BOD1L and RIF1 function within the same pathway to regulate resection.

It is well established that DSB resection is more prevalent in late S/G2 phases of the cell cycle (Heyer et al., 2010). As would therefore be expected, the base level of RPA2-positive cells was higher in G2 cells, with control cells being 31.0% focus-positive. Once again, depletion of BOD1L and RIF1 had significant and comparable impacts on the prevalence of RPA2 foci; there was no additive effect of depleting both proteins (figure 4.10c-d). It can be concluded from these observations that BOD1L and RIF1 co-operate to influence resection of DSBs during G2. These

results shed further light on the observations presented in Chapter 3, during which it was first demonstrated that BOD1L acts as a suppressor of DSB resection during G2.

4.2.8: Increased DSB resection during G1 is counteracted by depletion of CtIP and MRE11

As BRCA1 is required to stimulate short-range resection by CtIP and MRE11 (Chen et al., 2008), I hypothesised that the depletion of these nucleases would rescue the observed increase in resection during G1. CtIP and MRE11 were therefore depleted in isolation or in combination with BOD1L in HeLa cells. Whole-cell extracts were analysed by SDS-PAGE and immunoblotting using antibodies against BOD1L, CtIP, MRE11 and RPA2-P (S4/S8), confirming that BOD1L and both nucleases had been successfully depleted. In addition, in BOD1L-depleted cells, there was a considerable increase in the level of phosphorylated RPA2 compared to that of control cells. Upon depletion of CtIP or MRE11 – either individually or alongside BOD1L depletion – RPA2 phosphorylation returned to control levels (figure 4.11a). This suggests that aberrant resection in the absence of BOD1L is attributable to CtIP and MRE11.

As an alternative approach, siRNA-transfected cells were exposed to a dose of 3 Gy of IR and harvested for immunofluorescence analyses after 8 hours. RPA2 focus formation was assessed in these cells as described above. These immunofluorescence analyses showed that the depletion of BOD1L resulted in a significant increase in the recruitment of RPA2 in G1 (CENPF-negative) cells. In agreement with the immunoblotting data presented above, the

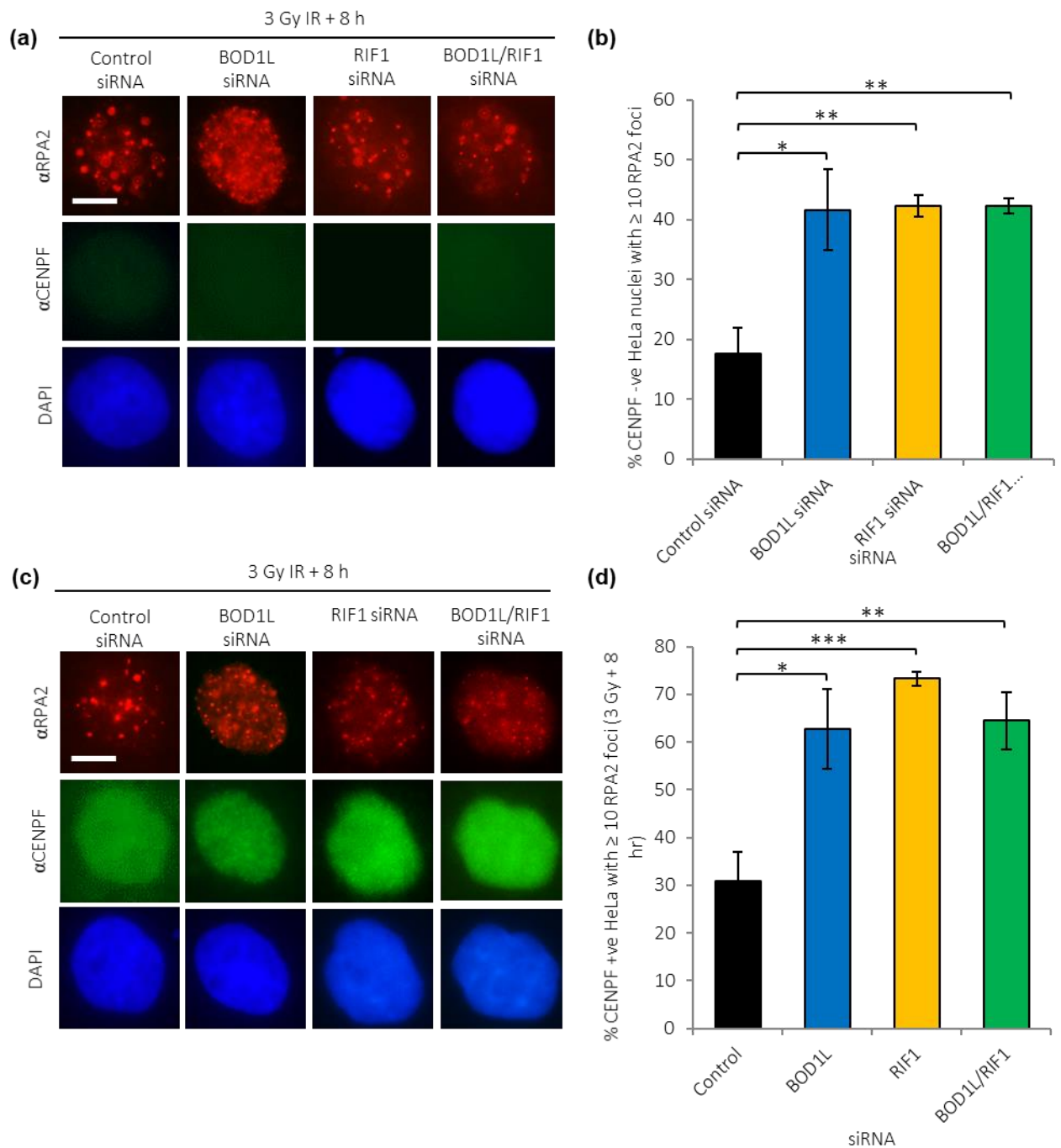


Figure 4.10: Accumulation of RPA2 at IR-induced DSBs is elevated in the absence of BOD1L and RIF1.

HeLa cells were transfected with BOD1L and RIF1 siRNA, individually and in combination. Transfected cells were grown on coverslips, exposed to 3 Gy IR and harvested after 8 hr for immunofluorescence analyses. Coverslips were stained with the indicated antibodies; CENPF was included as a marker of cell cycle phase. The proportion of G1 nuclei (those with no detectable CENPF) with at least 10 RPA2 foci was quantified. Representative images are shown in (a) with quantifications in (b). Statistics: Student's T-test for Control vs. KD. BOD1L: $p = 0.04$, RIF1: $p = 0.006$, BOD1L/RIF1: $p = 0.006$. Quantification of RPA2 focus-positive cells was also carried out for a sample of G2 nuclei; representative images are shown in (c) with quantifications in (d). Statistics: Student's T-test for Control vs. KD. BOD1L: $p = 0.02$, RIF1: $p = 0.0005$, BOD1L/RIF1: $p = 0.008$. Data shown in (b) and (d): 3 independent experiments, $n \geq 100$ cells/experiment. Error bars indicate SEM.

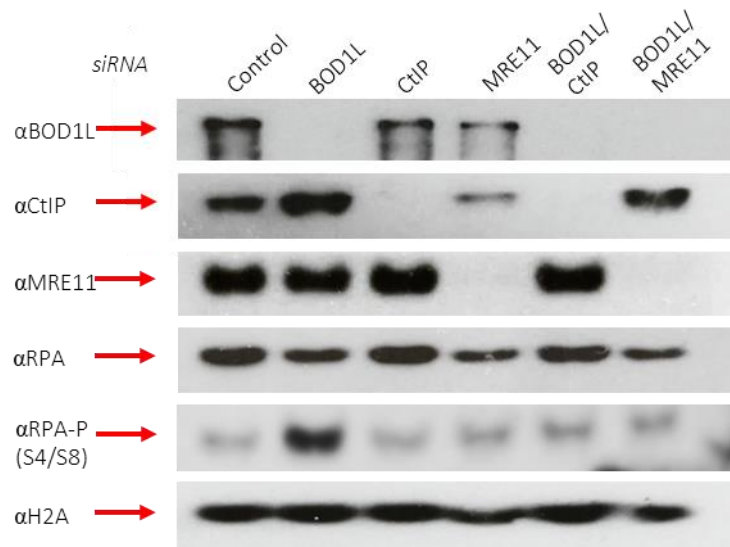
proportion of RPA2-positive cells was markedly reduced in the absence of CtIP or MRE11; in fact, CtIP depletion resulted in RPA2 levels significantly lower than those of control cells.

When CtIP or MRE11 were co-depleted with BOD1L, the elevated RPA2 chromatin localisation that was observed in the absence of BOD1L was completely abrogated (figure 4.11b-c). Taken together, these observations confirmed that CtIP and MRE11 are responsible for the elevated resection observed in BOD1L-depleted cells during G1.

4.2.9: Increased genome instability in the absence of BOD1L or RIF1

The sections above demonstrate that BOD1L and RIF1 interact and function within the same pathway to regulate nucleolytic resection in both G1 and G2. It was therefore important to discover whether the impairment of this interaction through the depletion of either protein had consequences at the cellular level. As nucleolytic resection is a vital aspect of the regulation of DSB repair (Symington & Gautier, 2011), it was postulated that the aberrant resection observed in the absence of BOD1L or RIF1 would lead to genome instability due to an inability to repair DSBs appropriately (Chapman et al., 2013, Naim and Rosselli, 2009). To investigate this, HeLa cells were treated with siRNA against BOD1L, RIF1, or a non-targeting control. These cells were seeded onto coverslips, irradiated as described previously, and harvested for analyses after 24 h. Coverslips were mounted in medium containing DAPI, and micronuclei were enumerated by immunofluorescence microscopy.

(a)



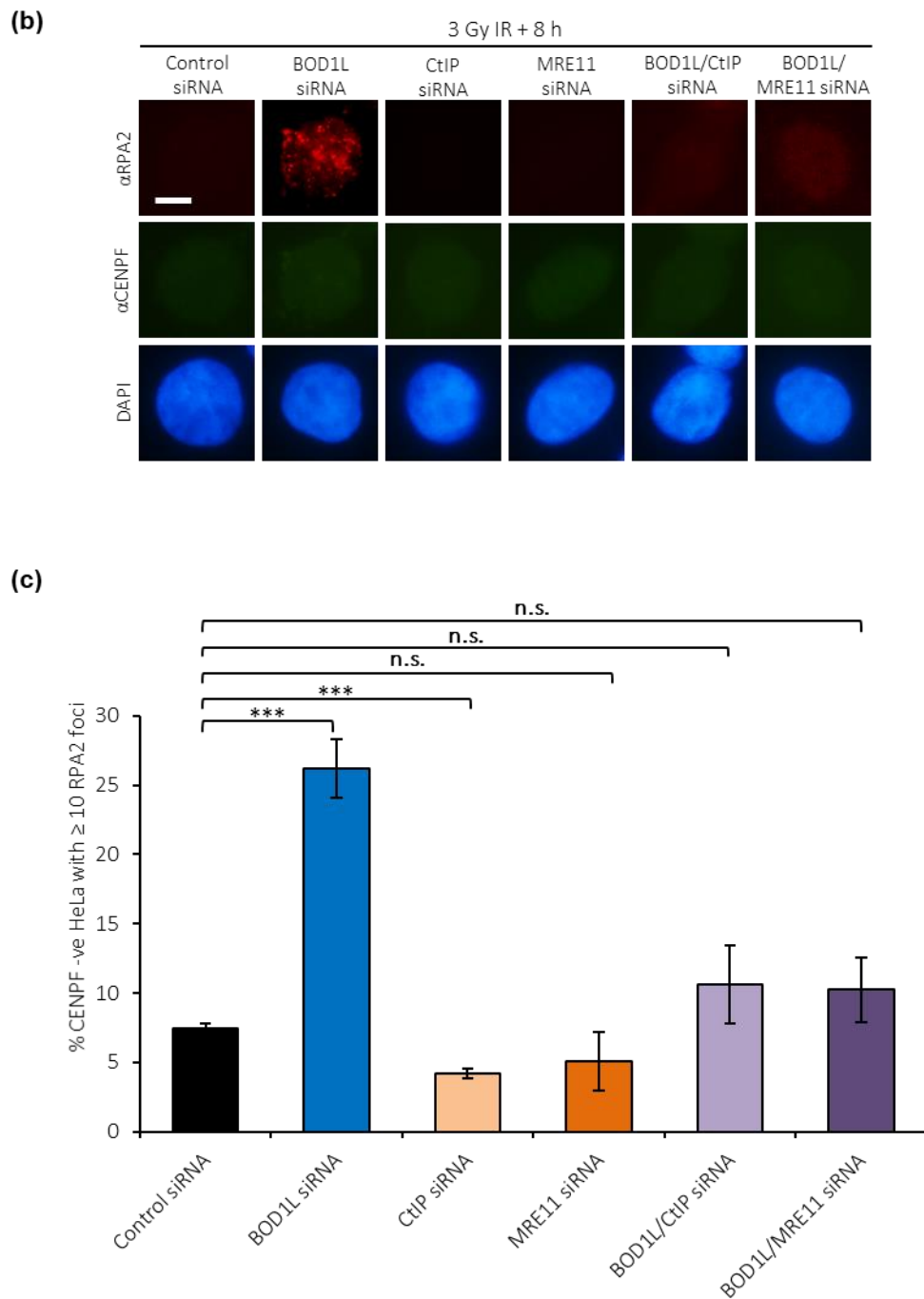


Figure 4.11: Increased G1 resection in the absence of BOD1L is counteracted by the depletion of CtIP or MRE11.

HeLa cells depleted of the named proteins were subjected to 15 Gy IR and harvested after 8 hr for analyses. Successful knockdowns of the proteins of interest was demonstrated by Western blot (a). The proportion of RPA2-positive G1 cells (CENPF-negative cells with ≥ 10 foci) was calculated. Representative images are shown in (b) with quantifications in (c). (Statistics: Student's T-test for Control vs. KD. BOD1L: $p = 0.0009$. CtIP: $p = 0.003$. MRE11: $p = 0.11$. BOD1L/CtIP: $p = 0.32$. BOD1L/MRE11: $p = 0.29$. Data shown in (c): 3 independent experiments, $n \geq 100$ cells/experiment. Error bars represent SEM.

In control-depleted cells, the proportion of cells with IR-induced micronuclei increased twofold upon depletion of BOD1L. Knockdown of RIF1 or BOD1L and RIF1 in combination yielded comparable results, with 27.5 % and 27.7 % of these cell populations having IR-induced micronuclei, respectively (Figure 4.12). These results confirm that genome stability is compromised in the absence of BOD1L or RIF1. Furthermore, the lack of any additive impact on micronucleation upon co-depletion of BOD1L and RIF1 reinforces the notion that these proteins function within the same pathway.

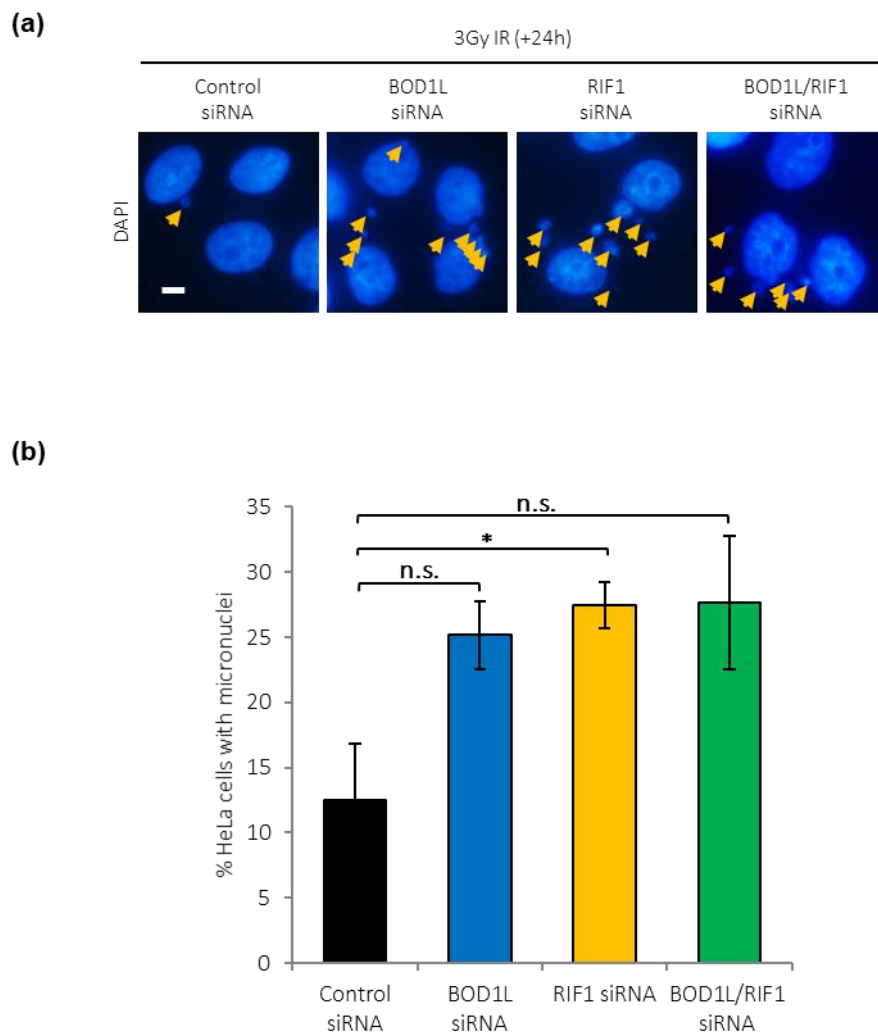


Figure 4.12: Depletion of RIF1 or BOD1L have a comparable impact on genome instability.

HeLa cells treated with the indicated siRNAs were subjected to a dose of 3 Gy IR and harvested after 24 hr for analysis. Mounted cells were examined with the DAPI channel of the microscope to assess and quantify micronucleus formation. Representative images are shown in (a) and quantifications in (b).

Data shown in (b): 3 independent experiments with ≥ 100 nuclei analysed per condition in each experiment. Statistics: Student's T-test for Control vs. KD. BOD1L: $p = 0.07$. RIF1: $p = 0.03$. BOD1L/RIF1: $p = 0.09$. Error bars indicate SEM.

4.3: Discussion

Alongside its published role during S-phase (Higgs et al., 2015), the data presented thus far demonstrate that BOD1L also functions to prevent aberrant resection of IR-induced DSBs. However, the mechanisms underlying this novel role had not been explored. The results presented in this chapter revealed a previously unknown interaction between BOD1L and RIF1, one of the principal effectors of the 53BP1-mediated network of resection antagonists that suppress unscheduled resection and promote NHEJ. RIF1 was identified as a potential novel interactor of BOD1L in a mass spectrometry screen (Prof. Simon Boulton & Valérie Borel, unpublished). The validity of this screen was supported by the enrichment of known interactors in murine Bod1L-containing complexes, such as components of the COMPASS histone methyltransferase complex (Couture and Skiniotis, 2013), lending credibility to the notion that BOD1L interacts with RIF1. This interaction was confirmed by immunoprecipitation, suggesting a means by which BOD1L may influence the resection of IR-induced DSBs.

Further characterisation of the BOD1L-RIF1 interaction by GST pull-down assays with BOD1L fragments highlighted the importance of the N- and C-terminal regions of BOD1L in mediating its interaction with RIF1. It was interesting to note that one of the implicated N-terminal fragments contains the Shg1H (Shg1 homology) domain: a region with sequence homology to Shg1, a component of the yeast methyltransferase COMPASS complex (Higgs *et al.*, 2018, PFAM: 05205, <http://pfam.xfam.org/family/PF05205>, Marchler-Bauer et al., 2011, Roguev et al., 2001). This domain is already known to be necessary and sufficient to mediate the interaction between BOD1L and the histone methyltransferase SETD1A (Higgs *et al.*, 2018). The

likely involvement of the Shg1H domain in the interaction between BOD1L and RIF1 suggests that this region may function as a general mediator of BOD1L's interactions with other proteins.

In contrast, the BOD1L C-terminus contains no recognisable structural or functional domains associated with mediating protein-protein interactions. The observation that this region is also important in promoting the BOD1L-RIF1 interaction suggests that the BOD1L C-terminus may harbour uncharacterised interaction domains.

Approaches based on the interaction behaviour of protein fragments are associated with several key caveats. Firstly, the tertiary protein structures of truncated fragments may differ from the *in vivo* conformation of the full-length protein. This is a particular risk when knowledge of the protein's domain structure is lacking (as is the case for BOD1L), and cannot therefore be used to inform the ideal start and end points of the fragments in an attempt to preserve key structural and functional domains. Furthermore, GST pull-down assays using individual protein fragments are unable to provide insight into potential co-operation between particular regions of BOD1L, which may be required to mediate its interaction with RIF1. As the N-terminal fragments F1 and F2 and C-terminal fragment F6 were each found to be sufficient to pull down endogenous RIF1, this suggests that full-length BOD1L may adopt a conformation that brings these regions into proximity in order to promote interaction with RIF1.

The discovery of the BOD1L-RIF1 interaction provided further insights into the regulation of nucleolytic resection and the role of BOD1L during G1. Firstly, analysis of RIF1 focus formation by immunofluorescence demonstrated that localisation of RIF1 to IR-induced DSBs during G1 is significantly impaired in the absence of BOD1L. RIF1's role during G1 is to antagonise the inappropriate accumulation of BRCA1 at damaged chromatin. In agreement, the significant and similar increase in G1 accumulation of BRCA1 to IR-induced DSBs upon depletion of BOD1L, RIF1 or both proteins supports the notion that these factors act in the same pathway to regulate BRCA1 recruitment. Based on the results in this chapter, it can therefore be concluded that BOD1L is recruited to IR-induced DSBs downstream of the apical resection antagonist 53BP1, but upstream of its key effector RIF1. Given that there is some functional redundancy between RIF1 and another 53BP1 effector, PTIP, it would also be of interest to determine whether BOD1L alters the recruitment of this latter factor to IR-induced DSBs in G1 or G2.

RIF1 is a vital effector of 53BP1-dependent CSR; several previous studies have revealed a significant impairment of this process in B-cells derived from *Rif1*-deficient mouse models (Chapman *et al.*, 2013, di Virgilio *et al.*, 2013). Chapman and colleagues further supported their observations by demonstrating that class switching in response to immunisation with a specific antigen was severely reduced in *Rif1*-deficient mice (Chapman *et al.*, 2013). Moreover, a study by di Virgilio and colleagues showed a mild increase in CSR following shRNA-mediated depletion of CtIP in RIF1-deficient B-cells (di Virgilio *et al.*, 2013), suggesting that aberrant DSB end resection plays a role in the CSR defects observed in the absence of RIF1. As BOD1L is recruited to IR-induced DSBs upstream of RIF1 and is required for RIF1 localisation to damaged

chromatin, it was conceivable that BOD1L depletion could have a comparable impact on CSR. The data presented herein demonstrate that this is indeed the case; CSR is considerably compromised in Bod1L-deficient mouse B-cells. These findings are in line with the role of BOD1L in modulating DSB resection through the recruitment of RIF1 to sites of DNA damage. These observations also imply that, as for RIF1, the role for BOD1L extends beyond end protection of DSBs induced by external sources – it also acts to restrict resection of programmed DSBs generated in physiological processes.

It would be valuable to extend the data presented in this chapter using complementation-based approaches. As a clear demonstration that the phenotypes observed upon knockdown of BOD1L or RIF1 can be attributed to the absence of these proteins, knockdown-resistant versions can be expressed in siRNA-treated cells with the intention of restoring the control phenotype. It would be of particular interest to show that RIF1 recruitment to IR-induced DSBs in G1 cells, which is impaired in the absence of BOD1L, could be rescued by the expression of siRNA-refractory BOD1L. Furthermore, complementation of BOD1L-depleted cells could be attempted using engineered BOD1L which lacks the N- and C-terminal regions (those represented by fragments F1-F2 and F6). Having demonstrated in this chapter that these regions interact with RIF1, I would hypothesise that a BOD1L fragment lacking these regions would be unable to rescue the phenotypes observed in BOD1L-depleted cells. This experiment would demonstrate the significance of the C- and N-termini of BOD1L in facilitating its interaction with RIF1 and would further support the importance of this interaction for DSB end protection.

During the G1 phase of the cell cycle, DNA replication has not taken place and resection as a precursor to HR is therefore typically down-regulated by the 53BP1 pathway. As discussed above, this DSB end protection pathway is compromised in the absence of BOD1L due to the perturbation of RIF1 recruitment (Feng et al., 2013, Chapman *et al.*, 2013, Escibano-Diaz et al., 2013, di Virgilio et al., 2013). As BOD1L- or RIF1-deficient cells are incapable of inhibiting inappropriate BRCA1 accumulation at G1 DSBs, it follows that the level of short-range resection (which requires the stimulation of CtIP activity by BRCA1) should be higher in these cells (Chen et al., 2008). This was indeed shown to be the case. In the absence of BOD1L or RIF1, analyses by immunoblotting showed elevated levels of RPA2 (S4/S8) phosphorylation. A G1-specific increase in resection was supported by a significant increase in RPA2 focus formation in CENPF-negative cells, as demonstrated by immunofluorescence microscopy. Consistent with the knowledge that BRCA1 stimulates CtIP- and MRE11-dependent short-range resection (Chen et al., 2008), the observed aberrant resection during G1 was restored to control levels by the knockdown of these nucleases on a background of BOD1L depletion.

It is worthy of note that alternative resection-dependent DSB repair pathways exist alongside HR. One such pathway is the RAD51-independent single-strand annealing (SSA) pathway. Homologous repeat sequences either side of the DSB are annealed to repair the break. This involves CtIP-mediated resection to expose 3' ssDNA tails and requires further endonucleolytic processing to remove any non-homologous sections prior to ligation. As for HR, it is inhibited by 53BP1 and its downstream effectors, including RIF1 (Bhargava et al., 2016). In a similar

manner, alternative end joining (alt-EJ) also involves short-range resection by CtIP, the annealing of sites of microhomology either side of the DSB and the deletion of genetic material across the break. As such, both pathways are associated with a high frequency of chromosomal translocations and genome instability (Bhargava et al., 2016, Symington and Gautier, 2011). It has also been shown recently that a resection-dependent form of canonical NHEJ (c-NHEJ) takes place in G1 cells; importantly, the resection which primes this form of repair differs in nature from that which takes place as a precursor to HR. Resection-dependent c-NHEJ requires phosphorylation of CtIP by Polo-like kinase 3 (Plk3), which enables CtIP to interact with BRCA1 and initiate resection; this step is supported by the activity of MRE11, EXO1 and EXD2, and Artemis is essential for the completion of repair. As for SSA and alt-EJ, resection-dependent c-NHEJ results in genomic aberrations (Biehs et al., 2017). It is plausible that the increased DSB resection observed in the absence of BOD1L may lead to an up-regulation of these mutagenic alternative pathways; a thorough examination of repair dynamics in BOD1L-depleted cells will be a valuable next step.

The results described here are in line with those of chapter 3 with respect to the role of BOD1L as a regulator of G2 DSB resection, but there may be distinct mechanisms in play during different cell cycle phases. It was shown that the depletion of BOD1L or RIF1 (individually and in combination) led to a significant increase in the recruitment of RPA2 to ssDNA in CENPF-positive irradiated cells. However, it must be pointed out that impairment of RIF1 recruitment in the absence of BOD1L, as observed in G1, may be too simplistic an explanation for increased resection in G2. Focus formation of 53BP1, RIF1 and REV7 at DSBs in CENPF-positive cells was

unaltered in the absence of BOD1L. In line with this observation, the depletion of BOD1L or RIF1 had no impact on IR-induced recruitment of BRCA1 to G2 DSBs. Taken together, this may suggest that BOD1L suppresses aberrant resection of G2 DSBs independently of RIF1 and BRCA1. However, this is somewhat at odds with the data presented in chapter 3, which suggest a prominent role for CtIP and MRE11 in the aberrant resection of DSBs in G2 cells; BRCA1 is a pre-requisite for the activity of these nucleases. One possible explanation for these discontinuities lies in the shortcomings of the immunofluorescence techniques used. Whilst the examination of focus formation at sites of DNA damage provides a useful visual indication of protein recruitment, it cannot be used to assess protein functionality. It may therefore be that BOD1L's control of resection depends on antagonising BRCA1 recruitment to DSBs via RIF1 in G1, and on influencing the activity of these proteins in G2.

Since the results from chapters 3 and 4 collectively demonstrated that BOD1L functioned in the suppression of resection both in G1 and G2 cells, it was intriguing to note that analyses of γ H2AX foci suggested that a DSB repair defect was only present in G2 cells. This observation implied that despite the alterations to G1 repair dynamics in the absence of BOD1L, IR-induced DSBs occurring in this phase may still be repaired. NHEJ would not be a viable repair pathway for DSBs subjected to extensive processing. As discussed above, the down-regulation of this pathway may result in a shift towards non-canonical pathways, such as single-strand annealing, which are resection-dependent but require no homologous template. Whilst DSBs may be repaired in this manner, leading to a resolution of γ H2AX foci, the use of these mutagenic

pathways may result in aberrations at the chromosomal level. This possibility warrants further investigation.

The downstream consequence of BOD1L or RIF1 depletion on cells was subsequently analysed by assessing micronucleation, which occurs through a failure to resolve DNA damage and complete DNA replication in an appropriate and timely manner (Naim and Rosselli, 2009). Upon depletion of BOD1L and/or RIF1, there was an increase in the prevalence of micronuclei in irradiated cells. Based on this observation, it can be concluded that BOD1L and RIF1 are required for the completion of DSB repair. Furthermore, the increase in micronuclei formation is strikingly similar for BOD1L- and RIF1-depleted cells, with no additive impact of depleting both proteins; this further reinforces the fact that the interaction between these proteins is required to preserve the stability of the genome.

In summary, this chapter demonstrates that BOD1L interacts with RIF1, a key player in 53BP1-mediated DSB end protection. BOD1L is required for the recruitment of RIF1 to DSBs; together, these proteins suppress the inappropriate accumulation of BRCA1 to DSBs during G1. As BRCA1 is required to stimulate the short-range nucleases, CtIP and MRE11, the activities of BOD1L and RIF1 suppress undesirable DSB resection during G1, thereby maintaining genome stability. It is evident that the interaction between BOD1L and RIF1 is fundamental to BOD1L's role as a modulator of DSB resection during G1. However, how this protein regulates resection during G2 remains to be discovered. It is likely that BOD1L operates via distinct mechanisms in G1 and G2 to suppress inappropriate DSB resection.

Having shed light on the mechanism by which BOD1L regulates nuclease activity to control the resection of IR-induced DSBs, the next chapter aims to characterise the effects of BOD1L depletion upon key DSB repair pathways.

Chapter 5: The impact of BOD1L on DSB repair

5.1: Introduction

In chapter 4, I demonstrated that BOD1L interacts with RIF1, a key downstream effector of 53BP1, and that together, BOD1L and RIF1 suppress the resection of IR-induced DSBs. In G1 cells, this was dependent on BOD1L's recruitment of RIF1 to damaged chromatin, thereby preventing the accumulation of BRCA1. It was apparent that BOD1L suppressed aberrant resection in G2 cells via a distinct mechanism, although the involvement of RIF1 could not be ruled out. Since BRCA1-mediated nucleolytic resection is a fundamental driver of repair pathway choice (Chen et al., 2008), it logically followed that the dysregulation of this process in cells lacking BOD1L would disrupt the balance of these DSB repair pathways. Indeed, this is known to be the case for 53BP1 and its downstream effectors, including RIF1. During G1, RIF1 inhibits the recruitment of BRCA1 to damaged chromatin, allowing cells to suppress resection in G1 (Isono et al., 2017, Feng et al., 2013, Chapman et al., 2013, Escribano-Diaz et al., 2013)). Attempting repair by HR would clearly be unfavourable during this phase due to the absence of an undamaged sister chromatid to use as a repair template (Heyer et al., 2010). Alongside the suppression of potentially deleterious resection during G1, RIF1 also promotes NHEJ of DSBs and de-protected telomeres (Chapman et al., 2013). Conversely, BRCA1 antagonises RIF1 activity during G2, when HR is a viable repair pathway; this is achieved in part through BRCA1-mediated dephosphorylation of 53BP1 in G2 cells, which inhibits its interaction with RIF1 (Isono et al., 2017). Furthermore, CDK-dependent phosphorylation at T847 is a pre-requisite for CtIP

activity, which ensures that this nuclease only functions in late S/G2 phases of the cell cycle (Huertas and Jackson, 2009, Huertas et al., 2008).

Although the importance of RIF1 for NHEJ is widely acknowledged, the consequence of RIF1 deficiency on HR remains a point of contention, with some studies showing a negligible impact on HR (Isobe et al., 2017), and others suggesting an increase in usage of this pathway in RIF1-depleted cells (Escribano-Diaz et al, 2013).

Due to the interaction between BOD1L and RIF1, I postulated that BOD1L may also act to promote NHEJ alongside its role in suppressing resection. The experiments presented in this chapter therefore sought to discover the impact of BOD1L and RIF1 depletion on DSB repair by HR, NHEJ and resection-dependent alternative pathways.

5.2: BOD1L regulates DSB repair as well as resection

BOD1L interacts with RIF1 to regulate nucleolytic resection of DSBs, and genome instability arises in the absence of BOD1L. However, whether BOD1L influenced DSB repair in cells was unclear. To investigate this, the impact of BOD1L and RIF1 depletion on HR-mediated repair was initially probed using an I-SceI-based reporter assay. Further investigations with immunofluorescence microscopy in specific phases of the cell cycle revealed a G1-specific increase in RAD51 focus formation. These observations suggested an increase in recruitment of RAD51 to IR-induced DSBs during this phase. Next, the impact of BOD1L and RIF1 depletion

on NHEJ was analysed using a telomere fusion assay, which demonstrated that BOD1L, like RIF1, was required for end-joining. Finally, the use of error-prone resection-dependent repair pathways was also investigated with an I-SceI-based reporter assay. Together, these data illustrated that BOD1L is required to promote NHEJ and suppress G1-specific localisation of RAD51 to DSBs, thereby preventing inappropriate HR.

5.2.1: Depletion of BOD1L has no impact on HR proficiency

Data presented in the preceding chapters have repeatedly demonstrated an increase in nucleolytic resection, a pre-requisite for HR, in the absence of BOD1L. It was therefore of particular importance to investigate the impact of BOD1L depletion on downstream levels of HR. To assess levels of HR, the well-characterised DR-GFP reporter cell line was used (Gunn and Stark, 2012). This cell line harbours a reporter cassette containing truncated N- and C-terminal GFP fragments interspersed with a recognition site for the rare-cutting I-SceI endonuclease (SceGFP). Downstream of SceGFP is a fragment encompassing the central region of the GFP coding sequence with no N- or C-terminal regions (iGFP). Transient expression of I-SceI induces a DSB in SceGFP, which is then repaired by HR using iGFP as a homologous template. This generates a functional GFP coding sequence, and consequent expression of GFP, in HR-proficient cells.

The workflow for the assay is summarised in figure 5.1a. DR-GFP cells were transfected with siRNA against BOD1L, RIF1 and a non-targeting control. BRCA1 siRNA was included as a positive control, since depletion of this key factor should impair HR. Forty-eight hours post-siRNA transfection, cells were transfected with an I-SceI expression plasmid and a plasmid encoding

RFP as an internal control for transfection efficiency. Repair of the I-SceI-induced DSB by HR was subsequently examined by measuring the proportion of GFP-positive cells by flow cytometry (figure 5.1a). Proportions were adjusted according to the transfection efficiency of pRFP, as determined by flow cytometry, and relative HR levels were normalised to control cells (figure 5.1b).

As expected, the proportion of HR-proficient cells was significantly reduced in the absence of BRCA1 compared to control cells. In accordance with previous literature, there was no detectable impact of depleting RIF1 (Isobe et al., 2017), suggesting that this factor did not influence HR-mediated DSB repair. The depletion of BOD1L, or of both factors in combination, resulted in relative HR efficiencies that were comparable to those of RIF1-depleted cells. These data implied that, as for RIF1, BOD1L did not affect the usage of HR.

5.2.2: Chromatin recruitment of RAD51 increases upon BOD1L depletion in G1 cells

As an alternative means of monitoring HR, IR-induced RAD51 accumulation at DSBs was examined by immunofluorescence microscopy. The loading of RAD51 onto ssDNA after nucleolytic resection to form RAD51 nucleofilaments is a key step in HR-mediated DSB repair (West, 2003); as such, RAD51 focus formation represents a robust proxy for HR. HeLa cells were treated with siRNA against BOD1L or a non-targeting control sequence, grown on coverslips, irradiated with a dose of 5 Gy IR, and harvested at multiple time points over a period of 24 h. Whole-cell extracts from siRNA-treated cells were harvested and immunoblotted against BOD1L to confirm depletion. In parallel, coverslips were pre-extracted, fixed and stained with

antibodies against RAD51, and the proportion of RAD51-positive nuclei was quantified at each time point.

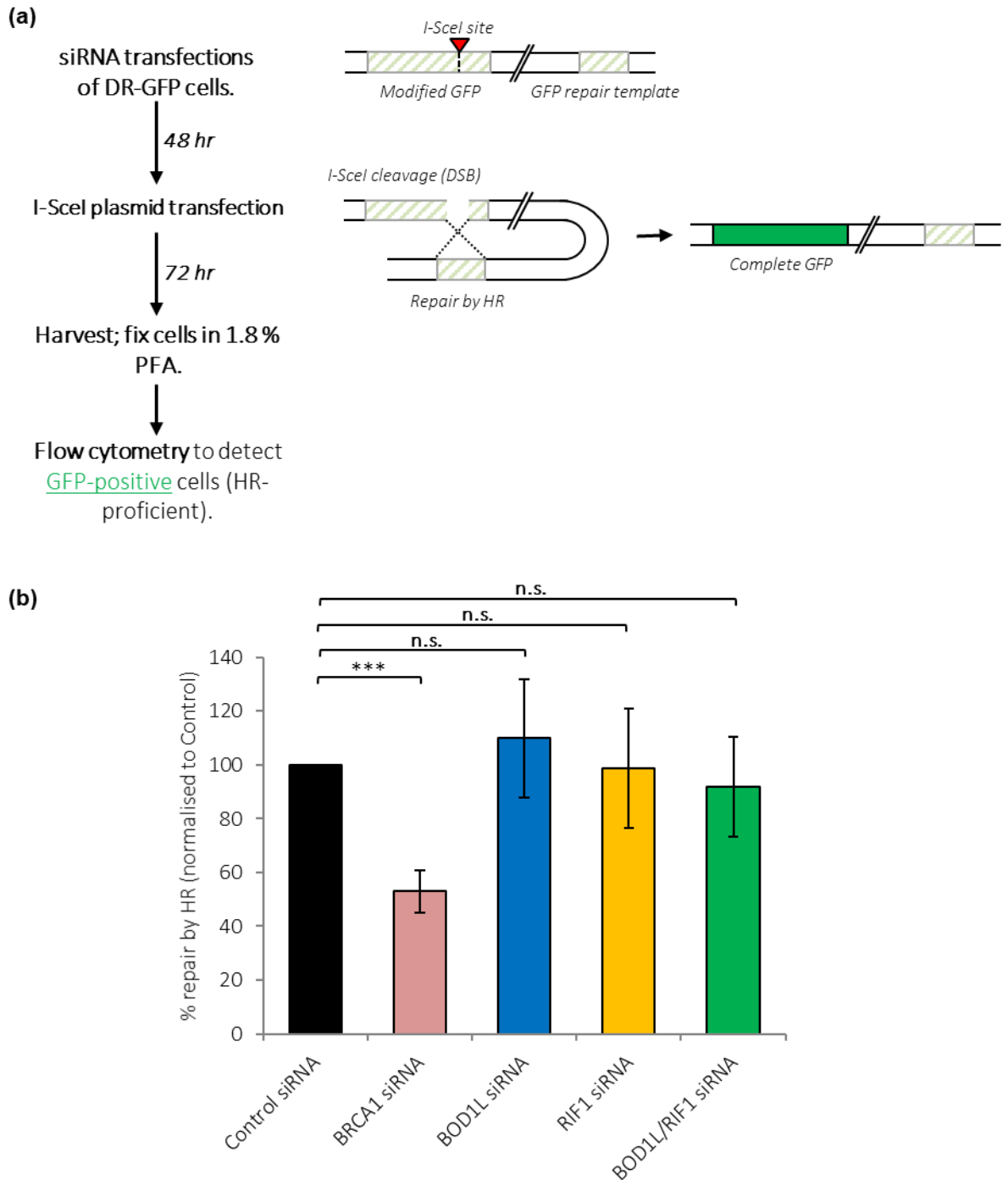


Figure 5.1: BOD1L and RIF1 depletion has no detectable impact on HR proficiency in asynchronous cells.

The DR-GFP cell line, harbouring a GFP reporter cassette, was transfected with siRNA against BRCA1, BOD1L, RIF1 and a non-targeting control. These cells were then transfected with an I-SceI expression vector. Upon expression, the rare-cutting endonuclease induced a DSB in the GFP reporter cassette. HR-proficient cells were able to repair the resultant DSB using a

downstream GFP repair fragment as a template, producing a complete GFP sequence. Three days after transfection with the I-SceI expression plasmid, cells were harvested and fixed in PFA. The proportion of GFP-positive cells was then analysed by flow cytometry. The workflow for the assay, including the status of the GFP reporter cassette at each step, is shown in (a). The proportion of HR-proficient cells (GFP-positive) is shown in (b). Data shown: ≥ 3 independent experiments. Statistics: Student's T-test for Control vs. KD. BRCA1: $p < 0.0001$. BOD1L: $p = 0.69$. RIF1: $p = 0.96$. BOD1L/RIF1: $p = 0.69$.

siRNA-mediated knockdown of BOD1L was first verified by Western blotting (figure 5.2a). Very few untreated control cells were RAD51-positive; this rose dramatically at 8 h after 5 Gy IR and had decreased again by 24 h post-treatment. Interestingly, the proportion of BOD1L-depleted cells with RAD51 foci was almost identical to that of the control cells at every time point (figure 5.2b-c), providing further evidence that BOD1L does not negatively influence DSB repair by HR, despite its demonstrated function as a suppressor of DSB resection.

The experiments described in chapter 4 demonstrated that the depletion of BOD1L or RIF1 results in the inappropriate accumulation of BRCA1 in G1 cells only. Since BRCA1-mediated stimulation of CtIP and MRE11 is a crucial prerequisite for HR, I hypothesised that this could lead to a G1-specific increase in RAD51 accumulation at DSBs. The formation of RAD51 foci was therefore quantified by immunofluorescence microscopy in G1 (CENPF-negative) cells. Control cells were largely negative for IR-induced RAD51 foci, with only 15.7% of G1 cells exhibiting foci. Interestingly, this rose two-fold in BOD1L-depleted cells. These data imply that, in agreement with the above predictions, BOD1L functioned to suppress inappropriate recruitment of RAD51 to resected DSBs during G1. Moreover, similar observations were made for cells depleted of RIF1 (figure 5.3). This further supported the notion that BOD1L and RIF1 function together to prevent inappropriate RAD51 recruitment.

Next, the proportion of CENPF-positive (G2) cells with RAD51 foci was enumerated on the same coverslips. While the vast majority of these cells exhibited RAD51 foci, there was a modest reduction in chromatin recruitment of RAD51 in the absence of BOD1L (Control 94.1%, siBOD1L

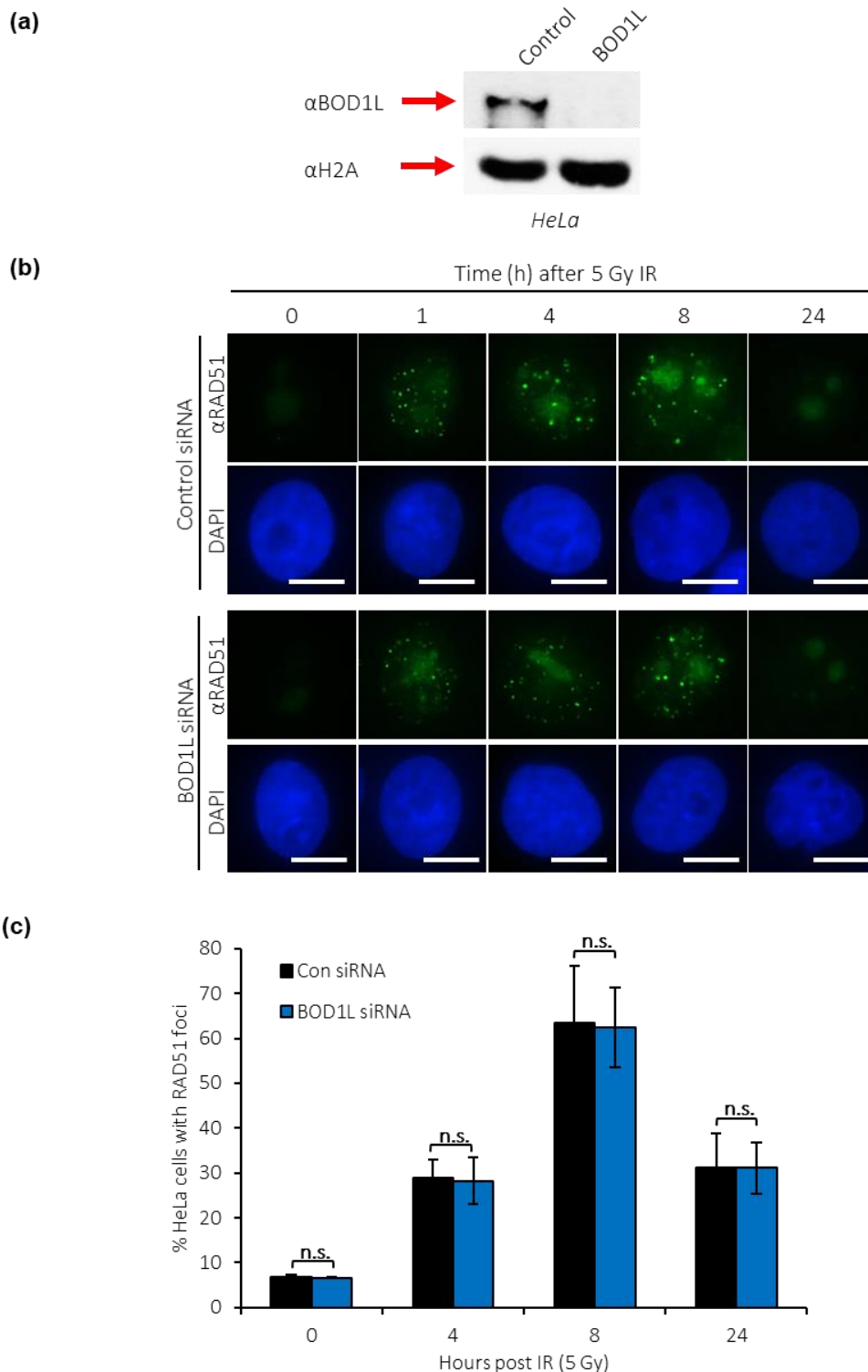
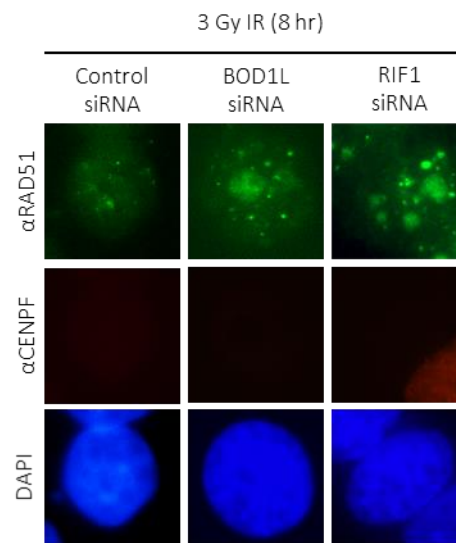


Figure 5.2: BOD1L depletion has no detectable impact on IR-induced RAD51 foci formation in an asynchronous pool of cells. HeLa cells were transfected with control and BOD1L siRNA. Depletions were confirmed by Western blotting (a). Cells were exposed to 5 Gy IR, harvested, pre-extracted, fixed in PFA and stained for RAD51. Representative images are shown in (b). The proportion of RAD51-positive cells was determined at the indicated time points after irradiation (c). Data in (c): 2 independent experiments with ≥ 100 nuclei analysed per condition in each experiment. Statistics: Student's T-test for Control vs. BOD1L. 0 (untreated): $p = 0.60$. 4 hr: $p = 0.90$. 8 hr: $p = 0.93$. 24 hr: $p = 0.99$.

(a)



(b)

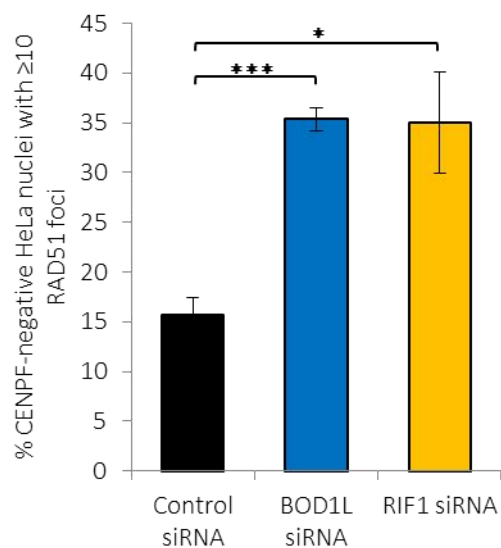


Figure 5.3: G1 recruitment of RAD51 increases in the absence of BOD1L or RIF1.

HeLa cells treated with the named siRNA were exposed to 3 Gy IR and harvested after 8 hr for analysis by immunofluorescence. After pre-extraction and fixation in PFA, cells were stained with antibodies against RAD51 and the S/G2 marker CENPF. The proportion of CENPF-negative (G1) cells with RAD51 foci was calculated for each condition. Representative images are shown in (a) with quantifications in (b).

Data shown in (b): 3 independent experiments with ≥ 100 cells analysed per condition in each experiment. Statistics: Student's T-test for Control vs. KD. BOD1L: $p = 0.0008$. RIF1: $p = 0.02$.

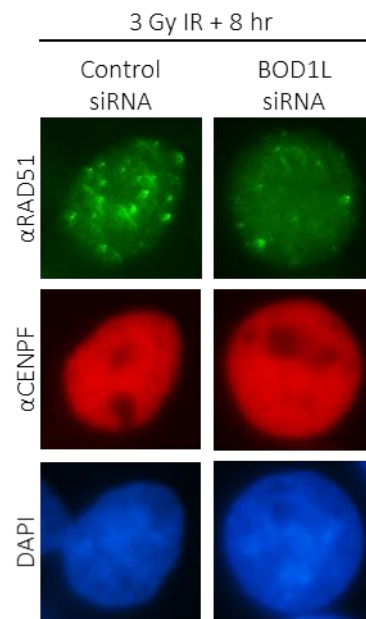
73.7%) (figure 5.4). However, this represented only a small reduction; the majority of G2 cells were still able to form RAD51 foci. It was therefore concluded that whilst BOD1L suppressed unscheduled HR in G1, it did not dramatically influence levels of HR in G2 cells.

5.2.3: BOD1L is required for NHEJ

53BP1, RIF1 and SHLD1-3 are required to promote non-homologous end-joining (Chapman *et al.*, 2013, Dev *et al.*, 2018, Gupta *et al.*, 2018, Noordermeer *et al.*, 2018, Findlay *et al.*, 2018). In telomere fusion assays, in which telomeres are artificially de-protected and exposed to NHEJ machinery within the nucleus, RIF1 loss reduced the proportion of chromosome end-to-end fusions (Chapman *et al.*, 2013), illustrating its role in promoting NHEJ in a physiological context.

In light of its interaction with RIF1, it was postulated that BOD1L may also influence NHEJ. To investigate this, HeLa cells were transfected with siRNA against BOD1L, RIF1, or a non-targeting control sequence. Twenty-four hours later, cells were transfected with a plasmid encoding TRF2^{ΔBAM}; this dominant negative mutant (Smogorzewska *et al.*, 2002) results in the collapse of the Shelterin complex, exposing telomeres to end-joining machinery. After 2 days, cells were then treated with Colcemid, which results in the de-polymerisation of the mitotic spindle and limits the formation of new microtubules, leading to cell cycle arrest at metaphase. The workflow is summarised in figure 5.5a. Cells were harvested, metaphase spreads prepared, and chromosomes visualised with DAPI. The proportion of chromosomes with end-to-end fusions was then quantified by immunofluorescence microscopy.

(a)



(b)

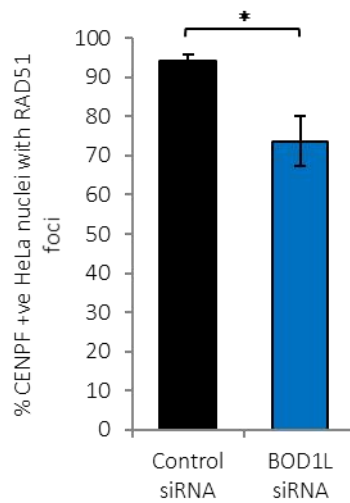


Figure 5.4: Depletion of BOD1L does not increase RAD51 recruitment to IR-induced DSBs in G2 cells.

HeLa cells were transfected with the named siRNA, treated with 3 μ M Aphidicolin, subjected to 3 Gy IR and harvested for immunofluorescence after 8 hr. Following pre-extraction and PFA fixation, cells were stained for RAD51 and the S/G2 marker CENPF. Representative images are shown in (a). The proportion of CENPF-positive cells with RAD51 foci was calculated in control and BOD1L-depleted cells (b).

Data shown in (b): 3 independent experiments with ≥ 100 nuclei analysed per condition in each experiment. Statistics: Student's T-test for Control vs. BOD1L, $p = 0.03$.

Upon expression of TRF2^{ΔBΔM} in control cells, 20.3% of chromosomes ends were fused; suggesting that unprotected telomeres were joined by the cellular NHEJ machinery. As expected, this fell sharply to 6.0% in cells depleted of RIF1. Moreover, loss of BOD1L phenocopied depletion of RIF1, with 5.6% of cells undergoing NHEJ-mediated telomere fusion (figure 5.5b-c). Taken together, these data support the hypothesis that BOD1L and RIF1 cooperate to drive NHEJ.

5.2.4: The impact of BOD1L on SSA, a non-canonical resection-dependent repair pathway

When the cellular capacity for NHEJ is reduced, alternative repair pathways compensate for this impairment to ensure that DNA damage is resolved (Mansour *et al.*, 2008). Furthermore, it was considered that there could be greater utilisation of non-canonical pathways in the event that the increased short-range resection in the absence of BOD1L or RIF1 was insufficient to prime HR (Bakr *et al.*, 2016, Ciccia and Elledge, 2010, Escribano-Diaz *et al.*, 2013). To investigate these scenarios, a non-canonical resection-dependent pathway, single-strand annealing (SSA), was investigated using an I-SceI-based reporter assay. This assay was performed in the SA-GFP cell line. The repair cassette in this cell line consists of a 5' section of the GFP coding sequence (5'GFP) with a downstream 3' section that contains the I-SceI recognition site (Sce3'GFP). The fragments share a short (~260nt) region of homology. Following expression of I-SceI, this homologous section is sufficient to act as a bridge across the resultant DSB; this facilitates repair by SSA, which generates a functional GFP sequence (Gunn and Stark, 2012).

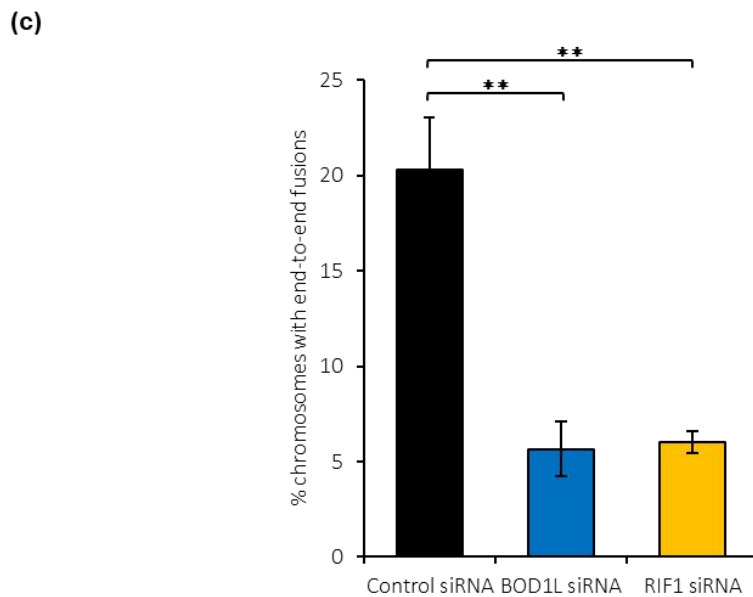
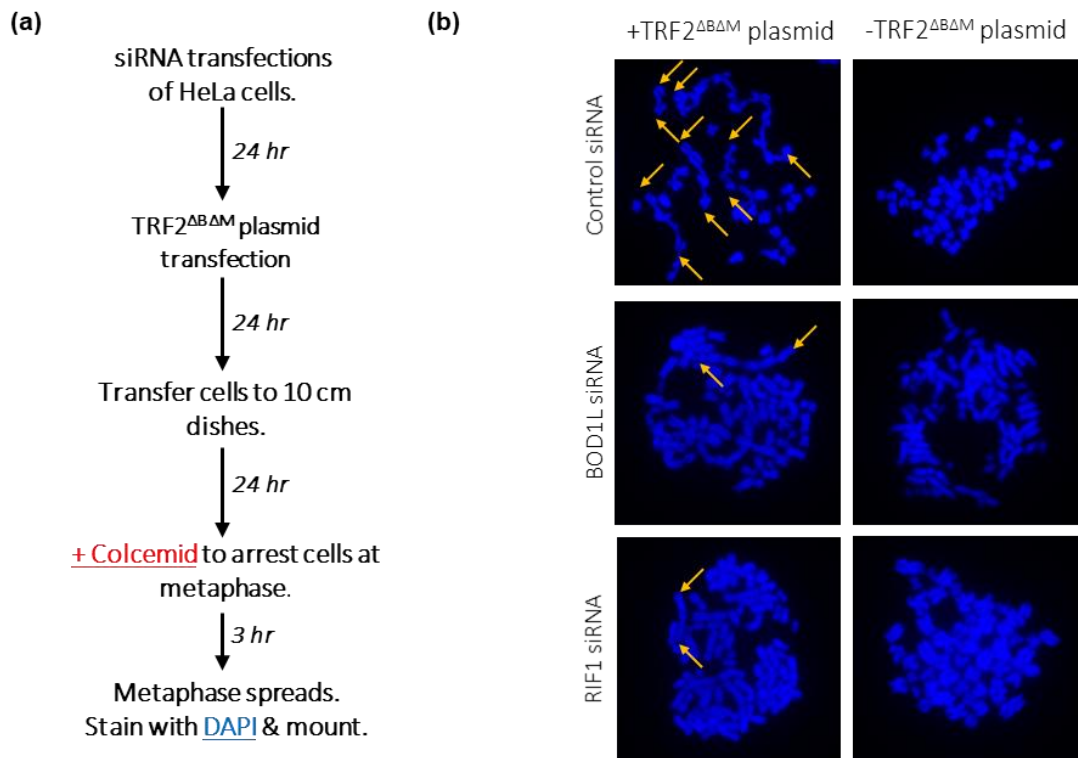


Figure 5.5: Non-homologous end joining of de-protected telomeres is suppressed by depletion of BOD1L or RIF1.

HeLa cells treated with the named siRNA were transfected with a mutant TRF2 expression plasmid (TRF2^{ΔBΔM}); this variant has a dominant-negative effect on the telomere protection complex, causing the collapse of the complex and exposing chromosome ends to NHEJ proteins. Three hours prior to harvesting, cells were treated with Colcemid to induce metaphase arrest. Cell samples were dropped from a height onto slides to spread chromosomes and the metaphase spreads were stained with mountant containing DAPI. The full workflow is summarised in (a). Representative images are shown in (b). The proportion of fused chromosomes was scored for each condition by immunofluorescence microscopy (c).

Data shown in (b): 3 independent experiments with ≥100 nuclei analysed per condition in each experiment. Statistics: Student's T-test for Control vs. KD. BOD1L: p = 0.009. RIF1: p = 0.007.

The workflow for the assay is summarised in figure 5.6a. Cells were transfected as described in section 5.3.1. For this assay, RAD52, a fundamental component of the SSA pathway (Symington, 2002) was depleted with siRNA as a positive control; the loss of this factor would be expected to reduce SSA proficiency. However, RAD52 depletion did not result in the anticipated reduction in GFP-positive cells, suggesting that there was no detectable impact on SSA in the absence of RAD52 in this assay. The results of this investigation were therefore inconclusive.

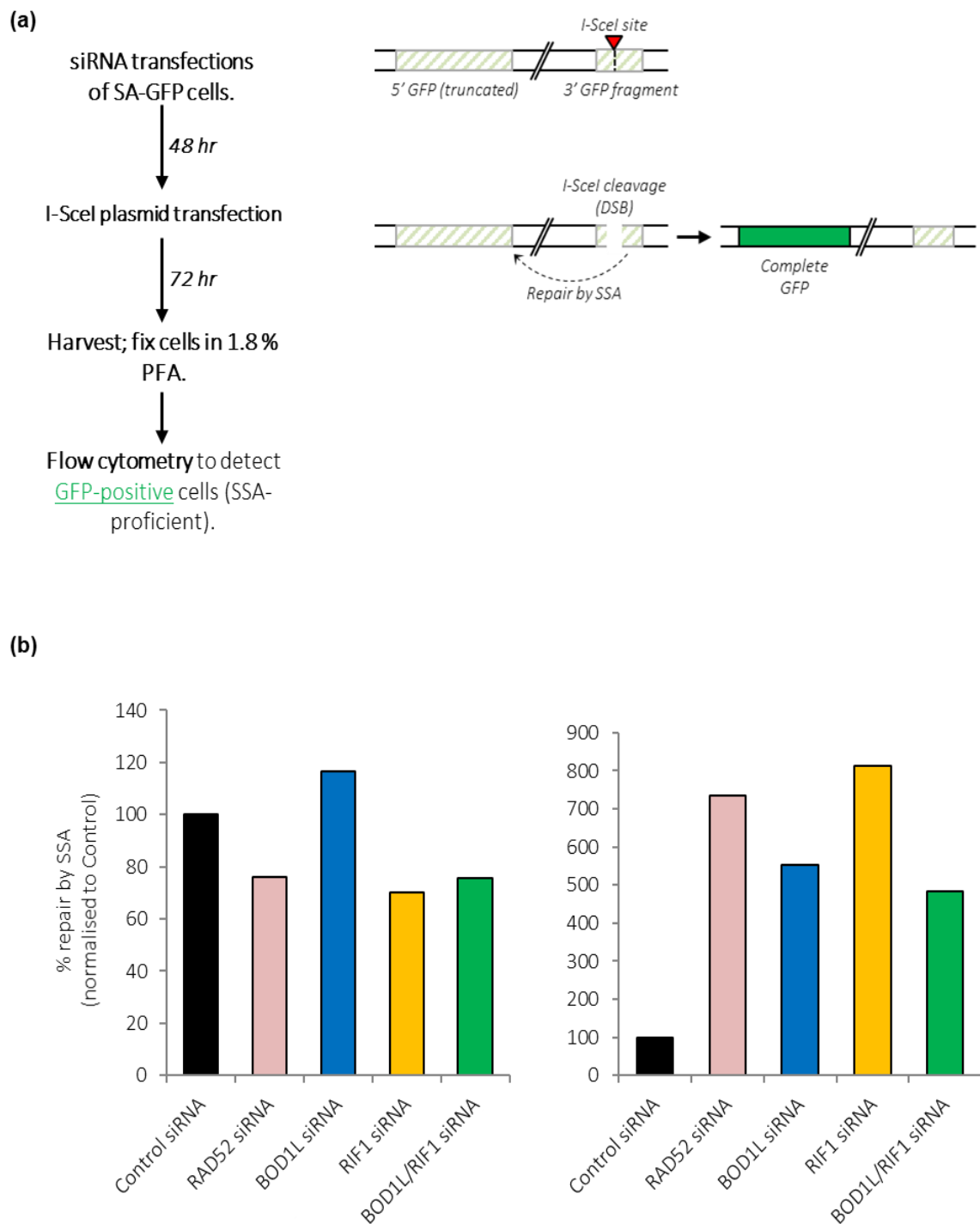


Figure 5.6: Single-strand annealing assay optimisation attempts.

The SA-GFP cell line, harbouring a GFP reporter cassette, was transfected with siRNA against RAD52, BOD1L, RIF1 and a non-targeting control. After 48 h, these cells were then transfected with an I-SceI expression vector. Upon expression, I-SceI induced a DSB in the GFP reporter cassette. SSA-proficient cells were able to repair the resultant DSB using a downstream 3' GFP repair fragment as a template, producing a complete GFP sequence. Seventy-two hours after transfection with the I-SceI expression vector, cells were harvested and fixed in preparation for flow cytometry. The proportion of GFP-positive cells was then analysed. The workflow is shown in (a), with a graphical representation of the state of the reporter cassette at each stage. Figures shown in (b) and (c) each represent a single independent experiment.

5.3: Discussion

Data from the preceding chapters demonstrated that BOD1L suppressed DSB resection following exposure of cells to IR. This modulation was likely to occur through its interaction with RIF1, one of the key downstream effectors of 53BP1-dependent DSB end protection. Whilst it is well established that RIF1 antagonises unscheduled BRCA1 recruitment to DSBs in G1 cells and promotes NHEJ, the influence of BOD1L on these processes had not been explored.

I hypothesised that the elevated resection observed in the absence of BOD1L may lead to a greater utilisation of HR-mediated repair. This was first investigated using an I-SceI-based GFP reporter assay. The results of this assay imply that, despite its down-regulation of resection, BOD1L has no impact on HR proficiency. This could be explained by the fact that a proportion of the unscheduled resection in the absence of BOD1L takes place in G1 cells, in which HR is not viable. Additionally, if the increase in CtIP-mediated short-range resection observed in BOD1L-deficient cells is not accompanied by long-range resection, this may be insufficient for the continuation of HR. This latter scenario was supported by the results of the native DNA fibre and foci analyses discussed in chapter 3, which pointed towards an increase in the number of DSBs resected in the absence of BOD1L, but no change in the extent of resection at individual breaks.

The data from the HR assay also confirmed that HR is unaffected in RIF1-depleted cells. These results agree with an earlier study by Isoibe and colleagues which used the same I-SceI-based

assay to investigate the influence of RIF1 on HR-mediated DSB repair (Isobe et al., 2017). This therefore supports the validity of my observations.

Given that HR is a cell cycle-controlled process which is restricted to late S and G2 phases, it would clearly be advantageous to monitor HR proficiency in specific phases upon depletion of BOD1L or RIF1. A standard technique for distinguishing between cell cycle phases in flow cytometry-based assays is co-staining fixed cells with propidium iodide (PI), an intercalating dye. PI fluorescence intensity is dependent on the DNA content in the cell; accordingly, G2 cells would be expected to produce a fluorescence intensity approximately twice that of G1 cells (Pozarowski and Darzynkiewicz, 2004). However, the inclusion of a separate transfection control in the assay setup described here rendered the use of PI co-staining impractical. Therefore, in order to investigate the impact of BOD1L and RIF1 depletion in a cell cycle-specific assay, RAD51 chromatin recruitment was examined in CENPF-negative and CENPF-positive cells, as well as in an asynchronous pool of cells. Notably, depletion of BOD1L or RIF1 had no detectable impact on IR-induced recruitment of RAD51 to DSBs when analyses were carried out in asynchronous cells; together with the results of the aforementioned reporter-based HR assay, these data suggest that HR is unaffected by the depletion of these proteins.

In contrast, the increase in RAD51 focal accumulation observed in BOD1L- and RIF1-depleted CENPF-negative cells implied a G1-specific increase in the recruitment of RAD51 to IR-induced DSBs. This is in line with the results of a previous study, which showed a slight increase in RAD51-positive nuclei upon depletion of RIF1 (Escribano-Díaz et al., 2013). My observation of

comparable results for BOD1L-depleted cells reinforced the notion that BOD1L and RIF1 function together to suppress recruitment of RAD51 during G1. One possibility to consider is that the inappropriate recruitment of RAD51 to G1 lesions in the absence of BOD1L or RIF1 is not simply a downstream consequence of aberrant resection, but is reflective of two distinct functions of BOD1L and RIF1: the suppression of RAD51 recruitment and the modulation of DSB resection. It may be that the former is specific to G1, whereas the latter can take place in G1 and G2; this would explain why there is no alteration in the recruitment of RAD51 to DSBs during G2 phase in BOD1L- or RIF1-depleted cells, despite increased resection in this context.

It is widely acknowledged that HR is normally restricted to late S/G2 cells that have completed DNA replication, ensuring a repair template is available. It therefore logically followed that altered levels of HR would be expected in G2 cells in the absence of BOD1L. This would manifest itself in greater recruitment of RAD51 to IR-induced DSBs in BOD1L-depleted cells. In contrast, however, a mild reduction in RAD51 recruitment was observed in G2 cells depleted of BOD1L, suggesting no increase in the utilisation of HR during this cell cycle phase in the absence of BOD1L. These results illustrate that whilst BOD1L suppressed unscheduled HR during G1, it did not actively promote this process during G2. This may reflect the fact that HR is a slow and complex process; even during G2, the majority of DSBs are repaired by other pathways (Mansour et al., 2008, Karanam et al., 2012). Increased resection alone may be insufficient to prompt a shift towards a greater use of HR. Instead, excess resected DSBs may be subjected to error-prone resection-dependent pathways which do not require RAD51.

Alongside its role in suppressing BRCA1 accumulation, RIF1 also actively promotes non-homologous end joining; previous studies have shown that NHEJ is impaired in the absence of RIF1 (Chapman *et al.*, 2013, Feng *et al.*, 2013, Escribano-Diaz *et al.*, 2013, di Virgilio *et al.*, 2013). As it has been demonstrated in chapter 4 that BOD1L and RIF1 interact and function within the same pathway, these proteins were expected to have a comparable impact on NHEJ. This was investigated with a telomere fusion assay, in which the expression of a dominant-negative mutant version of TRF2, a member of the protective Shelterin complex (TRF2^{ABΔM}), promotes de-protection of chromosome ends. This therefore provides an elegant and robust system for the investigation of the cellular capacity to perform NHEJ (Smogorzewska *et al.*, 2002). In accordance with my predictions, depletion of BOD1L and RIF1 suppressed the formation of end-to-end telomere fusions in the telomere de-protection assay. This illustrated that both of these proteins function in NHEJ; this pathway for DSB repair is therefore likely to be impaired in cells lacking either protein.

Previous studies have demonstrated that impairment of NHEJ results in greater utilisation of alternative repair pathways, including the non-canonical resection-dependent pathway, SSA (Mansour *et al.*, 2008, Escribano-Díaz *et al.*, 2013). Moreover, I considered the possibility that the increased short-range nucleolytic resection observed in the absence of BOD1L or RIF1 may not be coupled to elevated HR (Escribano-Díaz *et al.*, 2013, Bakr *et al.*, 2016, Cicca and Elledge, 2010). I therefore investigated the impact of BOD1L and RIF1 on SSA with a well-characterised I-SceI-based reporter assay (Gunn and Stark, 2012). The positive control selected for this assay was RAD52, a critical component of the SSA pathway. Following CtIP-mediated end resection

to expose 3' homologous flanking sequences, RAD52 mediates the re-annealing of these regions. This is followed by the removal of non-homologous sections and gap-filling by DNA polymerases. As such, severe impairment of SSA would be expected in the absence of RAD52 (Bhargava et al., 2016, Symington, 2002). However, attempts to optimise this assay proved to be unsuccessful. As shown in figure 5.6, depletion of RAD52 did not result in the predicted suppression of the GFP signal. Based on the results from this chapter and published literature, I would hypothesise that BOD1L-deficient cells would be forced to make greater usage of SSA as a repair pathway than their control counterparts due to the impairment of NHEJ in the absence of BOD1L. It would be worthwhile to make further attempts to optimise this assay in order to obtain conclusive results. Alternative siRNAs against RAD52 could be trialled to rule out inefficient protein depletion as a cause of the problems.

Collectively, these results demonstrate that BOD1L, along with RIF1, drives repair by NHEJ. Furthermore, in the absence of either protein, RAD51 focus formation increases during G1, suggesting that BOD1L and RIF1 co-operate to prevent inappropriate recruitment of RAD51 to DSBs in this phase. The role of BOD1L as an indirect regulator of HR appears to be confined to G1; my results suggest that it does not promote HR in G2 cells.

Previous investigations have sought to characterise the role of BOD1L during replication stress (Higgs *et al.*, 2015). The objectives of my thesis thus far have been to extend these investigations to examine the importance of BOD1L in the repair of IR-induced DSBs. The Topoisomerase I inhibitor Camptothecin (CPT) induces single-ended DSBs, which can be

regarded as a structural “intermediate” between a collapsed replication fork and a 2-ended DSB induced by IR. With this in mind, the work in the following chapter aimed to determine whether BOD1L was required for the resolution of CPT-induced lesions, and how other known DDR factors co-operate with BOD1L to effect repair.

Chapter 6: Role of BOD1L in repair of Camptothecin-induced double-strand breaks

6.1: Introduction

The earlier chapters of my thesis demonstrated that BOD1L acts as suppressor of DSB resection in cells exposed to IR. BOD1L also co-operates with RIF1 in promoting NHEJ and suppressing the inappropriate accumulation of RAD51 during G1, in which HR is inviable. However, BOD1L does not actively promote HR during G2. Previous studies and my work thus far have collectively investigated BOD1L's importance in the DDR in S-phase (during which collapsed replication forks result in DSB-like structures) (Higgs et al., 2015) and G2 (in which double-ended DSBs may be induced by IR). However, the potential role of BOD1L in the resection of single-ended DSBs in S-phase cells, which can be regarded as an intermediate between collapsed replication forks and G2 double-ended DSBs, remained unexplored.

Such breaks can be induced by the Topo-1 inhibitor Camptothecin (CPT). During DNA replication or transcription, unwinding of double-stranded DNA leads to torsional stress. The resultant supercoiling can be deleterious to cellular processes as it can impair the movement of key enzymes; as such, DNA supercoiling must be regulated carefully. To this end, a family of enzymes known as topoisomerases has evolved. Conserved across all kingdoms, these enzymes control supercoiling during S-phase through programmed DNA cleavage and re-ligation (Koster et al., 2010). CPT inhibits the activity of Topoisomerase-1 (Topo1) by binding

covalently to the Topo1-DNA complex and preventing the re-ligation of programmed nicks in the DNA. If this CPT-enzyme-DNA structure collides with an ongoing replication fork, a single-ended DSB forms. As with other DSBs, cell death may follow if this DSB cannot be promptly resolved (Liu et al., 2000).

Since CPT-induced DSBs occur during S-phase, they may be repaired by HR, provided that a template is available for repair. In order to facilitate repair of the DSB, the CPT-Topo1 adduct requires specialised processing in addition to nucleolytic resection. Multiple factors have been implicated in these processes. The ERCC1-XPF complex, typically associated with DNA crosslink resolution, has structure-specific nuclease activity and is thought to remove 3' phosphotyrosyl bonds in DNA-Topo1 complexes (Takahata et al., 2015). Additionally, based on studies of its yeast homologue, Fun30, it has been proposed that the chromatin remodeller SMARCAD1 is also crucial for the repair of CPT-induced DNA damage; depletion of this factor results in heightened sensitivity to CPT, whereas over-expression leads to genome instability in CPT-treated cells (Costelloe et al., 2012). Both CtIP and DNA2 are also involved in the resection of CPT-induced DSBs as a precursor to HR-mediated repair (Liu et al., 2016, Hartsuiker et al., 2009, Nakamura et al., 2010). Interestingly, my data, in combination with previous studies, attributed aberrant resection in the absence of BOD1L to these nucleases. However, whether they played an equivalent role in BOD1L-deficient cells exposed to CPT remained to be determined.

There had been no investigations of the potential role for BOD1L in the resection and resolution of single-ended S-phase DSBs, or those known to require complex processing due to the

presence of end adducts – both of which are characteristics of CPT-induced DNA damage. Moreover, the relevance of the interaction between BOD1L and RIF1 in this context was unexplored. This chapter therefore aimed to determine the importance of BOD1L and RIF1 in DSB resection, repair and genome stability following CPT exposure.

6.2: BOD1L is involved in the repair of CPT-induced DSBs

Since BOD1L modulates DSB resection and resection of replication forks in S-phase, I hypothesised that it may also contribute to the resolution of one-ended S-phase DSBs induced by CPT. To ascertain the importance of BOD1L in the repair of these lesions, the sensitivity of BOD1L- and RIF1-depleted cells to CPT was first assessed by clonogenic survival assays. Markers of CPT-induced genome instability and DNA damage signalling were subsequently quantified by immunofluorescence microscopy in cells depleted of BOD1L and RIF1. These results collectively suggested that BOD1L, along with RIF1, was involved in the maintenance of genome stability and preservation of cell viability following exposure to CPT. To shed further light on the role of BOD1L/RIF1 in this process, immunoblotting and immunofluorescence microscopy were used to examine the recruitment of RPA2, phosphorylated RPA32, RIF1 and BRCA1 to sites of DNA damage following CPT exposure in the absence of BOD1L. From these data, it was concluded that BOD1L suppressed resection of CPT-induced DSBs but did not influence the localisation of BRCA1. Finally, the role of BOD1L in HR-mediated repair after CPT was analysed by assessing the recruitment of RAD51 to sites of CPT-induced DNA damage.

6.2.1: BOD1L and RIF1 contribute to cell survival and genome stability after exposure to CPT

The potential role for BOD1L in the resolution of DSBs induced by CPT, which can be viewed as a structural intermediate between IR-induced two-ended DSBs and single-ended DSBs arising from replication fork collapse, had not been explored. Since BOD1L was shown to function in multiple aspects of the DDR to repair a variety of DNA lesions, I proposed that it may also participate in the resolution of CPT-induced DSBs, and that cell viability would be compromised in its absence. Furthermore, having demonstrated in chapter 4 that BOD1L and the 53BP1 effector RIF1 functionally interact, I hypothesised that comparable results would be obtained in RIF1-deficient cells.

To investigate cellular sensitivity to CPT in the absence of BOD1L or RIF1, I carried out clonogenic survival assays as described in section 3.3.1. HeLa cells depleted of BOD1L or RIF1 were subjected to doses of CPT ranging from 0.1 μ M to 2.0 μ M; the medium was washed out and replaced after 1 h. After incubation for a further 10 days in standard conditions, surviving colonies were stained with Crystal Violet solution, washed thoroughly and quantified manually. Additionally, transfected cells were plated at normal density, cultured and harvested after 3 days for Western blot analysis.

Depletion of BOD1L and RIF1 was initially confirmed by Western blotting (figure 6.1a). In the absence of either factor, there was a modest reduction in cell survival following treatment with CPT; this was most apparent after high-dose CPT (figure 6.1b). These data suggested that BOD1L and RIF1 contribute to the preservation of cell viability after exposure to CPT. However,

the defect was relatively mild. This observation implies that BOD1L and RIF1 play a less prominent role in the repair of CPT-induced lesions than a number of previously implicated factors, such as XRCC1 (Horton et al., 2017), MutS homologue 5 (MSH5) (Xu et al., 2015b), the structure-specific nuclease SLX4 (Kim et al., 2013), and TDP1 (Das et al., 2014).

Given that BOD1L functions in the repair of DNA damage and maintenance of genome stability after IR or during replication stress (Higgs et al., 2015), it was plausible to speculate that this factor also participated in the resolution of CPT-induced lesions, thereby maintaining genome stability in this context. Additionally, due to its interactions with BOD1L, I hypothesised that RIF1 would perform a parallel role.

To assess the importance of BOD1L and RIF1 in maintaining genome stability following exposure of cells to CPT, I examined the formation of micronuclei by immunofluorescence microscopy. HeLa cells were transfected with siRNA to deplete BOD1L, RIF1, or both factors in combination. Transfected cells were treated with 1 μ M CPT for 1 h; following wash-out of CPT and replacement of medium, cells were cultured for a further 24 h and harvested.

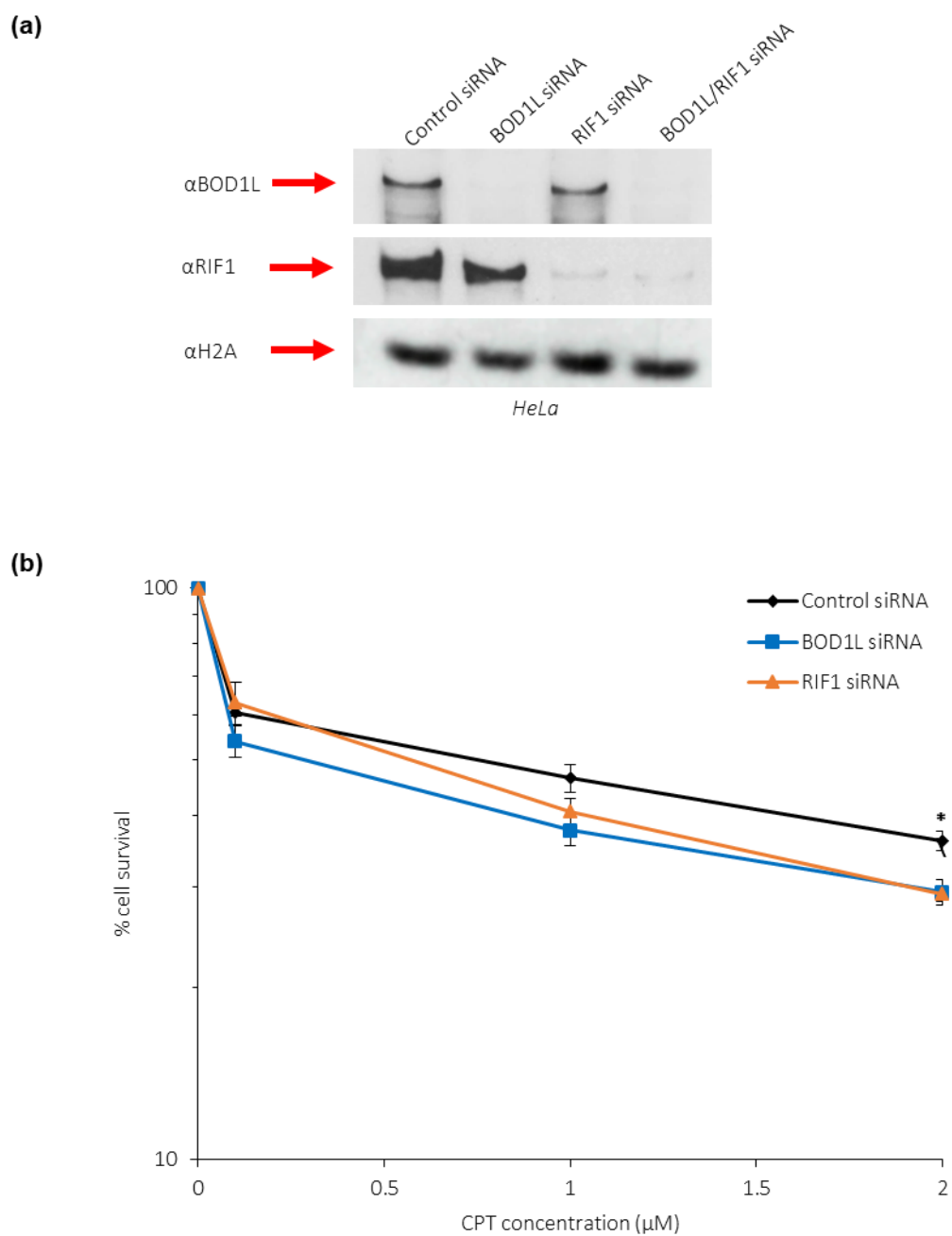


Figure 6.1: Depletion of BOD1L or RIF1 results in higher sensitivity to CPT.

Following siRNA-mediated depletion of BOD1L and RIF1 in HeLa cells, whole-cells extracts (WCEs) were prepared and analysed by Western blotting to confirm successful knockdowns of the named proteins (a). siRNA-treated cells were plated at low density and subjected to the indicated doses of CPT for 1 hr before washing out. Cells were allowed to proliferate for 10 days. At this time, the proportion of surviving colonies was calculated (b).

Data show in (b): 3 independent experiments with 3 dishes per condition for each experiment. Statistics: ANOVA. Con vs. BOD1L: $p = 0.02$. Con vs. RIF1: $p = 0.02$. BOD1L vs. RIF1: $p = 0.99$ (not significant).

Coverslips were pre-extracted, fixed and mounted with DAPI prior to enumeration of micronuclei by immunofluorescence microscopy.

In control cells, 7.4 % of nuclei exhibited CPT-induced micronucleation. This proportion approximately doubled upon depletion of BOD1L, RIF1, or both factors (figure 6.2); however, it was noted that the observed increase in micronucleation was not statistically significant when BOD1L was depleted singly. Therefore, whilst these data supported the notion that RIF1 contributed to genome stability following CPT exposure, potentially in co-operation with BOD1L, the importance of BOD1L to genome stability in this context could not be determined.

6.2.2: Resolution of CPT-induced DSBs is problematic in the absence of BOD1L or RIF1

Having demonstrated that cell survival after exposure to CPT is compromised in the absence of BOD1L or RIF1, I set out to determine the underlying cause of this defect. To this end, HeLa cells were transfected with siRNA against BOD1L, RIF1, or both factors in combination. Cells depleted of these proteins were treated with 1 μ M CPT for 1 h before washing out. Following treatment, coverslips were harvested at 1 h and 24 h time points, pre-extracted and fixed for immunofluorescence microscopy. Cells were stained with antibodies against γ H2AX to examine the repair of CPT-induced DNA damage, and the proportion of nuclei with at least 10 γ H2AX foci was assessed.

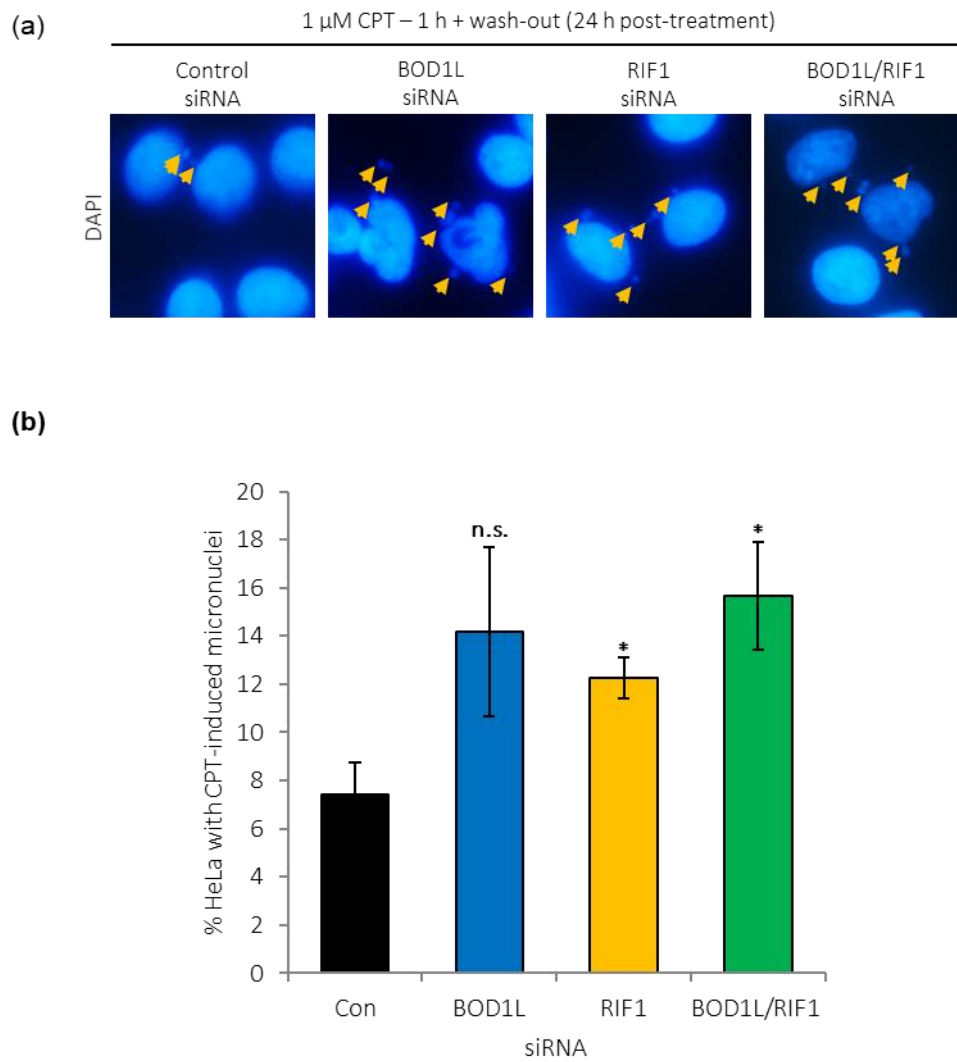


Figure 6.2: Cells depleted of BOD1L or RIF1 show more CPT-induced micronucleation.

HeLa cells treated with siRNA against BOD1L and RIF1, singly and in combination, were subjected to 1 μ M CPT for 1 hr before washing out. Cells were harvested 24 hr after treatment and mounted in medium containing DAPI. The number of cells with micronuclei was quantified by immunofluorescence microscopy. Representative images are shown in (a) and quantifications in (b).

Data shown in (b): ≥ 3 independent experiments with ≥ 100 nuclei quantified per condition in each experiment. Statistics: Student's T-test for Control vs. KD. BOD1L: $p = 0.15$. RIF1: $p = 0.02$. BOD1L/RIF1: $p = 0.03$. Error bars indicate SEM.

In cells depleted of BOD1L, RIF1 or both proteins, there was a two-fold increase in CPT-induced γ H2AX focus formation at 1 h post-treatment relative to control cells. Moreover, in the absence of these factors, the proportion of γ H2AX-positive cells remained elevated at 24 h after the induction of DNA damage. Interestingly, at both time points, the proportions of nuclei with γ H2AX foci were strikingly similar upon depletion of the above-named factors (figure 6.3). Collectively, these data implied that DSBs generated by exposure to CPT could not be fully resolved in BOD1L- or RIF1-deficient cells. Furthermore, the absence of any additive impact on γ H2AX recruitment to CPT-induced DSBs in cells depleted of both BOD1L and RIF1 suggested that these proteins act within the same pathway to resolve DNA damage after exposure to this genotoxin.

For further insight into the collective role of BOD1L and RIF1 in the repair of CPT-induced DSBs, I depleted these factors in HeLa cells using siRNA, treated cells with CPT and harvested coverslips for immunofluorescence microscopy after 24 h as described above. Cells were stained with antibodies against 53BP1, a well-established marker of DSBs (Symington & Gautier, 2011, Bothmer et al., 2010, Bunting et al., 2010). The proportion of cells with at least 10 53BP1 foci was examined by immunofluorescence microscopy.

Approximately 40 % of control cells contained 53BP1 foci 24 h after treatment with CPT; there was negligible alteration to this proportion upon depletion of the proteins of interest (figure

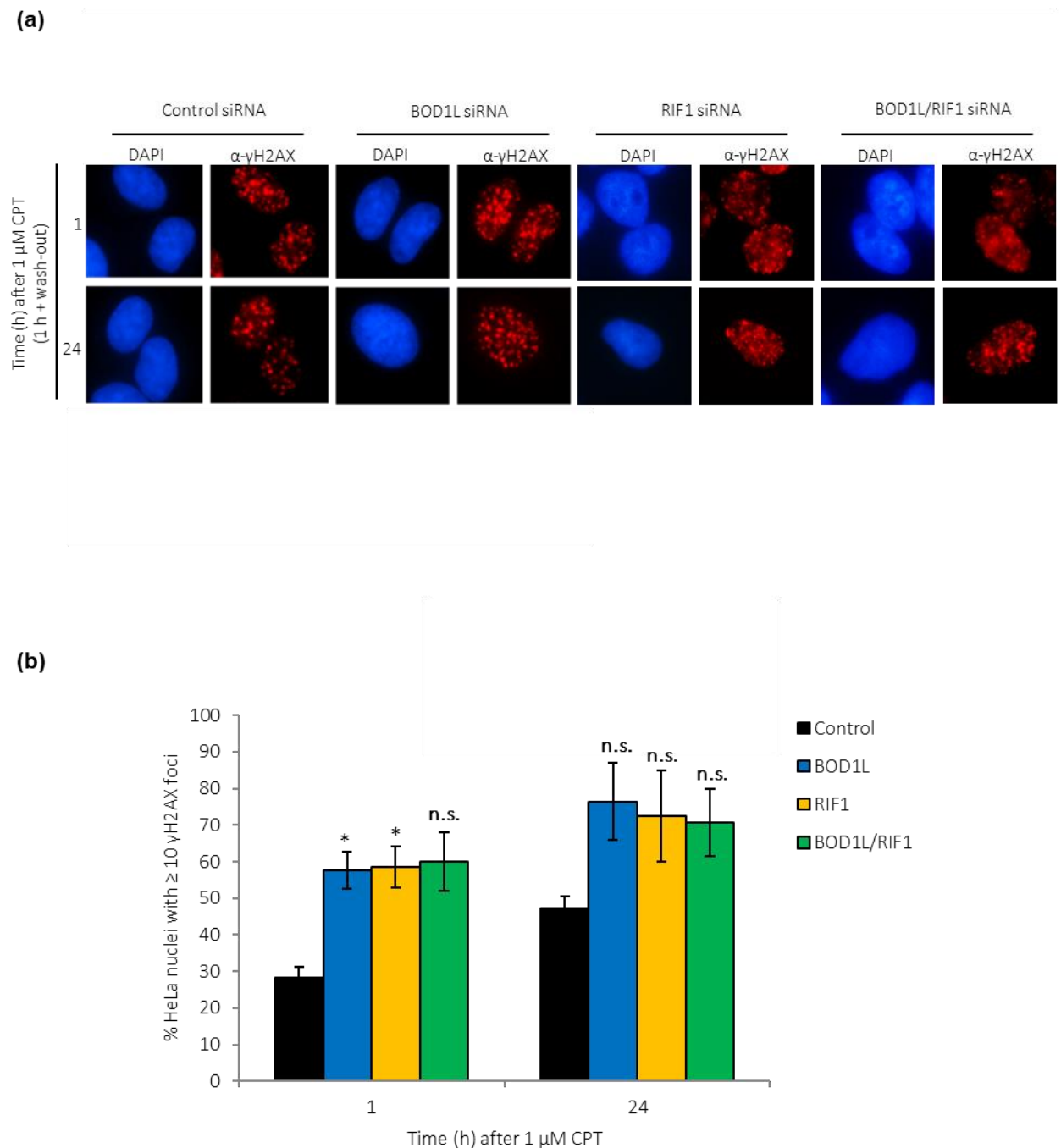


Figure 6.3: Resolution of CPT-induced DSBs is compromised in the absence of BOD1L or RIF1.

HeLa cells were transfected with the named siRNA, exposed to 1 μ M CPT for 1 h and harvested at the indicated time points following exposure. Cells were pre-extracted, fixed and stained with antibodies against γ H2AX, and the proportion of cells with at least 10 foci was assessed by immunofluorescence microscopy. Representative images are shown in (a) with quantifications in (b).

Data shown in (b): 3 independent experiments with at least 100 nuclei analysed per condition. Statistics: Student's T-test for Control vs. KD. 1 h: BOD1L: $p = 0.02$. RIF1: $p = 0.03$. BOD1L/RIF1: $p = 0.06$. 24 h: BOD1L: $p = 0.06$. RIF1: $p = 0.12$. BOD1L/RIF1: $p = 0.08$.

6.4). These observations demonstrated that the recruitment of 53BP1 to sites of CPT-induced damage was unaffected in the absence of these factors.

6.2.3: Resection of CPT-induced DSBs is increased in the absence of BOD1L or RIF1

The results of the previous section provided some evidence that BOD1L and RIF1 functioned together in the resolution of CPT-induced DSBs. Previous literature, as well as the earlier chapters of my thesis, illustrated that BOD1L and RIF1 suppressed inappropriate resection of stalled replication forks and IR-induced DSBs in order to facilitate their repair (Higgs et al., 2015, Garzon et al., 2019). I therefore proposed that these proteins also contributed to the repair of CPT-induced DSBs by modulating nucleolytic resection of these lesions. In order to determine whether BOD1L and RIF1 suppressed resection in this context, I analysed the recruitment of RPA2 to CPT-induced DSBs. HeLa cells were transfected with siRNA against BOD1L and RIF1, both singly and in combination. Transfected cells were treated with 1 μ M CPT and harvested after 1 h. After being pre-extracted and fixed, coverslips were stained with antibodies against RPA2 and co-stained with CENPF antibodies to permit the identification of late S-phase nuclei which had sustained CPT-induced damage. The proportion of CENPF-positive cells with at least 10 RPA2 foci was enumerated by immunofluorescence microscopy.

In control cells, 16.8 % of CENPF-positive nuclei exhibited RPA2 foci following exposure to CPT. This increased approximately two-fold in the absence of BOD1L, RIF1, or both factors in combination (figure 6.5), suggesting that resection of CPT-induced DSBs was elevated in the absence of these proteins.

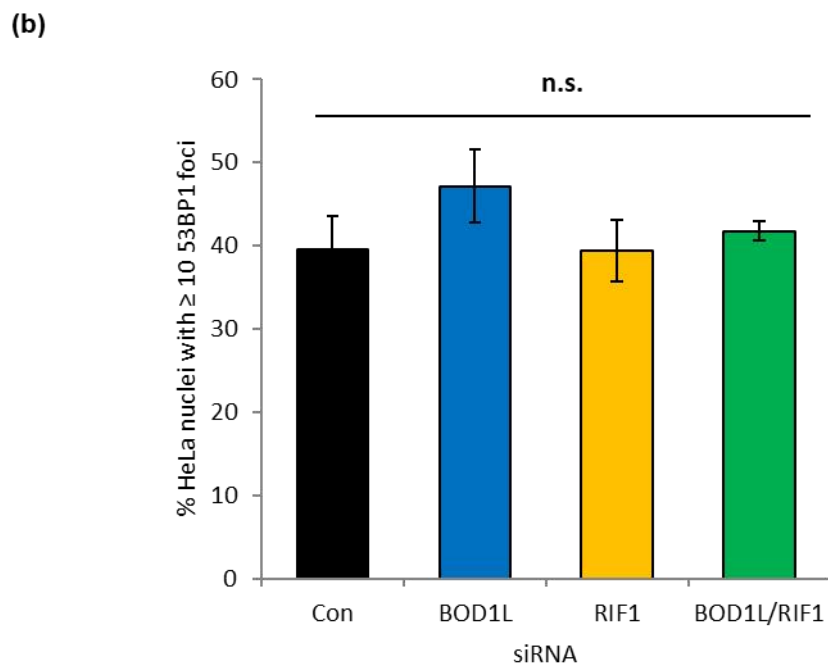
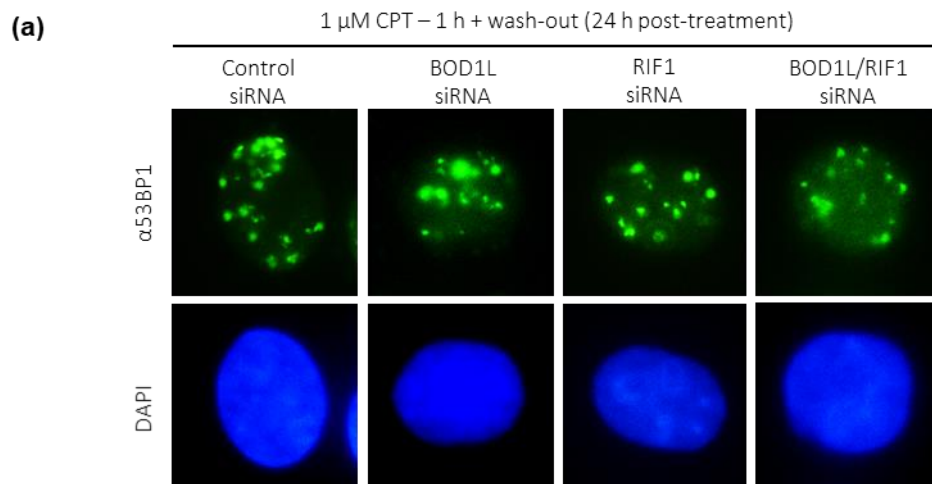


Figure 6.4: Recruitment of 53BP1 to sites of CPT-induced damage is unaffected in the absence of BOD1L or RIF1.

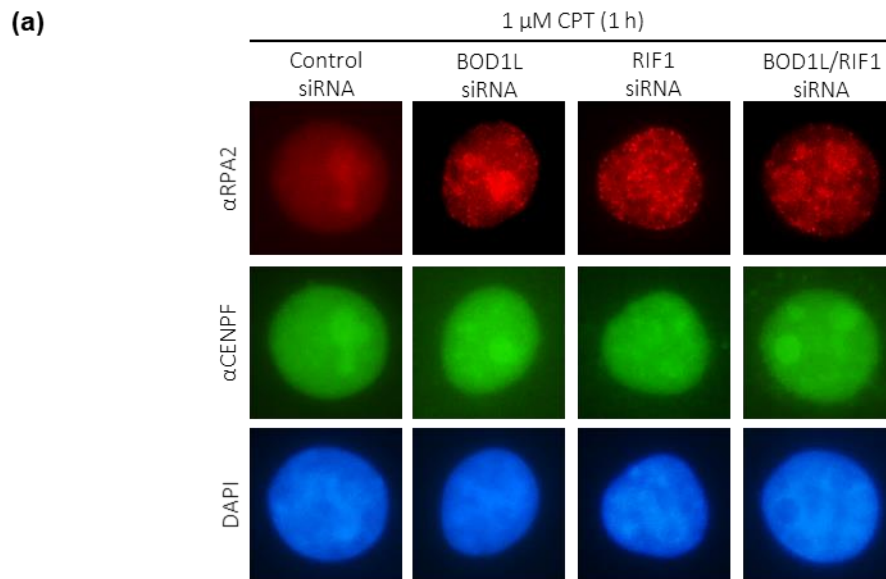
HeLa cells treated with the named siRNA were subjected to 1 μ M CPT for 1 h before washing out. Treated cells were harvested after 24 hr, stained with antibodies against 53BP1 and mounted in medium containing DAPI. The number of cells with at least 10 53BP1 foci was quantified by immunofluorescence microscopy. Representative images are shown in (a) and quantifications in (b).

Data shown in (b): ≥ 3 independent experiments with ≥ 100 cells quantified per condition in each experiment. Statistics: Student's T-test for Control vs. KD. BOD1L: $p = 0.25$. RIF1: $p = 0.98$. BOD1L/RIF1: $p = 0.62$. Error bars indicate SEM.

As a definitive indication of the impact of BOD1L and RIF1 depletion on resection of CPT-induced lesions, I extended my studies further to examine RPA32 phosphorylation in the absence of these factors after treatment with CPT. HeLa cells were transfected, treated and harvested as described above. In preparation for immunofluorescence microscopy, coverslips were stained with antibodies against RPA32-P (S4/S8) and CENPF, and the proportion of CENPF-positive nuclei with at least 10 RPA32-P foci was assessed. In parallel, HeLa cells treated with siRNA against BOD1L or a non-targeting control sequence were exposed to 1 μ M CPT and harvested 1 h and 4 h after treatment. Whole-cell extracts were prepared and analysed by Western blotting; membranes were probed with antibodies against BOD1L, RPA32-P (S4/S8) and as a subset of established targets of ATM, a master regulator of the DDR.

Western blotting confirmed the successful depletion of BOD1L. In the absence of this factor, cells exposed to CPT exhibited slightly higher levels of RPA32 phosphorylation than control cells; furthermore, there was a moderate increase in levels of CHK1-P (S345) and γ H2AX (figure 6.6a). Taken together, these results were suggestive of elevated resection of CPT-induced DSBs in cells depleted of BOD1L. This may have been accompanied by an increase in DDR signalling after CPT exposure in these cells.

Immunofluorescence microscopy analyses also revealed an increase in phosphorylated RPA32 after CPT exposure from 21.7% in control cells to 56.6% in cells depleted of BOD1L. Comparable increases in RPA32-P were observed upon depletion of RIF1 or RIF1 in



(b)

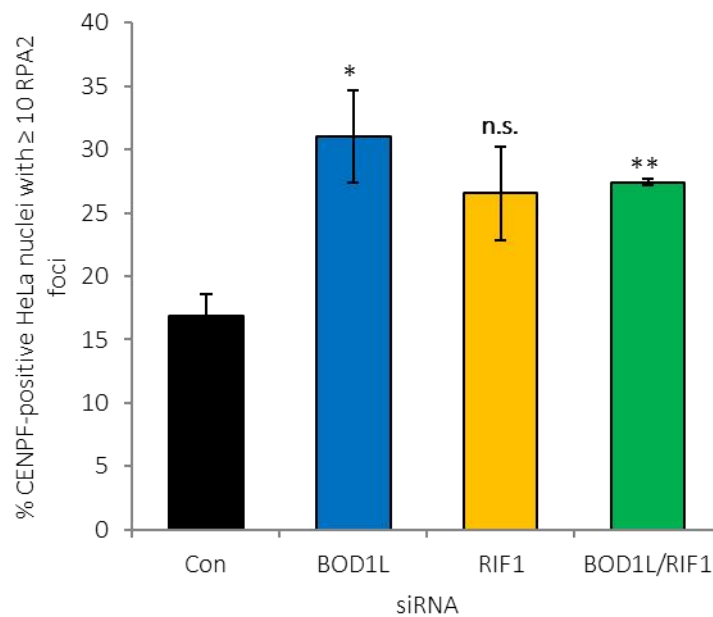


Figure 6.5: BOD1L- and RIF1-depleted cells exhibit increased accumulation of RPA2 at CPT-induced DSBs.

HeLa cells treated with the indicated siRNA were subjected to 1 μ M CPT for 1 h before washing out. Treated cells were harvested after 24 hr, stained with antibodies against CENPF and RPA2 and mounted with DAPI. The proportion of cells with at least 10 RPA2 foci was assessed by immunofluorescence microscopy. Representative images are shown in (a) and quantifications in (b).

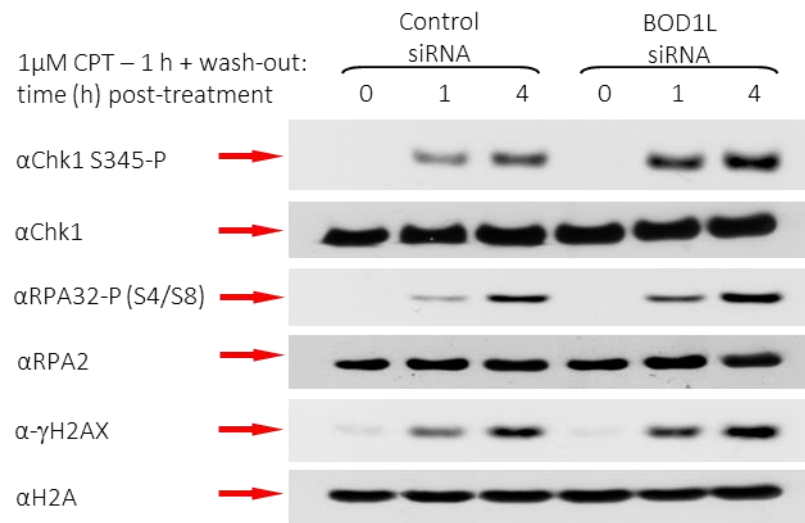
Data shown in (b): ≥ 3 independent experiments with ≥ 100 cells quantified per condition in each experiment. Statistics: Student's T-test for Control vs. KD. BOD1L: $p = 0.03$. RIF1: $p = 0.08$. BOD1L/RIF1: $p = 0.004$. Error bars indicate SEM.

combination with BOD1L. These data provided further evidence of a co-operative role for BOD1L and RIF1 in suppressing inappropriate resection of CPT-induced DSBs.

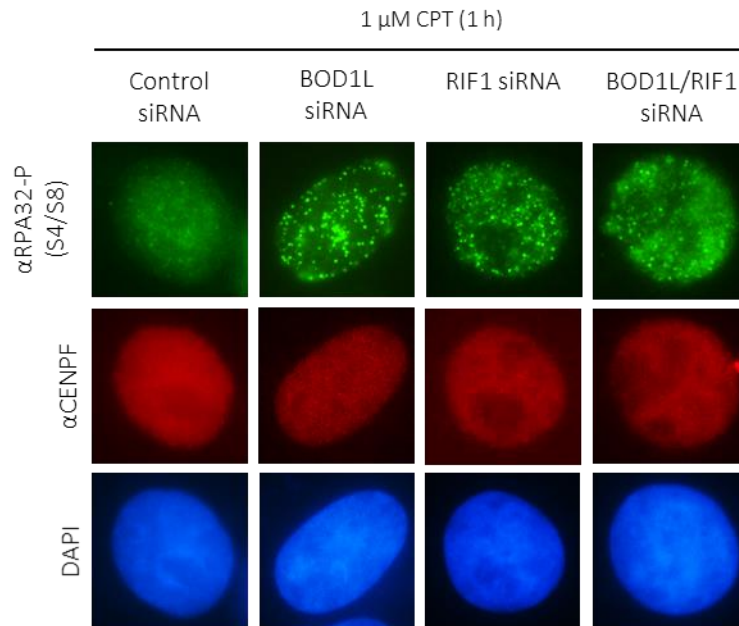
As for IR-induced DSBs, unscheduled resection of CPT-induced lesions in the absence of BOD1L or RIF1 could have manifested itself as an increase in the extent of resection per individual break, or a greater number of lesions resected per cell. To distinguish between these potential scenarios, I transfected HeLa cells with siRNA against BOD1L, RIF1 or a non-targeting control sequence, cultured these cells for 24 h with 10 μ M IdU and exposed them to 1 μ M CPT for 1 h. The following day, I harvested cells for native DNA fibre analysis (omitting the HCl denaturation step) and immunofluorescence microscopy. After spreading, DNA fibres were stained with antibodies against IdU, and tracts of resected ssDNA were measured using ImageJ. Coverslips for immunofluorescence microscopy were pre-extracted twice, fixed and stained with antibodies against IdU, and IdU foci were enumerated.

Native fibre analysis did not show any detectable difference in the length of ssDNA tracts between control cells and those depleted of BOD1L. However, there was a modest increase in tract length in RIF1-depleted cells (figure 6.7). The number of IdU foci per nucleus in CPT-treated cells was unaffected by the absence of either factor (figure 6.8). These analyses implied that RIF1 suppressed the extent of resection at individual CPT-induced DSBs, but BOD1L was dispensable for this function. IdU focus quantification did not support a role for either protein in curbing the number of lesions resected.

(a)



(b)



(c)

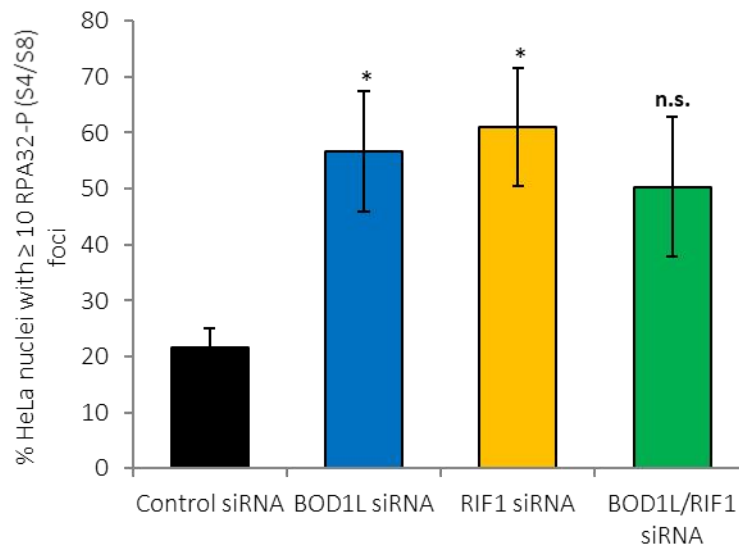
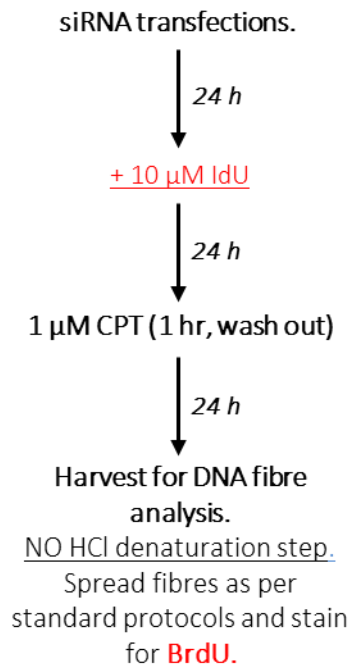


Figure 6.6: Depletion of BOD1L or RIF1 results in greater RPA32 phosphorylation in cells exposed to CPT.

HeLa cells treated with siRNA against BOD1L or a non-targeting control sequence were exposed to 1 μ M CPT for 1 h prior to washing out. Cells were harvested and whole-cell extracts prepared for Western blot analysis at the indicated time points after treatment with CPT. Membranes were probed with the named primary antibodies, incubated with HRP-conjugated secondary antibodies and visualised with chemiluminescence (a). In parallel, cells transfected and treated as in (a) were harvested 1 h post-CPT. Coverslips were pre-extracted, fixed and stained with antibodies against RPA32-P (S4/S8) and CENPF, and the proportion of CENPF-positive cells with at least 10 RPA32-P foci was assessed by immunofluorescence microscopy. Representative images are shown in (b) with quantifications in (c).

Data shown in (c): 3 independent experiments with ≥ 100 nuclei per condition analysed in each experiment. Statistics: Student's T-test for Control vs. KD. BOD1L: $p = 0.04$. RIF1: $p = 0.02$. BOD1L/RIF1: $p = 0.09$.

(a)



(b)

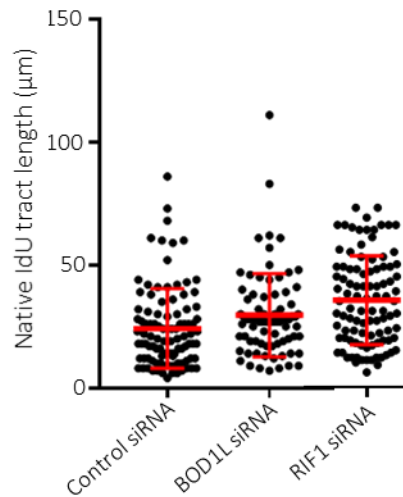
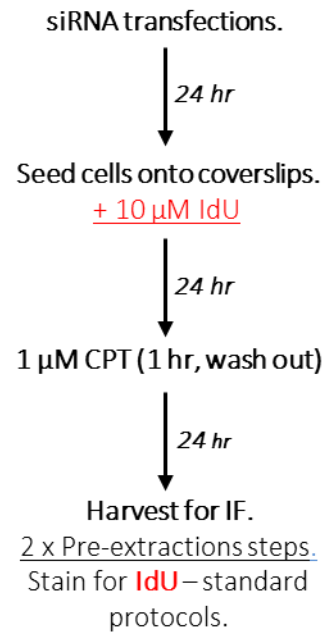


Figure 6.7: RIF1 depletion, but not BOD1L depletion, has a mild impact on the extent of resection of individual CPT-induced DSBs.

HeLa cells were transfected with siRNA against BOD1L, RIF1 or a non-targeting control sequence. The following day, the culture medium was supplemented with IdU. After 24 h, cells were treated with 1 μ M CPT; the medium was replaced after 1 h. Cells were harvested, stained with antibodies against IdU and spread for DNA fibre analysis, omitting the HCl denaturation step. Fluorescence microscopy images were acquired and native IdU tract length was measured using ImageJ software. The workflow is summarised in (a); native IdU tract lengths are shown in (b).

Data shown in (b) acquired from a single experiment with ≥ 100 tracts measured per condition. Bars indicate the standard deviation from the population mean.

(a)



(b)

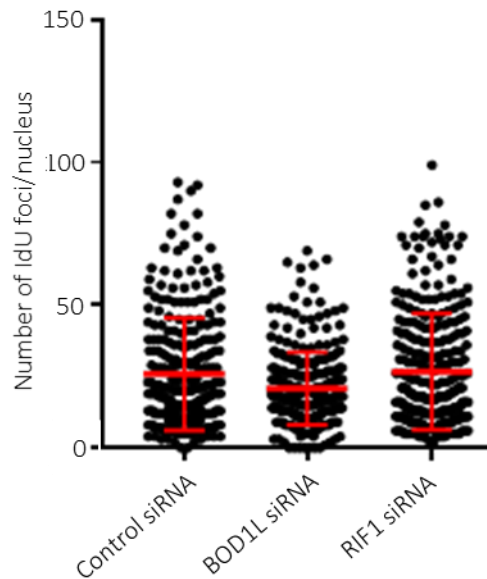


Figure 6.8: Depletion of BOD1L or RIF1 has no detectable impact on the number of CPT-induced DSBs resected.

HeLa cells were transfected with Control, BOD1L or RIF1 siRNA and cultured with 10 μ M IdU. After 24 h, cells were treated with 1 μ M CPT; this treatment was washed out after 1 h. Coverslips were harvested and stained with antibodies against IdU and the S/G2 marker CENPF. The number of IdU foci per CENPF-positive cell was quantified by immunofluorescence microscopy. The workflow is summarised in (a); the numbers of foci per cell are shown in (b).

Data shown in (b): 2 independent experiments with ≥ 100 nuclei analysed per condition in each experiment. Bars indicate the standard deviation from the population mean.

6.2.4: BOD1L is required for the recruitment of RIF1 to CPT-induced DSBs but does not affect BRCA1 localisation

The role of the 53BP1 effector RIF1 as a suppressor of DSB end resection has been researched extensively. It is known that RIF1 antagonises the recruitment of BRCA1 to lesions that are unsuitable for repair by resection-dependent pathways, thereby preventing short-range resection by CtIP, which is dependent on BRCA1 (Feng et al., 2013, Chapman *et al.*, 2013, Escribano-Diaz et al., 2013, di Virgilio et al., 2013). Moreover, in chapter 4 of my thesis, I demonstrated that BOD1L interacted with RIF1 and was required for its recruitment to IR-induced DSBs, where both proteins play a role in modulating resection. I therefore proposed that the mechanism for BOD1L's suppression of DSB resection following exposure to CPT could be based on its recruitment of RIF1 to these lesions.

To determine the importance of BOD1L in the localisation of RIF1 to CPT-induced DSBs, HeLa cells were depleted of BOD1L, RIF1, or both factors in combination using siRNA. Transfected cells were exposed to 1 μ M CPT and harvested for analysis by immunofluorescence microscopy after 1 h. Coverslips were pre-extracted, fixed and stained with antibodies against RIF1. Cells were co-stained with antibodies against CENPF to permit identification of late S-phase cells, and the proportion of CENPF-positive nuclei with at least 10 RIF1 foci was enumerated.

Approximately 18.0% of CENPF-positive nuclei were positive for RIF1 foci. As would be expected, RIF1 focus formation was almost entirely abrogated upon depletion of RIF1. There was a three-fold reduction in this proportion in the absence of BOD1L (figure 6.9). This

illustrates that the recruitment of RIF1 to CPT-induced DSBs is compromised in BOD1L-deficient cells.

Having demonstrated that BOD1L was required for localisation of RIF1 to sites of DNA damage in CPT-treated cells, it was important to determine whether impaired RIF1 recruitment resulted in excessive recruitment of BRCA1 to these sites. HeLa cells were transfected and treated with CPT as described above. After harvesting, pre-extraction and fixation, coverslips were stained with antibodies against BRCA1 and CENPF in preparation for immunofluorescence microscopy. The proportion of CENPF-positive cells with at least 10 BRCA1 foci was then assessed.

In control cells, approximately half of CENPF-positive nuclei contained BRCA1 foci. This proportion increased only slightly in cells deficient of BOD1L, RIF1 or both factors in combination (figure 6.10). Based on these results, I concluded that BOD1L and RIF1 collectively play a minimal role in antagonising recruitment of BRCA1 to CPT-induced DSBs.

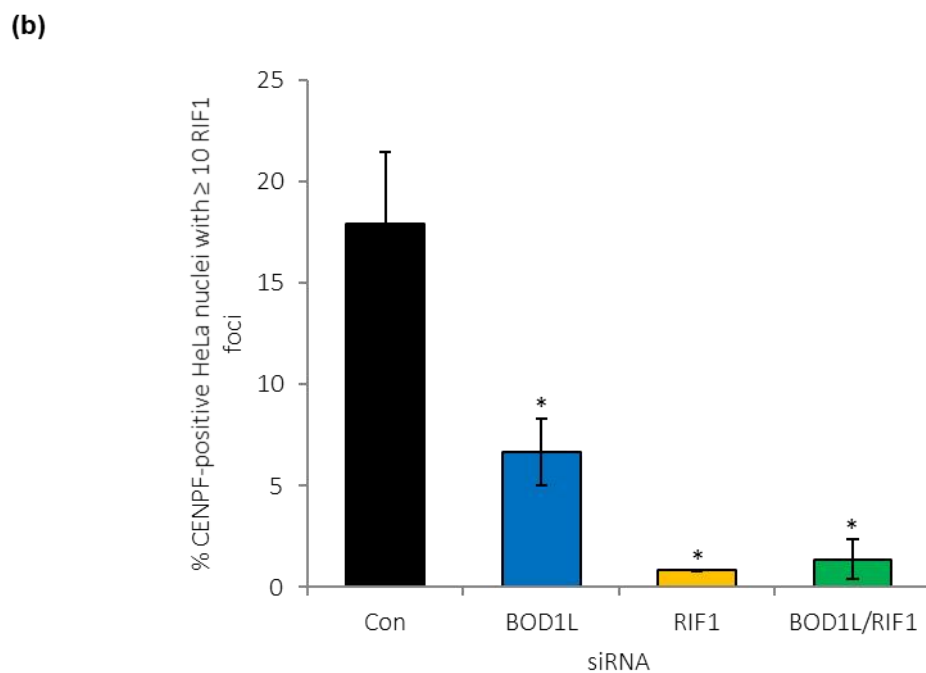
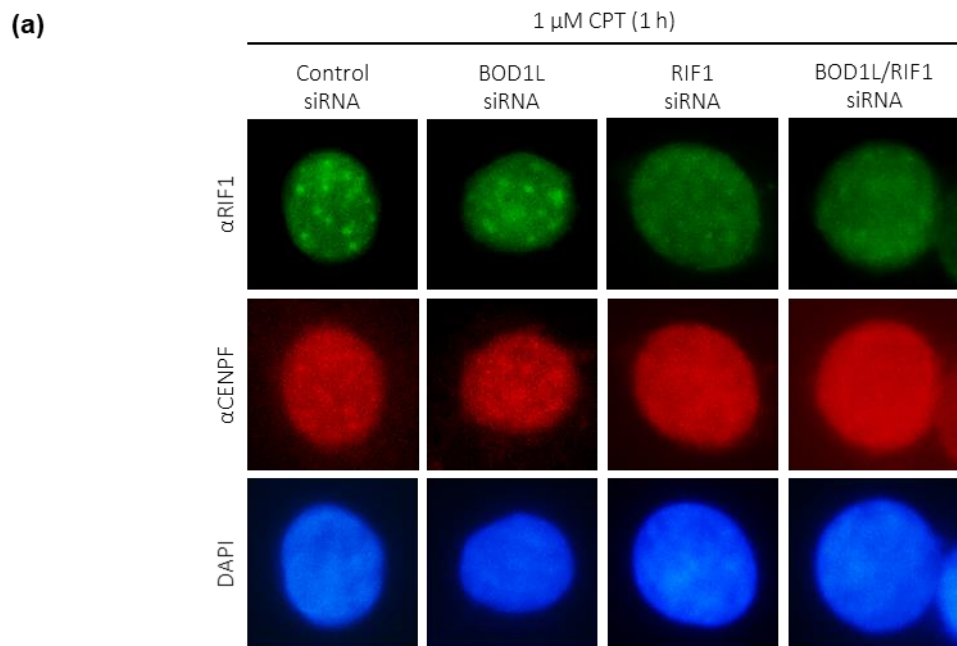


Figure 6.9: Recruitment of RIF1 to CPT-induced DSBs is impaired in the absence of BOD1L.

HeLa cells treated with the named siRNA were exposed to 1 μ M CPT for 1 h. Coverslips were then harvested, pre-extracted, fixed and stained with antibodies against RIF1 and CENPF. Stained coverslips were mounted with DAPI and the proportion of CENPF-positive cells with at least 10 RIF1 foci was quantified by immunofluorescence microscopy. Representative images are shown in (a) with quantifications in (b).

Data shown in (b) are from 3 independent experiments with ≥ 100 nuclei analysed per condition in each experiment.

Statistics: Student's T-test for Control vs. KD. BOD1L: $p = 0.04$. RIF1: $p = 0.009$. BOD1L/RIF1: $p = 0.01$.

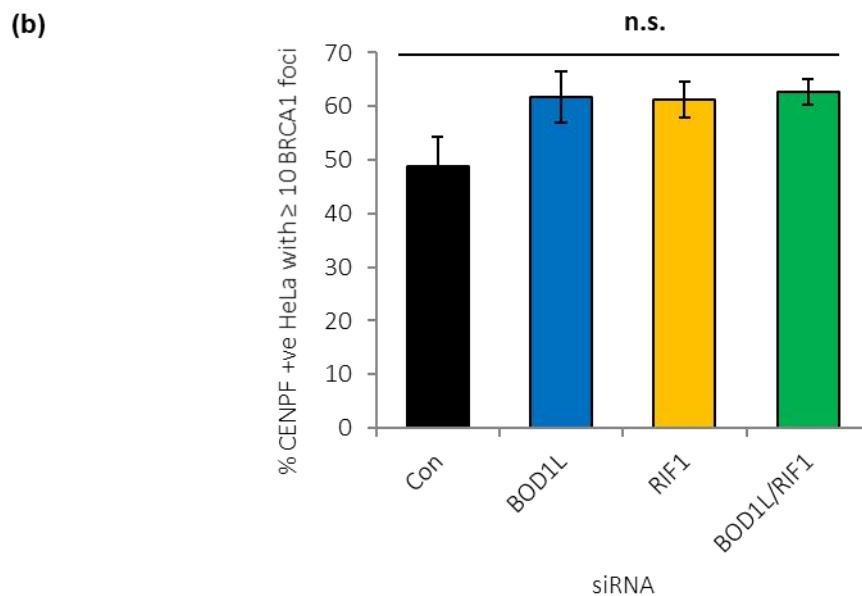
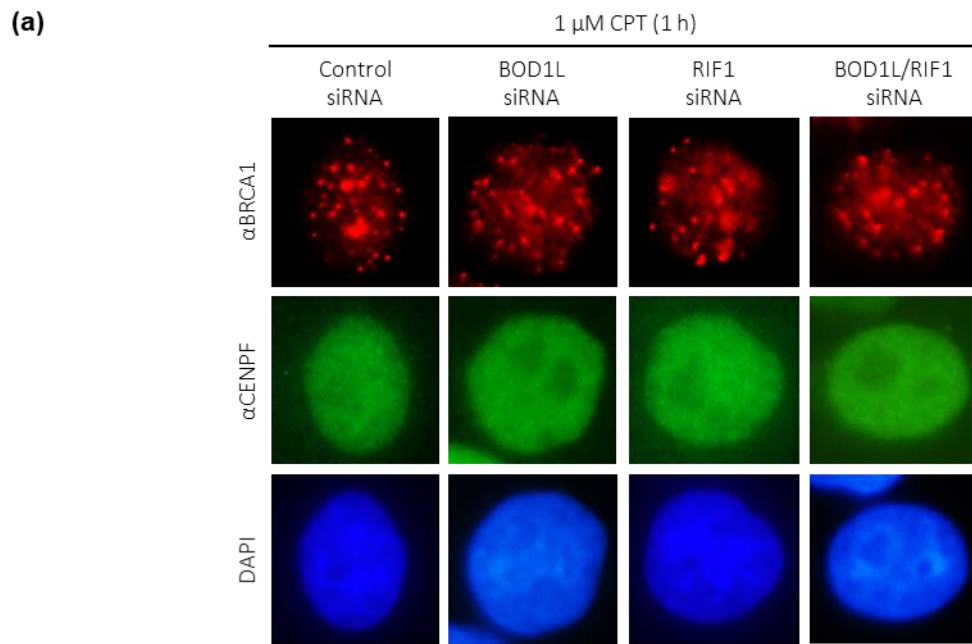


Figure 6.10: Recruitment of BRCA1 to CPT-induced DSBs is unaffected by depletion of BOD1L or RIF1.

HeLa cells were transfected with siRNA against BOD1L, RIF1 or a non-targeting control sequence. Transfected cells were exposed to 1 μ M CPT. After 1 h, cells were harvested, pre-extracted, fixed and stained with antibodies against BRCA1 and CENPF. The proportion of CENPF-positive cells with at least 10 BRCA1 foci was quantified by immunofluorescence microscopy. Representative images are shown in (a) with quantifications in (b).

Data shown in (b): 3 independent experiments with ≥ 100 nuclei analysed per condition in each experiment. Statistics: Student's T-test for Control vs. KD. BOD1L: $p = 0.15$. RIF1: $p = 0.13$. BOD1L/RIF1: $p = 0.09$.

6.2.5: Repair of CPT-induced DSBs by HR is unaffected in the absence of BOD1L or RIF1

Having demonstrated that BOD1L and RIF1 suppress resection of CPT-induced DSBs, I was interested to discover the impact of dysregulated resection in the absence of these proteins on the repair of CPT-induced lesions by resection-dependent DDR pathways. The principal resection-dependent mechanism for repair of late S- and G2-phase DSBs is HR; since CPT inflicts DNA damage during S-phase through inhibition of TopoI, the resultant lesions may be repaired by this pathway (Adachi et al., 2004, Adachi et al., 2003). It was plausible to speculate that HR utilisation could increase as a result of elevated resection in the absence of BOD1L or RIF1. To investigate this hypothesis, I studied the recruitment of the key HR factor RAD51 to CPT-induced DSBs.

HeLa cells depleted of BOD1L, RIF1, or both factors with siRNA were exposed to 1 μ M CPT for 1 h. These cells were harvested, pre-extracted, fixed and stained with antibodies against RAD51 and CENPF, and the percentage of cells with RAD51 foci was examined by immunofluorescence microscopy.

Nearly 80.0% of CENPF-positive nuclei contained RAD51 foci, and there was negligible fluctuation in this proportion in the absence of BOD1L or RIF1 (figure 6.11). It was therefore concluded that HR-mediated repair of CPT-induced DSBs was unaffected by depletion of these proteins.

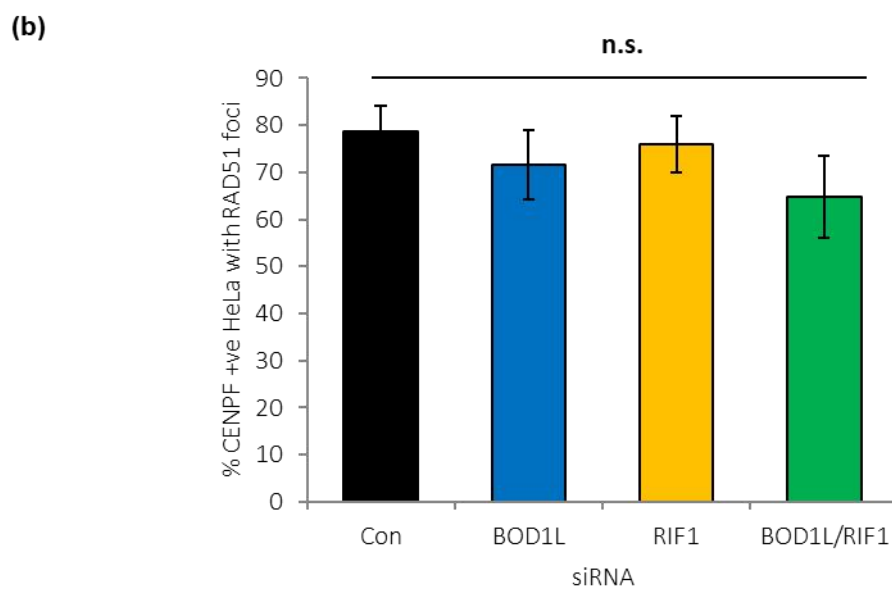
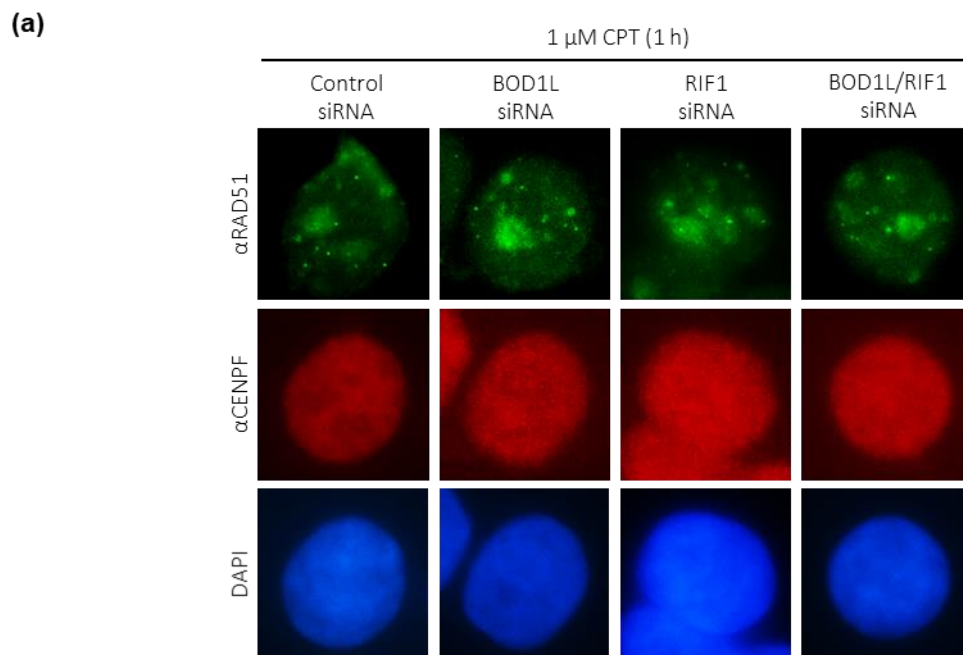


Figure 6.11: HR-mediated repair of CPT-induced DSBs is unaffected in the absence of BOD1L or RIF1.

HeLa cells transfected with the named siRNA were treated with 1 μ M CPT and harvested after 1 h. Coverslips were pre-extracted, fixed and stained with antibodies against RAD51 and CENPF before being mounted with DAPI. The proportion of CENPF-positive cells with RAD51 foci was examined by immunofluorescence microscopy. Representative images are shown in (a) with quantifications in (b).

Data shown in (b): 3 independent experiments with ≥ 100 nuclei per condition analysed in each experiment. Statistics: Student's T-test for Control vs. KD. BOD1L: $p = 0.49$. RIF1: $p = 0.77$. BOD1L/RIF1: $p = 0.25$.

6.3: Discussion

In the previous chapters of my thesis, I demonstrated that BOD1L suppresses unscheduled resection of IR-induced DSBs through its interaction with the 53BP1 effector RIF1. Together, these proteins antagonise the inappropriate recruitment of BRCA1 to DSBs during G1, thereby preventing short-range resection by CtIP and MRE11. Down-regulation of resection is advantageous during this phase as HR is not a viable repair pathway due to the absence of a suitable repair template. Accordingly, BOD1L was also shown to promote NHEJ.

The TopoI inhibitor CPT induces single-ended DSBs during S-phase. This type of lesion can be regarded as a structural intermediate between single-ended DSBs that arise during S-phase upon replication fork collapse and double-ended DSBs induced in G2 by IR. However, the importance of BOD1L, as well as its interaction with RIF1, had not previously been investigated in cells exposed to CPT.

I proposed initially that BOD1L and RIF1 may be required for the maintenance of genome stability and overall cell viability following exposure to CPT; this was tested by the enumeration of micronuclei with immunofluorescence microscopy, as well as clonogenic survival assays. In line with its known functions during replication stress and in cells exposed to IR, BOD1L was also found to play a role in ensuring cell survival after CPT. The knockdown of RIF1 had a comparable impact to that of BOD1L depletion, and the depletion of both factors did not have any additive impact, confirming that BOD1L and RIF1 function together to preserve cell viability

after CPT-induced DNA damage. However, the mild increase in CPT-induced micronucleation in the absence of BOD1L or RIF1 was insufficient to support a prominent role for either factor in the maintenance of genome stability.

It is plausible that crosstalk between BOD1L, RIF1 and additional factors may be crucial for the maintenance of genome stability and cell viability following exposure to CPT. One promising candidate protein is TDP1, which is known to play a vital role in the repair of CPT-induced lesions by the removal of trapped TopoI cleavage complexes; furthermore, it was demonstrated recently that TDP1, as for BOD1L and RIF1, is required for NHEJ (Li et al., 2017). There is also scope for interplay between BOD1L and the versatile nuclease/scaffold factor SLX4 – alternatively designated FANCP, a *bona fide* FA pathway protein. SLX4 regulates a multitude of DNA repair pathways, including the response to CPT via its interaction with the structure-specific endonuclease MUS81 (Kim et al., 2013, Ceccaldi et al., 2016b). Through its recently-demonstrated interaction with the FA pathway, it is plausible that BOD1L may co-operate with SLX4 in the resolution of CPT-induced DSBs (Higgs et al., 2015).

Cell survival and genome stability are reliant on intact DDR pathways. I therefore hypothesised that the repair of CPT-induced DSBs was compromised in the absence of BOD1L and RIF1. To investigate this hypothesis, I depleted cells of BOD1L and RIF1 with siRNA and analysed the recruitment of γ H2AX and 53BP1 recruitment to sites of CPT-induced damage by immunofluorescence microscopy and Western blotting – a well-established method for monitoring the repair of DSBs. I observed an increase in γ H2AX focus formation and protein

levels at early time points after CPT exposure, as well as a failure to resolve foci after 24 h. This implied that the repair of CPT-induced DSBs was problematic in the absence of these factors, and further demonstrated the co-operation between BOD1L and RIF1 in this context. Conversely, the depletion of either factor was inconsequential for the recruitment of 53BP1 to CPT-induced DSBs. This could be explained by the fact that BOD1L and RIF1 are both recruited downstream of 53BP1 (Chapter 4, Feng et al., 2013, Chapman *et al.*, 2013, Escribano-Diaz et al., 2013, di Virgilio et al., 2013); the absence of these factors would not therefore be expected to compromise the recruitment of 53BP1.

The mechanism by which BOD1L and RIF1 influenced the repair of CPT-induced DSBs was then considered. Due to the demonstrated roles of BOD1L in the inhibition of excessive resection during replication stress and following exposure to IR (Higgs et al., 2015, chapters 3-4), I speculated that it could perform a parallel role in CPT-treated cells. I set out to determine whether this was the case by examining the recruitment of the ssDNA-binding protein RPA2 and phosphorylated RPA32 to CPT-induced DSBs by immunofluorescence microscopy. In agreement with my predictions, there was an increase in CPT-induced focus formation of both proteins upon depletion of BOD1L or RIF1, confirming that these factors suppressed resection of lesions induced by this genotoxin. This was further supported by the increase in RPA32 (S4/S8) phosphorylation observed by Western blotting.

I extended my investigations using native fibre analysis and the quantification of IdU foci by immunofluorescence microscopy in order to determine the nature of aberrant resection in the

absence of BOD1L or RIF1. It was of interest to determine whether this defect manifested itself in the resection of a greater number of CPT-induced DSBs, or a greater extent of resection at individual lesions. Whilst neither factor appeared to influence the number of CPT-induced lesions resected per cell, there was a slight increase in the length of resected ssDNA tracts in the absence of RIF1. This observation suggested that RIF1 may function to suppress the extent of resection at DSBs in cells exposed to CPT, although it will be critical to verify this finding with additional experiments. Following exposure to IR, the results of the equivalent investigations suggested that BOD1L limited the number of lesions resected, but did not have an impact on resection tract length (chapter 3). Based on these contrasting results, I considered the possibility that BOD1L and RIF1 may function by distinct mechanisms to enable cells to cope with a variety of genotoxins.

My results suggested that BOD1L and RIF1 functioned within the same pathway to limit resection of CPT-induced DSBs. Since my earlier work demonstrated that BOD1L is required for the recruitment of RIF1 to IR-induced DSBs, I hypothesised that it may also be required for the localisation of RIF1 to DSBs induced by CPT. I assessed RIF1 focus formation in CPT-treated cells in the absence of BOD1L with immunofluorescence microscopy. As predicted, RIF1 recruitment to CPT-induced DSBs was impaired in BOD1L-depleted cells, confirming that RIF1 localisation was reliant upon BOD1L in the context of CPT treatment as well as IR exposure.

Without proper localisation of RIF1 to IR-induced DSBs, BRCA1 accumulated at these lesions in G1 cells, resulting in inappropriate CtIP-mediated resection (chapter 4). It therefore logically

followed that BRCA1 recruitment to CPT-induced DSBs may be altered in the absence of BOD1L. To this end, I next investigated BRCA1 focus formation by immunofluorescence microscopy in BOD1L- and RIF1-deficient cells following treatment with CPT. However, BRCA1 localisation to CPT-induced DSBs in the absence of either or both factors was unaffected. This result was in line with my observations of BRCA1 recruitment to IR-induced DSBs in G2 cells; in this case, the localisation of both BRCA1 and RIF1 was independent of BOD1L. A key consideration when assessing DNA damage foci by immunofluorescence microscopy is that this methodology cannot give any indication that a recruited protein is functioning appropriately. With this caveat in mind, I consequently proposed a mechanism by which BOD1L may modulate the function of BRCA1 at CPT-induced DSBs in order to influence resection without altering its recruitment.

A key unanswered question is the identity of the DDR components involved in inappropriate resection of CPT-induced DSBs in cells depleted of BOD1L or RIF1. During periods of replication stress, BOD1L limits the access of DNA2 to stalled replication forks to prevent uncontrolled resection, thereby preserving genome stability (Higgs et al., 2015). In contrast, CtIP was found to be prominently involved in aberrant resection of IR-induced DSBs in the absence of BOD1L or RIF1 (chapters 3-4). Both of these nucleases, along with BRCA1 and MRE11, are also known to be involved in the resolution of CPT-induced DSBs (Hartsuiker et al., 2009, Nakamura et al., 2010, Liu et al., 2016), and are therefore attractive candidate factors. As described in chapter 3, co-depletion of BOD1L and RIF1 along with a panel of candidates may serve to identify those specifically associated with aberrant CPT-induced resection in the absence of BOD1L or RIF1.

As well as CtIP, MRE11 and DNA2, it would also be worthwhile to include other factors known to be involved in the repair of CPT-induced DNA damage, such as ERCC1-XPF (Takahata et al., 2015) and SMARCAD1 (Costelloe et al., 2012).

Having demonstrated a role for BOD1L in suppressing resection of CPT-induced DSBs, which appeared to be linked to its interaction with RIF1, I speculated that downstream repair pathways in CPT-treated cells may be compromised in the absence of these proteins. Since CPT inflicts DNA damage during S-phase, a proportion of these lesions may therefore be suitable for repair by HR. It was possible that the elevated resection of CPT-induced DSBs observed in the absence of BOD1L or RIF1 may result in greater utilisation of HR to repair these lesions. To determine whether this was the case, I analysed the recruitment of RAD51 to CPT-induced DSBs by immunofluorescence microscopy in cells depleted of BOD1L or RIF1, with the expectation that RAD51 focus formation would increase if more HR-mediated repair were taking place. However, no alteration in RAD51 recruitment was detected in the absence of either protein. A similar result was observed for IR-induced DSBs in G2 cells (chapter 5), suggesting that an increase in resection alone may be insufficient to drive greater use of this complex and time-consuming repair pathway. It was also of note that this observation was at odds with BOD1L's role in stabilising RAD51 at stalled replication forks (Higgs et al., 2015), suggesting that this particular function of BOD1L may be restricted to cells experiencing replication stress. To confirm this, future experiments could involve co-depleting BOD1L with BLM or FBH1, which are known to destabilise RAD51 in the absence of BOD1L during replication stress (Higgs et al., 2015), before exposing cells to CPT and examining RAD51 focus formation

by immunofluorescence microscopy. Time course analyses of RAD51 foci in these cells may also provide valuable insights into the kinetics of RAD51 recruitment to CPT-induced DSBs.

To conclude, the data presented in this chapter demonstrated that BOD1L played a role in the repair of CPT-induced DSBs and contributes to the maintenance of genome stability in this context. However, the absence of BOD1L had a considerably milder impact in cells treated with CPT than those exposed to IR or inducers of replication stress, suggesting that the repair of CPT-induced DNA damage was more dependent on alternative factors. As has been shown for stalled replication forks and IR-induced DSBs, BOD1L fulfilled its function by suppressing resection of CPT-induced lesions. Co-operation with RIF1 appeared to be required; there was no additive impact of depleting both proteins. The factors involved in aberrant resection in the absence of either factor remains to be determined. Finally, the repair of DNA damage by HR following exposure to CPT was unaffected in the absence of BOD1L or RIF1, and the function of BOD1L as a stabiliser of RAD51 appeared to be confined to states of replication stress.

Chapter 7: Discussion

7.1: Summary and Model

Robust mechanisms for the repair of damaged DNA are fundamental to the maintenance of genome stability. Earlier published work by Higgs and colleagues identified BOD1L as a key safeguard of genome stability. BOD1L was shown to be involved in the prevention of replication stress-induced DNA damage by suppressing uncontrolled nucleolytic resection of stalled replication forks (Higgs et al., 2015). However, the potential role of BOD1L in the cellular response to other forms of DNA damage had not been investigated. This provided the rationale for my thesis.

My data have illustrated that the importance of BOD1L as a genome stability factor was not confined to cells experiencing replication stress; it also functioned in the modulation of nucleolytic resection at IR- and CPT-induced DSBs. A key aspect of BOD1L-mediated suppression of resection is its interaction with RIF1, a critical downstream effector of the repair pathway regulator 53BP1. My results demonstrated that BOD1L was required to recruit RIF1 to IR-induced DSBs, thereby antagonising the localisation of BRCA1 to G1 DSBs and consequently suppressing the number of sites targeted by CtIP-mediated resection. Although BOD1L also appeared to suppress CtIP activity during G2, there was no apparent impact on the localisation of RIF1 or BRCA1 to IR- or CPT-induced DSBs in the absence of BOD1L during this phase. It is possible that the functionality of these proteins is impaired in the absence of BOD1L during G2, despite their successful recruitment. Alternatively, there may simply be a masking of the focal defect in G2. The proposed mechanism is summarised in figure 7.1.

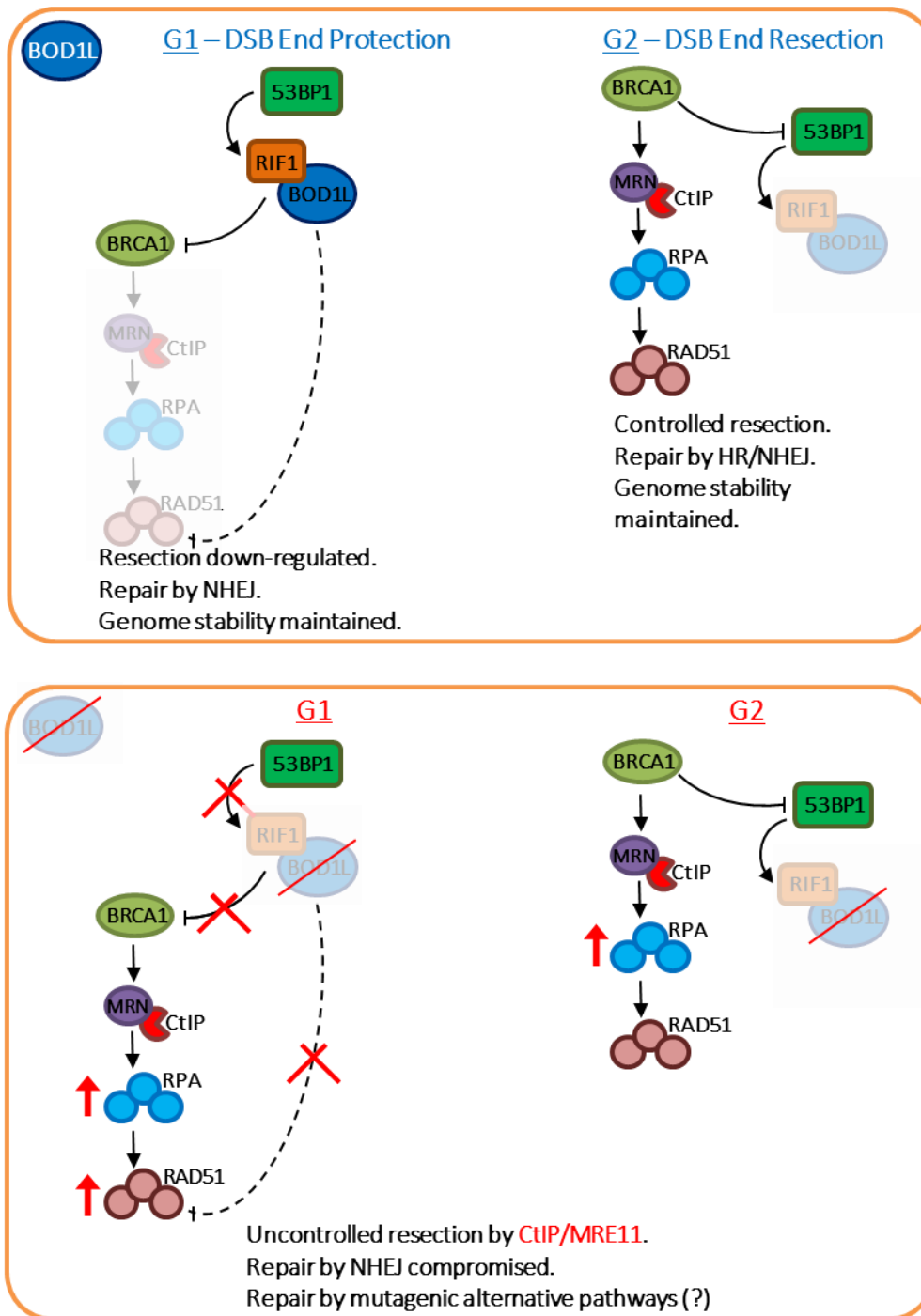


Figure 7.1: BOD1L-mediated regulation of DSB repair.

BOD1L functions differently in G1 and G2 to regulate resection and pathway choice during the repair of IR-induced DSBs. During G1, BOD1L is recruited to DSBs downstream of 53BP1. It interacts with the effector RIF1, facilitating its localisation at the site of damage. Collectively, BOD1L and RIF1 antagonise BRCA1 recruitment to DSBs, thereby suppressing CtIP/MRE11-dependent resection. The complex may also prevent inappropriate recruitment of RAD51. Repair of DSBs by NHEJ follows. In G2 cells, 53BP1 and its effectors are driven from DSBs by BRCA1, allowing for controlled CtIP/MRE11-mediated resection. HR and NHEJ are both viable repair pathways during this phase. In the absence of BOD1L, G1 cells fail to prevent the localisation of BRCA1 to DSBs, resulting in uncontrolled resection and greater accumulation of RPA and RAD51. Dysregulated resection is also observed in G2 cells, as evidenced by an increase in RPA accumulation. In both phases, NHEJ-mediated repair is compromised, potentially resulting in greater utilisation of mutagenic non-canonical repair pathways.

7.2: BOD1L and the 53BP1/RIF1-mediated DSB end protection pathway

Through a combination of affinity purification mass spectrometry and immunoprecipitations, I demonstrated a previously unknown interaction between BOD1L and RIF1, key effector of 53BP1. Subsequent immunofluorescence analyses of IR-induced focus formation revealed that BOD1L was recruited to DSBs downstream of 53BP1 but was required for the recruitment of RIF1 to DSBs.

These observations support the notion that BOD1L is a novel member of the 53BP1-dependent DNA end protection complex, alongside RIF1, REV7, PTIP and the Shieldin heterotrimer, which functions in G1 and G2 phases to restrict nucleolytic resection. BOD1L was also shown to promote 53BP1-dependent cellular functions, including NHEJ – both in the context of CSR to resolve programmed DSBs, and to repair DNA damage inflicted by exogenous agents.

7.2.1: The interaction between BOD1L and RIF1

Further characterisation of the interaction between BOD1L and RIF1 revealed that the N- and C-terminal regions of BOD1L were necessary and sufficient to mediate an association with endogenous RIF1. Conversely, the intervening region of BOD1L was dispensable for the interaction. This observation suggests that BOD1L may adopt a looped conformation, bringing its N- and C-termini into proximity to promote its interaction with RIF1 with no involvement of the central region (figure 7.2). Such a conformational change would be in line with BOD1L's

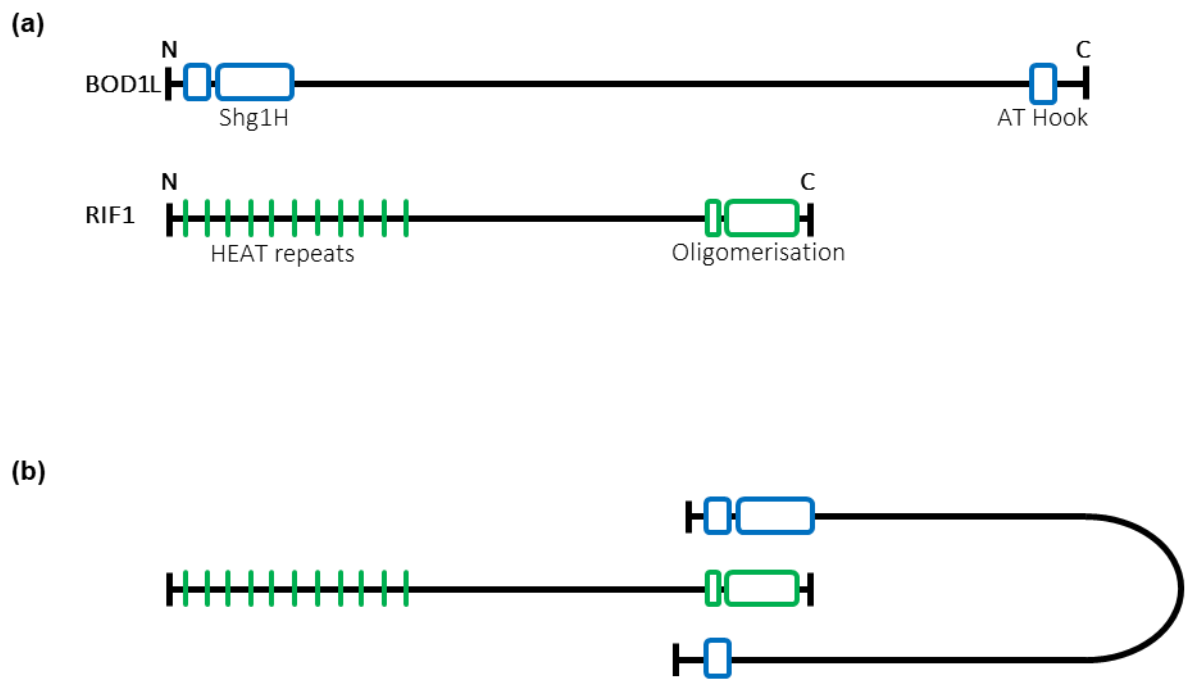


Figure 7.2: The interaction between BOD1L and RIF1.

Simplified structures and key domains of BOD1L and RIF1 are shown in (a). BOD1L may adopt a looped conformation to allow its N- and C-termini to interact with RIF1 (b).

likely role as a DDR scaffold protein; this is consistent with the fact that no catalytic activity of this protein has been identified to date, and that there are no sequence moieties that would suggest a catalytic function. Moreover, the C-terminal oligomerisation domains of RIF1 are known to mediate its interaction with other proteins, including BLM and PP1, whilst the N-terminal HEAT repeats are required for its localisation to DSBs (Escribano-Diaz et al., 2013). These observations are consistent with a model whereby RIF1 interacts with BOD1L via its oligomerisation domain.

The drivers for the assembly of the BOD1L-RIF1 complex remain unexplored. It is not known whether the assembly of the complex is constitutive, regulated by the cell cycle or enhanced upon detection of DNA damage. Based on the presence of multiple confirmed and putative S/TQ motifs in the sequence of BOD1L, I would hypothesise that ATM/ATR-mediated phosphorylation may enhance its interaction with RIF1. Furthermore, this post-translational modification is known to be important for 53BP1-dependent end protection. Phosphorylation of 53BP1 by ATM at 28 N-terminal motifs is essential for its interaction with RIF1 (Symington and Gautier, 2011, Bunting et al., 2010, Bothmer et al., 2011). It therefore logically follows that the interaction between BOD1L and RIF1 may be enhanced in the presence of DSBs in response to phosphorylation of BOD1L by ATM or ATR.

The results presented in chapter 5 of my thesis demonstrated that BOD1L is dispensable for successful HR, but is required for successful end joining. This observation is in keeping with its

interaction with RIF1, which is known to promote NHEJ at the expense of HR, and further highlights the importance of BOD1L in DSB repair pathway choice.

7.2.2: Suppression of nucleolytic resection

The initial characterisation of BOD1L highlighted the anti-resection role of this factor in cells experiencing replication stress (Higgs et al., 2015). Since it is well established that there is redundancy across different DDR pathways in terms of the proteins involved, it was unsurprising to discover that BOD1L's role in suppressing nucleolytic resection was not confined to stalled replication forks. Indeed, multiple proteins have been shown to function during replication stress as well as in the resolution of DSBs. For example, BLM co-operates with the FA pathway to suppress the formation of micronuclei during replication stress alongside its key role in nucleolytic resection to prime DSBs for HR (Naim and Rosselli, 2009). Furthermore, RAD51 contributes to the repair of ICLs, a key cause of replication stress, independently of its function in HR-dependent DSB repair (Wang et al., 2015a).

In chapters 3 and 4 of my thesis, I demonstrated that BOD1L also negatively regulates resection of double-ended DSBs induced by IR in G1 and G2 phases of the cell cycle via its interaction with RIF1. Furthermore, as discussed in chapter 6, these factors also regulate resection of single-ended DSBs induced in S-phase by CPT.

The interplay between BRCA1-dependent promotion of DSB resection and end protection by the 53BP1 pathway has been researched extensively. Whilst 53BP1, RIF1 and additional downstream effectors impede resection, this block can be overcome by BRCA1 and CtIP when resection and repair by HR are deemed favourable. The prominent role of CtIP and MRE11 in DSB resection when BOD1L is depleted is in line with its demonstrated interaction with RIF1 and subsequent suppression of BRCA1-mediated nucleolytic activity. In G1 cells, RIF1 recruitment to DSBs was reduced in the absence of BOD1L, thereby impairing RIF1's ability to prevent the inappropriate localisation of BRCA1 to these sites. This underpinned the increase in CtIP- and MRE11-dependent resection observed. Since extensively processed DSBs cannot be repaired by NHEJ, this is likely to result in increased utilisation of error-prone resection-dependent pathways, such as SSA. Ultimately, this scenario may lead to reduced genome stability due to an overall reduction in DSB repair proficiency.

In G2 cells, however, a more complex mechanism appeared to be in play. During this phase, the recruitment of RIF1 to DSBs was unperturbed in the absence of BOD1L; accordingly, the localisation of BRCA1 was unchanged. Nevertheless, increased resection by CtIP and MRE11 was still observed in BOD1L-deficient cells. This pointed towards an undetectable defect in BRCA1 recruitment, or perhaps a regulatory problem further downstream. It is perhaps unsurprising that DSB end protection factors function via distinct mechanisms in different cell cycle phases due to the key differences in context. During G1, extensive resection has the potential to be highly deleterious to cells due to the absence of any template for HR-mediated repair. As outlined above, this may lead to an increase in the use of mutagenic repair pathways.

On the other hand, resection is not unfavourable during G2; indeed, for DSBs which require processing to remove adducts in advance of repair (such as those induced by IR), HR may be an advantageous pathway choice.

My research, in combination with recently-published literature, also sheds further light on the role of BOD1L as a replication fork protection factor. Garzón and colleagues highlighted a novel role for RIF1 in the protection of stalled replication forks from nucleolytic degradation. The mechanism proposed bore similarities to that of BOD1L-dependent fork protection. Most notably, BOD1L and RIF1 both prevented DNA2-mediated degradation of stalled replication forks (Higgs et al., 2015, Garzón et al., 2019). It is therefore logical to speculate that BOD1L and RIF1 may co-operate to preserve the integrity of stalled forks, but further investigations would be valuable to confirm this. In the absence of RIF1, WRN was shown to be the accessory helicase required for DNA2-mediated fork resection. The potential importance of WRN in the context of BOD1L-dependent fork protection has yet to be examined.

7.3: SETD1A: A novel fork protection factor that interactions with BOD1L

As discussed in previous sections, preventing uncontrolled nucleolytic processing of nascent DNA at stalled replication forks is fundamental for the maintenance genome stability. It is widely established that multiple members of the FA and HR pathways contribute to replication fork protection, and there is emerging evidence demonstrating that dynamic chromatin rearrangements and post-translational modifications are also vital to these processes. For

example, lysine methyltransferases (KMTs) have been shown to play roles in modulating fork resection through histone methylation. The yeast KMT Set1, a component of the conserved COMPASS protein complex, regulates the replication stress response through methylation of H3K4; loss of this protein impedes transition through S-phase during replication stress (Faucher and Wellinger, 2010). Furthermore, the activities of EZH2 and MLL2/3 both promote fork degradation (Rondinelli et al., 2017, Ray Chaudhuri et al., 2016).

Interestingly, SETD1A, a KMT recently identified as novel fork protection factor, interacts with BOD1L and appears to act within the same fork protection pathway (Higgs et al., 2018). This interaction was found to be dependent on the N-terminal Shg1 homology (Shg1H) domain of BOD1L – a region bearing sequence similarity to a component of the yeast COMPASS complex, Shg1 (Higgs et al., 2018, PFAM: 05205, <http://pfam.xfam.org/family/PF05205>, Marchler-Bauer et al., 2011, Roguev et al., 2001). SETD1A depletion was found to be epistatic with loss of BOD1L in cells exposed to MMC, an inducer of replication stress.

In parallel with published literature on BOD1L-mediated fork protection, it was demonstrated that SETD1A shields nascent DNA from excessive DNA2-mediated processing by suppressing the anti-recombinase activity of BLM and FBH1, thereby stabilising RAD51 at stalled forks.

Former studies have not suggested that BOD1L has any catalytic activity; however, SETD1A requires its methyltransferase activity for fork protection. Higgs and colleagues demonstrated

that SETD1A methylates histone H3K4 at stalled replication forks to mark them for protection. This modification limits access of the methyl 'reader' chromodomain helicase DNA-binding protein 4 (CHD4). Furthermore, methylation of stalled forks was found to be essential to facilitate histone chaperoning by FANCD2 in the vicinity of the stalled fork, ultimately leading to its protection from DNA2-mediated degradation (Higgs et al., 2018). These observations are consistent with the fact that BOD1L has also been shown to co-operate with the FA pathway during replication stress. However, it should be noted that recruitment of FANCD2 or its mono-ubiquitination – a fundamental step within the FA pathway – was unaffected in the absence of BOD1L. This suggests that BOD1L acts downstream of SETD1A-mediated histone methylation and the recruitment of the FA core complex and FANCD2/I (Higgs et al., 2015).

7.3.1: Interplay between fork protection mechanisms

In the preceding two sections, I have compared the mechanism of BOD1L-dependent fork protection with those of SETD1A- and RIF1-dependent protection. Below, I will discuss the similarities and contrasts between the fork protection pathways which rely on SETD1A and RIF1 and highlight the scope for interplay between all three pathways.

A point of contrast between SETD1A- and RIF1-dependent fork protection is the difference in regulatory post-translational modifications required in each case. Whilst RIF1-mediated fork protection relies on its interaction with protein phosphatase 1 (PP1) and the regulation of WRN phosphorylation, the SETD1A-dependent pathway is underpinned by histone methylation – a

pre-requisite for the histone chaperone activity of FANCD2 and subsequent fork protection (Garzón et al., 2019, Higgs et al., 2015, Higgs et al., 2018).

Nevertheless, the similarities between these mechanisms, as well as recent data from our lab and others, highlight the potential for a common pathway which may involve SETD1A, BOD1L and RIF1, or a series of closely linked pathways. Most notably, in each case, fork protection ultimately depends on the suppression of DNA2-mediated fork degradation (Higgs et al., 2018, Higgs et al., 2015, Garzón et al., 2019).

Furthermore, recent studies have highlighted that the conserved HEAT-like repeats in the N-terminus of RIF1 may serve as a 'reader' of histone methylation (Masai et al., 2018, Kobayashi et al., 2019). In agreement with this hypothesis, it has been demonstrated that RIF1 is able to bind *in vitro* to methylated H3K4; in fact, this methylation is a pre-requisite for the recruitment of RIF1 to DSBs (Dr. Rachel Bayley, unpublished). Taken together, these observations implicate RIF1 as an additional methylation 'reader', along with CHD4 (Higgs et al., 2018), which participates in SETD1A-dependent fork protection. Importantly, RIF1 and CHD4 have opposing roles. CHD4 is negatively regulated by histone methylation, and its recruitment to stalled forks promotes their degradation in the absence of BRCA2-dependent fork protection (Higgs et al., 2018). On the other hand, RIF1 is positively regulated by histone methylation and protects forks from excessive nucleolytic processing. Overall, it is therefore conceivable that BOD1L and SETD1A are both required to recruit RIF1 to stalled replication forks via direct interaction and histone methylation activity, respectively (chapter 4, Higgs et al., 2018). These forks are then

protected through a combination of the exclusion of CHD4 and the recruitment of RIF1. It would be valuable to elucidate the interplay between these pathways fully.

7.3.2: Replication fork protection and the acquisition of PARPi resistance

It has consistently been demonstrated that BRCA1-deficient cancer cells can acquire resistance to PARPi-based therapies with the concomitant loss of 53BP1 or its downstream effectors (D'Andrea, 2018). In light of BOD1L's interaction with RIF1 and with SETD1A, this may prompt the speculation that SETD1A depletion in cells deficient of BRCA1 may also result in resistance to PARPi. Indeed, there is emerging evidence to suggest that the depletion of SETD1A on a BRCA1-deficient background leads to PARPi resistance (Dr. Rachel Bayley and Rhiannon Moss, unpublished). The up-regulation of alternative fork protection pathways, such as those dependent on ATR and CHK1 (D'Andrea, 2018), has been established as a viable mechanism for the acquisition of PARPi resistance. Nevertheless, if future investigations demonstrate that the depletion of BOD1L also results in resistance to PARP inhibitors, I would speculate that this is underpinned by the impairment of 53BP1-dependent DSB end protection and the consequent restoration of HR, rather than the loss of BOD1L-mediated fork protection.

7.4: BOD1L and human disease

A robust DDR is fundamental to the maintenance of human health. As outlined in my introduction, several human diseases have been attributed to mutations in DDR pathway proteins; conversely, the inhibition of DDR proteins and pathways has attractive therapeutic

potential. My thesis, along with previously published material, suggests that BOD1L may also be a relevant factor in human disease.

7.4.1: Cancer therapeutics

PARP inhibitors (PARPi) remain a mainstay for the treatment of BRCA1- and BRCA2-deficient malignancies, such as familial breast and ovarian cancers. However, the acquisition of resistance to this therapy represents an ongoing clinical problem and has been the subject of extensive study. As stated above, one mechanism underpinning the development of PARPi resistance in BRCA1-deficient cancers is the impairment of 53BP1-dependent DNA end protection (D'Andrea, 2018). The loss of 53BP1 (Bouwman et al., 2010), RIF1 (Chapman et al., 2013, Escribano-Diaz et al., 2013), REV7 (Xu et al., 2015a) or any single component of the recently-identified trimeric Shieldin complex (Dev et al., 2018, Gupta et al., 2018b, Findlay et al., 2018, Noordermeer et al., 2018) can lead to the re-establishment of CtIP-mediated DNA end resection and consequent restoration of HR.

In chapters 4 and 5 of my thesis, I demonstrated that BOD1L and RIF1 interact, and that BOD1L is required for the recruitment of RIF1 to DSBs induced by IR and CPT. Accordingly, in the absence of BOD1L, DSB end protection is compromised, leading to an increase in CtIP/MRE11-mediated resection. Since BOD1L functions upstream of RIF1, I would hypothesise that the concomitant loss of BOD1L expression or function in BRCA1-deficient tumours may also confer resistance to PARPi. This has clear implications for clinical management of these cancers and is worthy of investigation.

7.4.2: Likely phenotypes for individuals harbouring BOD1L mutations

At the time of writing, no patients carrying mutations in BOD1L had been identified. However, in view of BOD1L's known associations with SETD1A, as well as the FA and 53BP1 pathways, it is possible to speculate regarding the likely clinical manifestations of BOD1L mutations.

Immunodeficiency. Several key studies have demonstrated the importance of RIF1 in 53BP1-dependent cellular processes. This includes the NHEJ-mediated resolution of programmed DSBs that occur during class switch recombination (CSR) (Chapman et al., 2013, di Virgilio et al., 2013, Escribano-Diaz et al., 2013). This process is a fundamental aspect of generating a robust immune system capable of responding to a diverse range of antigens. Through the induction and repair of DSBs in the 'switch' region of the immunoglobulin heavy chain, new B cell isotypes with altered effector properties are generated (Soulas-Sprauel et al., 2007, Khan and Ali, 2017). In the absence of RIF1, CSR is severely compromised; di Virgilio and colleagues proposed that in addition to defective NHEJ, aberrant DSB end resection contributes to this failure of CSR (di Virgilio et al., 2013).

Given the interaction between BOD1L and RIF1 that I demonstrated in the course of my research, along with BOD1L's role as a modulator of DSB resection, it logically followed that BOD1L deficiency might also impede CSR. Indeed, my data (in collaboration with Prof. Simon

Boulton) suggests this is the case, lending credibility to the notion that patients with mutations in BOD1L would likely be affected by immunodeficiency.

Fanconi Anaemia. Previous work by Higgs and colleagues revealed that BOD1L depletion phenocopies the loss of the FA core component FANCA, resulting in its designation as a FA-like protein (Higgs et al., 2015). Moreover, the 53BP1 effector REV7, which is recruited downstream of RIF1, was recently identified as a *bona fide* FA protein (Bluteau et al., 2016). As discussed in chapter 4, my investigations of REV7 localisation to IR-induced DSBs in the absence of BOD1L were inconclusive due to high antibody background signal. Nevertheless, it is not inconceivable that mutations in BOD1L may result in clinical features typically associated with FA due to its interactions with the FA and 53BP1 pathways, particularly given the fact that BOD1L is likely to function upstream of REV7 due to its functional association with RIF1. Such features may include congenital abnormalities of the thumb, café-au-lait spots, bone marrow failure, a predisposition to haematological cancers and genome instability at the cellular level (Ceccaldi et al., 2016b).

Haematological malignancies. A suite of mutations in BOD1L – predominantly in the Shg1H domain – is associated with chronic lymphocytic leukaemia (CLL) and myelodysplasia, a precursor to leukaemia development (Dr. Martin Higgs and Prof. Tatjana Stankovic, unpublished). Based on this observation, I would hypothesise that individuals harbouring such mutations may be predisposed to haematological malignancies. Given that the Shg1H domain of BOD1L has been shown to mediate its interaction with SETD1A (Higgs et al., 2018), it is likely

that these mutations may perturb the interaction between these proteins. Since this interaction has been shown to be critical for the maintenance of genome stability in cells experiencing replication stress (Higgs et al., 2018), its impairment may underpin the development of cancer in individuals with BOD1L mutations.

Neuropsychiatric disorders. Within the last five years, multiple exome sequencing studies have implicated rare loss-of-function mutations in *SETD1A* in the development of schizophrenia. These studies have further suggested that there may be a general role for chromatin modifiers in suppressing schizophrenia development (Takata et al., 2014, Singh et al., 2016). Two recent studies have highlighted the fact that loss of SETD1A results in key transcriptional changes in genes and pathways known to be relevant to neurodevelopment (Cameron et al., 2019, Mukai et al., 2019). However, the mechanistic basis of disease development in individuals with *SETD1A* mutations remains to be elucidated fully. There is the potential for BOD1L to play a role in the pathology of neuropsychiatric disease through its interaction with SETD1A.

7.5: Extending the current study

A number of key questions which arose during the course of my studies could not be addressed in full due to time constraints and lack of reagent availability. It would be valuable to extend the current study with a focus on the following areas.

7.5.1: Further insights into the role of BOD1L in 53BP1-dependent end protection

Having identified candidate regions in the N- and C-termini of BOD1L which appear to mediate its interaction with RIF1, it would be valuable to locate specific residues which are required for this interaction.

I would begin by extending the *in vitro* studies performed to date by generating shorter GST-tagged fragments which span the regions of BOD1L originally encompassed by fragments 1, 2 and 6 (refer to figure 4.3). GST pull-down assays would be used to identify the minimal fragments required for interaction; point mutations could be introduced into these fragments in an attempt to abrogate the interaction. Fragment 1 of BOD1L includes the Shg1H domain, which shares regions of sequence homology with the yeast methyltransferase Shg1 and is thought to mediate BOD1L's interaction with SETD1A (Higgs et al., 2018). Moreover, fragment 6 harbours an AT hook domain, which is known to facilitate DNA binding (Reeves and Nissen, 1990). The selection of residues to mutate can therefore be informed, at least in part, by a bioinformatics-based approach.

Once the key residues have been identified, these could be validated in an *in vivo* context using CRISPR-Cas9 to introduce the relevant substitutions into endogenous BOD1L. The resultant cell lines would provide a valuable means to investigate the impact of an impaired BOD1L-RIF1 interaction on DSB end resection and genome stability. Since I have shown that BOD1L is required for the recruitment of RIF1 to sites of DNA damage and for RIF1-dependent cellular

functions, such as CSR, it is likely that cells harbouring mutations in BOD1L which impair its interaction with RIF1 would phenocopy BOD1L- or RIF1-depleted cells.

Investigating the potential importance of ATM- and ATR-dependent phosphorylation for BOD1L's interaction with RIF1 and the impact of these modifications on the DDR would be valuable. To establish whether the BOD1L-RIF1 interaction is constitutive or enhanced by DNA damage, pull-down experiments could be repeated in irradiated and non-irradiated cells to detect any difference in the strength of the interaction. If more endogenous protein were pulled down in cells subjected to DNA-damaging agents, this would be suggestive of a role for DDR signalling in establishing the interaction. As a further control, such observations could be verified by treating cells with chemical inhibitors of ATM or ATR; this would be expected to lessen the BOD1L-RIF1 interaction if phosphorylation by these kinases were playing a stimulating role. These investigations could be supported by the use of BOD1L phospho-specific antibodies (Davies, 2015). *In vitro* approaches could subsequently be used to identify specific S/TQ motifs within BOD1L which are required for its interaction with RIF1. It would be worthwhile to focus future research on motifs located within the N- and C-terminal regions of BOD1L, which are known to mediate the interaction.

It would also be of interest to investigate the importance of BOD1L to the chromatin localisation of the 53BP1 effectors which are recruited downstream of RIF1 – particularly REV7 and the Shieldin complex. My investigations into the localisation of REV7 to IR-induced DSBs in the absence of BOD1L were hampered by non-specific antibody signal; however, during the course

of my research, no alternative antibodies against REV7 became available. Ideally, the experiments described in chapter 4 (figure 4.6) would be repeated with an alternative antibody or cell line expressing tagged versions of these proteins. Given that BOD1L is required to recruit RIF1 to damaged chromatin, and that the recruitment of REV7 is dependent on correctly-localised 53BP1 and RIF1 ((Xu et al., 2015a, Boersma et al., 2015), I would expect REV7 recruitment to be compromised in the absence of BOD1L.

Finally, the impact of BOD1L depletion on the recruitment of the most distal 53BP1 effector, the Shieldin complex (Dev et al., 2018, Gupta et al., 2018, Noordermeer et al., 2018, Findlay et al., 2018), remains unexplored. Due to the lack of commercial antibodies against these recently-characterised proteins at the time of writing, these investigations would have necessitated the generation of stable cell lines expressing tagged Shieldin components. This would have been impractical within the given time frame of my research. As for REV7, I would hypothesise that the Shieldin complex components would be mis-localised in the absence of BOD1L, which would be in line with my demonstration of increased DSB resection in BOD1L-depleted cells.

7.5.2: Impact of BOD1L depletion on DSB repair pathways

Immunofluorescence microscopy provides a robust and relatively straightforward means of gaining insights into DNA repair dynamics. Indeed, the analysis of DDR protein foci at sites of damage has been a mainstay of DNA damage repair research for multiple decades. An important consideration, however, is that the formation of foci demonstrates recruitment of

the factors concerned, but not necessarily correct functionality. Furthermore, captured images can, at best, represent only a snapshot of DNA repair activity. Given that the constituents of the DNA repair machinery can change within a timeline of seconds or minutes, particularly during the initiating stages of repair, it is entirely plausible that vital information may be missed when images are acquired over a time scale of hours. Techniques such as live cell imaging (refer to Karanam et al., 2012 for examples) or high-resolution microscopy to analyse DNA repair at the single-molecule level (such as the studies described by Graham et al., 2018 and Graham et al., 2016) may prove valuable to examine DSB repair in the absence of BOD1L in greater detail.

I experienced considerable technical difficulty whilst attempting to optimise the fluorescent reporter cell line assays described in chapter 5 (Gunn and Stark, 2012); the assays for non-canonical repair pathways proved particularly problematic. Alternative repair assays may provide a more comprehensive impression of the impact of BOD1L on DSB repair, potentially offering crucial insights into repair dynamics in the absence of this factor. For example, the GC92 cell line generated from human fibroblasts allows for the distinction of canonical NHEJ- versus alt-EJ-dependent repair outcomes, which result in the expression of CD4 or CD8, respectively (Rass et al., 2009). Alternatively, the SeeSaw reporter cell line provides a system for assessing the relative proportions of NHEJ and SSA; each outcome results in the expression of a different fluorescent protein (Gomez-Cabello et al., 2013). I would hypothesise that in absence of BOD1L, impairment of NHEJ-mediated repair would be accompanied by a greater utilisation of non-canonical pathways. It may be that SSA is favoured due to the increased resection of DSBs that occurs in cells lacking BOD1L.

The results of the telomere fusion assay described in chapter 5 were in agreement with published literature and my predictions based on the functional interaction between BOD1L and RIF1. The end-to-end fusion of de-protected telomeres was markedly reduced upon depletion of BOD1L or RIF1, demonstrating that both proteins were drivers of NHEJ. Whilst this assay is an elegant tool for examining the functionality of the cellular end-joining machinery, I was unable to optimise the detection of telomeres using fluorescence *in situ* hybridisation (FISH) probes. Further investigations of NHEJ proficiency in the absence of BOD1L would therefore be worthwhile to support the existing results. This could involve an I-SceI-based assay in a suitable reporter cell line (Gunn and Stark, 2012) or a similar assay, or the optimisation of the FISH approach.

7.5.3: Crosstalk between BOD1L and pro-/anti-recombinogenic pathways

The interplay between BOD1L and the pro- and anti-recombinogenic factors involved in DSB repair clearly warrants further investigation. In particular, the importance of RAD51 and BLM in the context of aberrant IR-induced DSB resection have yet to be fully elucidated in a BOD1L-deficient setting.

The results presented in chapter 3 of my thesis suggested differences in the significance of BLM at IR-induced DSBs and stalled replication forks in the absence of BOD1L. Whereas BLM activity has been shown to displace RAD51 from stalled replication forks in the absence of BOD1L,

leaving them exposed to uncontrolled resection (Higgs et al., 2015), BLM alone is insufficient to promote elevated resection of DSBs in BOD1L-depleted cells. This may be in keeping with the seemingly contradictory pro- and anti-resection roles of BLM demonstrated in earlier studies (Bugreev et al., 2007). However, it is unclear which of these roles predominates in BOD1L-depleted cells exposed to IR. In order to provide further insights into this unanswered question, it would be interesting to analyse IR-induced RAD51 focal formation in cells depleted of BOD1L and BLM, and to compare this between G1 and G2 cells.

It was intriguing to note that in BOD1L-deficient cells, elevated resection of DSBs was observed in G1 and G2, but a corresponding increase in RAD51 recruitment to resected DSBs only occurred in G1 cells. I cannot rule out the possibility that these observations are indicative of two distinct, cell cycle-dependent functions of BOD1L. It may be that this factor specifically acts to suppress the localisation of RAD51 to DSBs during G1, which would not be beneficial to cells because HR is inviable in this phase. In contrast, the anti-resection activity of BOD1L is functional in G1 and G2 phases. If this were the case, co-depletion of BOD1L with CtIP or MRE11 would not be expected to reduce RAD51 focal accumulation to control levels due to the absence of RAD51 suppression by BOD1L. However, if the accumulation of RAD51 at DSBs in the absence of BOD1L were merely a consequence of aberrant resection in G1, this would be rescued by the depletion of these key nucleases.

7.5.4: Potential interactions with RIF1- and CtIP-dependent fork protection pathways

BOD1L is known to operate within the same pathway as the KMT SETD1A to protect stalled replication forks from excessive nucleolytic degradation (Higgs *et al.*, 2018). The fork protection functions of RIF1 and CtIP have also recently been described (Garzón *et al.*, 2019, Przetocka *et al.*, 2017). However, whether BOD1L co-operates with these proteins to protect stalled forks from degradation remains unknown. A straightforward way to determine this would be to co-deplete BOD1L with RIF1 or CtIP and monitor the extent of fork resection using DNA fibre analysis. If these co-depletions resulted in an additive impact on fork resection, this would imply that distinct protective pathways are in play, with BOD1L and SETD1A functioning in one pathway and RIF1 in another, potentially along with CtIP (Higgs *et al.*, 2015, Higgs *et al.*, 2018, Garzón *et al.*, 2019, Przetocka *et al.*, 2017).

7.5.5: BOD1L and the repair of CPT-induced DSBs

Although the results presented in chapter 6 point towards a role for BOD1L and RIF1 in the resolution of DSBs following exposure to CPT, the identity of the other factors involved remains a key unanswered question.

Since it was apparent that BOD1L suppressed resection of CPT-induced DSBs, in line with its function during replication stress and following exposure to IR, it would be worthwhile to discover the nucleases which are regulated by BOD1L in this context. CtIP, MRE11 and DNA2 have been implicated in the processing of CPT-induced DSBs; furthermore, all have been shown to be regulated by BOD1L in other DNA repair pathways. Co-depletion of BOD1L with these

nucleases could be undertaken in order to identify those involved in aberrant resection of DSBs induced by CPT; as described in chapter 3, depletion of the relevant nucleases would be expected to suppress the elevated resection observed in the absence of BOD1L.

The depletion of BOD1L or RIF1 engendered only a mild increase in cellular sensitivity to CPT, comparable to that of 53BP1 depletion (Yoo et al., 2005). It is therefore reasonable to assume that these factors function as accessory proteins in repair pathways which combat CPT-induced damage, rather than playing prominent roles. siRNA-mediated depletion of BOD1L or RIF1 along with factors such as ERCC1, XPF and SMARCAD1 – key exponents of the repair of CPT-induced lesions (Takahata et al., 2015, Costelloe et al., 2012) – could be performed, and cell viability, genome stability and the resolution of DSBs over time could be examined by immunofluorescence microscopy. Owing to its common role in promoting NHEJ alongside its functions following CPT exposure, TDP1 is also a strong candidate for co-operation with BOD1L and RIF1 (Li et al., 2017). Furthermore, there is the potential for BOD1L to interact with SLX4, a *bona fide* FA protein involved in the resolution of CPT-induced damage (Kim et al., 2013, Ceccaldi et al., 2016b). This approach would facilitate the initial identification of factors with which BOD1L and RIF1 may co-operate during the resolution of CPT-induced DNA damage; no additive impact would be expected from the depletion of BOD1L/RIF1 and these proteins.

7.6: Concluding remarks

The studies presented herein represent a valuable extension to the existing characterisation of BOD1L, furthering our understanding of the role that this recently-identified protein plays in the DDR. Moreover, my thesis contributes to our knowledge of the regulation of DSB repair through the modulation of nucleolytic resection at sites of DNA damage. This regulation has key implications for DNA repair pathway choice. Finally, as has been discussed, my research may also have wider-reaching implications into the field of cancer therapeutics.

References

- ADACHI, N., SO, S. & KOYAMA, H. 2004. Loss of nonhomologous end joining confers camptothecin resistance in DT40 cells. Implications for the repair of topoisomerase I-mediated DNA damage. *J Biol Chem*, 279, 37343-8.
- ADACHI, N., SUZUKI, H., IIZUMI, S. & KOYAMA, H. 2003. Hypersensitivity of nonhomologous DNA end-joining mutants to VP-16 and ICRF-193: implications for the repair of topoisomerase II-mediated DNA damage. *J Biol Chem*, 278, 35897-902.
- ADAMS, K. E., MEDHURST, A. L., DART, D. A. & LAKIN, N. D. 2006. Recruitment of ATR to sites of ionising radioactivity induces DNA damage requires ATM and components of the MRN complex. *Oncogene*, 25, 3894-3904.
- AL-DOSARI, M. S., SHAHEEN, R., COLAK, D. & ALKURAYA, F. S. 2010. Novel CENPJ mutation causes Seckel syndrome. *J Med Genet*, 47, 411-414.
- APARICIO, T., BAER, R., GOTTESMAN, M. E. & GAUTIER, J. 2016. MRN, CtIP, and BRCA1 mediate repair of topoisomerase II-DNA adducts. *J Cell Biol*, 212, 399-408.
- ARNOULT, N., CORREIA, A., MA, J., MERLO, A., GARCIA-GOMEZ, S., MARIC, M., TOGNETTI, M., BENNER, C. W., BOULTON, S. J., SAGHATELIAN, A. & KARLSEDER, J. 2017. Regulation of DNA repair pathway choice in S and G2 phases by the NHEJ inhibitor CYREN. *Nature*, 549, 548-552.
- ASHLEY, A. K., SHRIVASTAV, M., NIE, J., AMERIN, C., TROSKA, K., GLANZER, J. G., LIU, S., OPIYO, S. O., DIMITROVA, D. D., LE, P., SISHC, B., BAILEY, S. M., OAKLEY, G. G. & NICKOLOFF, J. A. 2014. DNA-PK phosphorylation of RPA Ser4/Ser8 regulates replication stress checkpoint activation, fork restart, homologous recombination and mitotic catastrophe. *DNA Repair*, 21, 131-139.
- BAKR, A., KOCHER, S., VOLQUARDSEN, J., PETERSEN, C., BORGMANN, K., DIKOMEY, E., ROTHKAMM, K. & MANSOUR, W. Y. 2016. Impaired 53BP1/RIF1 DSB mediated end-protection stimulates CtIP-dependent end resection and switches the repair to PARP1-dependent end joining in G1. *Oncotarget*, 7, 57679-57693.
- BALDOCK, R. A., DAY, M., WILKINSON, O. J., CLONEY, R., JEGGO, P. A., OLIVER, A. W., WATTS, F. Z. & PEARL, L. H. 2015. ATM Localization and Heterochromatin Repair Depend on Direct Interaction of the 53BP1-BRCT2 Domain with gammaH2AX. *Cell Rep*, 13, 2081-9.
- BALL, L. G. & XIAO, W. 2005. Molecular basis of ataxia telangiectasia and related diseases. *Acta Pharmacologica Sinica*, 26, 897-907.
- BECK, C., ROBERT, I., REINA-SAN-MARTIN, B., SCHREIBER, V. & DANTZER, F. 2014. Poly(ADP-ribose) polymerases in double-strand break repair: focus on PARP1, PARP2 and PARP3. *Exp Cell Res*, 329, 18-25.
- BENITEZ, A., LIU, W., PALOVCAK, A., WANG, G., MOON, J., AN, K., KIM, A., ZHENG, K., ZHANG, Y., BAI, F., MAZIN, A. V., PEI, X.-H., YUAN, F. & ZHANG, Y. 2018. FANCA Promotes DNA Double-Strand Break Repair by Catalyzing Single-Strand Annealing and Strand Exchange. *Mol Cell*, 71, 621-628.
- BERMEJO, R., LAI, M. S. & FOIANI, M. 2012. Preventing replication stress to maintain genome stability: resolving conflicts between replication and transcription. *Mol Cell*, 45, 710-718.
- BHARGAVA, R., ONYANGO, D. O. & STARK, J. M. 2016. Regulation of Single-Strand Annealing and its Role in Genome Maintenance. *Trends Genet*, 32, 566-575.
- BHAT, K. P. & CORTEZ, D. 2018. RPA and RAD51: fork reversal, fork protection, and genome stability. *Nat Struct Mol Biol*, 25, 446-453.
- BIEHS, R., STEINLAGE, M., BARTON, O., JUHASZ, S., KUNZEL, J., SPIES, J., SHIBATA, A., JEGGO, P. A. & LOBRICH, M. 2017. DNA Double-Strand Break Resection Occurs during Non-homologous End Joining in G1 but Is Distinct from Resection during Homologous Recombination. *Mol Cell*, 65, 671-684.
- BITINAITE, J., WAH, D. A., AGGARWAL, A. K. & SCHILDKRAUT, I. 1998. FokI dimerization is required for DNA cleavage. *Proc Natl Acad Sci U S A*, 95, 10570-10575.
- BJORKMAN, A., DU, L., FELGENTREFF, K., ROSNER, C., PANKAJ KAMDAR, R., KOKARAKI, G., MATSUMOTO, Y., DAVIES, E. G., VAN DER BURG, M., NOTARANGELO, L. D., HAMMARSTROM, L. & PAN-HAMMARSTROM, Q. 2015. DNA-PKcs Is Involved in Ig Class Switch Recombination in Human B Cells. *J Immunol*, 195, 5608-15.
- BLEICHERT, F., BOTCHAN, M. R. & BERGER, J. M. 2017. Mechanisms for initiating cellular DNA replication. *Science*, 355.

- BLUTEAU, D., MASLIAH-PLANCHON, J., CLAIRMONT, C., ROUSSEAU, A., CECCALDI, R., DUBOIS D'ENGHIEN, C., BLUTEAU, O., CUCCUINI, W., GACHET, S., PEFFAULT DE LATOUR, R., LEBLANC, T., SOCIE, G., BARUCHEL, A., STOPPA-LYONNET, D., D'ANDREA, A. D. & SOULIER, J. 2016. Biallelic inactivation of REV7 is associated with Fanconi anemia. *J Clin Invest*, 126, 3580-4.
- BODER, E. & SEDGWICK, R. P. 1958. Ataxia-Telangiectasia: A Familial Syndrome of Progressive Cerebellar Ataxia, Oculocutaneous Telangiectasia and Frequent Pulmonary Infection. *Pediatrics*, 21, 526-554.
- BOERSMA, V., MOATTI, N., SEGURA-BAYONA, S., PEUSCHER, M. H., VAN DER TORRE, J., WEVERS, B. A., ORTHWEIN, A., DUROCHER, D. & JACOBS, J. J. 2015. MAD2L2 controls DNA repair at telomeres and DNA breaks by inhibiting 5' end resection. *Nature*, 521, 537-40.
- BOSMA, G. C., CUSTER, R. P. & BOSMA, M. J. 1983. A severe combined immunodeficiency mutation in the mouse. *Nature*, 301, 527-530.
- BOSMA, G. C., KIM, J., URICH, T., FATH, D. M., COTTICELLI, M. G., RUETSCH, N. R., RADIC, M. Z. & BOSMA, M. J. 2002. DNA-dependent protein kinase activity is not required for immunoglobulin class switching. *J Exp Med*, 196, 1483-95.
- BOTHMER, A., ROBIANI, D. F., DI VIRGILIO, M., BUNTING, S., KLEIN, I. A., FELDHAHN, N., BARLOW, J., CHEN, H.-T., BOSQUE, D., CALLEN, E., NUSSENZWEIG, A. & NUSSENZWEIG, M. C. 2011. Regulation of DNA End Joining, Resection, and Immunoglobulin Class Switch Recombination by 53BP1. *Mol Cell*, 42, 319-329.
- BOUWMAN, P., ALY, A., ESCANDELL, J. M., PIETERSE, M., BARTKOVA, J., VAN DER GULDEN, H., HIDDINGH, S., THANASOULA, M., KULKARNI, A., YANG, Q., HAFPTY, B. G., TOMMISKA, J., BLOMQVIST, C., DRAPKIN, R., ADAMS, D. J., NEVANLINNA, H., BARTEK, J., TARSOUNAS, M., GANESAN, S. & JONKERS, J. 2010. 53BP1 loss rescues BRCA1 deficiency and is associated with triple-negative and BRCA-mutated breast cancers. *Nat Struct Mol Biol*, 17, 688-695.
- BRODERICK, R., NIEMINUSZCZY, J., BADDOCK, H. T., DESHPANDE, R. A., GILEADI, O., PAULL, T. T., MCHUGH, P. J. & NIEDZWIEDZ, W. 2016. EXD2 promotes homologous recombination by facilitating DNA end resection. *Nat Cell Biol*, 18, 271-80.
- BUGREEV, D. V., YU, X., EGELMAN, E. H. & MAZIN, A. V. 2007. Novel pro- and anti-recombination activities of the Bloom's syndrome helicase. *Genes Dev*, 21, 3085-3094.
- BUISSON, R., BOISVERT, J. L., BENES, C. H. & ZOU, L. 2015. Distinct but Concerted Roles of ATR, DNA-PK, and Chk1 in Countering Replication Stress during S Phase. *Mol Cell*, 59, 1011-24.
- BUNTING, S., CALLEN, E., WONG, N., CHEN, H.-T., POLATO, F., GUNN, A., BOTHMER, A., FELDHAHN, N., FERNANDEZ-CAPETILLO, O., CAO, L., XU, X., DENG, C.-X., FINKEL, T., NUSSENZWEIG, M. C., STARK, J. M. & NUSSENZWEIG, A. 2010. 53BP1 Inhibits Homologous Recombination in Brca1-Deficient Cells by Blocking Resection of DNA Breaks. *Cell*, 141, 243-254.
- BYUN, T. S., PACEK, M., YEE, M. C., WALTER, J. C. & CIMPRICH, K. A. 2005. Functional uncoupling of MCM helicase and DNA polymerase activities activates the ATR-dependent checkpoint. *Genes Dev*, 19, 1040-52.
- CAMERON, D., BLAKE, D. J., BRAY, N. J. & HILL, M. J. 2019. Transcriptional Changes following Cellular Knockdown of the Schizophrenia Risk Gene SETD1A Are Enriched for Common Variant Association with the Disorder. *Mol Neuropsychiatry*, 5, 109-114.
- CARNEY, J. P., MASER, R. S., OLIVARES, H., DAVIS, E. M., LE BEAU, M., YATES III, J. R., HAYS, L., MORGAN, W. F. & PETRINI, J. H. 1998. The hMre11/hRad50 Protein Complex and Nijmegen Breakage Syndrome: Linkage of Double-Strand Break Repair to the Cellular DNA Damage Response. *Cell*, 93, 477-486.
- CECCALDI, R., RONDINELLI, B. & D'ANDREA, A. D. 2016a. Repair Pathway Choices and Consequences at the Double-Strand Break. *Trends Cell Biol*, 26, 52-64.
- CECCALDI, R., SARANGI, P. & D'ANDREA, A. D. 2016b. The Fanconi anaemia pathway: new players and new functions. *Nat Rev Mol Cell Biol*, advance online publication.
- CEJKA, P. 2015. DNA End Resection: Nucleases Team Up with the Right Partners to Initiate Homologous Recombination. *J Biol Chem*, 290, 22931-8.
- CHANG, H. H. Y., PANNUNZIO, N. R., ADACHI, N. & LIEBER, M. R. 2017. Non-homologous DNA end joining and alternative pathways to double-strand break repair. *Nat Rev Mol Cell Biol*, 18, 495-506.
- CHANOUX, R. A., YIN, B., URTISHAK, K. A., ASARE, A., BASSING, C. H. & BROWN, E. J. 2009. ATR and H2AX cooperate in maintaining genome stability under replication stress. *J Biol Chem*, 284, 5994-6003.
- CHAPMAN, J. R., BARRAL, P., VANNIER, J. B., BOREL, V., STEGER, M., TOMAS-LOBA, A., SARTORI, A. A., ADAMS, I. R., BATISTA, F. D. & BOULTON, S. J. 2013. RIF1 is essential for 53BP1-dependent nonhomologous end joining and suppression of DNA double-strand break resection. *Mol Cell*, 49, 858-71.

- CHAPMAN, J. R., TAYLOR, M. R. G. & BOULTON, S. J. 2012. Playing the End Game: DNA Double-Strand Break Repair Pathway Choice. *Mol Cell*, 47, 497-510.
- CHEN, L., NIEVERA, C. J., LEE, A. Y.-L. & WU, X. 2008. Cell Cycle-dependent Complex Formation of BRCA1-CtIP-MRN Is Important for DNA Double-strand Break Repair. *The Journal of Biological Chemistry*, 283, 7713-7720.
- CHEN, Q., KASSAB, M. A., DANTZER, F. & YU, X. 2018. PARP2 mediates branched poly ADP-ribosylation in response to DNA damage. *Nat Commun*, 9, 3233.
- CHOY, K. R. & WATTERS, D. J. 2018. Neurodegeneration in Ataxia-Telangiectasia: Multiple Roles of ATM Kinase in Cellular Homeostasis. *Developmental Dynamics*, 247, 33-46.
- CHRZANOWSKA, K. H., GREGOREK, H., DEMBOWSKA-BAGIŃSKA, B., KALINA, M. A. & DIGWEED, M. 2012. Nijmegen breakage syndrome (NBS). *Orphanet Journal of Rare Diseases*, 7, 13.
- CICCIA, A. & ELLEDGE, S. J. 2010. The DNA damage response: making it safe to play with knives. *Mol Cell*, 40, 179-204.
- CONLIN, M. P., REID, D. A., SMALL, G. W., CHANG, H. H., WATANABE, G., LIEBER, M. R., RAMSDEN, D. A. & ROTHENBERG, E. 2017. DNA Ligase IV Guides End-Processing Choice during Nonhomologous End Joining. *Cell Rep*, 20, 2810-2819.
- CONTI, C., SEILER, J. A. & POMMIER, Y. 2007. The mammalian DNA replication elongation checkpoint: implication of Chk1 and relationship with origin firing as determined by single DNA molecule and single cell analyses. *Cell Cycle*, 6, 2760-7.
- CORTEZ, D., GUNTUKU, S., QIN, J. & ELLEDGE, S. J. 2001. ATR and ATRIP: Partners in Checkpoint Signaling. *Science*, 294, 1713-1716.
- COSTANZO, V. 2011. Brca2, Rad51 and Mre11: performing balancing acts on replication forks. *DNA Repair (Amst)*, 10, 1060-5.
- COSTELLOE, T., LOUGE, R., TOMIMATSU, N., MUKHERJEE, B., MARTINI, E., KHADAROO, B., DUBOIS, K., WIEGANT, W. W., THIERRY, A., BURMA, S., VAN ATTIKUM, H. & LLORENTE, B. 2012. The yeast Fun30 and human SMARCAD1 chromatin remodellers promote DNA end resection. *Nature*, 489, 581-4.
- COUTO, C. A.-M., WANG, H.-Y., GREEN, J. C. A., KIELY, R., SIDDAWAY, R., BORER, C., PEARS, C. J. & LAKIN, N. D. 2011. PARP regulates nonhomologous end joining through retention of Ku at double-strand breaks. *J Cell Biol*, 194, 367-375.
- COUTURE, J.-F. & SKINIOTIS, G. 2013. Assembling a COMPASS. *Epigenetics*, 8, 349-354.
- D'ANDREA, A. D. 2018. Mechanisms of PARP inhibitor sensitivity and resistance. *DNA Repair*, 71, 172-176.
- DAS, B. B., HUANG, S. Y., MURAI, J., REHMAN, I., AME, J. C., SENGUPTA, S., DAS, S. K., MAJUMDAR, P., ZHANG, H., BIARD, D., MAJUMDER, H. K., SCHREIBER, V. & POMMIER, Y. 2014. PARP1-TDP1 coupling for the repair of topoisomerase I-induced DNA damage. *Nucleic Acids Res*, 42, 4435-49.
- DAVIES, A. M. 2015. *The functional and molecular characterisation of the novel DNA damage repair protein Bod1L*. Doctor of Philosophy, University of Dundee.
- DAVIES, O. R., FORMENT, J. V., SUN, M., BELOTSEKOVSKAYA, R., COATES, J., GALANTY, Y., DEMIR, M., MORTON, C. R., RZECHORZEK, N. J., JACKSON, S. P. & PELLEGRINI, L. 2015. CtIP tetramer assembly is required for DNA-end resection and repair. *Nat Struct Mol Biol*, 22, 150-157.
- DAVIS, A. J., CHEN, B. P. & CHEN, D. J. 2014. DNA-PK: a dynamic enzyme in a versatile DSB repair pathway. *DNA Repair (Amst)*, 17, 21-9.
- DE BONT, R. & VAN LAREBEKE, N. 2004. Endogenous DNA damage in humans: a review of quantitative data. *Mutagenesis*, 19.
- DEANS, A. J. & WEST, S. C. 2011. DNA interstrand crosslink repair and cancer. *Nat Rev Cancer*, 11, 467-480.
- DENSHAM, R. M., GARVIN, A. J., STONE, H. R., STRACHAN, J., BALDOCK, R. A., DAZA-MARTIN, M., FLETCHER, A., BLAIR-REID, S., BEESLEY, J., JOHAL, B., PEARL, L. H., NEELY, R., KEEP, N. H., WATTS, F. Z. & MORRIS, J. R. 2016. Human BRCA1-BARD1 ubiquitin ligase activity counteracts chromatin barriers to DNA resection. *Nat Struct Mol Biol*, 23, 647-655.
- DENSHAM, R. M. & MORRIS, J. R. 2017. The BRCA1 Ubiquitin ligase function sets a new trend for remodelling in DNA repair. *Nucleus*, 8, 116-125.
- DESHPANDE, R. A., LEE, J. H., ARORA, A. & PAULL, T. T. 2016. Nbs1 Converts the Human Mre11/Rad50 Nuclease Complex into an Endo/Exonuclease Machine Specific for Protein-DNA Adducts. *Mol Cell*, 64, 593-606.
- DEV, H., CHIANG, T.-W. W., LESCALE, C., 12, , DE KRIJGER, I., MARTIN, A., PILGER, D., COATES, J., SCZANIECKA-CLIFT, M., WEI, W., OSTERMAIER, M., HERZOG, M., LAM, J., SHEA, A., DEMIR, M., WU, Q., YANG, F., FU, B., LAI, Z., BALMUS, G., BELOTSEKOVSKAYA, R., SERRA, V., O'CONNOR, M. J., BRUNA, A., BELI, P., PELLEGRINI, L., CALDAS, C., DERIANO, L., JACOBS, J. J. L., GALANTY, Y. & JACKSON, S. P. 2018. Shieldin

- complex promotes DNA end-joining and counters homologous recombination in BRCA1-null cells. *Nat Cell Biol*, 20, 954-965.
- DI VIRGILIO, M., CALLEN, E., YAMANE, A., ZHANG, W., JANKOVIC, M., GITLIN, A. D., FELDHAHN, N., RESCH, W., OLIVEIRA, T. Y., CHAIT, B. T., NUSSENZWEIG, A., CASELLAS, R., ROBBIANI, D. F. & NUSSENZWEIG, M. C. 2013. Rif1 Prevents Resection of DNA Breaks and Promotes Immunoglobulin Class Switching. *Science*, 339, 711-715.
- DUPRÉ, A., BOYER-CHATENET, L., SATTLER, R. M., MODI, A. P., LEE, J.-H., NICOLETTE, M. L., KOPELOVICH, L., JASIN, M., BAER, R., PAULL, T. T. & GAUTIER, J. 2008. A forward chemical genetic screen reveals an inhibitor of the Mre11-Rad50-Nbs1 complex. *Nat Chem Bio*, 4, 119-125.
- EDWARDS, S. L., BROUGH, R., LORD, C. J., NATRAJAN, R., VATCHEVA, R., LEVINE, D. A., BOYD, J., REIS-FILHO, J. S. & ASHWORTH, A. 2008. Resistance to therapy caused by intragenic deletion in BRCA2. *Nature*, 451, 1111-5.
- ESCRIBANO-DIAZ, C., ORTHWEIN, A., FRADET-TURCOTTE, A., XING, M., YOUNG, J. T., TKAC, J., COOK, M. A., ROSEBROCK, A. P., MUNRO, M., CANNY, M. D., XU, D. & DUROCHER, D. 2013. A Cell Cycle-Dependent Regulatory Circuit Composed of 53BP1-RIF1 and BRCA1-CtIP Controls DNA Repair Pathway Choice. *Mol Cell*, 49, 872-883.
- FAUCHER, D. & WELLINGER, R. J. 2010. Methylated H3K4, a transcription-associated histone modification, is involved in the DNA damage response pathway. *PLoS Genet*, 6.
- FENG, L., FONG, K. W., WANG, J., WANG, W. & CHEN, J. 2013. RIF1 counteracts BRCA1-mediated end resection during DNA repair. *J Biol Chem*, 288, 11135-11143.
- FERRETTI, L. P., LAFRANCHI, L. & SARTORI, A. A. 2013. Controlling DNA-end resection: a new task for CDKs. *Frontiers in Genetics*, 4, 99.
- FINDLAY, S., HEATH, J., LUO, V. M., MALINA, A., MORIN, T., COULOMBE, Y., DJERIR, B., LI, Z., SAMIEI, A., SIMO-CHEYOU, E., KARAM, M., BAGCI, H., RAHAT, D., GRAPTON, D., LAVOIE, E. G., DOVE, C., KHALED, H., KUSANE, H., MANN, K. K., OROS KLEIN, K., GREENWOOD, C. M., TABACH, Y., PARK, M., COTE, J.-F., MASSON, J. Y., MARECHAL, A. & ORTHWEIN, A. 2018. SHLD2/FAM35A co-operates with REV7 to coordinate DNA double-strand break repair pathway choice. *EMBO J*, 37, e100158.
- FORGET, A. L. & KOWALCZYKOWSKI, S. C. 2010. Single-molecule imaging brings Rad51 nucleoprotein filaments into focus. *Trends Cell Biol*, 20, 269-76.
- FRAGKOS, M., GANIER, O., COULOMBE, P. & MECHALI, M. 2015. DNA replication origin activation in space and time. *Nat Rev Mol Cell Biol*, 16, 360-74.
- GAMBUS, A. 2017. Termination of Eukaryotic Replication Forks. *Adv Exp Med Biol*, 1042, 163-187.
- GARZON, J., URSICH, S., LOPES, M., HIRAGA, S. I. & DONALDSON, A. D. 2019. Human RIF1-Protein Phosphatase 1 Prevents Degradation and Breakage of Nascent DNA on Replication Stalling. *Cell Rep*, 27, 2558-2566 e4.
- GODIN, S. K., SULLIVAN, M. R. & BERNSTEIN, K. A. 2016. Novel insights into RAD51 activity and regulation during homologous recombination and DNA replication. *Biochem Cell Biol*, 94, 407-418.
- GODTHELP, B. C., WIEGANT, W. W., WAISFISZ, Q., MEDHURST, A. L., ARWERT, F., JOENJE, H. & ZDZIENICKA, M. Z. 2006. Inducibility of nuclear Rad51 foci after DNA damage distinguishes all Fanconi anemia complementation groups from D1/BRCA2. *Mutat Res*, 594, 39-48.
- GOMEZ-CABELLO, D., JIMENO, S., FERNANDEZ-AVILA, M. J. & HUERTAS, P. 2013. New tools to study DNA double-strand break repair pathway choice. *PLoS One*, 8, e77206.
- GOODMAN, L. S., WINTROBE, M. M., DAMESHEK, W., GOODMAN, M. J., GILMAN, A. & MCLENNAN, M. T. 1946. *J Am Med Assoc*, 132, 126-132.
- GOODSHIP, J. A., GILL, H., CARTER, J., JACKSON, A. P., SPLITT, M. & WRIGHT, M. 2000. Autozygosity Mapping of a Seckel Syndrome Locus to Chromosome 3q22.1-q24. *Am J Hum Genet*, 67, 498-503.
- GRAHAM, T. G., WALTER, J. C. & LOPARO, J. J. 2016. Two-Stage Synapsis of DNA Ends during Non-homologous End Joining. *Mol Cell*, 61, 850-8.
- GRAHAM, T. G. W., CARNEY, S. M., WALTER, J. C. & LOPARO, J. J. 2018. A single XLF dimer bridges DNA ends during nonhomologous end joining. *Nat Struct Mol Biol*, 25, 877-884.
- GUNN, A. & STARK, J. M. 2012. I-Sce-based assays to examine distinct repair outcomes of mammalian chromosomal double strand breaks. *Methods Mol Biol*, 920, 379-391.
- GUPTA, D., LIN, B., COWAN, A. & HEINEN, C. D. 2018a. ATR-Chk1 activation mitigates replication stress caused by mismatch repair-dependent processing of DNA damage. *Proc Natl Acad Sci U S A*, 115, 1523-1528.

- GUPTA, R., SOMYAJIT, K., NARITA, T., MASKEY, E., STANLIE, A., KREMER, M., TYPAS, D., LAMMERS, M., MAILAND, N., NUSSENZWEIG, A., LUKAS, J. & CHOUDHARY, C. 2018b. DNA Repair Network Analysis Reveals Shieldin as a Key Regulator of NHEJ and PARP Inhibitor Sensitivity. *Cell*, 173, 972-988.
- HARASHIMA, H., DISSMEYER, N. & SCHNITTGER, A. 2013. Cell cycle control across the eukaryotic kingdom. *Trends Cell Biol*, 23, 345-56.
- HARTSUIKER, E., NEALE, M. J. & CARR, A. M. 2009. Distinct Requirements for the Rad32^{Mre11} Nuclease and Ctp1^{CtIP} in the Removal of Covalently Bound Topoisomerase I and II from DNA. *Mol Cell*, 33, 117-123.
- HASHIMOTO, S., ANAI, H. & HANADA, K. 2016. Mechanisms of interstrand DNA crosslink repair and human disorders *Genes Env*, 38, 9-16.
- HELLEDAY, T., PETERMANN, E., LUNDIN, C., HODGSON, B. & SHARMA, R. A. 2008. DNA repair pathways as targets for cancer therapy. *Nat Rev Cancer*, 8, 193-204.
- HELMRICH, A., BALLARINO, M., NUDLER, E. & TORA, L. 2013. Transcription-replication encounters, consequences and genomic instability. *Nat Struct Mol Biol*, 20, 412-8.
- HER, J., RAY, C., ALTSHULER, J., ZHENG, H. & BUNTING, S. 2018. 53BP1 Mediates ATR-Chk1 Signaling and Protects Replication Forks under Conditions of Replication Stress. *Molecular and Cell Biology*, 38, e00472-17.
- HEYER, W. D., EHMSSEN, K. T. & LIU, J. 2010. Regulation of homologous recombination in eukaryotes. *Annu Rev Genet*, 44, 113-39.
- HIGGS, M. R., REYNOLDS, J. J., WINCZURA, A., BLACKFORD, A. N., BOREL, V., MILLER, E. S., ZLATANOU, A., NIEMINUSZCZY, J., RYAN, E. L., DAVIES, N. J., STANKOVIC, T., BOULTON, S. J., NIEDZWIEDZ, W. & STEWART, G. S. 2015. BOD1L Is Required to Suppress Deleterious Resection of Stressed Replication Forks. *Mol Cell*, 59, 462-77.
- HIGGS, M. R., SATO, K., REYNOLDS, J. J., BEGUM, S., BAYLEY, R., GOULA, A., VERNET, A., PAQUIN, K. L., SKALNIK, D. G., KOBAYASHI, W., TAKATA, M., HOWLETT, N. G., KURUMIZAKA, H., KIMURA, H. & STEWART, G. S. 2018. Histone Methylation by SETD1A Protects Nascent DNA through the Nucleosome Chaperone Activity of FANCD2. *Mol Cell*, 71, 25-41.
- HORTON, J. K., STEFANICK, D. F., ZHAO, M. L., JANOSHAZI, A. K., GASSMAN, N. R., SEDDON, H. J. & WILSON, S. H. 2017. XRCC1-mediated repair of strand breaks independent of PNKP binding. *DNA Repair (Amst)*, 60, 52-63.
- HSIANG, Y.-H., LIHOU, M. G. & LIU, L. F. 1989. Arrest of replication forks by drug-stabilized Topoisomerase I-DNA cleavable complexes as a mechanism of killing by Camptothecin. *Cancer Research*, 49, 5077-5082.
- HUERTAS, P. 2010. DNA resection in eukaryotes: deciding how to fix the break. *Nat Struct Mol Biol*, 17, 11-6.
- HUERTAS, P., CORTES-LEDESMA, F., SARTORI, A. A., AGUILERA, A. & JACKSON, S. P. 2008. CDK targets Sae2 to control DNA-end resection and homologous recombination. *Nature*, 455, 689-692.
- HUERTAS, P. & JACKSON, S. P. 2009. Human CtIP Mediates Cell Cycle Control of DNA End Resection and Double Strand Break Repair. *J Biol Chem*, 284, 9558-9565.
- HUNG, P. J., JOHNSON, B., CHEN, B.-R., BYRUM, A. K., BREDEMEYER, A. L., YEWDELL, W. T., JOHNSON, T. E., LEE, B. J., DEIVASIGAMANI, S., HINDI, I., AMATYA, P., GROSS, M. L., AMARASINGE, G. K., ZHA, S., TYLER, J. K. & SLECKMAN, B. P. 2018. MRI is a DNA damage response adaptor during classical non-homologous end joining. *Mol Cell*, 71, 332-342.
- HWANG, S. Y., KANG, M. A., BAIK, C. J., LEE, Y., HANG, N. T., KIM, B. G., HAN, J. S., JEONG, J. H., PARK, D., MYUNG, K. & LEE, J. S. 2019. CTCF cooperates with CtIP to drive homologous recombination repair of double-strand breaks. *Nucleic Acids Res*, 47, 9160-9179.
- ISOBE, S. Y., NAGAO, K., NOZAKI, N., KIMURA, H. & OBUSE, C. 2017. Inhibition of RIF1 by SCAI Allows BRCA1-Mediated Repair. *Cell Rep*, 20, 297-307.
- ISONO, M., NIIMI, A., OIKE, T., HAGIWARA, Y., SATO, H., SEKINE, R., YOSHIDA, Y., ISOBE, S. Y., OBUSE, C., NISHI, R., PETRICCI, E., NAKADA, S., NAKANO, T. & SHIBATA, A. 2017. BRCA1 Directs the Repair Pathway to Homologous Recombination by Promoting 53BP1 Dephosphorylation. *Cell Rep*, 18, 520-532.
- JACKSON, S. P. & BARTEK, J. 2009. The DNA-damage response in human biology and disease. *Nature*, 461, 1071-8.
- JAIN, R., AGGARWAL, A. K. & RECHKOBLIT, O. 2018. Eukaryotic DNA polymerases. *Curr Opin Struct Biol*, 53, 77-87.
- JIMENO, S., FERNANDEZ-AVILA, M. J., CRUZ-GARCIA, A., CEPEDA-GARCIA, C., GOMEZ-CABELLO, D. & HUERTAS, P. 2015. Neddylation inhibits CtIP-mediated resection and regulates DNA double strand break repair pathway choice. *Nucleic Acids Res*, 43, 987-99.
- KAKAROUGKAS, A. & JEGGO, P. A. 2014. DNA DSB repair pathway choice: an orchestrated handover mechanism. *Br J Radiol*, 87, 20130685.

- KALAY, E., YIGIT, G., ASLAN, Y., BROWN, K. E., POHL, E., BICKNELL, L. S., KAYSERILI, H., LI, Y., TÜYSÜZ, B., NÜRNBERG, G., KIESS, W., KOEGL, M., BAESSMANN, I., BURUK, K., TORAMAN, B., KAYIPMAZ, S., KUL, S., IKBAL, M., TURNER, D. J., TAYLOR, M. S., AERTS, J., SCOTT, C., MILSTEIN, K., DOLLFUS, H., WIECZOREK, D., BRUNNER, H. G., HURLES, M. E., JACKSON, A. P., RAUCH, A., NÜRNBERG, P., KARAGÜZEL, A. & WOLLNIK, B. 2011. CEP152 is a genome maintenance protein disrupted in Seckel syndrome. *Nat Genet*, 43, 23-26.
- KARANAM, K., KAFRI, R., LOEWER, A. & LAHAV, G. 2012. Quantitative Live Cell IMaging Reveals a Gradual Shift between DNA Repair Mechanisms and a Maximal Use of HR in Mid S Phase. *Mol Cell*, 47, 320-329.
- KEE, Y. & HUANG, T. T. 2015. Role of Deubiquitinating Enzymes in DNA Repair. *Mol Cell Biol*, 36, 524-544.
- KENT, T., CHANDRAMOULY, G., MCDEVITT, S. M., OZDEMIR, A. Y. & POMERANTZ, R. T. 2015. Mechanism of microhomology-mediated end-joining promoted by human DNA polymerase theta. *Nat Struct Mol Biol*, 22, 230-7.
- KHAN, F. A. & ALI, S. O. 2017. Physiological roles of DNA double-strand breaks. *Journal of Nucleic Acids*, 2017, 6439169.
- KHETARPAL, P., DAS, S., PANIGRAHI, I. & MUNSHI, A. 2016. Primordial dwarfism: overview of clinical and genetic aspects. *Mol Genet Genomics*, 291, 1-15.
- KIEFER, K., OSHINSKY, J., KIM, J., NAKAJIMA, P. B., BOSMA, G. C. & BOSMA, M. J. 2007. The catalytic subunit of DNA-protein kinase (DNA-PKcs) is not required for Ig class-switch recombination. *Proc Natl Acad Sci U S A*, 104, 2843-2848.
- KIM, H. & D'ANDREA, A. D. 2012. Regulation of DNA cross-link repair by the Fanconi anemia/BRCA pathway. *Genes Dev*, 26, 1393-408.
- KIM, Y., SPITZ, G. S., VETURI, U., LACH, F. P., AUERBACH, A. D. & SMOGORZEWSKA, A. 2013. Regulation of multiple DNA repair pathways by the Fanconi anemia protein SLX4. *Blood*, 121, 54-63.
- KLUG, A. R., HARBUT, M. B., LLOYD, R. S. & MINKO, I. G. 2012. Replication bypass of N2-deoxyguanosine interstrand cross-links by human DNA polymerases η and ι . *Chem Res Toxicol*, 25, 755-762.
- KNIES, K., INANO, S., RAMIREZ, M. J., ISHIAI, M., SURRALLES, J., TAKATA, M. & SCHINDLER, D. 2017. Biallelic mutations in the ubiquitin ligase RFW3 cause Fanconi anemia. *J Clin Invest*, 127, 3013-3027.
- KOBAYASHI, S., FUKATSU, R., KANO, Y., KAKUSHO, N., MATSUMOTO, S., CHAEN, S. & MASAI, H. 2019. Both a Unique Motif at the C Terminus and an N-Terminal HEAT Repeat Contribute to G-Quadruplex Binding and Origin Regulation by the Rif1 Protein. *Mol Cell Biol*, 39.
- KOLINJIVADI, A. M., SANNINO, V., DE ANTONI, A., ZADOROZHNY, K., KILKENNY, M., TECHER, H., BALDI, G., SHEN, R., CICCIA, A., PELLEGRINI, L., KREJCI, L. & COSTANZO, V. 2017. Smarcal1-Mediated Fork Reversal Triggers Mre11-Dependent Degradation of Nascent DNA in the Absence of Brca2 and Stable Rad51 Nucleofilaments. *Mol Cell*, 67, 867-881 e7.
- KOMANDER, D. & RAPE, M. 2012. The ubiquitin code. *Annu Rev Biochem*, 81, 203-29.
- KOSTER, D. A., CRUT, A., SHUMAN, S., BJORNSTI, M. A. & DEKKER, N. H. 2010. Cellular strategies for regulating DNA supercoiling: a single-molecule perspective. *Cell*, 142, 519-530.
- KOTTEMANN, M. C. & SMOGORZEWSKA, A. 2013. Fanconi anaemia and the repair of Watson and Crick DNA crosslinks. *Nature*, 493, 356-63.
- KROKAN, H., WIST, E. & KROKAN, R. H. 1981. Aphidicolin inhibits DNA synthesis by DNA polymerase α and isolated nuclei by a similar mechanism. *Nucleic Acids Res*, 9, 4709-4719.
- LAFRANCHI, L., DE BOER, H. R., DE VRIES, E. G. E., ONG, S.-E., SARTORI, A. A. & VAN VUGT, M. A. T. M. 2014. APC/C^{Cdh1} control CtIP stability during the cell cycle and in response to DNA damage. *EMBO J*, 33, 2860-2879.
- LEE, J.-H. & SKALNIK, D. G. 2005. CpG-binding Protein (CXXC Finger Protein 1) Is a Component of the Mammalian Set1 Histone H3-Lys4 Methyltransferase Complex, the Analogue of the Yeast Set1/COMPASS Complex. *J Biol Chem*, 280, 41725-41731.
- LEMAN, A. R. & NOGUCHI, E. 2012. Local and global functions of Timeless and Tipin in replication fork protection. *Cell Cycle*, 11, 3945-55.
- LENGAUER, C., KINZLER, K. W. & VOGELSTEIN, B. 1998. Genetic instabilities in human cancers. *Nature*, 396.
- LI, J., SUMMERLIN, M., NITISS, K. C., NITISS, J. L. & HANAKAHI, L. A. 2017. TDP1 is required for efficient non-homologous end joining in human cells. *DNA Repair (Amst)*, 60, 40-49.
- LI, X., WANG, W. & CHEN, J. 2015. From pathways to networks: connecting dots by establishing protein-protein interaction networks in signaling pathways using affinity purification and mass spectrometry. *Proteomics*, 15, 188-202.

- LIANG, C. C., ZHAN, B., YOSHIKAWA, Y., HAAS, W., GYGI, S. P. & COHN, M. A. 2015. UHRF1 Is a Sensor for DNA Interstrand Crosslinks and Recruits FANCD2 to Initiate the Fanconi Anemia Pathway. *Cell Rep*, 10, 1947-1956.
- LIU, L. F., DESAI, S. D., LI, T. K., MAO, Y., SUN, M. & SIM, S. P. 2000. Mechanism of action of camptothecin. *Ann N Y Acad Sci*, 922, 1-10.
- LIU, W., ZHOU, M., LI, Z., LI, H., POLACZEK, P., DAI, H., WU, Q., LIU, C., KARANJA, K. K., POPURI, V., SHAN, S. O., SCHLACHER, K., ZHENG, L., CAMPBELL, J. L. & SHEN, B. 2016. A Selective Small Molecule DNA2 Inhibitor for Sensitization of Human Cancer Cells to Chemotherapy. *EBioMedicine*, 6, 73-86.
- LOMBARDI, P. M., MATUNIS, M. J. & WOLBERGER, C. 2017. RAP80, ubiquitin and SUMO in the DNA damage response. *J Mol Med (Berl)*, 95, 799-807.
- LORD, C. J. & ASHWORTH, A. 2012. The DNA damage response and cancer therapy. *Nature*, 481, 287-294.
- MALACARIA, E., PUGLIESE, G. M., HONDA, M., MARABITTI, V., AIELLO, F. A., SPIES, M., FRANCHITTO, A. & PICHIERRI, P. 2019. Rad52 prevents excessive replication fork reversal and protects from nascent strand degradation. *Nat Commun*, 10, 1412.
- MALYARCHUK, S., CASTORE, R., SHI, R. & HARRISON, L. 2013. Artemis is required to improve the accuracy of repair of double-strand breaks with 5'-blocked termini generated from non-DSB-clustered lesions. *Mutagenesis*, 28, 357-366.
- MAMO, T., MLADEK, A. C., SHOGREN, K. L., GUSTAFSON, C., GUPTA, S. K., RIESTER, S. M., MARAN, A., GALINDO, M., VAN WIJNEN, A. J., SARKARIA, J. N. & YASZEMSKI, M. J. 2017. Inhibiting DNA-PKCS radiosensitizes human osteosarcoma cells. *Biochemical and Biophysical Research Communications*, 486, 307-313.
- MANSOUR, W. Y., BORGMANN, K., PETERSEN, C., DIKOMEY, E. & DAHM-DAPHI, J. 2013. The absence of Ku but not defects in classical non-homologous end-joining is required to trigger PARP1-dependent end-joining. *DNA Repair (Amst)*, 12, 1134-42.
- MANSOUR, W. Y., SCHUMACHER, S., ROSSKOPF, R., RHEIN, T., SCHMIDT-PETERSEN, F., GATZEMEIER, F., HAAG, F., BORGMANN, K., WILLERS, H. & DAHM-DAPHI, J. 2008. Hierarchy of nonhomologous end-joining, single-strand annealing and gene conversion at site-directed DNA double-strand breaks. *Nucleic Acids Res*, 36, 4088-98.
- MARECHAL, A. & ZOU, L. 2015. RPA-coated single-stranded DNA as a platform for post-translational modifications in the DNA damage response. *Cell Res*, 25, 9-23.
- MASAI, H., KAKUSHO, N., FUKATSU, R., MA, Y., IIDA, K., KANO, Y. & NAGASAWA, K. 2018. Molecular architecture of G-quadruplex structures generated on duplex Rif1-binding sequences. *J Biol Chem*, 293, 17033-17049.
- MATEOS-GOMEZ, P. A., GONG, F., NAIR, N., MILLER, K. M., LAZZERINI-DENCHI, E. & SFEIR, A. 2015. Mammalian polymerase theta promotes alternative NHEJ and suppresses recombination. *Nature*, 518, 254-7.
- MATSUOKA, S., BALLIF, B. A., SMOGORZEWSKA, A., MCDONALD III, R., HUROV, K. E., LUO, J., BAKALARSKI, C. E., ZHAO, Z., SOLIMINI, N., LERENTHAL, Y., SHILOH, Y., GYGI, S. & ELLEDGE, S. J. 2007. ATM and ATR Substrate Analysis Reveals Extensive Protein Networks Responsive to DNA Damage. *Science*, 316, 1160-1166.
- MATSUURA, S., TAUCHI, H., NAKAMURA, A., KONDO, N., SAKAMOTO, S., ENDO, S., SMEETS, D., SOLDER, B., BELOHRADSKY, B. H., DER KALOUSTIAN, V. M., OSHIMURA, M., ISOMURA, M., NAKAMURA, Y. & KOMATSU, K. 1998. Positional cloning of the gene for Nijmegen breakage syndrome. *Nat Genet*, 19, 179-181.
- MATTIROLI, F., VISSERS, J. H. A., VAN DIJK, W. J., IKPA, P., CITTERIO, E., VERMEULEN, W., MARTEIJN, J. A. & SIXMA, T. K. 2012. RNF168 Ubiquitinates K13-15 on H2A/H2AX to Drive DNA Damage Signaling. *Cell*, 150, 1182-1195.
- MAZOUZI, A., VELIMEZI, G. & LOIZOU, J. I. 2014. DNA replication stress: Causes, resolution and disease. *Exp Cell Res*, 329, 85-93.
- MEEK, K., KIENKER, L., DALLAS, C., WANG, W., DARK, M. J., VENTA, P. J., HUIE, M. L., HIRSCHHORN, R. & BELL, T. 2001. SCID in Jack Russell terriers: a new animal model of DNA-PKcs deficiency. *J Immunol*, 167, 2142-50.
- MEHTA, A. & HABER, J. E. 2014. Sources of DNA Double-Strand Breaks and Models of Recombinational DNA Repair. *Cold Spring Harbor Perspectives in Biology*, 6.
- MICHL, J., ZIMMER, J. & TAROUNAS, M. 2016. Interplay between Fanconi anemia and homologous recombination pathways in genome integrity. *EMBO J*.
- MIJIC, S., ZELLWEGER, R., CHAPPIDI, N., BERTI, M., JACOBS, K., MUTREJA, K., URSICH, S., RAY CHAUDHURI, A., NUSSENZWEIG, A., JANSACK, P. & LOPES, M. 2017. Replication fork reversal triggers fork degradation in BRCA2-defective cells. *Nat Commun*, 8, 859.

- MOKRANI-BENHELLI, H., GAILLARD, L., BIASUTTO, P., LE GUEN, T., TOUZOT, F., VASQUEZ, N., KOMATSU, J., CONSEILLER, E., PICARD, C., GLUCKMAN, E., FRANCCANNET, C., FISCHER, A., DURANDY, A., SOULIER, J., DE VILLARTAY, J. P., CAVAZZANA-CALVO, M. & REVY, P. 2012. Primary Microcephaly, Impaired DNA Replication, and Genomic Instability Caused by Compound Heterozygous ATR Mutations. *Human Mutation*, 34, 374-384.
- MORENO, S. P. & GAMBUS, A. 2015. Regulation of Unperturbed DNA Replication by Ubiquitylation. *Genes (Basel)*, 6, 451-68.
- MORIO, T. 2017. Recent advances in the study of immunodeficiency and DNA damage response. *Int J Hematol*, 106, 357-365.
- MUKAI, J., CANNAVO, E., CRABTREE, G. W., SUN, Z., DIAMANTOPOULOU, A., THAKUR, P., CHANG, C. Y., CAI, Y., LOMVARDAS, S., TAKATA, A., XU, B. & GOGOS, J. A. 2019. Recapitulation and Reversal of Schizophrenia-Related Phenotypes in Setd1a-Deficient Mice. *Neuron*, 104, 471-487 e12.
- MUNOZ, S. & MENDEZ, J. 2017. DNA replication stress: from molecular mechanisms to human disease. *Chromosoma*, 126, 1-15.
- NAIM, V. & ROSSELLI, F. 2009. The FANCD pathway and BLM collaborate during mitosis to prevent micro-nucleation and chromosome abnormalities. *Nat Cell Biol*, 11, 761-769.
- NAKAJIMA, N. I., HAGIWARA, Y., OIKE, T., OKAYASU, R., MURAKAMI, T., NAKANO, T. & SHIBATA, A. 2015. Pre-exposure to ionizing radiation stimulates DNA double strand break end resection, promoting the use of homologous recombination repair. *PLoS One*, 10, e0122582.
- NAKAMURA, K., KOGAME, T., OSHIUMI, H., SHINOHARA, A., SUMITOMO, Y., AGAMA, K., POMMIER, Y., TSUTSUI, K. M., TSUTSUI, K., HARTSUIKER, E., OGI, T., TAKEDA, S. & TANIGUCHI, Y. 2010. Collaborative Action of Brca1 and CtIP in Elimination of Covalent Modifications from Double-Strand Breaks to Facilitate Subsequent Break Repair. *PLoS Genet*, 6, e1000828.
- NEPAL, M., CHE, R., ZHANG, J., MA, C. & FEI, P. 2017. Fanconi Anemia Signaling and Cancer. *Trends Cancer*, 3, 840-856.
- NIMONKAR, A. V., GENSCHEL, J., KINOSHITA, E., POLACZEK, P., CAMPBELL, J. L., WYMAN, C., MODRICH, P. & KOWALCZYKOWSKI, S. C. 2011. BLM-DNA2-RPA-MRN and EXO1-BLM-RPA-MRN constitute two DNA end resection machineries for human DNA break repair. *Genes Dev*, 25, 350-62.
- NOLL, D. M., MCGREGOR MASON, T. & MILLER, P. S. 2006. Formation and Repair of Interstrand Cross-Links in DNA. *Chem Rev*, 106, 277-301.
- NOORDERMEER, S. M., ADAM, S., SETIAPUTRA, D., BARAZAS, M., PETTITT, S. J., LING, A. K., OLIVIERI, M., ÁLVAREZ-QUILÓN, A., MOATTI, N., ZIMMERMANN, M., ANNUNZIATO, S., KRASDEV, D. B., SONG, F., BRANDSMA, I., FRANKUM, J., BROUGH, R., SHERKER, A., LANDRY, S., SZILARD, R. K., MUNRO, M. M., MCEWAN, A., GOULLET DE RUGY, T., LIN, Z.-Y., HART, T., MOFFAT, J., GINGRAS, A. C., MARTIN, A., VAN ATTIKUM, H., JONKERS, J., LORD, C. J., ROTTENBERG, S. & DUROCHER, D. 2018. The shieldin complex mediates 53BP1-dependent DNA repair. *Nature*, 560, 117-121.
- O'CONNOR, M. J. 2015. Targeting the DNA Damage Response in Cancer. *Mol Cell*, 60, 547-560.
- O'DRISCOLL, M., RUIZ-PEREZ, V. L., WOODS, C. G., JEGGO, P. A. & GOODSHIP, J. A. 2003. A splicing mutation affecting expression of ataxia-telangiectasia and Rad3-related protein (ATR) results in Seckel syndrome. *Nat Genet*, 33, 497-501.
- OGI, T., WALKER, S., STIFF, T., HOBSON, E., LIMSIRICHAIKUL, S., CARPENTER, G., PRESCOTT, K., SURU, M., BYRD, P. J., MATSUSE, M., MITSUTAKE, N., NAKAZAWA, Y., VASUDEVAN, P., BARROW, M., STEWART, G. S., TAYLOR, A. M. R., O'DRISCOLL, M. & JEGGO, P. A. 2012. Identification of the First ATRIP-Deficient Patient and Novel Mutations in ATR Define a Clinical Spectrum for ATR-ATRIP Seckel Syndrome. *PLoS Genet*, 8, e1002945.
- PAULL, T. T. 2015. Mechanisms of ATM Activation. *Annu Rev Biochem*, 84, 711-38.
- PEARS, C. J., COUTO, C. A. M., WANG, H.-Y., BORER, C., KIELY, R. & LAKIN, N. D. 2012. The role of ADP-ribosylation in regulating DNA double-strand break repair. *Cell Cycle*, 11, 48-56.
- PELLEGRINO, S., MICHELENA, J., TELONI, F., IMHOF, R. & ALTMAYER, M. 2017. Replication-Coupled Dilution of H4K20me2 Guides 53BP1 to Pre-replicative Chromatin. *Cell Rep*, 19, 1819-1831.
- PETERMANN, E., ORTA, M. L., ISSAEVA, N., SCHULTZ, N. & HELLEDAY, T. 2010. Hydroxyurea-Stalled Replication Forks Become Progressively Inactivated and Require Two Different RAD51-Mediated Pathways for Restart and Repair. *Mol Cell*, 37, 492-502.
- PINTO, C., KASACIUNAITE, K., SEIDEL, R. & CEJKA, P. 2016. Human DNA2 possesses a cryptic DNA unwinding activity that functionally integrates with BLM or WRN helicases. *Elife*, 5.

- POLATO, F., CALLEN, E., WONG, N., FARYABI, R., BUNTING, S., CHEN, H. T., KOZAK, M., KRULAK, M. J., RECZEK, C. R., LEE, W. H., LUDWIG, T., BAER, R., FEIGENBAUM, L., JACKSON, S. & NUSSENZWEIG, A. 2014. CtIP-mediated resection is essential for viability and can operate independently of BRCA1. *J Exp Med*, 211, 1027-36.
- PORTER, I. M., MCCLELLAND, S. E., KHOUDOLI, G. A., HUNTER, C. J., ANDERSEN, J. S., MCAINSH, A. D., BLOW, J. J. & SWEDLOW, J. R. 2007. Bod1, a novel kinetochore protein required for chromosome biorientation. *J Cell Biol*, 179, 187-197.
- POZAROWSKI, P. & DARZYNKIEWICZ, Z. 2004. Analysis of cell cycle by flow cytometry. *Methods Mol Biol*, 281, 301-311.
- PRIEGO MORENO, S., JONES, R. M., POOVATHUMKADAVIL, D., SCARAMUZZA, S. & GAMBUS, A. 2019. Mitotic replisome disassembly depends on TRAIPI ubiquitin ligase activity. *Life Sci Alliance*, 2.
- PRZETOCKA, S., PORRO, A., BOLCK, H. A., WALKER, C., LEZAJA, A., TRENNER, A., VON AESCH, C., HIMMELS, S. F., D'ANDREA, A. D., CECCALDI, R., ALTMAYER, M. & SARTORI, A. A. 2018. CtIP-Mediated Fork Protection Synergizes with BRCA1 to Suppress Genomic Instability upon DNA Replication Stress. *Mol Cell*, 72, 568-582 e6.
- QUINET, A., LEMACON, D. & VINDIGNI, A. 2017. Replication Fork Reversal: Players and Guardians. *Mol Cell*, 68, 830-833.
- QVIST, P., HUERTAS, P., JIMENO, S., NYEGAARD, M., HASSAN, M. J., JACKSON, S. P. & BØRGLUM, A. D. 2011. CtIP Mutations Cause Seckel and Jawad Syndromes. *PLoS Genet*, 7, e1002310.
- RASS, E., GRABARZ, A., PLO, I., GAUTIER, J., BERTRAND, P. & LOPEZ, B. S. 2009. Role of Mre11 in chromosomal nonhomologous end joining in mammalian cells. *Nat Struct Mol Biol*, 16, 819-24.
- RAY CHAUDHURI, A., CALLEN, E., DING, X., GOGOLA, E., DUARTE, A. A., LEE, J. E., WONG, N., LAFARGA, V., CALVO, J. A., PANZARINO, N. J., JOHN, S., DAY, A., CRESPO, A. V., SHEN, B., STARNES, L. M., DE RUITER, J. R., DANIEL, J. A., KONSTANTINOPOULOS, P. A., CORTEZ, D., CANTOR, S. B., FERNANDEZ-CAPETILLO, O., GE, K., JONKERS, J., ROTTENBERG, S., SHARAN, S. K. & NUSSENZWEIG, A. 2016. Replication fork stability confers chemoresistance in BRCA-deficient cells. *Nature*, 535, 382-7.
- REEVES, R. & NISSEN, M. S. 1990. The A.T-DNA-binding domain of mammalian high mobility group I chromosomal proteins. A novel peptide motif for recognizing DNA structure. *J Biol Chem*, 265, 8573-8582.
- RODRÍGUEZ-LÓPEZ, A. M., JACKSON, D. A., IBORRA, F. & COX, L. S. 2002. Asymmetry of DNA replication fork progression in Werner's syndrome. *Aging Cell*, 1, 30-39.
- RONDINELLI, B., GOGOLA, E., YUCEL, H., DUARTE, A. A., VAN DE VEN, M., VAN DER SLUIJS, R., KONSTANTINOPOULOS, P. A., JONKERS, J., CECCALDI, R., ROTTENBERG, S. & D'ANDREA, A. D. 2017. EZH2 promotes degradation of stalled replication forks by recruiting MUS81 through histone H3 trimethylation. *Nat Cell Biol*, 19, 1371-1378.
- ROSSI, M. J. & MAZIN, A. V. 2008. Rad51 Protein Stimulates the Branch Migration Activity of Rad54 Protein. *J Biol Chem*, 283, 24698-24706.
- RYCENGA, H. B. & LONG, D. T. 2018. The evolving role of DNA inter-strand crosslinks in chemotherapy. *Curr Opin Pharmacol*, 41, 20-26.
- SAKAI, W., SWISHER, E. M., KARLAN, B. Y., AGARWAL, M. K., HIGGINS, J., FRIEDMAN, C., VILLEGAS, E., JACQUEMONT, C., FARRUGIA, D. J., COUCH, F. J., URBAN, N. & TANIGUCHI, T. 2008. Secondary mutations as a mechanism of cisplatin resistance in BRCA2-mutated cancers. *Nature*, 451, 1116-20.
- SALEH-GOHARI, N. & HELLEDAY, T. 2004. Conservative homologous recombination preferentially repairs DNA double-strand breaks in the S phase of the cell cycle in human cells. *Nucleic Acids Res*, 32, 3683-3688.
- SARKAR, S., DAVIES, A. A., ULRICH, H. J. & MCHUGH, P. J. 2006. DNA interstrand crosslink repair during G1 involves nucleotide excision repair and DNA polymerase ϵ . *EMBO J*, 25, 1285-1294.
- SARTORI, A. A., LUKAS, C., COATES, J., MISTRICK, M., FU, S., BARTEK, J., BAER, R., LUKAS, J. & JACKSON, S. P. 2007. Human CtIP promotes DNA end resection. *Nature*, 450, 509-14.
- SAVITSKY, K., BAR-SHIRA, A., SHLOMIT GILAD, ROTMAN, G., ZIV, Y., VANAGAITE, L., TAGLE, D. A., SMITH, S., UZIEL, T., SFEZ, S., ASHKENAZI, M., PECKER, I., FRYDMAN, M., HARNIK, R., PATANJALI, S. R., SIMMONS, A., CLINES, G. A., SARTIEL, A., GATTI, R. A., CHESSA, L., SANAL, O., LAVIN, M. F., JASPERS, N. G. J., TAYLOR, A. M. R., ARLETT, C. F., MIKI, T., WEISSMAN, S. M., LOVETT, M., COLLINS, F. S. & SHILOH, Y. 1995. A Single Ataxia Telangiectasia Gene with a Product Similar to P1-3 Kinase. *Science*, 268, 1749-1753.
- SCHIPLER, A. & ILIAKIS, G. 2013. DNA double-strand-break complexity levels and their possible contributions to the probability for error-prone processing and repair pathway choice. *Nucleic Acids Res*, 41, 7589-7605.

- SCHLACHER, K., CHRIST, N., SIAUD, N., EGASHIRA, A., WU, H. & JASIN, M. 2011. Double-strand break repair-independent role for BRCA2 in blocking stalled replication fork degradation by MRE11. *Cell*, 145, 529-42.
- SCHWERTMAN, P., BEKKER-JENSEN, S. & MAILAND, N. 2016. Regulation of DNA double-strand break repair by ubiquitin and ubiquitin-like modifiers. *Nat Rev Mol Cell Biol*, 17, 379-94.
- SECKEL, H. P. G. 1960. Bird-headed dwarfs: studies in developmental anthropology including human proportions. *CC Thomas*.
- SHAKEEL, S., RAJENDRA, E., ALCON, P., O'REILLY, F., CHOREV, D. S., MASLEN, S., DEGLIESPOSTI, G., RUSSO, C. J., HE, S., HILL, C. H., SKEHEL, J. M., SCHERES, S. H. W., PATEL, K. J., RAPPILBER, J., ROBINSON, C. V. & PASSMORE, L. A. 2019. Structure of the Fanconi anaemia monoubiquitin ligase complex. *Nature*, 575, 234-237.
- SHIBATA, A., CONRAD, S., BIRRAUX, J., GEUTING, V., BARTON, O., ISMAIL, A., KAKAROUGKAS, A., MEEK, K., TAUCHER-SCHOLZ, G., LOBRICH, M. & JEGGO, P. A. 2011. Factors determining DNA double-strand break repair pathway choice in G2 phase. *EMBO J*, 30, 1079-92.
- SHIBATA, A., MOIANI, D., ARVAI, A. S., PERRY, J., HARDING, S. M., GENOIS, M. M., MAITY, R., VAN ROSSUM-FIKKERT, S., KERTOKALIO, A., ROMOLI, F., ISMAIL, A., ISMALAJ, E., PETRICCI, E., NEALE, M. J., BRISTOW, R. G., MASSON, J. Y., WYMAN, C., JEGGO, P. A. & TAINER, J. A. 2014. DNA double-strand break repair pathway choice is directed by distinct MRE11 nuclease activities. *Mol Cell*, 53, 7-18.
- SHRIVASTAV, M., DE HARO, L. P. & NICKOLOFF, J. A. 2008. Regulation of DNA double-strand break repair pathway choice. *Cell Research*, 2008, 134-147.
- SILVERMAN, J., TAKAI, H., BUONOMO, S. B. C., EISENHABER, F. & DE LANGE, T. 2004. Human Rif1, ortholog of a yeast telomeric protein, is regulated by ATM and 53BP1 and functions in the S-phase checkpoint. *Genes Dev*, 18, 2108-2119.
- SIMONETTA, M., DE KRIJGER, I., SERRAT, J., MOATTI, N., FORTUNATO, D., HOEKMAN, L., BLEIJERVELD, O. B., ALTELAAR, A. F. M. & JACOBS, J. J. L. 2018. H4K20me2 distinguishes pre-replicative from post-replicative chromatin to appropriately direct DNA repair pathway choice by 53BP1-RIF1-MAD2L2. *Cell Cycle*, 17, 124-136.
- SINGH, B. & WU, P. J. 2019. Regulation of the program of DNA replication by CDK: new findings and perspectives. *Curr Genet*, 65, 79-85.
- SINGH, T., KURKI, M. I., CURTIS, D., PURCELL, S. M., CROOKS, L., MCRAE, J., SUVISAARI, J., CHHEDA, H., BLACKWOOD, D., BREEN, G., PIETILAINEN, O., GERETY, S. S., AYUB, M., BLYTH, M., COLE, T., COLLIER, D., COOMBER, E. L., CRADDOCK, N., DALY, M. J., DANESH, J., DIFORTI, M., FOSTER, A., FREIMER, N. B., GESCHWIND, D., JOHNSTONE, M., JOSS, S., KIROV, G., KORKKO, J., KUISMIN, O., HOLMANS, P., HULTMAN, C. M., IYEGBE, C., LONNQVIST, J., MANNIKKO, M., MCCARROLL, S. A., MCGUFFIN, P., MCINTOSH, A. M., MCQUILLIN, A., MOILANEN, J. S., MOORE, C., MURRAY, R. M., NEWBURY-ECOB, R., OUWEHAND, W., PAUNIO, T., PRIGMORE, E., REES, E., ROBERTS, D., SAMBROOK, J., SKLAR, P., ST CLAIR, D., VEIJOLA, J., WALTERS, J. T., WILLIAMS, H., SWEDISH SCHIZOPHRENIA, S., STUDY, I., STUDY, D. D. D., CONSORTIUM, U. K., SULLIVAN, P. F., HURLES, M. E., O'DONOVAN, M. C., PALOTIE, A., OWEN, M. J. & BARRETT, J. C. 2016. Rare loss-of-function variants in SETD1A are associated with schizophrenia and developmental disorders. *Nat Neurosci*, 19, 571-7.
- SIRBU, B. M., COUCH, F. B. & CORTEZ, D. 2012. Monitoring the spatiotemporal dynamics of proteins at replication forks and in assembled chromatin using isolation of proteins on nascent DNA. *Nat Protoc*, 7, 594-605.
- SMITS, A. H. & VERMEULEN, M. 2016. Characterizing Protein-Protein Interactions Using Mass Spectrometry: Challenges and Opportunities. *Trends Biotech*, 34, 825-834.
- SMOGORZEWSKA, A., KARLSEDER, J., HOLTGREVE-GREZ, H., JAUCH, A. & DE LANGE, T. 2002. DNA Ligase IV-Dependent NHEJ of Deprotected Mammalian Telomeres in G1 and G2. *Curr Biol*, 12, 1635-1644.
- SOBHIAN, B., SHAO, G., LILLI, D. R., CULHANE, A. C., MOREAU, L. A., XIA, B., LIVINGSTON, D. M. & GREENBERG, R. A. 2007. RAP80 Targets BRCA1 to Specific Ubiquitin Structures at DNA Damage Sites. *Science*, 316.
- SORIA-BRETONES, I., CEPEDA-GARCIA, C., CHECA-RODRIGUEZ, C., HEYER, V., REINA-SAN-MARTIN, B., SOUTOGLOU, E. & HUERTAS, P. 2017. DNA end resection requires constitutive sumoylation of CtIP by CBX4. *Nat Commun*, 8, 113.
- SOULAS-SPRAUEL, P., RIVERA-MUNOZ, P., MALIVERT, L., LE GUYADER, G., ABRAMOWSKI, V., REVY, P. & DE VILLARTAY, J. P. 2007. V(D)J and immunoglobulin class switch recombinations: a paradigm to study the regulation of DNA end-joining. *Oncogene*, 26, 7780-7791.
- STEWART, G. S., MASER, R. S., STANKOVIC, T., BRESSAN, D. A., KAPLAN, M. I., JASPERS, N. G. J., RAAMS, A., BYRD, P. J., PETRINI, J. H. J. & TAYLOR, A. M. R. 1999. The DNA Double-Strand Break Repair Gene *hMRE11* is Mutated in Individuals with an Ataxia-Telangiectasia-like Disorder. *Cell Research*, 99, 577-587.

- STEWART, G. S., PANIER, S., TOWNSEND, K., AL-HAKIM, A. K., KOLAS, N. K., MILLER, E. S., NAKADA, S., YLANKO, J., OLIVARIUS, S., MENDEZ, M., OLDREIVE, C. E., WILDENHAIN, J., TAGLIAFERRO, A., PELLETIER, L., TAUBENHEIM, N., DURANDY, A., BYRD, P. J., STANKOVIC, T., TAYLOR, A. M. R. & DUROCHER, D. 2009. The RIDDLE Syndrome Protein Mediates a Ubiquitin-Dependent Signaling Cascade at Sites of DNA Damage. *Cell*, 136, 420-434.
- STEWART, G. S., WANG, B., BIGNELL, C. R., TAYLOR, A. M. R. & ELLEDGE, S. J. 2003. MDC1 is a mediator of the mammalian DNA damage checkpoint. *Nature*, 421, 961-966.
- SUTHERLAND, B. M., BENNETT, P. V., SUTHERLAND, J. C. & LAVAL, J. 2002. Clustered DNA damaged induced by X rays in human cells. *Radiat Res*, 157, 611-616.
- SYMINGTON, L. S. 2002. Role of RAD52 Epistasis Group Genes in Homologous Recombination and Double-Strand Break Repair. *Microbiology and Molecular Biology Reviews*, 66, 630-670.
- SYMINGTON, L. S. & GAUTIER, J. 2011. Double-Strand Break End Resection and Repair Pathway Choice. *Annu Rev Genet*, 45, 247-271.
- TAALMAN, R. D., JASPERS, N. G. J., SCHERES, J. M., DE WIT, J. & HUSTINX, T. W. 1983. Hypersensitivity to ionizing radiation, in vitro, in a new chromosomal breakage disorder, the Nijmegen Breakage Syndrome. *Mut Res*, 112, 23-32.
- TAKAHATA, C., MASUDA, Y., TAKEDACHI, A., TANAKA, K., IWAI, S. & KURAOKA, I. 2015. Repair synthesis step involving ERCC1-XPF participates in DNA repair of the Top1-DNA damage complex. *Carcinogenesis*, 36, 841-51.
- TAKATA, A., XU, B., IONITA-LAZA, I., ROOS, J. L., GOGOS, J. A. & KARAYIORGOU, M. 2014. Loss-of-function variants in schizophrenia risk and SETD1A as a candidate susceptibility gene. *Neuron*, 82, 773-80.
- TAYLOR, A. M. R. & BYRD, P. J. 2005. Molecular pathology of ataxia telangiectasia. *J Clin Pathol*, 58, 1009-1015.
- TAYLOR, A. M. R., GROOM, A. & BYRD, P. J. 2004. Ataxia-telangiectasia-like disorder (ATLD)—its clinical presentation and molecular basis. *DNA Repair*, 3, 1219-1225.
- TAYLOR, A. M. R., HARNDEN, D. G., ARLETT, C. F., HARCOURT, S. A., LEHMAN, A. R., STEVENS, S. & BRIDGES, B. A. 1975. Ataxia telangiectasia: a human mutations with abnormal radiation sensitivity. *Nature*, 258, 427-429.
- TIMSON, J. 1975. Hydroxyurea. *Mut Res*, 32, 115-132.
- TKAC, J., XU, G., ADHIKARY, H., YOUNG, J. T., GALLO, D., ESCRIBANO-DIAZ, C., KRIETSCH, J., ORTHWEIN, A., MUNRO, M., SOL, W., AL-HAKIM, A., LIN, Z. Y., JONKERS, J., BORST, P., BROWN, G. W., GINGRAS, A. C., ROTTENBERG, S., MASSON, J. Y. & DUROCHER, D. 2016. HELB Is a Feedback Inhibitor of DNA End Resection. *Mol Cell*, 61, 405-18.
- TOMIMATSU, N., MUKHERJEE, B., CATHERINE HARDEBECK, M., ILCHEVA, M., VANESSA CAMACHO, C., LOUISE HARRIS, J., PORTEUS, M., LLORENTE, B., KHANNA, K. K. & BURMA, S. 2014. Phosphorylation of EXO1 by CDKs 1 and 2 regulates DNA end resection and repair pathway choice. *Nat Commun*, 5, 3561.
- TUCKER, J. D. & PRESTON, R. J. 1996. Chromosome aberrations, micronuclei, aneuploidy, sister chromatid exchanges, and cancer risk assessment. *Mut Res*, 365, 147-159.
- UCKLEMANN, M. & SIXMA, T. K. 2017. Histone ubiquitination in the DNA damage response. *DNA Repair*, 56, 92-101.
- VAN DEN BOSCH, M., BREE, R. T. & LOWNDES, N. F. 2003. The MRN complex: coordinating and mediating the response to broken chromosomes. *EMBO reports*, 4, 844-849.
- VESELA, E., CHROMA, K., TURI, Z. & MISTRİK, M. 2017. Common Chemical Inductors of Replication Stress: Focus on Cell-Based Studies. *Biomolecules*, 7, 19.
- VUJANOVIC, M., KRIETSCH, J., RASO, M. C., TERRANEO, N., ZELLWEGER, R., SCHMID, J. A., TAGLIALATELA, A., HUANG, J. W., HOLLAND, C. L., ZWICKY, K., HERRADOR, R., JACOBS, H., CORTEZ, D., CICCIA, A., PENENGO, L. & LOPES, M. 2017. Replication Fork Slowing and Reversal upon DNA Damage Require PCNA Polyubiquitination and ZRANB3 DNA Translocase Activity. *Mol Cell*, 67, 882-890 e5.
- WANG, A. T., KIM, T., WAGNER, J. E., CONTI, B. A., LACH, F. P., HUANG, A. L., MOLINA, H., SANBORN, E. M., ZIERHUT, H., CORNES, B. K., ABHYANKAR, A., SOUGNEZ, C., GABRIEL, S. B., AUERBACH, A. D., KOWALCZYKOWSKI, S. C. & SMOGORZEWSKA, A. 2015a. A Dominant Mutation in Human RAD51 Reveals Its Function in DNA Interstrand Crosslink Repair Independent of Homologous Recombination. *Mol Cell*, 59, 478-90.
- WANG, B. & ELLEDGE, S. J. 2007. Ubc13/Rnf8 ubiquitin ligases control foci formation of the Rap80/Abraxas/Brca1/Brcc36 complex in response to DNA damage. *Proc Natl Acad Sci U S A*, 104, 20759-20763.

- WANG, J., AROUMOUGAME, A., LOBRICH, M., LI, Y., CHEN, D., CHEN, J. & GONG, Z. 2014. PTIP associates with Artemis to dictate DNA repair pathway choice. *Genes Dev*, 28, 2693-2698.
- WANG, J., DING, Q., FUJIMORI, H., MOTEGI, A., MIKI, Y. & MASUTANI, M. 2015b. Loss of CtIP disturbs homologous recombination repair and sensitizes breast cancer cells to PARP inhibitors. *Oncotarget*, 7.
- WEEMAES, C. M., HUSTINX, T. W., SCHERES, J. M., VAN MUNSTER, P. J., BAKKEREN, J. A. & TAALMAN, R. D. 1981. A new chromosomal instability disorder: the Nijmegen breakage syndrome. *Acta Paediatr Scand*, 70, 557-564.
- WEST, S. C. 2003. Molecular views of recombination proteins and their control. *Nat Rev Mol Cell Biol*, 4, 435-445.
- WILER, R., LEBER, R., MOORE, B. B., VANDYK, L. F., PERRYMAN, L. E. & MEEK, K. 1995. Equine severe combined immunodeficiency: A defect in V(D)J recombination and DNA-dependent protein kinase activity. *Proc Natl Acad Sci U S A*, 92, 11485-11489.
- WILLIAMS, H., GOTTESMAN, M. E. & GAUTIER, J. 2013. The differences between ICL repair during and outside of S-Phase. *Trends Biochem Sci*, 38, 386-393.
- WRIGHT, W. D., SHAH, S. S. & HEYER, W. D. 2018. Homologous recombination and the repair of DNA double-strand breaks. *J Biol Chem*, 293, 10524-10535.
- WYMAN, C. & KANAAR, R. 2006. DNA Double-Strand Break Repair: All's Well that Ends Well. *Annu Rev Genet*, 40, 363-383.
- XU, G., CHAPMAN, J. R., BRANDSMA, I., YUAN, J., MISTRICK, M., BOUWMAN, P., BARTKOVA, J., GOGOLA, E., WARMERDAM, D., BARAZAS, M., JASPERS, J. E., WATANABE, K., PIETERSE, M., KERSBERGEN, A., SOL, W., CELIE, P. H., SCHOUTEN, P. C., VAN DEN BROEK, B., SALMAN, A., NIEUWLAND, M., DE RINK, I., DE RONDE, J., JALINK, K., BOULTON, S. J., CHEN, J., VAN GENT, D. C., BARTEK, J., JONKERS, J., BORST, P. & ROTTENBERG, S. 2015a. REV7 counteracts DNA double-strand break resection and affects PARP inhibition. *Nature*, 521, 541-4.
- XU, Y. & BALTIMORE, D. 1996. Dual roles of ATM in the cellular response to radiation and in cell growth control. *Genes Dev*, 10, 2401-2410.
- XU, Y., WU, X. & HER, C. 2015b. hMSH5 Facilitates the Repair of Camptothecin-induced Double-strand Breaks through an Interaction with FANCD1. *J Biol Chem*, 290, 18545-58.
- YOO, E., KIM, B. U., LEE, S. Y., CHO, C. H., CHUNG, J. H. & LEE, C. H. 2005. 53BP1 is associated with replication protein A and is required for RPA2 hyperphosphorylation following DNA damage. *Oncogene*, 24, 5423-30.
- ZEMAN, M. K. & CIMPRICH, K. A. 2014. Causes and consequences of replication stress. *Nature*, 16.
- ZHAI, Y., LI, N., JIANG, H., HUANG, X., GAO, N. & TYE, B. K. 2017. Unique Roles of the Non-identical MCM Subunits in DNA Replication Licensing. *Mol Cell*, 67, 168-179.
- ZHAO, W., STEINFELD, J. B., LIANG, F., CHEN, X., MARANON, D. G., JIAN MA, C., KWON, Y., RAO, T., WANG, W., SHENG, C., SONG, X., DENG, Y., JIMENEZ-SAINZ, J., LU, L., JENSEN, R. B., XIONG, Y., KUPFER, G. M., WIESE, C., GREENE, E. C. & SUNG, P. 2017. BRCA1-BARD1 promotes RAD51-mediated homologous DNA pairing. *Nature*, 550, 360-365.
- ZHU, X., MANCINI, M. A., CHANG, K.-H., LIU, C.-Y., CHEN, C.-F., SHAN, B., JONES, D., YANG-FENG, T. L. & LEE, W.-H. 1995. Characterization of a Novel 350-Kilodalton Nuclear Phosphoprotein That Is Specifically Involved in Mitotic-Phase Progression. *Mol Cell Biol*, 15, 5017-5029.
- ZIMMERMANN, M. & DE LANGE, T. 2014. 53BP1: pro choice in DNA repair. *Trends Cell Biol*, 24, 108-17.
- ZUAZUA-VILLAR, P., GANESH, A., PHEAR, G., GAGOU, M. E. & MEUTH, M. 2015. Extensive RPA2 hyperphosphorylation promotes apoptosis in response to DNA replication stress in CHK1 inhibited cells. *Nucleic Acids Res*, 43, 9776-87.